Habilitation Thesis

Optimum Design of the Motorization of Electric Vehicles based on Multiphysic Approach

Daniel FODOREAN

Lecturer at Technical University of Cluj-Napoca

Faculty of Electrical Engineering

Department of Electrical Machines and Drives

June, 2013

ABSTRACT

The present habilitation thesis summarizes the achievements and the perspectives of the teaching and research activities of the author. The report is structured on the main topics related to the optimization of the motorization of light electric vehicles (EVs). First of all, we will introduce the frame in which the research activities have been employed.

The research experience of the author has been started with a co-tutoring PhD thesis, at the initiative of the *University of Technology from Belfort-Montbéliard* (UTBM) - France, and the *Technical University of Cluj-Napoca* (TUCN) - Romania. The subject of the research (a novelty, at that time, for both partners) has been proposing the study of a wide speed range motorization solution based on hybrid excited machines. (The hybrid excitation refers to a main field source, the permanent magnet, and auxiliary an electromagnet used to vary the constant field of the magnet.) After a consistent study, which gave encouraging results, the author's public defense of the PhD thesis report took place in 12 July 2005 in France. This moment, was followed (from the author's point of view) by a rich experience in both universities – which are now partners in several educational programs or research projects.

At UTBM, firstly as a PhD student and next, for two years as *Attaché Temporaire d'Enseignement et Recherche* (between 2003-2004 and 2005-2006) and for another two year as Associated Professor (between 2007-2009), the author has been benefited of the experience of a high quality research personal in the field of power electronics, microcontrollers and digital signal processors programming. At home, at the TUCN, firstly as a student and after that as a master-student, PhD student, Assistant Lecturer (2005-2006, 2009-2011) and Lecturer (since 2011) the author's study has been focused in the field of electrical engineering in general, and in the topic of design and control of electrical machines and their drives, in particular.

In this context, the author has assimilated interdisciplinary competences which should contribute to the transfer of knowledge towards the industrial environment. Thus, the author has been involved in several research projects, financed by the Romanian Government or by the industrial partners. To be more precisely, the author was or he is the project manager for 5 research contracts:

- two research contracts with industrial partners from Switzerland (XANTOS and HYTEN).
- three national contracts: of TD type (for PhD students); of TE type (for your researchers); of PCCA type (partnership or cooperation research project, involving industrial partners).

These contracts have permitted the acquisition of high quality and performance equipment which is now in the custody of the CAREESD research center from TUCN. This should increase the confidence of our industrial partners with regard to the quality of our research.

At the UTBM, as research team leader, the author has been involved in several projects with industrial applicability, where we put in place a testing platform for electric motors with hybrid supply for the propulsion of light electric vehicles (golf cars and electric scooters).

With the occasion of the research employed at UTBM, the author has been involved in a collaboration which dates now from 2009. This research cooperation concerns the optimization of electrical machines involved in the electric vehicles and power generation for insulated wind power plants. This research subject was realized with a French colleague, Associated Professor Lhassane IDOUMGHAR (habilitated to be PhD supervisor, in informatics, since 2012) from University of Haute-Alsace (UHA), Mulhouse-France. At the UHA the author had two research stages, and in May 2013 he has been "invited professor".

The author has also participated to several international courses, namely:

- „*Sensorless Control of Permanent Magnet Machines*" course organized by Aalborg University (Denmark).

- „FPGA-Basics" and „FPGA-EDrive" courses organized by dSPACE GmbH (Germany).

All this experience in interdisciplinary fields had the final goal of obtaining competitive solutions for the motorization of light electric vehicles, in terms of performances and cost, capable to contribute to the progress of the technology involved in hybrid-electric vehicles.

The visibility of the scientific results plays an important role in promoting the local research. This has motivated the author to employ a consistent dissemination activity which has produced the following results (starting from the PhD thesis public defense): 4 books in national edition and 1 book chapter in international edition, 12 journal articles (10 of ISI type), 29 international conference articles and 1 national patent proposition.

In order to keep a high level of his research, the author has been involved in editorial activity, as scientific secretary, for the *International Journal of Electrical Engineering in Transportation*. Also, the author is a member of the IEEE scientific organization and reviewer for the journals: *IEEE Transactions in Industrial Electronics* and *IEEE Transactions on Vehicular Technology*.

In perspective, the author is intending to study an entirely magnetic traction system (the mechanical gear being replaced by a magnetical one) and the limits of high speed motorization for the propulsion of electric vehicles. These approaches could contribute to the increase of the electric vehicles' autonomy.

REZUMAT

Actualul raport de teză de abilitare prezintă în rezumat realizările și perspectivele didactice și de cercetare ale autorului. Raportul este structurat pe principale tematici de cercetare utilizate la optimizarea optimală a motorizării vehiculelor electrice. Mai întâi de toate, va fi amintit cadrul în care au fost desfășurate activitățile de cercetare.

Experiența în cercetare a autorului a demarat cu ocazia unei teze de doctorat în cotutelă, inițiată de *Université de Tehnologie de Belfort-Montbéliard* (UTBM) - Franța, și de *Universitatea Tehnică din Cluj-Napoca* (UTCN). Subiectul tezei (o noutate la acea vreme, pentru ambii parteneri) urmărea propunerea unei soluții de motorizare în plajă largă de viteze pentru vehicule electrice ușoare, pe baza unui motor cu excitație hibridă. (Excitația hibridă la o mașină electrică presupune existența unui magnet permanent, ca sursă principală de câmp, și auxiliar un electromagnet care să permită variația fluxului constant al magnetului). După un studiu consistent și cu rezultate științifice promițătoare, urmat de susținerea publică a tezei de doctorat în data de 12 Iulie 2005, au urmat o serie de experiențe didactice și de cercetare, atât la UTCN cât și la UTBM.

La UTBM, mai întâi ca și doctorand, apoi, timp de patru ani de zile, în calitate de *Attaché Temporaire d'Enseignement et Recherche* (perioada 2003-2004 și 2005-2006) și respectiv Conferențiar (perioada 2007-2009) autorul a beneficiat din plin de experiența cercetătorilor colectivului francez în privința următoarelor domenii de interes: electronică de putere, programarea microcontrolerelor și a procesoarelor digitale de semnal. Acasă, la UTCN, mai întâi ca student, masterand și doctorand, iar ulterior ca Asistent (2005-2006, 2009-20011) și Șef Lucrări (din 2011) autorul s-a format în domeniul electrotehnicii și al proiectării și controlului mașinilor electrice și a convertizoarelor statice asociate.

În acest context de cooperare s-au pus bazele unor competențe interdisciplinare care să contribuie atât la formarea autorului cât și la transferul cunoștințelor în zona aplicativă, industrială. În consecință, autorul a fost și este implicat în diverse contracte de cercetare, dintre care se amintesc cele în calitate de director de proiect:

- două contracte cu parteneri industriali din Elveția (firmele XANTOS și HYTEN).

- trei contracte naționale: *de tip TD* (pentru tineri doctoranzi); *de tip TE* (pentru tinere echipe de cercetare); *de tip PCCA* (cu parteneri industriali).

Aceste contracte de cercetare au permis echiparea centrului de cercetare CAREESD (din cadrul UTCN) cu echipamente de calitate și performante, infrastructură care aduce un plus de valoare și credibilitate în vederea implicării partenerilor industriali.

La UTBM, în calitate de responsabil de echipă de cercetare, autorul a fost implicat în diverse proiecte cu aplicație industrială, dintre se amintesc: platforma de teste pentru motorizări și hibridizare a alimentării (folosind baterii și ultracondensatoare) pentru vehicule electrice ușoare (carturi și scutere electrice). Tot în acest cadru, s-au pus bazele unei colaborări de cercetare care datează din anul 2009. Această colaborare vizează optimizarea proiectării mașinilor electrice pentru aplicațiile de propulsie electrică sau sisteme eoliene. Această tematică a fost realizată alături de colegul Conferențiar Lhassane IDOUMGHAR (abilitat să conducă cercetare din anul 2012) de la Université de Haute Alsace (Mulhouse, Franța), unde subsemnatul a efectuat 2 stagii de formare, și a fost în calitate de "profesor invitat" (Mai, 2013).

Autorul a participat de asemenea la diverse cursuri de formare, și anume:

- cursul „*Sensorless Control of Permanent Magnet Synchronous Machine*" organizat la Aalborg University (Danemarca).
- cursurile „*FPGA-Basics*" și „*FPGA-Edrives*" organizate de compania dSPACE GmbH (Germania).

Toată această experiență, formare interdisciplinară și competențe în domeniul propulsiei electrice are ca scop final propunerea unor soluții competitive ca performanțe și cost, care să

contribuie la progresul tehnologiei din domeniul vehiculelor electrice-hibride. În acest sens, vizibilitatea rezultatelor obținute joacă un rol important în promovarea cercetării autohtone, motiv pentru care autorul a întreprins o activitate de publicare consistentă, soldată (de la momentul susținerii tezei de doctorat) cu următoarele publicații: 4 cărți în edituri naționale și 1 capitol de carte în editură internațională, 12 articole de revistă (dintre care 10 de tip ISI), 29 de articole de conferință internațională și o propunere de brevet național.

În vederea menținerii calității în cercetare, autorul a întreprins activități editoriale la revista *International Journal of Electrical Engineering in Transportation*, fiind și recenzor pentru articole științifice propuse spre publicare în jurnalele *IEEE Transactions in Industrial Electronics* și *IEEE Transactions on Vehicular Technology*. De asemenea, autorul este membru al organizației IEEE.

Daca până în prezent activitatea de cercetare a autorului a fost concentrată spre motorizarea și managementul energiei la vehiculele electrice-hibride ușoare, în perspectivă se urmărește studiul sistemului de tracțiune în totalitate magnetic (cu reductor magnetic care să-l înlocuiască pe cel mecanic) și forțarea limitelor propulsiei folosind mașini de mare viteză. Aceste cercetări se estimează a fi soluții viabile în vederea creșterii autonomiei vehiculului electric.

To my wife, Ligia, and children, Carina & Andrei

ACKNOWLEDGMENTS

Even if the habilitation thesis must prove the scientific independence of the researcher, this does not mean that the content of the thesis is the exclusive result of his solitary effort. On the contrary, this requires collaboration, understanding and communion which can be found while working alongside colleagues or benefit from the experiences of partners or strangers whose scientific papers animates knowledge. That is why, the acknowledgments are sincere in every word. Thanks are not shown here for free and cannot fully express the appreciation and gratitude that is due.

I would start first of all to recognize that some of the results presented here would not have been possible without the involvement of my mentors, Professor Ioan Adrian VIOREL (Technical University of Cluj-Napoca - TUCN) and Professor Abdellatif MIRAOUI (Univeristy of Technology from Belfort-Montbéliard - UTBM), the scientific leaders of my PhD thesis carried out in co-tutoring. Dear Professors, I am truly grateful to you for all your involvement.

From my PhD thesis public defense, 8 years have been past. During this time I had the opportunity to work in two universities and research groups: the CAREESD research center, from TUCN, and the SET research laboratory, from UTBM. This scientific environment has offered me many opportunities and occasions to assimilate and to progress in my research work. Dear colleagues and friends from Belfort, Mulhouse and Cluj-Napoca, thank you very much for your cooperation.

I wish also to express my recognition to the professors that took part in the habilitation jury, who had consecrated important time and energy to read and to make constructive critics on the manuscript, which finally permitted me to improve the quality of the report. So, special thanks to: Professor Humberto HENAO (University Picardie “Jules-Verne”, Amiens, France), Professor Marcel ISTRATE (Technical University “Gh.Asachi” from Iasi) and Professor Dumitru TOADER (University “Politehnica” from Timisoara).

Finally, I would like to express all my gratitude to my best friend and precious people in my life, for their continuous support, understanding and love: my wife Ligia, my daughter Carina and my son Andrei. I love you!

SUMMARY

PART 1

TEACHING AND RESEARCH ACTIVITY ACHIEVEMENTS

1 INTRODUCTION

1.1 The structure of the thesis

The present thesis report represents the summary of scientific and teaching achievements of the author with respect to the propulsion of the Electric Vehicle (EV). The EV application is a common research topic today, mainly because of the gas emission and fossil fuel depletion worldwide. But in order to compete with thermal vehicles, researches need to be done especially with regard to the energy storage units and the traction chain. Of course, on board of an EV there are many other auxiliaries which affect the energy consumption (i.e., all micro-motors used for the electric chairs/windows/mirrors, steering, braking, air-conditioning etc.), being responsible for an important part of energy consumption. But the battery, the major supplying source from an EV (even for hybrid electric configurations) is mainly affected by the traction motor. For important accelerations ramps the electric motor consuming the most important part of the stored energy. In order to spare as much as possible the battery, an improved energy management of the traction chain should be assured. Thus, optimizing motorization, controlling with improved energetic performances and optimal energy management are the key elements to respond to the EV's need: the improved autonomy.

In FIGURE 1-1 are presented the main elements from a traction chain: the supplying source, which could be battery, fuel cell (FC) or ultracapacitor (UC); the control system, formed by a controller unit and the static power converter; and finally the electrical machine (EM). These are the main scientific themes treated in this thesis.

The present thesis report is structured in 8 chapters and the references. The copies of the author's most significant scientific papers are presented at the end of the manuscript.

The 1st chapter presents a short state-of-the-art of the EV, the most important moments in its history, starting from his birth and up to its present, and taking a prospective look towards the next 50 years. Also, the author's main results and achievements will conclude this chapter.

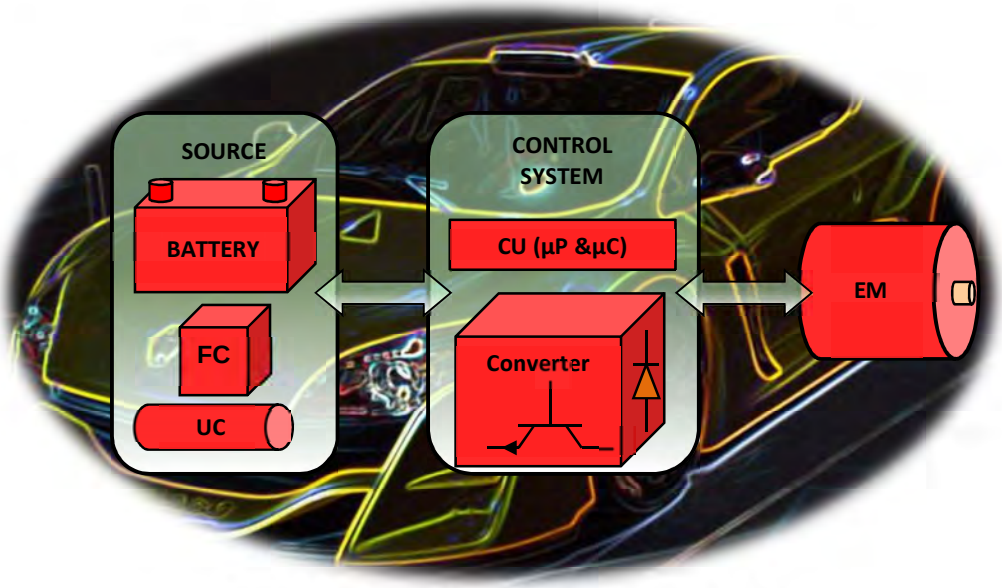

FIGURE 1-1. The main devices in the propulsion of an EV.

The 2nd chapter is dedicated to the motorization variants, especially for light EVs, while the 3rd chapter will present the main designing elements for several types or topologies of EM. The design is mainly validated numerically based on the finite element method.

In order to exploit the maximum performances of the motorization it is needed to optimize the core of the traction chain: the electric motor. Thus, in the 4th chapter several optimization techniques are presented. An important aspect of the motorization is related to a sensitive problem: the thermal behavior of the machine, knowing that the EM should assure the safe operation for an imposed driving cycle. Thus, the heat transfer for several electrical machines and its implication will be evaluated in the 5th chapter.

In the 6th chapter will be discussed the control techniques used for the motorization of the EV, the motor-drive capability to operate in faulty conditions and the conditions of working beyond the rated speed in the *constant power zone*. The energy, necessary to assure the motor's operation, comes from battery (most commonly), ultracapacitors or fuel cells. Thus, the subject of the energy management will be presented in the 7th chapter.

The conclusions and the scientific perspectives are presented in the 8th chapter, where new research topics are emphasized: the high speed motorization, the magnetic gears, and the controllability at high switching frequency. From teaching perspective, the author intends to employ in his future courses the concepts of Hardware-in-the-Loop and Rapid Control Prototyping, which are the key elements in studying the hybrid-electric vehicle with competitive performances. Also, some conclusions are emphasized at the end of the 8th chapter.

1.2 Framework and summary of main results

It would be difficult to identify which project or research study is more linked to the topic of electric vehicle (EV), because almost the entire research work of the author is dedicated to this subject. Thus, the author thinks that is rather appropriated to cite two books, written in English (actually a monograph and a book chapter), which are mainly dedicated to EV application:

- D. Fodorean, F.Jurca, M.Ruba and D.C. Popa. *Motorization Variants for Light Electric Vehicles – design, magnetic, mechanical and thermal aspects*, AlmaMater, June 2013.
- D.Fodorean: *Global Design and Optimization of a Permanent Magnet Synchronous Machine used for Light Electric Vehicle* – book chapter in monograph *Electric Vehicles – Modelling and Simulations*, edited by Serif Soylu. Intech, 2011.

The following subchapters will describe the EV's state-of-the-art and the main teaching activities and research achievements, to prove the relevance of the work and the author's independency in producing scientific results.

1.3 The research context

One of the greatest problems of our modern society, in particular for industrialized countries, is the pollution [1]. According to several studies, the largest share of pollution from urban areas comes from vehicles' emissions and because of the explosive growth of the number of cars. The pollution effect is more obvious especially in large cities. Consequently, finding a solution to reduce (or eliminate) the pollution is a vital need. If in public transports (trains, buses and trams) were found non-pollutant solutions (electrical ones), for the individual transport, the existent variants cannot yet meet the autonomy expectations. Even though historically the electric vehicle precedes the thermal vehicle, the power/fuel-consumption ratio and the reduced time to refill the tank has made the car powered by diesel or gasoline the ideal candidate for individual transport. Lately there were some rumors regarding the depletion of fossil resources, but according to recent studies the earth resources can be assured for many

years from now. So, the problem of breathing clean air remains the main advantage of the electric vehicle (EV). However, beside the renewable energy subject, the electric transportation is one of the common topics of the researchers today.

An *electric vehicle* by its definition is supplied from a purely electric source, being propelled by an electrical machine (in motor regime for the traction phase and in generator regime when employing energy recovery in breaking phase). Regarding the available power sources, we can have electrified vehicles (train, tram, trolleybus) or automobiles (with embedded power source) which can be charged at home or, nowadays, on streets and dedicated supplying stations [2]-[10].

Regarding the *hybrid* term linked to the *vehicle*, the common opinion of the researchers in this field is to consider a hybrid vehicle (HV) when the propulsion is assured with an internal combustion engine (ICE) and an electric motor (EM), alternately or in the same time. On the other hand, the term *hybrid-electric* refers to the mixt character of the power source, which can be battery (most often), or fuel cell (FC) stack, connected in parallel with ultracapacitors (UC), the propulsion being assured only with EM (or at least two EMs, when the EV is propelled by in-wheel motors); this is the *hybrid electric vehicle* (HEV).

In FIGURE 1-2 are presented the main EV, HV and HEV configurations currently employed in the automobile industry [2], [3], [4], [10], [11], [12].

In the case of EV or HEV the traction can be intermediate by a mechanical transmission (gear and distribution system), or with no transmission, when the EM is built in outer-rotor configuration – being called *in-wheel motor*. (In FIGURE 1-2 the dotted line refers to the electric power flow, while the "CU" acronym refers to the control unit which manages the power flow.)

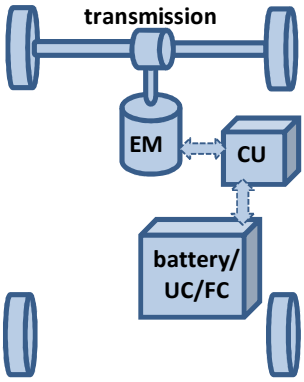

EV (HEV) with transmission

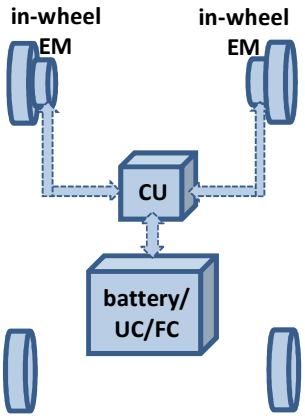

EV (HEV) with no transmission

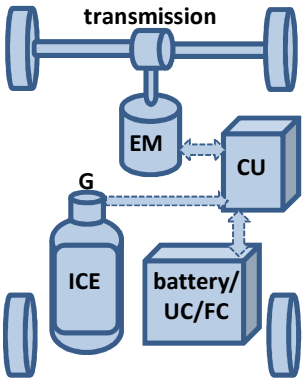

HV series configuration

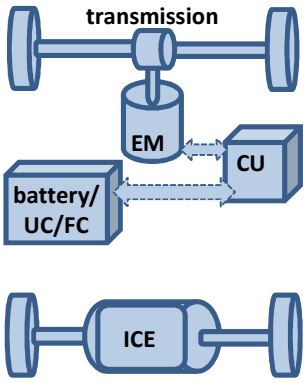

HV parallel configuration

FIGURE 1-2. EV, HV and HEV configurations.

For the fully electric topologies, the power source can be formed by one unit (battery, UC or FC) or by a mixed source (battery – for continuous regime – with UC – for high acceleration ramps – or FC with UC). For a FC system, other elements should be taken into consideration: a high speed compressor which assures the air flow into the FC stack, an oxygen tank, etc. The FC stack is not very big in volume, but the needed auxiliaries force the use of such a technology rather in static applications, not for automobiles.

Concerning the technology of the motorization and of the power supply, we can speak of several possibilities: for the motorization: direct current (dc) or alternative current (ac) machines; for the batteries: most commonly lead-acid, or nichel-metal-hybrid, sodium and lithium based batteries; for the FC: proton exchange membrane, solid oxide etc.; for the UC: the technology is similar for all manufacturers.

For the HV there are two possible configurations: series and parallel. For the series HV variant, the internal combustion engine (ICE) is linked to an electric generator (G) to feed the power source; the motorization is based on EM. For the HV in parallel configuration, there are several possible variants [3].

Nowadays the hybrid vehicles can be seen on streets, having satisfactory price and autonomy. But it seems logic that this is just an intermediary step to the fully electric automobiles, which are still in searching of an appropriate supplying solution, capable to assure satisfactory autonomy, with reduced refilling time [13]-[17].

Another source of electricity generation is the flywheel, which finds its place in the hybrid-source configuration, but due to its reduced power density it is rather used in static application.

1.3.1 Brief history of the electric vehicle

In FIGURE 1-3 is depicted in brief the evolution of the EV since its birth, in the 2nd quarter of the 19th century, until nowadays when it is possible to speak about the *electric concept cars*, plug-in vehicles (EVs fed directly on streets) and EVs on highways.

The exact date of the first ever build EV is not surely known. Two dates are indicated: 1832 or 1835 [2]. At that time it was the beginning of an era which will influence not only the transportation/travelling concept, but even the existence of the mankind. The first steam locomotive was built in USA in 1804. The first train used to transport humans, propeled by steam locomotive, was seen in 1825, in England. If the railway transportation was financed by country governments, the individual transportation was rather animated by the hobby of wealthy people. The first electric battery in mass production appeared in 1802, designed by William Cruickshank. Based on his technology and the electric motor proposed by Michael Faraday (who builds the first dc motor, in 1821), the EV appeared in the second quarter of the 19th century.

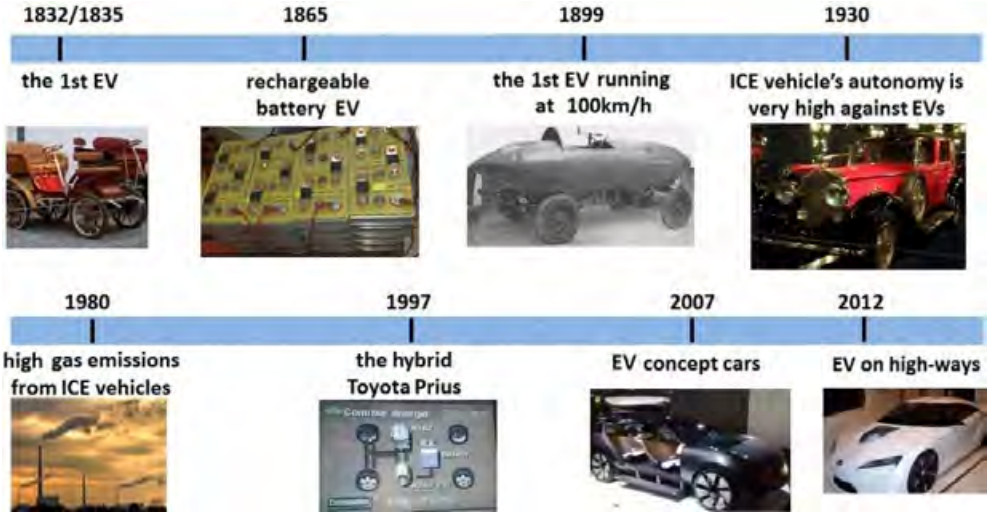

FIGURE 1-3. Main events in the history of the EV.

The first rechargeable battery has been built in 1836, and after years of technology improvement, a similar battery was used to propel an EV in 1865 [2]. In parallel with the electric car, the first electric locomotive, powered by a non-rechargeable battery was built by Robert Davidson in 1837, and the first electrified locomotive was running on a main of 6.4 km, in Baltimore, USA [3]. The first tram was put into service in Sankt-Petersburg, RUSSIA, and the first electric car which reached the 100 km/h has been tested in 1899 [3].

At the end of the 19th century the EV was more spread than the thermal vehicle. With the beginning of the 20th century the humanity entered into a new stage marked by the first flying machine: the ancestor of the airplane. The demands in autonomy, important recharging time and reduced power density made the EV to loose important terrain against the ICE vehicle. While mankind was entering in the industrialized era, the use of fossil resources determined a reorientation. Thus, after 100 years from the first EV, the thermal automobile became most spread all over the world.

The evolution of the electrified train has known a different road. Some of the main history events of the train are presented in FIGURE 1-4.

FIGURE 1-4. Photographs with trains: the evolution of train powered by electric machines.

For diesel locomotive, which had the fuel installed on board, the advantage of power density was not so obvious. On a contrary, the power source of the electric locomotive was not installed on the train and so the whole system could be smaller, lighter and faster (and consequently cheaper, capable to assure the supply of several trains in the same time). Such a train is presented in FIGURE 1-4-top-left. Moreover, the capability of the dc motor to offer a very important speed variation made the electric locomotive its own competitor in establishing the world speed record. In 20th March, 1950, the world record of an electrified locomotive was established at 331 km/h: it belongs to a train made by the French company, ALSTOM, FIGURE 1-4-top-right. Also, the capability of the electric machine to recover energy in breaking regime was a huge advantage against the steam or diesel locomotive. Such a train and technology are presented in FIGURE 1-4-middle. The French company proposed after that the high speed train, known as *Train à Grande Vitesse* (TGV), which has established several times the speed record for trains, like the one in 2007 FIGURE 1-4-bottom (ALSTOM reported, in April 2007, a top speed of 574.8 km/h.).

Other companies from Japan, and lately from China, are proposing similar trains. The government from Japan is prepared to eliminate the airplanes from internal transportation, starting from 2045: by using the MAGLEV train (magnetically levitated), capable to transport 350 persons at 500 km/h (source: http://www.fiicurios.ro/stiai-ca/acesta-este-trenul-care-zboara-cu-500-de-km-h-japonezii-se-pregatesc-sa-renunte-la-cursele-aeriene-interne.html - web page accessed on 11 March 2013).

Concerning the personal transportation, we can say that the electric car developed in this period is rather the fruit of personal ambition of some researchers or industrial companies who refused to abandon this topic. The EVs were rather used for specific applications like merchandise manipulation, golf tournaments etc., but not for personal transportation. The reduced autonomy and the important time to recharge the battery have determined the use of only very light vehicles (FIGURE 1-5-left), fed from low voltage batteries (to reduce the overall weight), or alternatively, for sport events, using solar panels (FIGURE 1-5-rigth).

FIGURE 1-5. Photographs with light electric cars, supplied from batteries or solar panel.

Regarding the urban transportation, in 1960-1970 the diesel busses were much spread. Nowadays we can speak of an entirely electrified network transportation system. In European countries, most of the travelers are using electrified vehicles: metros, trams, trolleybuses; even the buses are now fuelled by methanol, which is less pollutant than the diesel or gasoline variants. In Romania, similar decisions have been taken by the government and private funds, to find solutions oriented for the use of non-polluting transportation. In FIGURE 1-6 is presented a photograph of the tram running in Cluj-Napoca (Romania).

FIGURE 1-6. Tramway in Cluj-Napoca (Romania).

Coming back to the history evolution of the EV from FIGURE 1-3, with the increase of earth population (but also due to living standards improvement and the necessity for fast and long-distance transport) two issues appeared, at the beginning of the year 1980: the problem of pollution and its negative consequences in urban areas, on one hand, and on the other hand the problem of depletion of Earth's natural resources. Conjunction with the monopoly of certain countries to the oil resources, which generated or were pretext to wars, determined the humanity to find alternative solutions. In the beginning of the 9th decade of the 20th century, the industrial companies and the governments started to speak about the necessity of using hybrid vehicles. In 1997, Toyota came up with a hybrid solution in series production: the first generation of the hybrid Toyota Prius. Since then, other generations of Toyota have come to life, and other car manufacturers have developed their hybrid variants. More researches have been made in the storage field, different materials have been tested and new devices were proposed. The European, American or Asian countries have established through specific international partnerships the new trend in this field, like the acceptable gas emissions, the autonomy etc. Practically, from the year 2007 every car manufacturer has proposed different variants of *concept car* which could respond to the gas emissions criteria. Today, we can see the hybrid cars on streets, as well as the plug-in EV (supplied directly on street). The EV, running only on electric propulsion was limited to urban area, few years before. But now, at the end of 2012, the car manufacturers are proposing EV running on highways. So, the trend is clear and the researchers have a lot to do in this field.

1.3.2 The electric vehicle in the present

With regard to automobiles, there have been several attempts of establishing a maximum acceptable level of pollution. Thus, several car manufacturers have prepared a declaration called *Partnership for a New Generation of Vehicles* (PNGV), also named *SUPERCAR* [2]. This concept states, for a certain power, the expected performances from a thermal or hybrid car. Virtually, every car manufacturer proposes its own automobile at *SUPERCAR* standards, see Table 1-1. In this table are presented only some of the world's concept cars. Of course, at concept level, the investment is not a criterion for the construction of EVs, as in the case of series manufacturing (where profits are severely quantified). For example, nowadays the price of 1 kW of power provided by FC is around 4’000 €; thus, a FC of 100 kW would cost 400’000 € (which is practically prohibitive in terms of costs, for series manufacturing).

By consulting Table 1-1, it can be noticed the interest of all car manufacturers to get reduced pollution vehicles, with highest possible autonomy. Nowadays, the hybrid vehicles can be seen on streets. Although the cost of a hybrid car is not much higher than for the classical thermal one (about 15-25% higher), however, the first one requires maintenance higher costs.

TABLE 1-1. SEVERAL TYPES OF ELECTRIC CAR CONCEPTS - [2]

CONCEPT CARS	*TECHNICAL DATA*	*PERFORMANCES*
AUDI metroproject quattro	turbocharged four-cylinder engine and an electric machine of 30 kW; lithium-ion battery	100km range on electric-only; 0-100 km/h in 7.8 s; maximum speed 200 km/h
BMW x5 hybrid SUV	for 1000 r/min, there is a V-8 engine providing 1000 Nm; the electric motor gives 660 Nm	fuel economy is improved by an estimated 20%.
CHRYSLER eco voyager FCV	propulsion of 200 kW; hydrogen is feed to a PEM fuel cell (FC)	range of 482 km and a 0–60 km/h in less than 8 s.
CITROËN c-cactus hybrid	diesel engine provides 52 kW and the electric motor gives 22 kW	fuel consumption is 2.0 L/100 km; maximum speed is 150 km/h
FORD hySeries EDGE	Li-ion battery providing 130 kW, and the FC provides 35 kW	range of 363 km (limited by the amount of hydrogen for the FC)
HONDA FCX	electric vehicle with 80 kW propulsion engine, combining ultracapacitors (UC) and PEM FC	55% for overall efficiency, driving range of 430 km
HYUNDAI I-blue FCV	FC stack produces 100 kW; 100 kW electric machine (front wheels) and 20 kW EM for each rear wheel	estimated range: 600 km
JEEP renegade diesel–electric	1.5 L diesel engine provides 86 kW and is teamed with 4 electric motors (4WD) of 85 kW combined power	the diesel provides range extension up to 645 km beyond the 64 km electric-only range (diesel fuel tank holds 38 L)
KIA FCV	a 100 kW FC supplies 100 kW front wheels EM, while the motor driving the rear wheels is 20 kW	range is stated to be 610 km
MERCEDES BENZ s-class direct hybrid	3.5 L (V-6) gasoline engine with motor/generator combined power of 225 kW and torque of 388 Nm	acceleration time from 0-100 km/h in 7.5 s
MITSUBISHI pure EV	Li-ion battery and wheel-in-motors of 20 kW	150 kg Li-ion battery give a range of 150 km (2010 prospective range of 250 km
OPEL flextreme	a series hybrid topology (diesel engine) with Li-ion battery; the EM has 120 kW peak power	fuel consumption of 1.5 L/100 km; electric only mode has range of 55 km
PEUGEOT 307 hybrid	it is diesel/electric hybrid automobile	the estimated fuel economy is 82 mpg; this is a hybrid that matches the PNGV goals
SUBARU G4E	five passengers EV, using Li-ion batteries	driving range: 200 km; the battery fully charged at home in 8 h (an 80% charge is possible in 15 min)
TOYOTA 1/X plug-in hybrid	thermal engine 0.5 L, with a huge reduction of mass to 420 kg (based of carbon fibre composites)	low mass also means low engine power and fuel consumption
VOLKSWAGEN Blue FC	a 12 kW FC mounted in the front charges 12 Li-ion batteries at the rear; The 40 kW motor is located at the rear	the electric-only range is 108 km; top speed is 125 km/h, and the acceleration time from 0-100 km/h is 13.7 s
VOLVO recharge	series hybrid with lithium polymer batteries; the engine is of 4-cylinder type with1.6 L; it has 4 electric wheels motors (AWD)	electric-only range is 100 km; for a 150 km trip, the fuel economy is 1.4 L/100 km

With the improvements in the storage system, the manufacturers of EVs have proposed increased autonomy vehicles, capable to run on highway. The top 10 best-selling highway EVs are presented in Table 1-2 [18].

TABLE 1-2. ELECTRIC VEHICLES TODAY: TOP 10 BEST SELLING HIGHWAY ELECTRIC CARS PRODUCED SINCE 2008 - [18]

MODEL	*MARKET LAUNCH*	*GLOBAL SALES (BY DECEMBER 2012)*
Nissan Leaf	December 2010	49 117
Mitsubishi i MiEV	July 2009	~ 24 000
Renault Kangoo Z.E.	October 2011	6 665
Mitsubishi Minicab MiEV	December 2011	3 234
Renault Fluence Z.E.	2011	2 861
Tesla Model S	June 2012	2 650
Tesla Roadster	March 2008	~ 2 418
Smart electric drive	2009	~ 2 200
BYD e6	May 2010	2 124
Bolloré Bluecar	December 2011	1 942

Japan and the U.S. are the largest highway-capable electric car country markets in the world, followed by several European countries and China. In Japan, more than 28 000 all-electric cars have been sold through, with sales led by the *Nissan Leaf* (21 000 units sold since 2010). Around 27 000 all-electric cars have been sold in the U.S. since 2008 (sales led by the *Nissan Leaf*, with 19 512 units sold through December 2012). In Europe, the best-selling electric car in 2012 was *Opel Ampera* [18].

In this moment, for an electric car not the acquisition price will be the most important issue, but the investment necessary to assure the vehicle's maintenance. A comparison of two variants, with thermal and hybrid motorization, is presented in FIGURE 1-7 to show that the selling price of an HV is 25% higher that a thermal vehicle [2]. Due to lack of appropriate infrastructure and monopoly for EV parts, the maintenance costs are huge for electric cars.

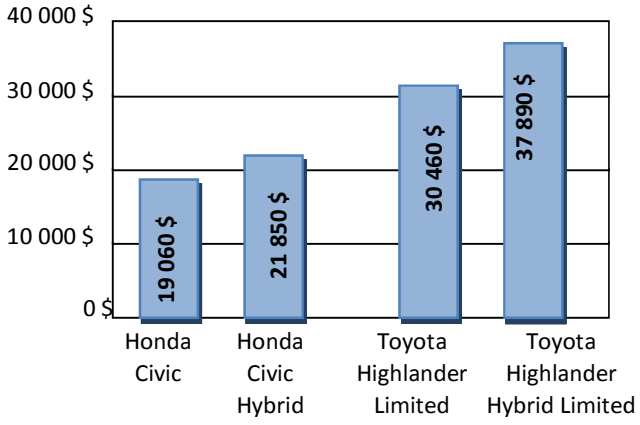

FIGURE 1-7. Comparison between thermal and hybrid motorization.

1.3.3 The electric vehicle: perspectives

Compared to thermal vehicles, the number of selling units of EVs is still reduced, but the trend is clear. The number of EVs seen on streets will increase in the nearest future. Some predictions on the EV's are presented in FIGURE 1-8 [2].

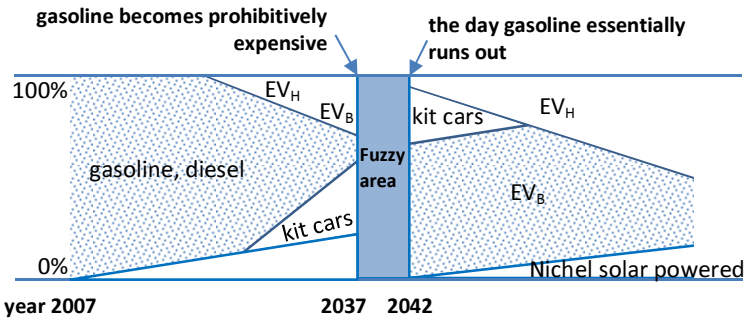

FIGURE 1-8. Estimated prospective of the EV of the future.

Based on [2], in the previsions for the nearest future it seems that the number of thermal automobiles decreases, while the hybrid ones are taking their place. By 2037 the transition electric car (called *kit car*) will replace entirely the old vehicles motorized with ICE. After a fuzzy period, when the entire electric distribution network should replace the currently gas stations, the vehicles will be supplied based on non-polluted systems with new energy storage units, by that passing to a new philosophy of building and using the automobiles. (In FIGURE 1-8 "kit cars" refers to a new generation of EVs, "EV_B" denotes the EVs using non-conventional electric sources and "EV_H" refers to EV build based on new materials, supplying stations and a new transport philosophy.)

So, one of the challenges of personal transport refers to finding clean solutions, with enhanced autonomy [11], [12]. This was the motivation of the author's research activity, all these years. By taking a closer look to the magnetical, mechanical, thermal phenomena which take place in an electric machine, and searching the best suited variant in terms of optimum weight, energetic performances controllability and fault tolerance, the author proposes his point of view with regards to the improvements that can be done in order to obtain competitive EVs.

1.4 The main achievements of the teaching activity

Even from the PhD period, the teaching and research responsibilities have prepared the interdisciplinary approach of the author. Teaching in two establishments was an important opportunity, having colleagues and friends with similar or new interest which contributed to the author's formation as independent researcher. The first university where the author worked most of the time in the doctoral period was the University of Technology from Belfort-Montbéliard (UTBM), Belfort, France. The second university, where the author has obtained the *Engineer* and *Master of Science* diploma, and presently he is a Lecturer, is the Technical University of Cluj-Napoca (TUCN).

At the UTBM, the author has obtained the PhD degree after the public defense of his thesis, in July, 12, 2005. Here, between 2005-2006, as *Attaché Temporaire d'Enseignement et Recherche* (ATER)[1] the author has concentrated his efforts in teaching *Finite Element Method based on Computer Added Design (FEM-CAD)* and *Electrotechnic (Elec)*. After receiving "*la qualiff de Maître de Conferences*" (MC)[2], the author get the Associated Professor position at the same French university. Here, from 2007-2009 the author have teach courses in *Modeling of Electrical Machines and Drives (MEMD)*, *Mechanical for Electrical Engineering (MEE)*, and *Programming*

[1] *Teaching and Research Assistant*

[2] It is recognition of the Universities National Council from France, based on the scientific background of the researcher, regarding the right to participate at job contest for obtaining the university degree of *Associate Professor* (called in French *Maître de Conferences* - MC).

Digital Signal Processors (PDSP). He was responsible for the *MEMD* and MEE courses. He was elected in the Council of the Electrical Engineering Department (EED), he participated at the students' selection for the EED, and he was coordinator for more than 30 students in their bachelor project.

At the TUCN, the author had teaching responsibilities and activities in a various courses and laboratories, like: *classical Electrical Machines* (EM), *Special Electrical Machines* (SEM), *Modeling of Electromechanical Systems* (MES), *Maintenance for Industrial Systems* (MIS), *Advanced Control in Electromechanical Systems* (ACES), *Testing and Diagnosis of Electrical Systems* (TDES). These teaching activities were carried out while having the quality of *Assistant Lecturer* (AL), between 2006, 2009-2011, and *Lecturer* (L), since 2011.

The summary of the teaching activities is presented in Table 1-3. Several devices were constructed for the aforementioned teaching activities, few of them being shown in FIGURE 1-9.

TABLE 1-3. TEACHING EXPERIENCE

UNIVERSITY	TEACHING POSITION	COURSE-C, SEMMINARY-S, LOBORATORY-L	PERIOD	STUDENTS' LEVEL
UTBM	ATER	FEM-CAD (L)	2005-2006	2nd year, Eng.
		Elec (L, S & C)		1st year, Eng.
	MC	MEMD (L, S & C)	2007-2009	3rd year, Eng.
		MEE (L & C)		3rd year, Eng.
		PDSP (L & S)		1st year, Eng.
TUCN	AL	EM (L)	2005-2006, 2009-2011	3rd year, Eng.
		SEM (L)		5thyear, Eng.
		MES (C & L)		4th year, Eng.
		MIS (L)		4th year, Eng.
		ACES (L)		4th year, Eng.
	L	EM (L)	Since 2011	3rd year, Eng.
		MES (C & L)		4th year, Eng.
		TDES (L)		1st year,Master

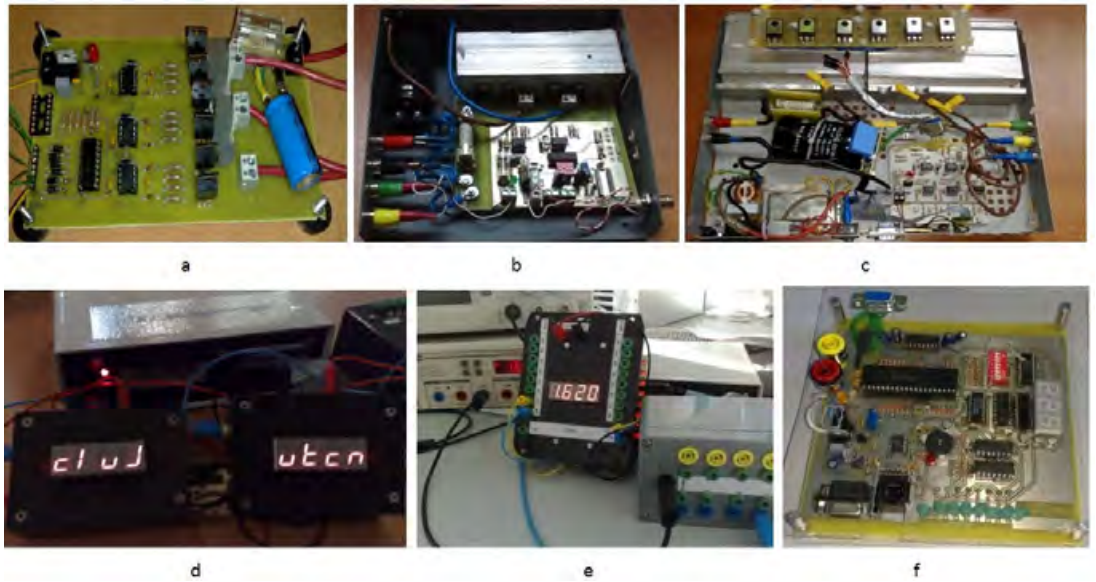

FIGURE 1-9. Sample of constructed equipment for employing the laboratory activities:
a): 1 kW inverter; b) 1 kW H-bridge; c) 6 kW inverter; d) advertising message; e) digital voltmeter based on TMS320LF2407A; f) development board based on dsPIC30F4011.

The author would like to mention that for the MIS and ACES topics he prepared new laboratory tutorials and test benches. For the SEM and MES topics he prepared partially the tutorials and test benches. As a result of the teaching activity, 3 books were written, in Romanian. Other 2 books, written in English, have resulted from the research activity: one book-chapter in international edition, and one book in national edition.

1.5 The main results and achievements of the research activity

In order to have an idea on the research activity evolution, all the published papers of the author will be detailed in this section. From the PhD period, one can distinguish the following scientific achievements: 1 research project as project manager, 5 articles presented in international conferences and 2 articles in international journals; all the other results belong to the "post-PhD period".

For the articles published in ISI type journals we will indicate the **I**mpact **F**actor (**IF**) announce by Thomson Reuters for the 2011 year, while the **R**elative **I**nfluence **S**core (**RIS**) was established by UEFISCDI, in January 2012.

1.5.1 Summary of results from the scientific research activity

The summary of the author's scientific published papers (after the PhD period) are shown in Table 1-4.

TABLE 1-4. SCIENTIFIC RESULTS AFTER PHD PERIOD: **PUBLISHED PAPERS, CITATIONS* AND PATENTS**

CATEGORY / *YEAR*	*BOOKS*	*JOURNAL ARTICLES*		*CONFERENCE ARTICLES*	*CITATIONS IN ISI JOURNALS*	*PATENT PROPOSITIONS*
		ISI[3]	IDB[4]			
2013	1	1	-	-	6	-
2012	-	4	-	4	10	1
2011	1	-	-	4	9	-
2010	1	1	-	4	5	-
2009	1	1	1	2	2	-
2008		2	-	7	-	-
2007	1	1	-	4	-	-
2006	-	-	1	4	-	-
TOTAL	**5**	**10**	**2**	**29**	**32**	**1**

* The citations were collected from, SCOPUS in June 2013.

The details on the published papers are presented in the next subchapter

A good quality research can be assured only with appropriate funds. Thus, the involvement of adequate organism is vital. The author was involved, as a member in several research contracts, with national or European funding. As project manager the author has assured the appropriate budget for the logistic and materials which are now detained by the CAREESD research center at TUCN. The amount spend on equipment surpasses 100 k€ (programmable dc power sources of 5kW and 45 kW, programmable ac/dc power load of 1.8kW, dSPACE DS1004, DS1103 and DS1006, torque/speed transducer, digital oscilloscopes, high frequency current transducers, digital multimeters, electronic power sources, electronic devices

[3] refers to the Thomson Reuters indexed journals.

[4] refers to International Data Bases

for static converter constructions, PCs etc.). More details on the bought equipment can be found on the projects' web-sites: www.wheel-ee.utcluj.ro and www.hitech-hev.utcluj.ro.

The author was or is involved in numerous research projects, funded by the Romanian Government or by European Union (FP7 projects), but here, only a summary of the research contracts for which he is project manager are presented, see Table 1-5, where the reader can identify the Young Research Team (TE) project type, as well as the Partnership and Cooperation (PCCA) project type.

TABLE 1-5. SCIENTIFIC RESULTS AFTER JULY 2005 MOMENT: **CONTRACTS AS PROJECT MANAGER**

PROJECT ACRONYM	***PROJECT TYPE AND NUMBER***	***FUNDING ORGANISM***	***PERIOD***	***BUDGET***
WHEEL-EE	TE-250/2010	Romanian Government	28 July2010 – 27 July 2013	Aprox.200'000€
Xantos Project	Industrial project	XANTOS company, from Switzerland	March-May 2011	15387€
Hyten Project	Industrial project	HYTEN company, from Switzerland	June-December 2011	6486€.
HiTECH-HEV	PCCA-191/2012	Romanian Government	2 July 2012 – 1 July 2015	Aprox. 660'000€ + 220'000€ private budget

1.5.2 Details on the result of the scientific research activity

Here are presented the details of all the published papers, obtained contracts and patent proposition of the author.

Books (5)

B1. D. Fodorean, F.Jurca, M.Ruba and D.C. Popa. *Motorization Variants for Light Electric Vehicles – design, magnetic, mechanical and thermal aspects*, AlmaMater 2013, ISBN 978-606-504-160-8.

B2. D.Fodorean: *Global Design and Optimization of a Permanent Magnet Synchronous Machine used for Light Electric Vehicle*, Intech 2011, (Croatia) – book chapter in monograph *Electric Vehicles – Modelling and Simulations*, edited by Serif Soylu, ISBN 978-953-307-477-1.

B3. D.Fodorean: *Initiation in programming the digital signal processors of TMS320LF2407(A) type* (original title in Romanian: *Iniţiere în programarea procesoarelor digitale de semnal din clasa TMS320LF2407(A)*), UT Press 2010, ISBN 978-973-662-533-6.

B4. L.Szabo and D.Fodorean: *Simulation of the converter-machine assembly used in electromechanical systems* (original title in Romanian: *Simularea ansamblului convertor-masina utilizat in sisteme electromecanice*), UT Press 2009, ISBN 978-973-662-480-3.

B5. I-A.Viorel, D.Fodorean, F.N.Jurca: *Special Electrical Machines - Applications* (original title in Romanian: *Masini Electrice Speciale – Aplicatii*), Mediamira 2007, ISBN 978-973-713-183-6.

Journals (14)

ISI journals - 10

J1. D. Fodorean, L. Idoumghar, and L. Szabo, "Motorization for electric scooter by using permanent magnet machines optimized based on hybrid metaheuristic algorithm", IEEE Transaction on Vehicular Technology, vol.62, n.1, pp.39-49, January 2013, ISSN 0018-9545. **(IF=1.921, RIS=2.167)**

J2. M. Ruba, D. Fodorean, "Analysis of Fault-Tolerant Multiphase Power Converter for a Nine-Phase Permanent Magnet", IEEE Transaction on Industry Applications, vol.48, nr.6, pp.2092-2101, November/December 2012, ISSN 0093-9994. **(IF=1.657, RIS=1.917)**

J3. D.Fodorean, L.Idoumghar, A.N'diaye, D.Bouquain and A.Miraoui: "Simulated Annealing Algorithm for the Optimisation of an Electrical Machine", IET Electric Power Applications, vol.6, n°9, pp.735-742, November, 2012, ISSN 1751-8660. **(IF=1.173, RIS=1.326)**

J4. A.R. Matyas, K.A. Biro, D. Fodorean, "Multi-Phase Synchronous Motor Solution for Steering Applications", Progress In Electromagnetics Research, vol.131, pp.63-80, Sept. 2012, ISSN 1559-8985. **(IF=5.298, RIS=1.761)**

J5. D. Fodorean, D.C. Popa, M. Ruba, "On the Fault-Tolerance of Permanent Magnet Synchronous Machines and Drives used in Hybrid Vehicle Application", International Review of Electrical Engineering, vol.7, n.2, pp.3795-3803, March-April 2012, ISSN 1827-6660. **(IF=0, RIS=0)**

J6. T.Raminosoa, B.Blunier, D.Fodorean and A.Miraoui, "Design and optimisation of a Switched Reluctance Motor driving a Compressor for a PEM Fuel Cell System for Automotive Applications", IEEE Transactions on Industrial Electronics, vol.57, n°9, pp.2988-2997, September 2010, ISSN 0278-0046. **(IF=5.16, RIS=1.872)**

J7. D.Fodorean, S.Giurgea, A.Djerdir, A.Miraoui: "Numerical Approach for Optimum Electromagnetic Parameters of Electrical Machines used in Vehicle Traction Applications", Energy Conversion and Management (Elsevier), vol.50, pp.1288-1294, Mai 2009, ISSN 0196-8904. **(IF=2.216, RIS=1.516)**

J8. S.Giurgea, D.Fodorean, G.Cirrincione, A.Miraoui, M. Cirrincione: "Multimodel Optimization Based on the Response Surface of the Reduced FEM Simulation Model With Application to a PMSM", IEEE Transactions on Magnetics, vol.44, n°9, pp.2153-2157, Septembre 2008, ISSN 0018-9464. **(IF=1.363, RIS=0.832)**

J9. D.Fodorean, I.A.Viorel, A.Djerdir, A.Miraoui: "Performances for a Synchronous Machine with Optimized Efficiency while Wide Speed Domain is Attempted", IET Electric Power Applications, vol.2, n°1, pp.64-70, January 2008, ISSN 1751-8660. **(IF=1.173, RIS=1.326)**

J10. D.Fodorean, A.Djerdir, I.A.Viorel, A.Miraoui: "A Double Excited Synchronous Machine for Direct Drive Application - Design and Prototype Tests", IEEE Transactions on Energy Conversion, vol.22, n.3, pp.656-665, September 2007, ISSN 0885-8969. **(IF=2.272, RIS=2.661)**

International journals - 2

Ji11. D.Fodorean, A. Miraoui, "Rapid design of permanent magnet synchronous machines (original title in French: Dimensionnement rapide des Machines Synchrones à Aimants Permanents (MSAP))", Technique de l'Ingénieur, Paris, France, 2009, Document D3554 – 24 pages, ISSN:1963-062X.

Ji12. D.Fodorean, I.A.Viorel, A.Djerdir, A.Miraoui: "On a Double-Excited Synchronous Motor with Wide Speed Range, Numerical and Experimental Results", Iranian Journal of Electrical and Computer Engineering IJECE, vol.5, n°1, 2006, pp.63-68, ISSN 1682-0053.

University Periodicals - 2

Ji13. M.Gutman, I.A.Viorel, D.Fodorean, C.Stet: "Different variants of permanent magnet synchronous motors with field weakening possibilities", University Oradea Annals, Electrotehnical Section, Oradea, Romania, 2005, pp. 150-154, ISSN 1223-2106.

Ji14. D.Fodorean, I.A.Viorel, A.Miraoui, A.Djerdir, M.Gutman: "On the performances of a synchronous motor with different rotor configurations", University Oradea Annals, Electrotehnical Section, Oradea, Romania, 2004, pp. 105-109, ISSN 1223-2106.

Conference Proceedings Articles (34)

International conference proceedings articles - 32

C1. D. Fodorean, L. Szabo, "Control of a permanent magnet synchronous motor for electric scooter application", International Symposium on Power Electronics, Electrical Drives, Automation and Motion - SPEEDAM 2012, Sorrento, Italy, June 20-22, 2012, pp.1178-1181, ISBN-978-1-4673-1300-1.

C2. M. Ruba, L. Szabo, D. Fodorean, "Design and analysis of low voltage high current SRM for small automotive applications", International Symposium on Power Electronics, Electrical Drives, Automation and Motion - SPEEDAM 2012, Sorrento, Italy, June 20-22, 2012, pp.341-346, ISBN-978-1-4673-1300-1.

C3. F. Jurca, D. Fodorean, "Axial Flux Interior Permanent Magnet Synchronous Motor for Small Electric Traction Vehicle", International Symposium on Power Electronics, Electrical Drives, Automation and Motion - SPEEDAM 2012, Sorrento, Italy, June 20-22, 2012, pp.365-368, ISBN-978-1-4673-1300-1.

C4. F. Jurca, C. Martis, D. Fodorean, "Analysis of a radial flux synchronous machine with outer rotor for integrated starter-alternator", International Symposium on Power Electronics, Electrical Drives, Automation and Motion - SPEEDAM 2012, Sorrento, Italy, June 20-22, 2012, pp.496-500, ISBN-978-1-4673-1300-1.

C5. D. Fodorean, D.C. Popa, F. Jurca, M. Ruba: "Optimizing the Design of Radial/Axial PMSM and SRM used for Powered Wheel-Chairs", Proceedings of the International Conference on Electrical, Computer, Electronics and Communication Engineering, Paris, France, 14-16 November 2011, pp.120-125.

C6. D. Fodorean, F. Jurca, C. Oprea, L. Szabo: "Permanent Magnet Synchronous Machines with Improved Energetic Performances and Reduced Torque Ripples used for Electric Vehicles", Proceedings of the 3rd International Conference on Clean Electrical Power (ICCEP'11), 14-16 June 2011, pp.289-292.

C7. F. Jurca, Claudia S. Martis, C. Oprea, D. Fodorean: "Claw-Pole Machine Design and Tests for Small Scale Direct Driven Applications", Proceedings of the 3rd International Conference on Clean Electrical Power (ICCEP'11), 14-16 June 2011, pp.237-242.

C8. C. Oprea, Claudia S. Martis, F. Jurca, D. Fodorean, L. Szabo: "Permanent Magnet Linear Generator for Renewable Energy Applications: Tubular vs. Four-Sided Structures", Proceedings of the 3rd International Conference on Clean Electrical Power (ICCEP'11), 14-16 June 2011, pp.588-592.

C9. D.Fodorean, M.Ruba, D.C.Popa and A.Miraoui: "Fault Tolerant Permanent Magnet Machines used in Automobile Applications", Proceedings of the 19th International Conference on Electrical Machines, 6-8 September 2010, pp.1-6, ISBN 978-1-4244-4175-4.

C10. D.Fodorean, A.N'diaye, D.Bouquain and A.Miraoui: "Characterization and control of a permanent magnet synchronous motor used in vehicle application", Proceedings of the IEEE International Conference on Automation Quality and Testing Robotics (AQTR), 28-30 May 2010, pp.1-6, ISBN 978-1-4244-6724-2.

C11. L.Idoumghar, D.Fodorean and A.Miraoui: "Using Hybrid Constricted Particles Swarm and Simulated Annealing Algorithm for Electric Motor Design", Proceedings of the 14th Biennial IEEE Conference on Electromagnetic Field Computation, Chicago, Illinois, USA, May 2010.

C12. L.Idoumghar, D.Fodorean and A.Miraoui: "Simulated Annealing Algorithm for Multi-Objective Optimization: Application to Electric Motor Design", Proceedings of the 29th IASTED International Conference: Modeling, Identification and Control'10 February 2010, pp.190-196.

C13. D.Fodorean, D. Bouquain, M.B. Camara and A.Miraoui, "Energy Management on board of a Reduced Scale Hybrid Automobile", Proceedings of the International Electrical Machines and Drives Conference, May 2009, pp.197-201, ISBN 9781424442515.

C14. D.Fodorean, L. Szabo and A.Miraoui: "Generator Solutions For Stand Alone Pico-Electric Power Plants", Proceedings of the International Electrical Machines and Drives Conference, May 2009, pp.434-438, ISBN 9781424442515.
C15. D.Fodorean, A.Miraoui: "Permanent Magnets Thermal Operation Limits in a Hybrid Excited Synchronous Machine used on Wide Speed Applications", Proceedings of the 11th IEEE International Conference on Optimization of Electrical and Electronic Equipment – OPTIM'08, Brasov, Romania, 22-24 May 2008, pp.21-26, ISBN 978-973-131-028-2.
C16. L.Szabo, M.Ruba, D.Fodorean: "Study on a Simplified Converter Topology for Fault Tolerant Motor Drives", Proceedings of the 11th IEEE International Conference on Optimization of Electrical and Electronic Equipment – OPTIM'08, Brasov, Romania, 22-24 May 2008, pp.197-202, ISBN 978-973-131-028-2.
C17. D.Fodorean, M.Ruba, L.Szabo, A.Miraoui: "Comparison of the Main Types of Fault-Tolerant Electrical Drives used in Automobile Applications", Proceedings of the IEEE International Symposium on Power Electronics, Electrical Drives, Automation and Motion – SPEEDAM'08, Ischia, Italy, 11-13 June 2008, pp.895-900, ISBN 978-1-4244-1664-6.
C18. M.B.Camara, D.Fodorean, H.Gualous, D; Bouquain, A.Miraoui: "Hybrid Sources Control for Electric Drives Traction Applications", Proceedings of the IEEE International Symposium on Power Electronics, Electrical Drives, Automation and Motion – SPEEDAM'08, Ischia, Italy, 11-13 June 2008, pp.744-749, ISBN 978-1-4244-1664-6.
C19. M.Ruba, L.Szabo, D.Fodorean: "On the Fault Tolerant Switched Reluctance Machines", MICROCAD'08, Miskolz, Hungary, 2008, pp.73-78, ISBN 978-963-661-812-6.
C20. L.Szabo, M.Ruba, D.Fodorean: "Simple converter structure for fault tolerant motors", Proceedings of the IEEE International Conference on Automation Quality and Testing Robotics – AQTR'08, Cluj-Napoca, Romania, 22-25 May 2008, pp.244-249, ISBN:978-1-4244-2576-1.
C21. T.Raminosoa, B.Blunier, D.Fodorean, A. Miraoui: "Design and Comparison of High Speed Switched and Synchronous Reluctance Machines to Drive the Compressor of an Automotive PEM Fuel Cell", Proceedings of the IEEE International Conference on Electrical Machines – ICEM'08, Vilamoura, Portugal, 6-9 September 2008, paper ID 792, ISBN: 978-1-4244-1736-0.
C22. D.Fodorean, A.Djerdir, A.Miraoui, I.A.Viorel: "FOC and DTC Techniques for Controlling a Double Excited Synchronous Machine", Proceedings of the IEEE International Electric Machines and Drives Conference – IEMDC'07, Antalya, Turkye, 3-5 May 2007, pp.1258-1263, ISBN:1-4244-0743-5.
C23. D.Fodorean, S. Giurgea, I.A.Viorel, A.Djerdir, A.Miraoui: "Adequate Parameters Determination for Three Types of Electric Machines with Enlarged Speed Domain via an Optimization Procedure and Magnetic Field Calculation", Proceedings of the 16th Conference on the Computation of the Electromagnetic Fields - COMPUMAG'07, Aachen, Germany, 24-28 July 2007, pp.371-372.
C24. S.Giurgea, D.Fodorean, G.Cirrincione, A.Miraoui, M.Cirrincione: "Multi Model Optimization Strategies Applied to a PMSM", Proceedings of the 16th Conference on the Computation of the Electromagnetic Fields - COMPUMAG'07, Aachen, Germany, 24-28 July 2007, pp.1129-1130.
C25. D.Fodorean, I.A.Viorel, A.Djerdir, A.Miraoui: "Mechanical and Thermal Designing Aspects for a PM Synchronous Machine with Wound Rotor", International Aegean Conference on Electric Machines, Power Electronics and Electromotion Joint Conference - ACEMP-Electromotion'07, Bodrun, Turkey, 10-12 Sept. 2007, pp.502-506, ISBN 978-975-93410-2-2.
C26. D.Fodorean, I.A.Viorel, A.Djerdir, A.Miraoui: "Improved Efficiency for an In-Wheel Motor in Large Speed Operating", Proceedings of the 12th IEEE Conference on Electromagnetic Field Computation - CEFC 2006, Miami, Florida-USA, 29-03 May, 2006, Digest-Book, pp.313, ISBN 1-4244-0319-7.

C27. I.A.Viorel, D.Fodorean, A.Viorel, L.Szabó: "Stand-Alone Double Excited Synchronous Generator Operating on a Variable Load", Proceedings of the International Conference on Power Electronics, Intelligent Motion and Power Quality (PCIM '2006), Nürnberg (Germany), 30 May-1 June, 2006, pp. 675-680. ISBN 3-928613-43-6.

C28. D.Fodorean, I.A.Viorel, A.Djerdir, A.Miraoui: "Wide Speed Control of a Hybrid Excited Synchronous Machine", Proceedings of the 17th International Conference on Electrical Machines - ICEM '06, Chania, Crete Island, Greece, 2-5 Sep. 2006, pp. 290, on CD.

C29. I.A.Viorel, R.Munteanu, D.Fodorean, L.Szabo: "On the possibility to use a Hybrid Synchronous Machine as an Integrated Starter-Generator", Proceedings of the 5th IEEE International Conference on Industrial Technology - ICIT '06, Mumbai, India, 15-17 Dec. 2006, pp. 1195-1200, ISBN 1-4244-0726-5.

C30. M. Gutman, I.A. Viorel, D.Fodorean: "Extended speed range drive system with synchronous motors", Proceedings of the 5th International Conference on Electromechanical and Power System (SIELMEN '2005), Chişinău (Moldova), 2005, vol.2, pp.815-818, ISBN 973-716-230-7.

C31. D.Fodorean, I.A.Viorel, A.Miraoui, M.Gutman: "Comparison of Hybrid Excited Synchronous Motors for Electrical Vehicle Propulsion", Proceedings of Aegean Conferences on Electrical Machines and Power Electronics - ACEMP '04, Istambul, Turkey, 26-28 May, 2004, pp. 52-57, ISBN 975-93410-1-8.

C32. D.Fodorean, A.Djerdir, A.Miraoui, I.A.Viorel: "Flux Weakening Performances for a Double-Excited Machine", Proceedings of the 16th International Conference on Electrical Machines - ICEM '04, Krakow-Poland, 5-8 Sep. 2004, paper number 434, on CD, ISBN 12-345678-90.

Other international conferences - 2

Co33. A.Miraoui, D.Fodorean, I.A.Viorel: "Hybrid Synchronous Motor with Flux Weakening Winding", Proceedings of the Workshop on Variable Reluctance Electrical Machines, Cluj (Romania), 2003, pp. 10-15, ISBN 973-8335-98-1.

Co34. A.Miraoui, I.A.Viorel, D.Fodorean: "Synchronous Direct Drive System with Extended Speed Domain", Workshop on Electrical Drives and Control System in Industry, 25-26 July, 2002, Cluj-Napoca (Romania), pp. 15-21.

Research projects (5)

International research projects - 2

Gi1. Project name: *Design of two types of special electrical machine*. Project type: industry project between Technical University of Cluj-Napoca and XANTOS (Switzerland). Project manager: Daniel FODOREAN. Project duration: 1 March – 31 May 2011. Budget: 15 387 €.

Gi2. Project name: *Assistance for the manufacturing and the testing phases of special electrical machines*. Project type: industry project between Technical University of Cluj-Napoca and HYTEN (Switzerland). Project manager: Daniel FODOREAN. Project duration: 1 July – 31 December 2011. Budget: 6 486 €.

National research projects - 3

Gn3. Project name: *Hardware-in-the-Loop Modular Platform for Testing the Energy Management of Competitive & Highly-Efficient Hybrid-Electric Vehicles*. PCCA grant, code 191/2012. Project manager: Daniel FODOREAN. Approved state budget for July 2012 – June 2015: 2 809 700lei (aprox.660 000 €) – the project has a supplementary private budget coming from two industrial companies, in total amount of 949 200 lei (aprox.220 000 €).

Gn4. Project name: *Intelligent Hybrid Vehicle for Individual Transportation of People with Reduced Mobility* (original title in Romanian: *Vehicul Hibrid Inteligent pentru Transportul*

Individual al Persoanelor cu Mobilitate Redusă). PN II-CNCSIS grant, code TE-250, project number 32/28.07.2010. Project manager: Daniel FODOREAN. Approved budget for 28 July 2010 – 27 July 2013: 813 700lei (aprox.200 000 €).

Gn5. *Design and control for a double excited synchronous machine* (original title in Romanian: Proiectarea si controlul unei masini sincrone dublu excitate). Funder: National Agency for Science, Technology and Innovation (ANSTI); Grant type TD-39, grand number nr: 33532/2002-2005. Project manager: D. Fodorean. Budget 9 900 lei (aprox.2 500 €).

Patent proposition

P1 M. Ruba and D. Fodorean, "Mașină cu reluctanță comutată cu autoventilație internă la rotor", nr. A00884/2012.

1.6 Other results and achievements

Some of other important achievements of the author are presented here briefly:

- Elected member in the council of the Electrical Engineering Department from UTBM (2008-2009).
- Member in the UTBM council responsible for the evaluation of the *ATER*s candidates for all departments from the UTBM (2009).
- Member in the jury of bachelor at TUCN (2006, 2010) and UTBM (2007-2009) and member in the *Students Scientific Communication Session* at TUCN (2010).
- Scientific secretary for the *International Journal of Electrical Engineering in Transportation* (www.ijeet.org) between 2007-2010.
- IEEE member, since 2007.
- Reviewer for several international conferences, and for ISI journals: *IEEE Transactions on Industrial Electronics* (since 2008) and *IEEE Transaction of Vehicular Technology* (since 2009).
- Postdoctoral research, between June 2010 and April 2013 within the 4D-POSTDOC project employed at the TUCN with the subject: "*Optimal Energy Management for Light Hybrid-Electric Vehicles*".
- Research stages and scholarships: scholarship at UTBM in the PhD period (2002-2005), research stages at Université de Haute-Alsace (Mulhouse, France) in January 2011 and August 2012.
- Participation at training courses: „*Sensorless Control of Permanent Magnet Synchronous Machines*" course organized by Aalborg University from Denmark and „FPGA-Basics" and „FPGA-EDrive" courses organized by dSPACE GmbH company from Germany.
- Invited professor at the Université de Haute-Alsace in Mai 2013.

2 MOTORIZATION OF LIGHT ELECTRIC VEHICLES

2.1 Framework and summary of main results

In this chapter are presented the main results with regard to the studied variants for the motorization of light EVs. A quality research activity can be carried out only with appropriate founds. Thus, here will be recalled the projects which assured the budget for this research topic.

- Project name: *Intelligent Hybrid Vehicle for Individual Transportation of People with Reduced Mobility* (original title in Romanian: *Vehicul Hibrid Inteligent pentru Transportul Individual al Persoanelor cu Mobilitate Redusă*). Grant, code TE-250, project number 32/28.07.2010. Project manager: Daniel FODOREAN. Acronym**: WHEEL-EE**.
- (Postdoctoral research). Project theme proposed by Daniel FODOREAN: "*Optimal Energy Management for Light Hybrid-Electric Vehicles*" within the frame of the 4D-POSTDOC[5] program funded my European Community. Program Manager: Aurel VLAICU. Period: June 2010 - April 2013. Research subject acronym: **MOEVEHU**.
- *Design and control for a double excited synchronous machine* (original title in Romanian: *Proiectarea si controlul unei masini sincrone dublu excitate*). Funder: National Agency for Science, Technology and Innovation (ANSTI); Grant type TD-39, grant number: 33532/2002-2005. Project manager: D. Fodorean. Acronym**: DCDESM**.

The research results on this topic have been presented in several journals, proceedings of international conferences, books and book chapters. Here, only 3 articles are indicated, which contain the main achievements of the author's research related to the light EV's motorization:

- D. Fodorean, L. Idoumghar, and L. Szabo, "Motorization for electric scooter by using permanent magnet machines optimized based on hybrid metaheuristic algorithm", IEEE Transaction on Vehicular Technology, vol.62, n.1, pp.39-49, January 2013.
- D. Fodorean, D.C. Popa, F. Jurca, M. Ruba: "Optimizing the Design of Radial/Axial PMSM and SRM used for Powered Wheel-Chairs", Proceedings of the International Conference on Electrical, Computer, Electronics and Communication Engineering, Paris, France, 14-16 November 2011, pp.120-125.
- D.Fodorean, I.A.Viorel, A.Djerdir, A.Miraoui: "On a Double-Excited Synchronous Motor with Wide Speed Range, Numerical and Experimental Results", Iranian Journal of Electrical and Computer Engineering IJECE, vol.5, n°1, Winter-Spring 2006, pp.63-68.

In the category of light electric vehicles we can consider bicycles, carts, *all-terrain vehicles* (ATVs), small vehicles for golf tournament, scooters and all other vehicles used for indoor cargo handling or cleaning (found in the market places, railways stations and airports). Practically, for indoor and other applications which do not request very high autonomy, the all-electric motorization is used. The classical motorization variants are based on dc machine, and usually with mechanical transmission. The new motorization variants are rather mounted in the wheel; such a variant is called *in-wheel motor*. In FIGURE 2-1 are presented two in-wheel motors for electric bicycle and scooter. For such a variant, the rotor is placed outside the stator, and usually the excitation is assured with permanent magnet (PM). The most common topology for such an in-wheel motor is the permanent magnet synchronous machine (PMSM).

[5] This is the acronym for the postdoctoral research program entitled: "Development and support of multidisciplinary postdoctoral programmes in major technical areas of national strategy of Research - Development - Innovation" 4D-POSTDOC, contract no. POSDRU/89/1.5/S/52603, project co-funded by the European Social Fund through Sectoral Operational Programme Human Resources Development 2007-2013"

in-wheel motor for bicycle

in-wheel motor for scooter

FIGURE 2-1. Photographs of in-wheel motors used for electric bicycle and scooter.

The study of the electric scooter was one of the favorite topics of the author. Another similar topic has concerned the electric scooter dedicated for persons with reduced mobility (ES-PRM) [19]-[28]. A photograph with the technology for such devices is presented in FIGURE 2-2 and FIGURE 2-3.

FIGURE 2-2. Photography of the studied ES-PRM.

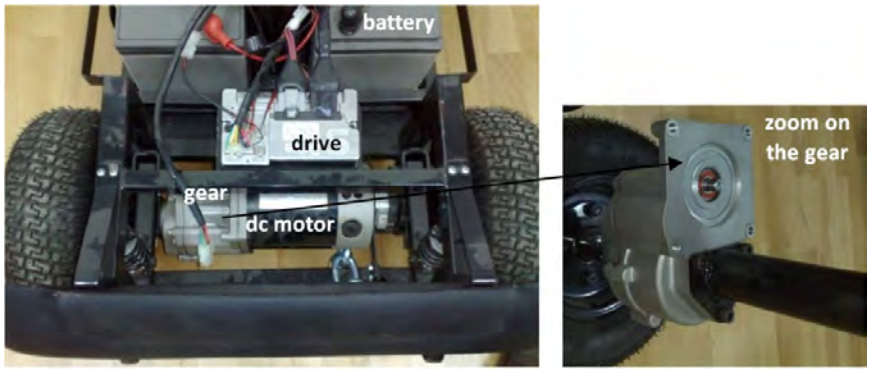

FIGURE 2-3. Photography on the electrical traction system of the ES-PRM.

Common electric scooter has two wheels and the motorization is rather based on only one in-wheel motor. For ES-PRM, the motorization is usually employed with one motor and a gear, because the use of two motors will significantly increase the vehicle's cost.

It is widely recognized that the common solution, the *dc* motor, has usually poor performances against *ac* motors. However, for small power electrical machines, this advantage is not always obvious, especially when the excitation is realized with PM. For ac machines, a

special attention should be paid to the efficiency and power factor (their calculation is given in the next chapters of the thesis) because these energetic performances will influence scooter's autonomy.

The ES-PRM was studied in the **WHEEL-EE** project. The research goal in this project was to propose a new technology for the traction chain and power supply of ES-PRM, keeping the investment within the market limits. For that, an ES-PRM was bought from the market (the one presented in FIGURE 2-2). The idea of the research is to replace the motorization, the battery and to employ an efficient and intelligent energy management, the goal being to increase the vehicle's autonomy. But firstly, it is needed to establish the application mechanical demands.

The mechanical design of an electric vehicles or scooter has been depicted in detail in [3], [9], [30]. Here, the main design parameters will be given, which are dependent on the scooter given data and expected performances.

For the ES-PRM bought from the market, the maximum speed and weight of the vehicle are 12 km/h and 220 kg, respectively. The tire for the wheel is 13 inches in diameter. The vehicle's dimensions are: 130 cm in length, 70 cm in width and 115 cm in height. The vehicle will be fed from a battery of 24 Vdc. More details about the scooter's data are given in Table 2-1.

TABLE 2-1. MAIN DATA OF THE STUDIED ELECTRIC SCOOTER IN THE WHEEL-EE PROJECT

PARAMETER	*VALUE*	*UNIT*
Maximum Speed	12	km/h
Autonomy	80	km
Maximum Load	220	kg
Scooter's Length	130	cm
Scooter's Width	70	cm
Scooter's Height	115	cm
Scooter's Weight	115	kg
Climbing Degree	6	%
Wheel Diameter	13	inch
Battery Capacity	75	Ah

First, it is needed to calculate the output power of the electric motor [1]. Since the mechanical power is the product between the torque and angular speed, firstly we should establish the speed of the vehicle at the wheel (tire):

$$n_t = \frac{v \cdot 60}{\pi \cdot D_t} \tag{2.1}$$

where n_t is the velocity measured at the vehicle's tire (in r/min), v is the vehicle speed, D_t is the outer diameter of the wheel (the tire height included).

Next, the rated torque has to be established. Since the torque is proportional to the wheel radius and the force acting on it, we should establish the force involved by the vehicle's weight and rolling conditions. The electric motor has to be capable to produce a mechanical force to balance all other forces which interfere in vehicle's rolling. Thus, the motor force is:

$$F_m = F_{acc} + F_h + F_d + F_w + F_r \tag{2.2}$$

where F_{acc} is the acceleration force, F_h is the climbing force, F_d is the aerodynamic drag force, F_w is a resistive force due to the wind, and F_r is the rolling force. Even if for this EV the acceleration is not an important criterion, it is however possible the estimate the resistant force due to acceleration based on the following expression [9]:

$$F_{acc} = C_{acc} \cdot M_{tot} \cdot acc \cdot g \tag{2.3}$$

where C_{acc} is the acceleration constant, M_{tot}, is the total mass of the vehicle, acc is the acceleration of the vehicle and g is the gravitational constant.

When the vehicle goes hill climbing (with an angle of incline, θ), the climbing force is:

$$F_h = M_{tot} \cdot g \cdot \sin(\theta) \tag{2.4}$$

Usually, the degree of incline is given in percentage. For this special electric scooter we have considered a maximum of 6% degree of incline. 1% degree of incline represents: 1 meter of rise on a distance of 100 meters. Thus, 1%=atan(0.01)=0°34' (zero degrees and 34 minutes). For an incline of 6% the angle is 3.43 degrees (or 3°25').

The drag force takes into account the aerodynamics of the vehicle. This force is proportional with the square of the speed, the frontal area of the vehicle and the aerodynamic coefficient, C_d, (empirically determined, for each category of vehicle) [9]:

$$F_d = A_{fr} \cdot v^2 \cdot g \cdot C_d \quad (2.5)$$

The resistant force due to wind, cannot be precisely computed. It depends on various conditions like, for common automobiles, the fact that windows are entirely or partially open. Also, the wind will never blow at constant speed. However, an expression, empirically obtained, which will take into account the speed of wind, v_w, can be written as [9]:

$$F_w = \left(\left(0.98 \cdot \left(\frac{v_w}{v}\right)^2 + 0.63 \cdot \frac{v_w}{v}\right) \cdot C_{rw} - 0.4 \cdot \frac{v_w}{v}\right) \cdot F_d \quad (2.6)$$

where C_{rw} is the wind relative coefficient, depending on the vehicle's aerodynamics.

The resistant force due to rolling depends on the hardness of the road's surface, C_r, being proportional with the weight of the vehicle and the angle of incline, [9]:

$$F_r = C_r \cdot M_{tot} \cdot g \cdot \cos(\theta) \quad (2.7)$$

A more precise computation of the rolling resistant force could take into account the shape and the width of the tires, but these elements are not critical at low speeds.

After the computation of the resistant forces, the needed wheel torque can be determined and finally the rated torque of the electrical machine, see Table 2.

TABLE 2-2. THE FORCES AND THE LOAD TORQUE OF THE STUDIED ES-PRM

PARAMETER	*VALUE*	*UNIT*
Resistance force due to acceleration	190.57	N
Resistance force due to hill climbing	129.21	N
Aerodynamic Drag Force	0.088	N
Resistance force due to wind	1.25	N
Rolling Force	21.57	N
The total resistance force	342.7	N
Load Torque	3.13	N·m
Speed at the wheel	3.21	m/s

For this value of the torque and speed at the wheel, with the gear ratio of 1:19, and by estimating the efficiency of the gear at 95%, it is possible to propose the electrical machine which responds to the ES-PRM demands: 1200 W, 3400 r/min, 3.37 N·m. Four electrical machines have been proposed for the ES-PRM. They will be presented in the next subchapter. A similar approach has been employed for the MOEVEHU project, where an electric scooter has been under study and for which several outer-rotor (in-wheel) topologies have been evaluated.

2.2 Radial, axial and transverse flux topologies

This chapter presents a short summary on the motorization variants found on the literature for the light electric vehicles (L-EV) [31]-[43]. The common motorization solution for L-EV is the dc machine, due to its simple control. But, its weak points, reduced efficiency and power density, associated to the need for high autonomy (which is affected by these parameters) led to a shift towards cars powered by ac drives. Also, in the category of AC machines used for L-EV, the permanent magnet synchronous machine (with radial or axial flux, with inner or outer rotor) is exclusively used, while the induction machine is dedicated for

industrial applications with reduced dynamics (due to the relatively reduced efficiency and power density, and increased heat on the rotor armature). Another machine which do not uses the magnets and can be considered for high temperature applications is the switched reluctance machine, lately used for washing machines. The latest machine under study here will be the transverse flux machine, which, normally, has the best torque/mass ratio.

Based on the scientific literature, the author has realized a brief comparison (see Table 2-3) on the existing electrical machines (EM) based on several criteria: the power density (power/weight ratio), the torque/current ratio, the machines' capability to operate beyond the base speed in the flux weakening region, the torque ripples, the temperature level (for example, the temperature affects directly the rear earth PMs, and an important risk of irreversible demagnetization arises), the robustness of the machine seen as a system, the noise level, the efficiency and power factor, the construction simplicity and the cost of the machine and of the static converter.

TABLE 2-3. BRIEF COMPARISON OF THE EM'S PERFORMANCES

CRITERION	*DC*	*IM*	*BLDC*	*BLAC*	*SRM*	*VRSM*	*TFM*
power density	-	-	+	+	-	-	+
torque/current ratio	-	-	+	+	-	-	-
speed variation capability	+	-	-	-	+	+	-
torque ripples	+	+	-	+	-	-	+
temperature	-	-	-	-	+	+	-
robustness	-	+	-	-	+	-	-
noise	-	+	+	+	-	-	+
efficiency	-	-	+	+	-	-	+
power factor		-	+	+	-	+	-
construction simplicity	-	+	-	-	+	-	-
motor cost	+	+	-	-	+	+	-
converter cost	+	+	+	+	-	+	+
TOTAL of "+"	**4/11**	**6/12**	**6/12**	**7/12**	**5/12**	**5/12**	**5/12**

Acronyms: DC-direct current machine; IM-induction machine; BLDC-brushless direct current machine; BLAC-brushless alternative current machine; SRM-switched reluctance machine; VRSM-variable reluctance synchronous machine; TFM-transverse flux machine.

In Table 2-3 the "-" denotes a weak point or disadvantage, and the "+" denotes an advantage or strong point. At the end of the table is presented a summary of results based on the applied criteria.

Based on the above table it can be said that, function of the application, the designer could choose the most suited variant, since all the machines have sensitive equal performances. For high power and reduced speed applications the use of permanent magnet machine will not be a smart choice, because of the high cost of the PMs. On the other hand, from micro-motors, the DC variant, which offers control simplicity, will be the preferred choice.

To justify a choice for our applications (electric scooter and ES-PRM), we are presenting the following comments:

- The DC is still used in trolleybuses and in the light EVs despite of its weak efficiency and reduced power density (even for PMs excited variants). Having in mind an increased autonomy, we have considered studying another machine.
- The IM is rather consecrated for industrial applications. Even if lately it has been tested for traction application, the starting torque and controllability issues (due to sliding) have lead us to study another type of machine.

- The BLDC and BLAC do not differ from the machine's point of view, but from current profile injected into the winding. The studied machine will be the permanent magnet synchronous machine (PMSM), fed with sinusoidal currents, which offers a smoother torque (in BLDC the torque ripples are quite important, since the injected current is of rectangular shape) [32]-[37].
- The switched reluctance machine, the cheapest from the construction point of view, was considered to be evaluated in this ES-PRM application. A high number of phases could reduce the torque ripples, which is very important for such machine [32], [38]-[40].
- The variable synchronous reluctance machine is usually used for high speed variation applications because of the possibility to have very high direct-quadrature inductances ratio. The rotor is built with axially laminated sheets. This employs some construction difficulties and we have decided not to consider for our ES-PRM.
- The transverse flux machine, the newest topology among the other machines, being proposed in the late of the 1990s. This machine was considered here due to the very promising power density capability [41]-[43].

2.2.1 The permanent magnet synchronous machine with radial flux

The first machine presented here is the radial flux permanent magnet synchronous machine (RF-PMSM) [1]. A photograph of the studied and constructed PMSM-RF is shown in FIGURE 2-4 . In order to have the best power density, the permanent magnets (PMs) are placed on the rotor surface.

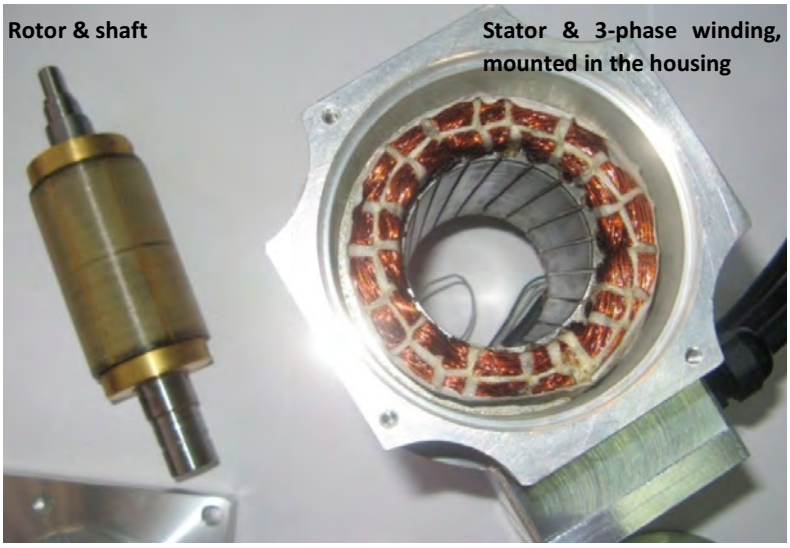

FIGURE 2-4. Photography of the studied RF-PMSM: stator core, rotor with PMs and passive parts [1]

Since the application is not running at very high speed, a simple bandage on the magnets is sufficient to strength them on the rotor surface. The PMs are glued on the rotor core with a Loctite resin. The number of pair of poles is three (thus, there are 6 magnetic poles). On the stator armature, a three phase winding of polar pitch type is disposed in 18 slots, meaning that the number of slots per pole and per phase is 1. This implies that the winding factor is also equal to unity. The material for the permanent magnet is Neodymium-Iron-Boron (Nd-Fe-B), type N38SH. For the steel, the M530 material type was used. The sheets were cut at 0.35 mm, to form the stator stack. Another reason to have thin sheets is to reduce the iron loss from the stator core. The layout of the three phase winding is shown in FIGURE 2-5.

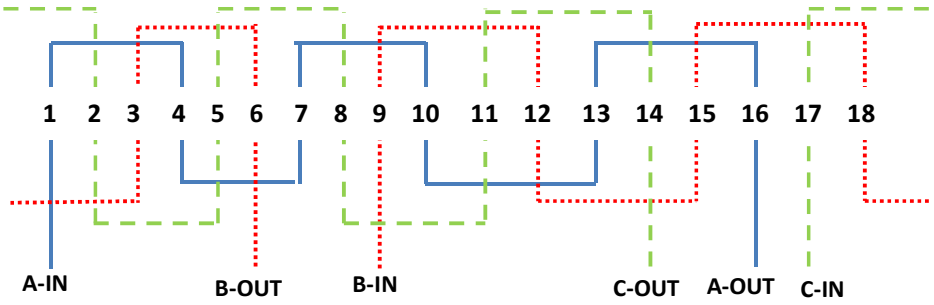

FIGURE 2-5. Drawing on the three-phase winding of the RF-PMSM. [1]

2.2.2 The axial flux permanent magnet synchronous machine

The second machine under study here is the axial flux permanent magnet synchronous machine (AF-PMSM) [1]. Usually, the axial flux topologies present the best power density, being more compact than the radial type machines. The motorization of the ES-PRM imposes volume limitations, the machine's housing being very close to the scooter's chassis – see FIGURE 2-3.

Usually, an axial flux machine has a high diameter, in comparison with its length. This is due not only for compactness, but also for winding manufacturing reasons (if the diameter is too small, the slots will be very thin and the turns could not be inserted into the slots). To overcome this problem, we have studied a double-sided stator armature has to be considered. Between this double-sided armature the rotor is placed, having only the PMs – there is no yoke in this configuration, only passive parts to fix the PMs at the rotor. A photograph of the studied/constructed AF-PMSM is presented in FIGURE 2-6.

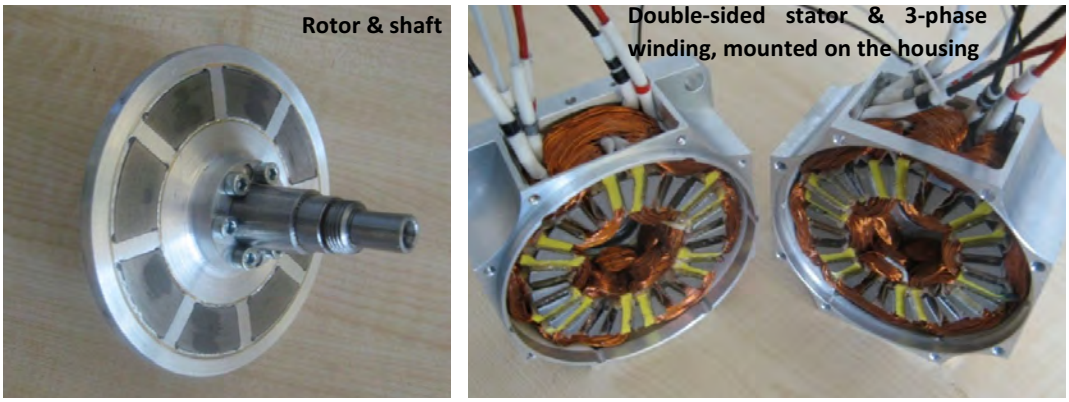

FIGURE 2-6. Photography of the studied AF-PMSM: double stator, rotor with PMs and passive parts. [1]

The stator core can be made also of massive iron, in which case Somaloy material should be used (for such material, the magnetic flux can flow in two directions). But usually the stator is made of sheets, to reduce the iron loss and to avoid overheating. There are multiple configurations of AF-PMSM [36]. If the length of the application will permit, other stator and rotor modules can be added.

For the AF-PMSM studied here, a double-sided stator configuration was considered, with the rotor placed between the armatures. If more than 2 stators are use, another rotor should be mounted on the shaft. The limitation of the number of rotor modules is imposed to limit the increase of the machine's inertia, which will have a direct influence on the control's dynamics.

The winding of the AF-PMSM machine is similar to the one of the RF-PMSM.

2.2.3 The switched reluctance machine

The simplest solution for the traction of light EV - and less expensive – is the switched reluctance machine (SRM), having a passive rotor and stator poles surrounded by coils [1]. That is all for the active part of this type of machine and this is the reason of SRM's simplicity and reduced cost.

The SRM works like a dc machine, even if it is a multiphase type machine. At each displacement of the rotor, the electric power feds only one phase. Thus, each fed phase should assure the desired electromagnetic torque. This is the reason for having a high instantaneous current in the phases of the SRM. This high current per phase involves local heating of the machine. It means that the cross section of one turn of the conductor should be quite big

The studied and constructed SRM is presented in FIGURE 2-7. It is an 8/6 variant, with 4 phases formed by two series connected coils. The stator and rotor core is made of steel sheets of M530 material. The reason of making the rotor of sheets (not massive iron) is to reduce the iron losses within the rotor, as well as the heat, because of the high switching frequency currents injected.

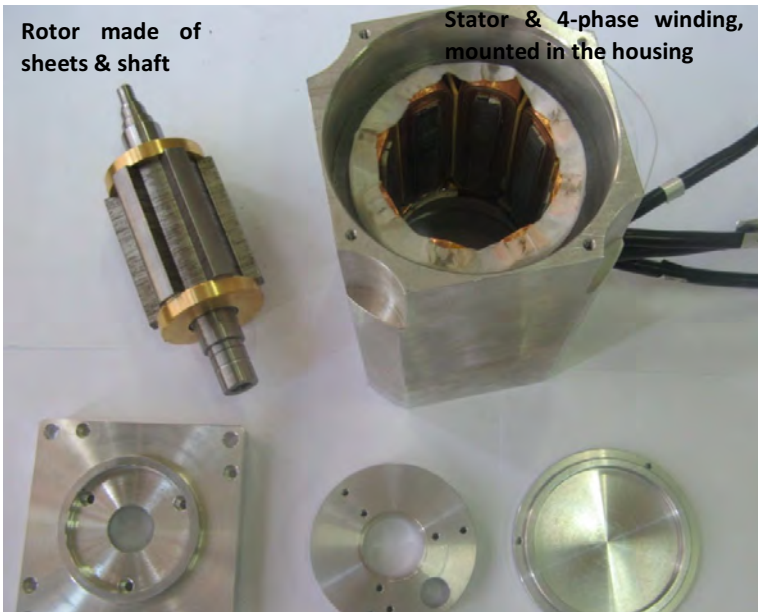

FIGURE 2-7. Photograph of the studied SRM, 8/6: stator, rotor and passive parts. [1]

2.2.4 The transverse flux permanent magnet machine

The transverse flux machine (TFPMM) is the newest electrical machine, being derived from claw pole machines [1]. Its construction is complex, though expensive. The difference between the claw pole and the transverse flux machine is on the stator winding, which this time is of homopolar type. The rotor is usually excited through permanent magnets (PMs), or can be of passive type, when the machine works on the minimum reluctance alignment principle.

In order to have a rotating (or linear) movement, the stator poles or rotor poles should be shifted with a specific angle. It could be mentioned that the stator poles, belonging to a winding, are not magnetically linked; thus, in the case of short-circuit in one phase, the other phases will not be affected. There is a specific ratio between the stator poles and the rotor magnetic poles. The usually shape of the stator poles is of "U" type. Several rotor configurations are available: with passive rotor, with PMs placed on the rotor surface or with flux concentration configuration.

Special material is needed for the construction of the stator poles of the transverse flux machine, since the magnetic flux can flow in X-Y or Y-Z direction. The so called Soft Magnetic Composite material, or Somaloy, is used. It has quite good magnetic properties, but saturates faster. The Somaloy capability to have a multidirectional flux flow makes it practically the exclusive material type used for such type of machines.

A drawing of the TFPMM is shown in FIGURE 2-8. Here a three phase TFPMM is presented. This topology has inclined "U" type poles and the rotor poles are placed to realize the so called flux concentration. The rotor poles belonging to the first phase are shifted against the rotor poles of the second winding, and consequently to the third winding with a specific angle. A high number of poles is needed to reduce as much as possible the outer diameter of the machine, but this involves an increased frequency, and finally a decrease of the machines efficiency. Also, due to the homopolar winding type the power factor is quite reduced. Thus, such a machine could be interested for low-speed high-power applications.

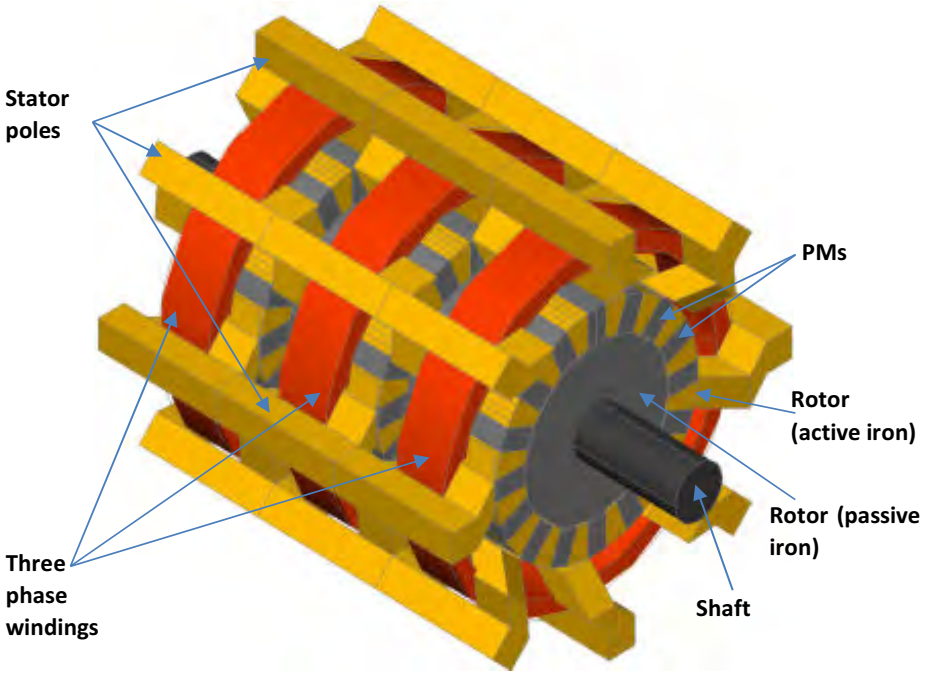

FIGURE 2-8. Draw of the studied transverse flux permanent magnet machine. [1]

The RF-PMSM, AF-PMSM and SRM and TFPMM have been designed (see the approach in chapter 3, where the performances were also presented - only for the constructed machines). Next, the machines were optimized based on simple or complex optimization algorithms (chapter 4), they were analyzed numerically based on finite element method (see subchapter3.5) and from thermal point of view (chapter 5), and their energetic performances and controllability was evaluated (chapter 6).

Unfortunately, the TFPMM could not respond to applications demands (while trying to increase the number of pole, to reduce the diameter of the machine, we have reached the acceptable frequency supplying level); thus, we have decided not to construct the TFPMM. After the construction of the motors and their test the conclusion of the study was that all the machine respond to the application requirements, stated in Table 2-1, and that only the cheapest motor, the SRM, was heavier than the DC motor install on the bought ES-PRSM. The AF-PMSM has 4.6kg, the RF-PMSM has 6.2kg, the DC motor is of 6.5kg and the SRM is 8.1kg.

In order to conclude the subject of the ES-PRM motorization, the author would like to present here the test bench on which the machines are or have been tested, see FIGURE 2-9.

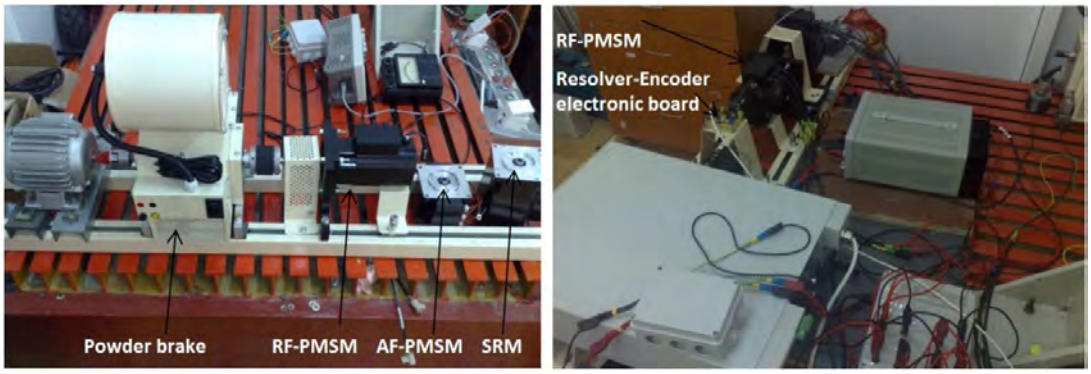

FIGURE 2-9. Test benches for the motorization of the ES-PRM (top: the three constructed prototypes; bottom: the RF-PMSM with electronic board for Resolver-Encoder converter).

2.3 Double-excited motorization variants

The *double-excitation* (or *hybrid excitation*) refers to the fact that in the excitation circuit, in addition to the PM as the main component of the flux source, there is also an auxiliary winding who's MMF can control the air gap field, and consequently, the speed. Up to the base speed, the auxiliary excitation MMF can, if required, to strengthen the PM field.

Double-excited synchronous machine (DESM) can have either *series* [44], or *parallel* [45]-[50] excitation circuits. Another classification criterion refers to the auxiliary winding location: it can be placed on rotor [44], [45], or on the armature [46]-[50]. If the auxiliary winding is placed on the stator core, the flux density can be controlled locally at the air-gap level. In this case, however, the source is bi-directional fed and the control is difficult, since exist the risk of instabilities [49]. The parallel excitation circuit, in all its topologies, suffers from the drawback of construction complexity, but the sliding contact, for feeding the field winding, is absent. The series excitation circuit has two important advantages: the simplicity and the global decrease of the flux density, which permits a decrease of the iron loss (thus obtaining an increased efficiency); its drawback: the sliding contact.

The main advantage of the DESM appears especially in those applications where the electric drives operate under partial loads [50] most of the time. For such applications, the electric motor should not only have the highest efficiency at a given partial load, but should also be able to operate in full load conditions. Unlike classical machines (induction, dc, synchronous), where these requirements are quite difficult to achieve, the DESM, thanks to its hybrid excitation field, is able to satisfy these specifications. Indeed, the PMs are designed in size to produce the desired electromagnetic torque. Moreover, at full load or in the flux-weakening operating mode, the excitation winding is fed either to produce the additional torque or to weaken the PMs field in order to increase the speed.

In the DCDESM project the author has studied several hybrid-excited variants based on the scientific literature, see topology examples in FIGURE 2-10. He also proposed several original DESM variants, see FIGURE 2-11. Finally, he has constructed one prototype of DESM, having a classical polar pitch winding placed on 36 slots and 4 poles with surface mounted PMs; the auxiliary winding is placed around rotor poles, see FIGURE 2-12.

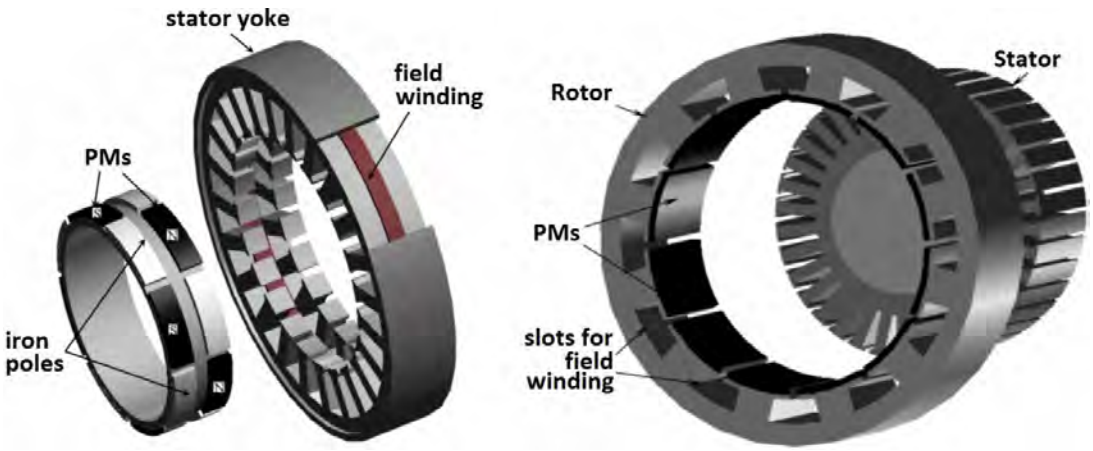

FIGURE 2-10. DESM topologies found in the literature.

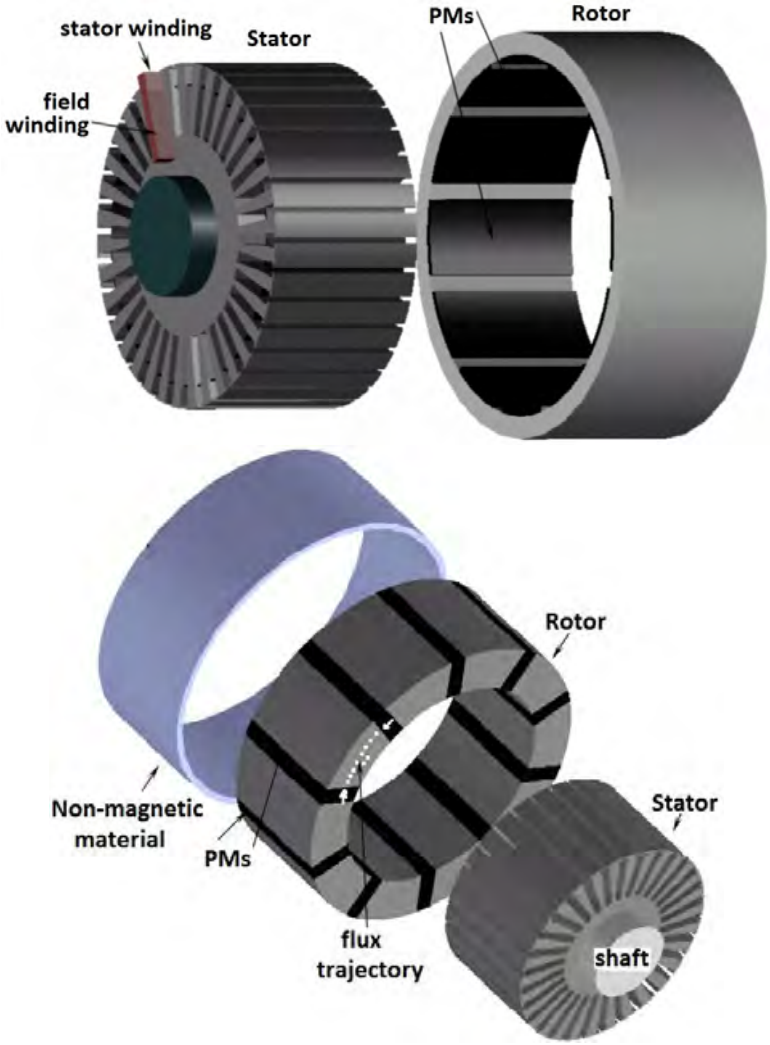

FIGURE 2-11. DESM original topologies proposed by the author:
-top: outer rotor DESM with surface mounted PMs; auxiliary winding on the stator, supplied on DC.
- bottom: outer rotor DESM with flux concentration PMs; auxiliary winding on the stator, supplied on DC.

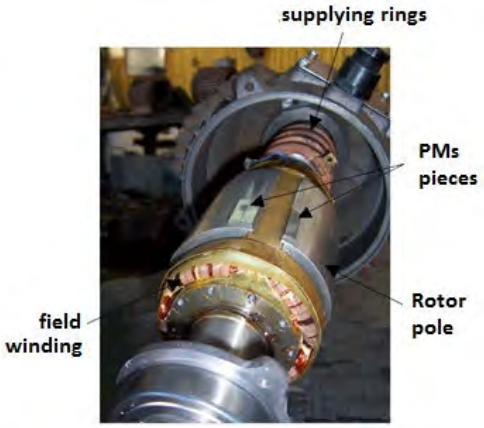

FIGURE 2-12. Photograph on the rotor of the constructed DESM.

The use of the auxiliary winding for such a DESM can be depicted from the results shown in FIGURE 2-13. For surface mounted machines, the flux weakening operation (the machine working beyond the rated speed) is not easy to be obtained and the machine can go up to 1.5 the rated speed. By taking advantage of the auxiliary winding, the DESM can work even at 2.6 time the rated speed, while the iron loss are decreased because the entire machine is demagnetized (the flux density in the machine's iron is decreased significantly). This is the most important advantage of the machine. Of course, a special attention should be paid to the demagnetization risk of the PMs, which could be partially damaged at high temperatures.

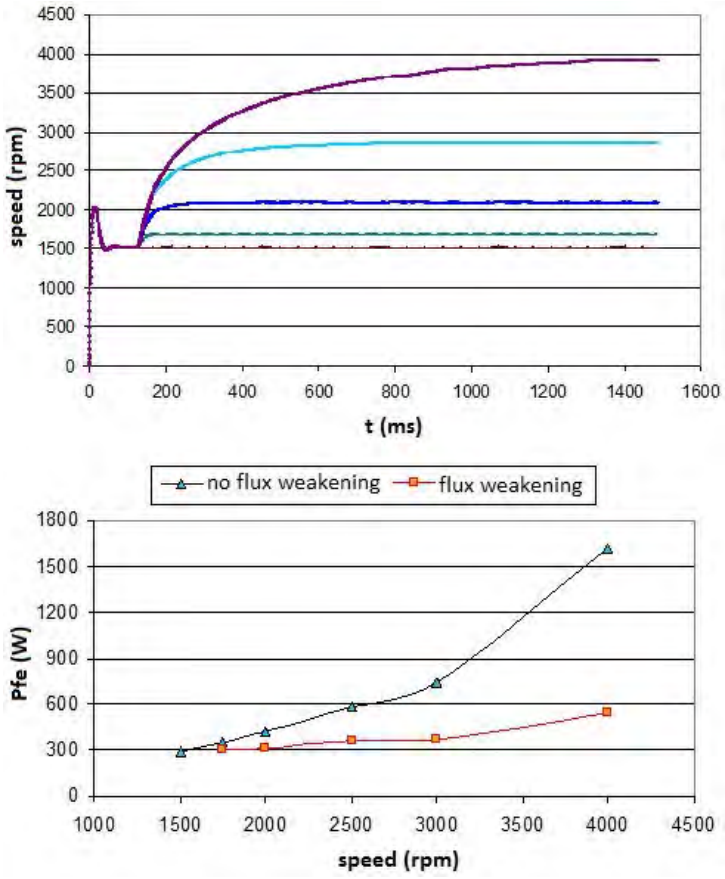

FIGURE 2-13. Numerical simulated results of the DESM running in flux weakening or not.

2.4 Outer-rotor topologies and fractional slot winding variants

The problem of the in-wheel motor was studied even in the PhD period, when several double excited machines were evaluated. But the construction and experimental validation for such a variant came mainly in the 4D-POSTDOC program, regarding the research theme MOEVEHU, where an electric scooter was under study.

In order to find the best motorization solution for the electric scooter application, the author' attention was focused on the existing variants found on the scientific literature [53]-[56]. Some scientists propose variants that use classical electrical motors (squirrel cage induction motor, DC-brushed or brushless synchronous motor excited by permanent magnets) and a belt transmission [9]. Considering a thermal scooter, no special construction and few modifications are needed to obtain an electric propelled one. This involves the use of a new power converter, but a relatively robust machine and drive can be employed. Such type of motorization is presented in FIGURE 2-14-left. The controllability for such a solution is an advantage, while the supplementary free place and the use of the belt are its major drawbacks.

A second solution is the in-wheel motorization, FIGURE 2-14-right, where the rotating part is outside the motor itself and mounted into the wheel. No supplementary place is needed to install the motor [53]-[56]. The lack of the belt and the compact topology of the motorization are the major advantages for such solution. On the other hand, due to mechanical shocks while the scooter is running on the road, there is an important risk to have a friction between the stator and the moving rotor, which will permanently damage the motor. Anyway, based on the aforementioned advantages, the authors have focused their attention on the in-wheel motorization topology.

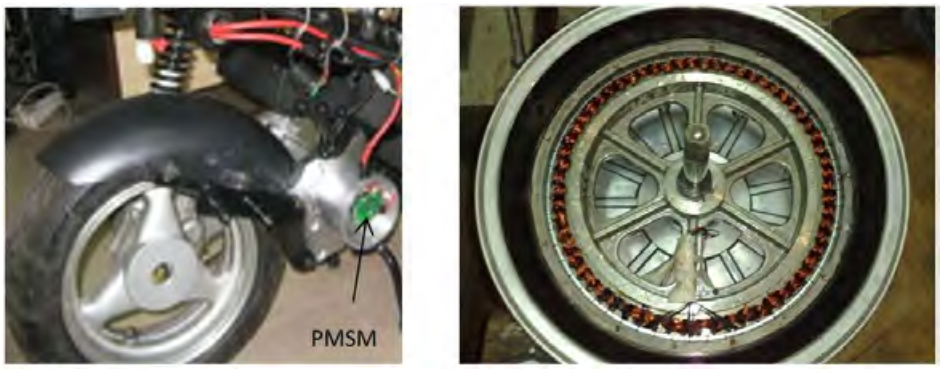

FIGURE 2-14. Scooter motorization variants: with belt transmission (left - http://www.icpe.ro/ro/d/3/p/scooter) and the in-wheel variant (right).

The use of in-wheel topology involves several mechanical issues and its outer diameter is imposed by the tire. The use of water cooling is not really necessary since the outside air can be used to cool the stator case directly, on both sides. On the other hand, the application requests to have the best power density ratio (to get the desired torque or output power, at the lowest mass of the machine) with the best improved energetic performances. Regarding the drive choice, the use of a common three phase inverter was also imposed (to avoid complexity).

It is obvious that a machine excited by permanent magnets (PMs) produces the best power/mass ratio. Moreover, the authors wanted to avoid the brushes. Thus, the motorization will be assured by a permanent magnet synchronous machine (PMSM). For such machine, the reluctance of the PMs produces waves on the torque characteristics [53]. To have a good controllability, especially in transients (and for a scooter which is involved in traffic, the transients are the normal operation), the torque characteristics needs to be as smooth as possible.

The supply for our application will be assured from a battery of 48 Vdc, the output power being 1.5 kW, while the rated speed of the PMSM is 420 r/min.

In order to respond to all this constraints, three motorization solutions have been analyzed: the first one with a reduced number of poles and distributed winding type, and the other two with fractional-slot pitch.

If all conductors per pole of one phase of an AC machine would be concentrated in one slot, the coil would become excessively large, with negative impact on the lamination and end-turn size. Thus, the power/weight ratio is decreased. In order to reduce the size of the coil, the practical solution is to divide the initial coil into multiple coils, thus having a distributed winding. Moreover, if the mechanical performances are very severe (very smooth torque is demanded), the fractional slot winding will be the right solution [58], [59]. The reduced torque ripples are due to very smooth induced electromotive force (emf), meaning very low harmonics of the wave. One of the conclusions from [58] was that in distributed winding topologies the length of the machine is greater than in the case of fractional slot configuration. Moreover, if the fractional slot winding is disposed in two layers, the length of the machine becomes smaller.

Unfortunately, the fractional slot configuration can reduce drastically the magnitude of the developed torque, due to winding factor (k_w) decrease. If N_t is the number of turns per one phase, the effective number of turns which will participate to the torque development is $N_{eff} = k_w \cdot N_t$. Ideally, $k_w = 1$, but, practically, for fractional slots, it is not possible. A special attention should be paid to the k_w parameter. Different poles-slots configurations have been investigated in [58], [59]. It has been reported the possible configurations which are maximizing the winding factor, with values between 0.86 (6 slots, 4 poles) and 0.96 (12 slots and 10 poles) [59]. Inadequate configurations can produce poor winding factors: 0.247 (21 slots and 16 poles), or 0.117 (9 slots and 32 poles) [58].

The calculation of k_w, for PMSM-17/39 variant for example, is very difficult, because the winding is not periodically distributed. But it can be computed based on the emf phasor diagram representation, FIGURE 2-15. Knowing that the winding factor represents the ratio between the *resultant phasor of the induced emf* (FIGURE 2-15-right) and the sum of *winding elements which are composing that resultant vector*, and with a coil pitch of 156.92°, k_w equals 0.9356. This value is satisfactory for the development of the desired torque, while the torque wave will be very smooth (this will be proved in the next section).

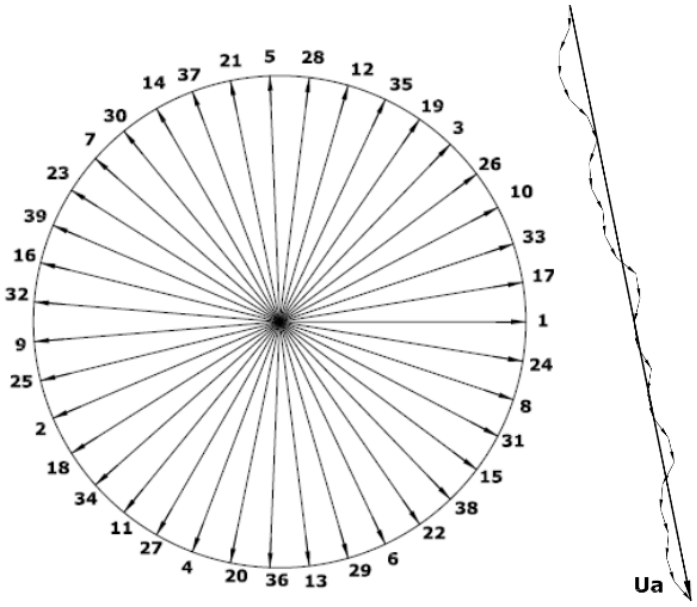

FIGURE 2-15. The emf phasors winding representation and the phase A vector for the PMSM-17/39.

PMSM-9/54

The first analyzed variant for the motorization of the electric scooter is based on a PMSM with 9 pair of poles, while on the stator there is a polar pitch three phase winding and 54 slots. (Using a reduced number of poles – to get a reduced frequency – is not possible for such a structure, where a high number of poles mean an improvement in the power/mass ratio.)

PMSM-17/39

The second analyzed machine has 17 pairs of poles and fractional pitch on the stator winding; the coils being distributed on 39 slots (see FIGURE 2-15). At 420 r/min, the rated frequency is of 119 Hz. Compared to the previously topology with 18 poles (which has 56 Hz) practically the frequency is doubled. Later on, one will see how the frequency will affect the machine's operation (efficiency).

PMSM-23/51

The third studied topology of PMSM has 23 pair of poles and 51 slots on the stator, with fractional winding pitch. The idea of testing this variant is to study the limit of using the fractional slot topology related to the smoothest possible torque, with good energetic performances (i.e., efficiency and power factor). For 46 poles, the rated frequency of the supply will be 161 Hz. Is this increase in frequency acceptable in terms of reduced torque ripples against a weakened efficiency? The answer will be given in the next paragraphs.

The analytical design of the studied machines is based on the equivalent magnetic reluctances circuit [60]. Here, only the calculated results will be presented, for a first evaluation of the designed machines, in order to have a comparison of power density and energetic performances.

The calculated results of the designed machines are presented in Table 2-4.

TABLE 2-4. THE DESIGN RESULTS OF THE STUDIED VARIANTS OF PMSM, AT RATED OPERATION [61]

MACHINE'S TYPE / *PARAMETER*	*PMSM-9/54*	*PMSM-17/39*	*PMSM-23/51*
Rated torque (N·m)	34	34	34
Number of phases (-)	3	3	3
Number of pole pairs (-)	9	17	23
Frequency (Hz)	63	119	161
Number of slots (-)	54	39	51
Outer diameter (mm)	223	223	223
Stack length (mm)	50	50	50
Air-gap length (mm)	1	1	1
Air-gap flux density (T)	0.828	0.849	0.843
Phase resistance (Ω)	0.073268	0.044453	0.059563
Rated current (A)	21.32	20.76	24.78
Total losses (W)	141.91	131.27	190.82
Power factor (%)	92.27	92.03	80.19
Efficiency (%)	90.53	91.24	87.27
Active part costs (€)	80.2	73.99	79.3
Active part mass (kg)	6.73	5.91	6.25
Power/mass ratio (W/kg)	222.8	253.8	240

For the same rated torque, number of phases, machine's length, outer diameter and air-gap length, the reader can identify the main results: the rated current, the total losses, the

energetic performances (efficiency and power factor), the mass of the active parts of the machine and its estimated cost. Except the power factor, where the first variant (PMSM-9/54) has the best value, for all other performances the PMSM-17/39 presents the best results. This last one has the lowest mass, thus the lowest cost, and the best power density. Moreover, in terms of efficiency, the second variant is better than the first one. Even if the iron loss is higher for PMSM-17/39, the improved efficiency is justified since the amount of copper (which influences the phase resistance) used for the windings is more reduced. The efficiency of the third machine is the lowest due to the iron loss increase (which are proportional with the square of the frequency).

(The reference price, for the active parts of the machine, is: 50 €/kg for the PMs and 7.6 €/kg for the copper and stator/rotor iron. These prices refer only to the raw material, and do not include the manufacturing.)

In order to validate the calculated results, the studied machines were analyzed numerically, by using the finite element method (FEM). For that, the Flux 2D software has been used. The flux-density distribution in the active parts of the studied machines is shown in FIGURE 2-16. It seems that the highest level of flux density is obtained in the core of the third variant; this is because of the high number of teeth.

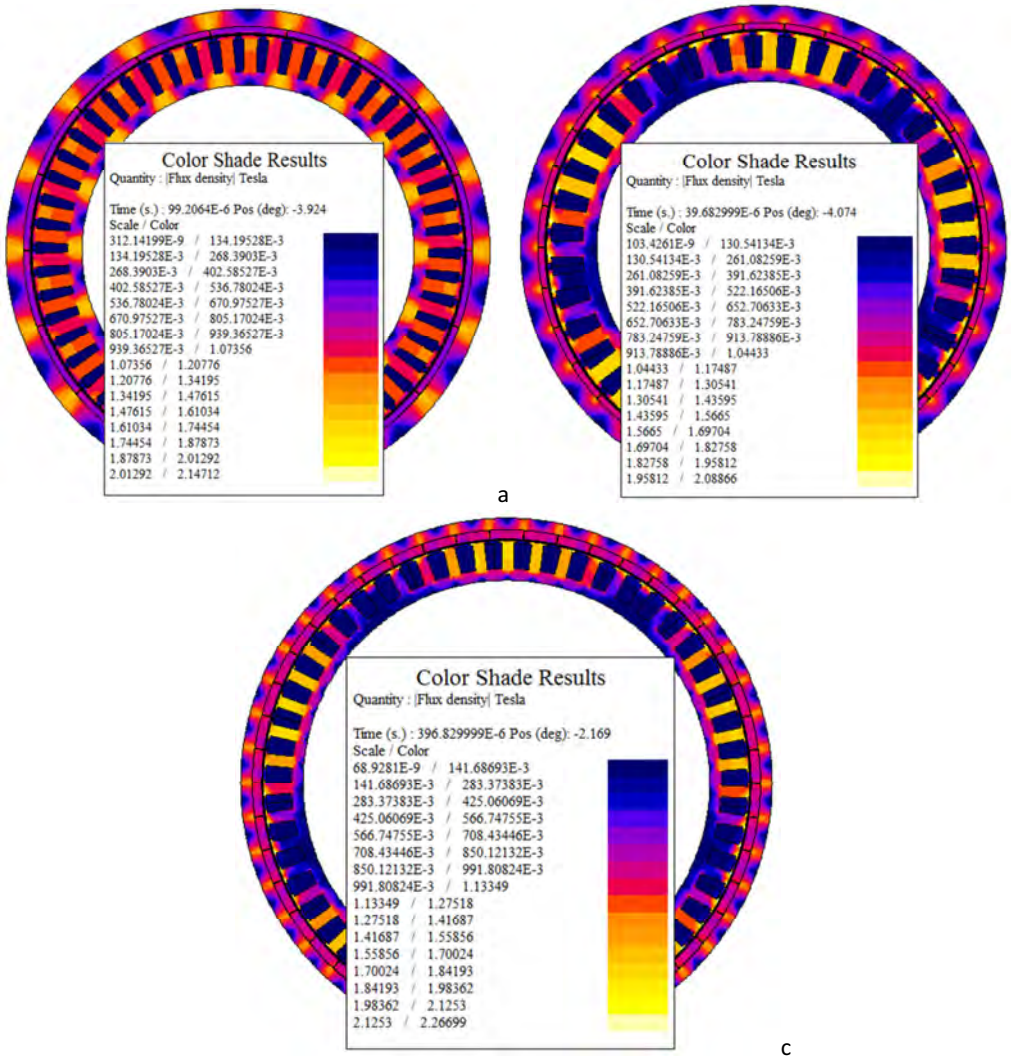

FIGURE 2-16. Flux-density distribution in the active parts of the studied machines:
a) PMSM-9/54; b) PMSM-17/39; c) PMSM-23/51. [61]

(It is true that the first variant has more teeth, but, as it was stated in the second section, the winding coefficient is better for the polar pitch than the fractional pitch winding type. Thus, a higher current is needed to produce the desired torque, and finally the flux density in the iron is increased for the third variant). This will increase the copper loss, by that reducing the efficiency of the machine. For the second topology the iron is less saturated because of the reduced number of teeth and current level.

All machines were simulated both in generator and in motor operating regime [61]. One can notice the harmonic content of the air-gap flux density, FIGURE 2-17, as well as the electromotive force (emf), FIGURE 2-18. It is obvious that the fractional slot winding configuration produces the lowest harmonic content, thus justifying our choice.

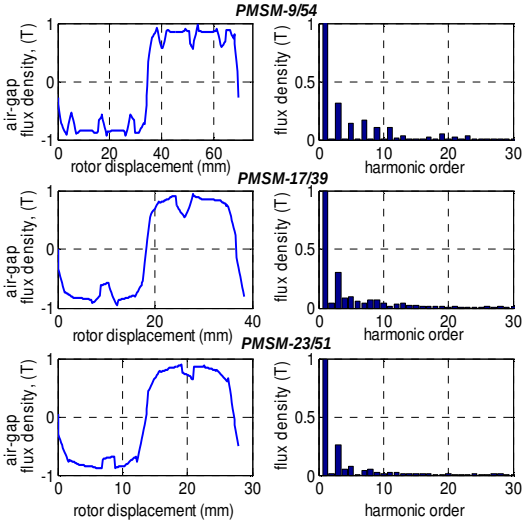

FIGURE 2-17. Air-gap flux density on the machines.

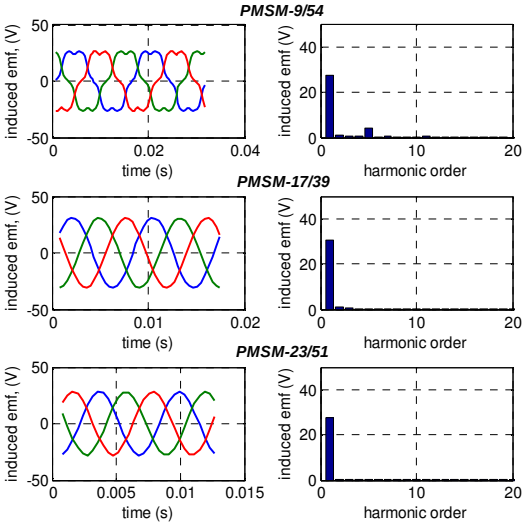

FIGURE 2-18. Induced emf on the studied machines.

In motor operating, by injecting a sinusoidal current into the phase winding we get the rated torque, as well as the iron loss. For example, the motor operating regime results of the PMSM-9/54 are depicted in FIGURE 2-19. It is obvious that, due to the specific poles-slots configuration, this machine produces important ripples; this is its major drawback..

Another parameter which helps us to evaluate the machines performances for the scooter application is the iron losses, which are shown in FIGURE 2-20. For the PMSM-9/54 variant, the iron loss is of 42 W. For the other two machines, due to high frequency, the iron loss is high: 73.8 W for PMSM-17/39, and 81 W for PMSM-23/51. Even if the iron loss is reduced for the first variant, due to supplementary current needed to obtain the desired torque, the efficiency of the PMSM-9/54 is decreased. This explains the fact that the efficiency is better for the PMSM-17/39.

The other important criterion which helps us to decide which machine is best suited for the scooter application is the torque wave form. It has been shown that the lowest ripples were obtained for the third variant, PMSM-23/51. Furthermore, the torque for the second and third variant are presented for comparison in FIGURE 2-21-top. It is clear again than the fractional slot topology, with the highest number of poles gives us better performances in terms of torque wave. There is a sensitive difference between these last two variants.

Since the lowest iron loss level was obtained with the first topology, with reduced number of poles, the author has tried to take advantage of the first topology, while trying to diminish the torque ripples. For that, the author has studied the skewing effect of the PMSM-9/54. Another solution could be to control the direct and quadrature current in the machine, but it is known that acting on the current components will reduce the torque, too.

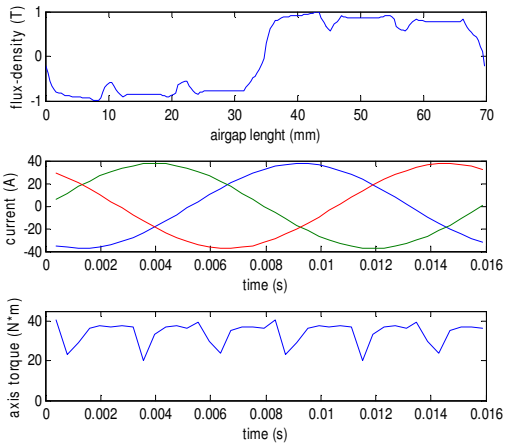

FIGURE 2-19. PMSM-9/54 results. [61]

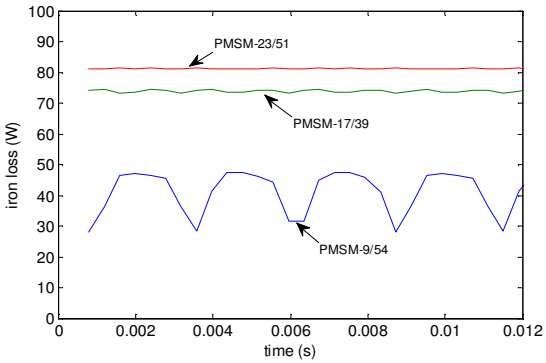

FIGURE 2-20. Iron loss for the studied machines. [61]

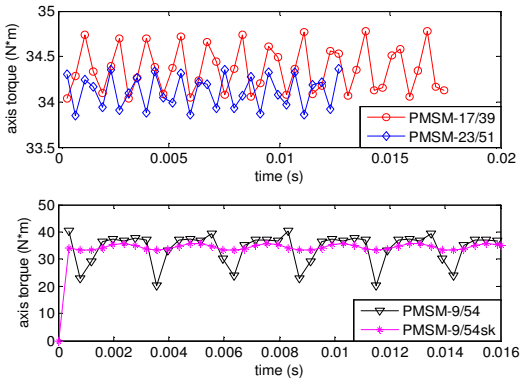

FIGURE 2-21. Torque waves. [61]

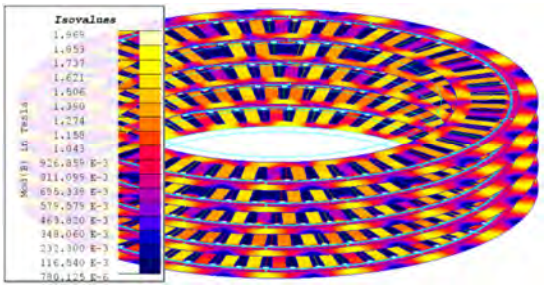

FIGURE 2-22. Flux density in the skewed PMSM-9/54. [61]

The stator was skewed with an angle equal to the tooth pitch. The flux density repartition within the active parts of the skewed PMSM is presented in FIGURE 2-22. In the same time, the torque wave, for the skewed and un-skewed PMSM-9/54, was presented in FIGURE 2-21-bottom.

One can see that the torque ripples have been drastically reduced, but the desired torque has been obtained at an increased current (25 A). Practically, by skewing the machine, the output performances are reduced, too. In order to obtain the rated torque, one should consider a much higher current, (thus, increasing the loss and decreasing the efficiency of the machine).

In Table 2-5 the torque and iron loss computed results are presented, for comparison.

TABLE 2-5. THE IRON LOSSES AND TORQUE RIPPLES FOR THE STUDIED MACHINES [61]

MACHINE'S TYPE / *PARAMETER*	*PMSM-9/54*	*PMSM-17/39*	*PMSM-23/51*
torque ripples (%)	55.8	1.88	1.23
iron losses (W)	42	73.8	81

Based on the above comments and conclusions obtained from Table 2-4 and Table 2-5, it can be concluded that the most suited variant for our application is the PMSM-17/39. This variant has been optimized based on methauristic optimization approach (see chapter 4), constructed and tested on a bench. Some photo and results of the tested PMSM-17/39 are presented in FIGURE 2-23.

The prototype

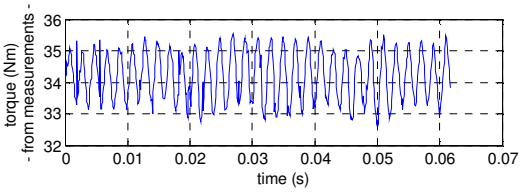

Measured torque

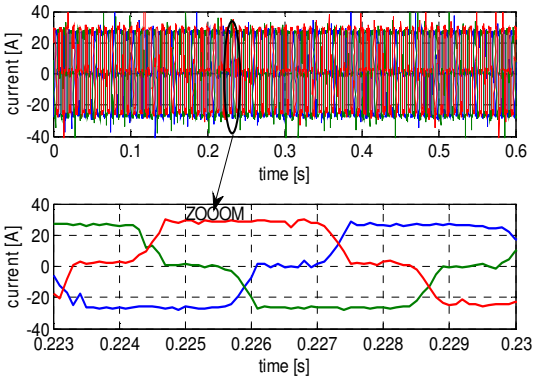

Measured current

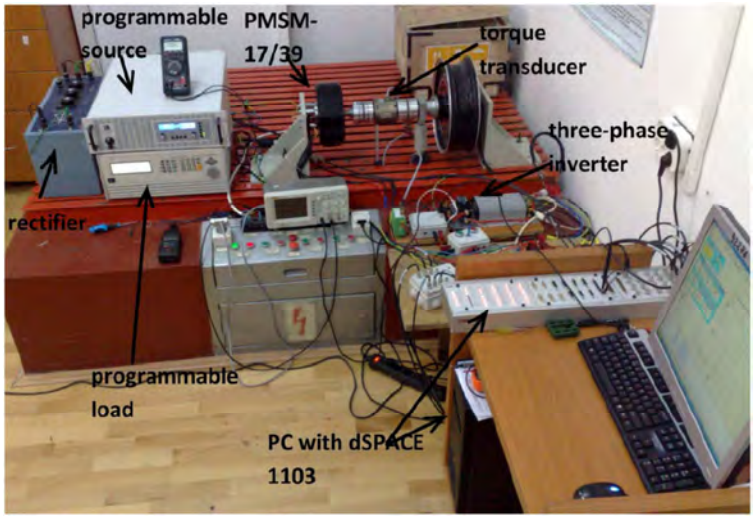

The test bench

FIGURE 2-23. Constructed prototype, the test bench and some results of the studied PMSM-17/39. [61]

3 THE DESIGN OF THE EV'S MOTORIZATION

3.1 Framework and summary of main results

The design of the EV's motorization was studied in all the author's projects, but it has been exclusively treated in the following industrial projects:

- Project name: *Design of two types of Special Electrical Machine*. Project type: industry project between Technical University of Cluj-Napoca and XANTOS (Switzerland). Project manager: Daniel FODOREAN. Period: March–May 2011. Project Acronym **D2SEM**.
- Project name: *Assistance for the Manufacturing and the Testing phases of Special Electrical Machines*. Project type: industry project between Technical University of Cluj-Napoca and HYTEN (Switzerland). Project manager: Daniel FODOREAN. Period: July–December 2011. Project Acronym: **AMT-SEM**.

The above projects, D2SEM and AMT-SEM, were financed of industrial companies from Switzerland and, based on confidential agreement, all the obtained results were given to the owner; none of the obtained results were published. Thus, here we will present the main results from the WHEEL-EE project and some of the research activities from UTBM and UTCN:

- D. Fodorean, F.Jurca, M.Ruba and D.C. Popa. *Motorization Variants for Light Electric Vehicles – design, magnetic, mechanical and thermal aspects*, AlmaMater, June 2013.
- D.Fodorean: *Global Design and Optimization of a Permanent Magnet Synchronous Machine used for Light Electric Vehicle*, Intech, June 2011 –chapter of 24 pages in monograph *Electric Vehicles – Modelling and Simulations*, edited by Serif Soylu.
- D.Fodorean, A. Miraoui, *Dimensionnement rapide des Machines Synchrones à Aimants Permanents (MSAP)*, Technique de l'Ingénieur, Paris, France, 2009, Document D3554.
- D.Fodorean, A.Djerdir, I.A.Viorel, A.Miraoui: *A Double Excited Synchronous Machine for Direct Drive Application - Design and Prototype Tests*, IEEE Transactions on Energy Conversion, vol.22, n.3, pp.656-665, September 2007.

The design of the EV's motorization was realized based on the scientific literature [31], [52], [60], [62]-[66]. When designing an electrical machine, there are two possible starting points: the calculation of the air-gap's diameter, where the torque is produced based on the linkage flux, coming from the main flux source, and the armature's reaction. For the PM machines, another approach consists in estimating the volume of the magnets needed to produce the desired output power. For all the studied machines, the author's approach is based on the air-gap diameter calculation. In this chapter, only the main parameters from the design process will be presented. With some geometry particularities, the PM's machine design approach presented here can be adapted for other configurations (radial, axial, or transverse flux machines). The SRM case is treated separately.

3.2 The PM machines design approach

3.2.1 PMSM's main designing elements, parameters and characteristics

The output power of an electric machine, when the leakage reactance is neglected, is proportional with the number of phases of the machine, n_{ph}, the phase current, i(t), and the inducted electromotive force (emf), e(t):

$$P_{out} = \eta \cdot \frac{n_{ph}}{T} \cdot \int_0^T e(t) \cdot i(t) dt = \eta \cdot n_{ph} \cdot k_p \cdot E_{max} \cdot I_{max} \quad (3.1)$$

where T is the period of one cycle of emf, E_{max}, and I_{max} represent the peak values of the emf and phase current, k_p is the power coefficient, and η is the estimated efficiency.

The peak value of the emf is expressed by introducing its coefficient, k_E:

$$E_{max} = k_E \cdot N_t \cdot B_{gap} \cdot D_{gap} \cdot L_m \cdot \frac{f_s}{pp} \tag{3.2}$$

where N_t is the number of turns per phase, B_{gap} and D_{gap} are the air-gap flux density and diameter, L_m is the length of the machine, f_s is the supplying frequency and pp is the number of pole pairs.

By introducing a geometric coefficient, $k_L=L_m/D_{gap}$, and a current coefficient (related to the currents wave form, [63]) k_i, and defining the phase load ampere-turns as:

$$A_{th} = \frac{2}{\pi} \cdot N_t \cdot \frac{I_{rms}}{D_{gap}} \tag{3.3}$$

it is possible to define the air-gap diameter of the machine:

$$D_{gap} = \sqrt[3]{\frac{2 \cdot p \cdot P_{out}}{\pi \cdot n_{ph} \cdot A_t \cdot k_E \cdot k_i \cdot k_p \cdot k_L \cdot \eta \cdot B_{gap} \cdot f_s}} \tag{3.4}$$

The phase load ampere-turns can be estimated, function of the power of the machine. Thus, the number of turns per phase can be calculated.

The coefficients k_E, k_i, k_p depend on the wave forms of the current and induced emf [63].

The air-gap flux density can be estimated by applying the Ampere's law and neglecting the iron permeability, based on the following equation:

$$B_{gap} = \frac{B_{rpm} \cdot \frac{h_{pm}}{\mu_{rpm}}}{\delta_0 + \frac{h_{pm}}{\mu_{rpm}}} \cdot k_{dpm} \tag{3.5}$$

where B_{rpm}, is the remanent flux density of the PM, h_{pm} is the height of the PM on the magnetization direction, k_{pm} is a demagnetization coefficient which takes into account the armature reaction (usually between 0.7..0.9 for rear-earth PMs), μ_{rpm} is the relative magnetic permeability of the PM and δ_0 is the air-gap length.

The expression given in (3.5) is for the surface mounted PMs, FIGURE 3-1a. For other rotor configurations, meaning with inset PMs (FIGURE 3-1b), with buried PMs (FIGURE 3-1c) or with flux concentration topology (FIGURE 3-1d) the calculation of the air-gap flux density can be made based on the following equations (to replace the (3.5) equation):

$$B_{gap} = \frac{B_{rpm} \cdot h_{pm}}{\frac{D_{is}}{2} - \delta_0 \cdot \left[\ln\left(\frac{\frac{D_{is}}{2} - \delta_c}{\frac{D_{or}}{2}} \right) + \mu_{rpm} \cdot \ln\left(\frac{\frac{D_{is}}{2}}{\frac{D_{or}}{2} - \delta_c} \right) \right]} \quad \text{for FIGURE 3-1b}$$

$$B_{gap} = \frac{B_{rpm} - B_{max} \cdot \frac{2 \cdot x}{w_{pm}}}{\frac{D_{or}}{pp \cdot w_{pm}} + \delta_c \cdot \frac{\mu_{rpm}}{h_{pm}}} \quad \text{for FIGURE 3-1c}$$

$$B_{gap} = \frac{B_{rpm}}{\sigma \cdot \frac{S_p}{S_{pm}} + \frac{1}{\mu_0} \cdot \frac{B_{rpm}}{H_{cpm}} \cdot \frac{2 \cdot \delta_c}{h_{pm}}} \quad \text{for FIGURE 3-1d}$$

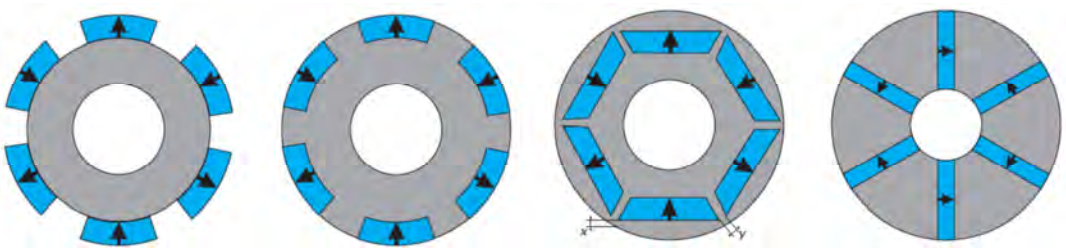

a b c d

FIGURE 3-1. Rotor topologies with PMs: a) on surface; b) inset; c) buried; d) for flux concentration. [64]

where δ_c is the air-gap length modified by Carter's coefficient, x is defined in FIGURE 3-1c, the diameters of the active parts of the machine are given in FIGURE 3-2, B_{max} is the maximum flux density in the saturated part of the rotor (usually, the saturation value of the used steel), w_{pm} is the width of the PM polar piece, σ is a geometric coefficient for flux concentrated topologies (usually, at 1.1 value), S_p is the pole surface and S_{pm} is the PMs piece surface.

The PMs placement influences the value of the direct and quadrature axis inductances ratio. This ratio reflects the machine's capability to operate in the flux-weakening region (how many times the rated speed is increased at constant power operation). The air-gap flux density level against the remanent flux of the PM and the inductances ratio are given in Table 3-1, [64].

TABLE 3-1. INDUCTANCES RATIO AND AIRGAP FLUX DENSITY LEVEL FOR DIFFERENT ROTOR TOPOLOGIES

TOPOLOGY / *PARAMETER*	*SURFACE MOUNTED*	*INSET*	*BURIED*	*FLUX CONCENTRATION*
Inductances ratio	1	2…3	2…6	2…4
Air-gap and remanent flux density comparison	$B_\delta<B_{rpm}$	$B_\delta<B_{rpm}$	$B_\delta<B_{rpm}$	$B_\delta>B_{rpm}$

All the other geometric parameters will be computed based on the air-gap diameter. The designer has to choose only the shape of the PMs and stator slot, having in mind the needs of the application (reduced number of poles for high speed applications, high number of poles for high powers, polar pitch or fractional slot winding for a compromise between the power density and torque ripples level).

In order to have an idea about the geometry of the studied machine, in FIGURE 3-2 are presented the main parameters of the designed RF-PMSM. The following notation was used:

- $D_{os, is, pm, or, sh}$ denote the diameter of the outer stator, inner stator, at the exterior of the PMs, outer rotor and shaft.
- at the stator slot, we identify $w_{sb, st, so}$ are the width of the slot at the bottom, at the top and the slot opening, and $h_{is, s}$ are the height of the tooth isthmus (tooth tip) and of the slot. (Another important parameter not defined here is the tooth pitch, τ_t, which represents the length of the arc or the angle between the middle of two consecutive slots or teeth: 360/number_of_teeth.)
- at the rotor, the polar pitch, τ_p, represents the length of the arc of one pole: 360°/number_of_poles.

The saturation factor, k_s, has to be computed in order to take into account the non-linearity of the steel. k_s depends on the equivalent magneto-motive force, F_m, in each active part of the machine and in the air-gap:

$$k_s = \frac{2 \cdot F_{mt} + 2 \cdot F_{istm} + F_{my} + F_{mr} + 2 \cdot F_{mg}}{2 \cdot F_{mg}} \tag{3.6}$$

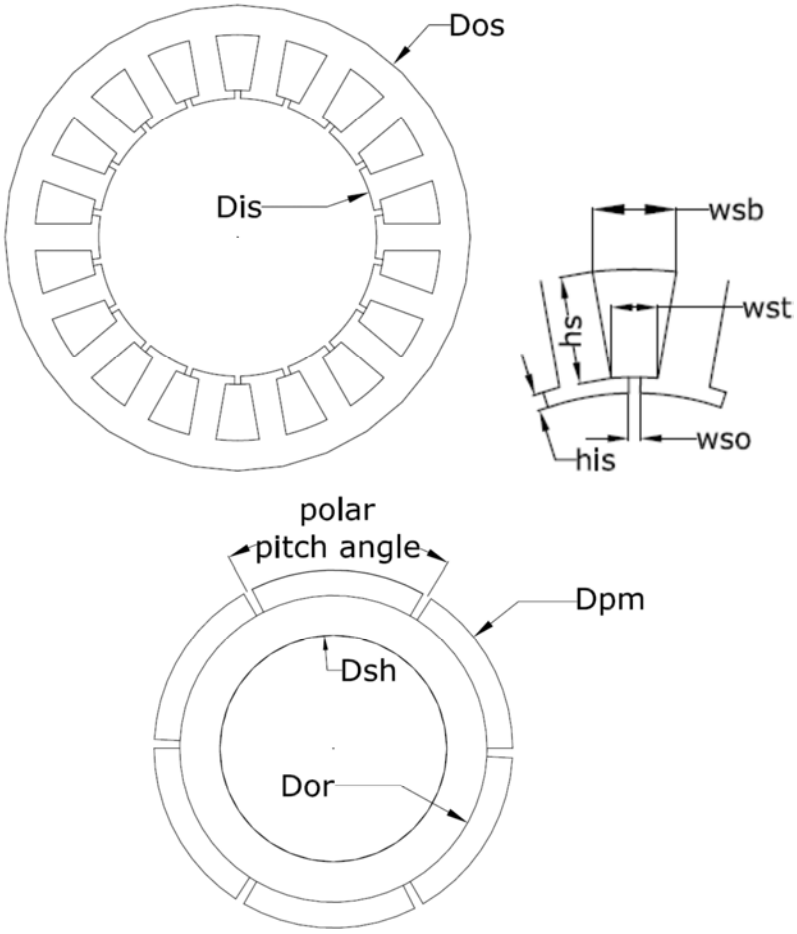

FIGURE 3-2. RF-PMSM: defining the geometric parameters. [1]

where 't', 'istm', 'y', 'r' and 'g' and indices referring to the stator teeth and isthmus, yoke, rotor core and air-gap, respectively. Each magneto-motive force is computed based on the magnetic field intensity (H) and the length (l) of the specific part of the machine, on the flux direction:

$$F_{mx} = H_x \cdot l_x \tag{3.7}$$

The generic equation (3.7) is used for the computation of the magneto-motive force in each active part of the machine, while 'x' replaces 't', 'y', 'r' and 'g' indices. The parameter l_x can be easily calculated. Further, the magnetic field intensity has to be expressed. The H_x value can be chosen from the supplier B(H) magnetic characteristic, function on the "B" value [1].

Next, the parameters of the machine should be determined. The phase resistance depends on the copper resistivity, ρ_{co}, the length of series turns, l_t, and it is inversely proportional with the conductor's cross section, S_c:

$$R_{ph} = \rho_{co} \cdot \frac{l_t}{S_c} \tag{3.8}$$

The *d-q* axis reactances are calculated based on the magnetizing (X_m) and leakage (X_σ) reactances:

$$X_{d,q} = X_\sigma + X_{m\_d,q} \cdot \frac{k_{a\_d,q}}{k_s} \tag{3.9}$$

The saliency coefficients, [1], $k_{a\_d,q}$, are calculated by:

$$k_{a\_d} = \frac{\pi \cdot \alpha_{pm} + \sin(\pi \cdot \alpha_{pm})}{4 \cdot \sin(\alpha_{pm} \cdot \pi/2)}$$
$$k_{a\_q} = \frac{\pi \cdot \alpha_{pm} - \sin(\pi \cdot \alpha_{pm}) + 2/3 \cdot \cos(\alpha_{pm} \cdot \pi/2)}{4 \cdot \sin(\alpha_{pm} \cdot \pi/2)} \quad (3.10)$$

where α_{pm} is a coefficient representing the percentage of magnet covering the rotor pole (for surface mounted PM machine, the saliency ratios are equal).

The *d-q* magnetizing reactances are:

$$X_{m\_d,q} = \frac{4 \cdot n_{ph} \cdot f_s \cdot \tau_p \cdot L_m \cdot (N_t \cdot k_{ws})^2 \cdot \mu_0 \cdot k_{a_{d,q}}}{\pi \cdot pp \cdot gap} \quad (3.11)$$

$$X_\sigma = \frac{4 \cdot \pi \cdot f_s \cdot (N_t)^2 \cdot \mu_0 \cdot \sum \Lambda_\sigma}{q} \quad (3.12)$$

where τ_p is the polar pitch, k_{ws} is the winding factor (equal to unity for most of the polar pitch winding variants (and has values of 0.93..0.96 for fractional slots windings), *q* is the number of slots per pole and per phase, and $\sum \Lambda_\sigma$ is specific leakage permeance.

This leakage permeance is obtained empirically, [62], by defining the specific slot permeances, the end-winding permeances, the tooth isthmus permeances and the differential leakage permeances (some of the geometrical parameters are presented in FIGURE 3-3):

$$\lambda_s = \frac{h_s}{3 \cdot w_{st}} + \frac{h_{sit}}{w_{st}} + \frac{h_{istm}}{w_{st} - w_{so}} \cdot \ln\left(\frac{w_{st}}{w_{so}}\right) \quad (3.13)$$

$$\lambda_{ew} = q \cdot \left(0.97 - 0.43 \cdot \frac{\tau_t}{w_{ew}}\right) \quad (3.14)$$

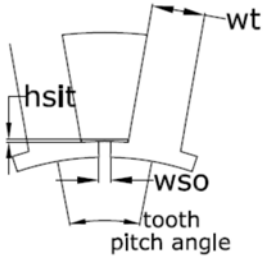

FIGURE 3-3. RF-PMSM: defining the slot parameters for leakage permeance calculation. [1]

$$\lambda_t = \frac{5 \cdot \frac{\delta_0}{w_{so}}}{5 + 4 \cdot \frac{\delta_0}{w_{so}}} \quad (3.15)$$

$$\lambda_d = \frac{n_{ph} \cdot q \cdot \tau_{t \cdot K_{fe}}}{\pi^2 \cdot \delta_c \cdot k_s} \cdot k_q \quad (3.16)$$

where h_{sit} is the height of the isolation material which keeps the conductors inside the slot, w_{ew} is the width of the end-winding, k_{fe} is the iron stack coefficient (is 0.93 for 0.2mm sheets, 0.95 for 0.35 mm sheets and 0.97 for 0.5mm sheets), k_q is a coefficient related to the tooth pitch and the number of slots per pole and per phase (graphically obtained, [62]), and δ_c is the air-gap modified by Carter's coefficient.

For the motor operation of the PMSM (with magnetic anisotropy), the typical load phasor diagram is considered, in *d-q* frame, FIGURE 3-4, [67]-[69].

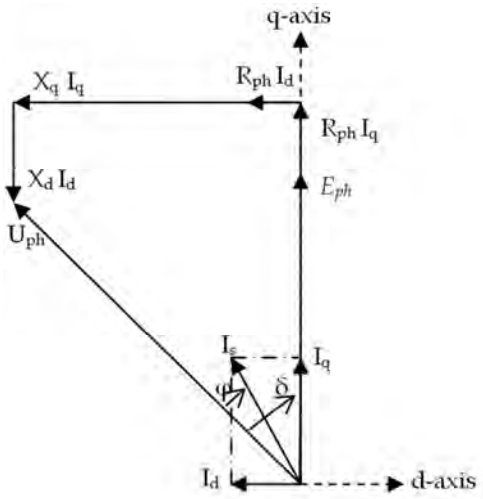

FIGURE 3-4. The phasor diagram of the PMSM in motor-load operation. [1]

From this phasor diagram one will get the *d-q* axis reactances equations, function of phase voltage, U_{ph}, phase electromotive force, E_{ph}, phase resistance, R_{ph}, *d-q* axis currents and internal angle, δ:

$$X_d = \frac{U_{ph} \cdot \cos(\delta) - E - R_{ph} \cdot I_q}{I_d}$$
$$X_q = \frac{U_{ph} \cdot \sin(\delta) + R_{ph} \cdot I_d}{I_q} \quad (3.17)$$

Thus, it is possible to compute the phase current, $I_{ph} = \sqrt{I_d^2 + I_q^2}$, knowing that the direct and quadrature current are obtained by developing (3.17):

$$I_d = \frac{U_{ph} \cdot \left(X_q \cdot \cos(\delta) - R_{ph} \cdot \sin(\delta)\right) - E_{ph} \cdot X_q}{R_{ph}^2 + X_d \cdot X_q}$$
$$I_q = \frac{U_{ph} \cdot \left(X_d \cdot \cos(\delta) + R_{ph} \cdot \sin(\delta)\right) - E_{ph} \cdot R_{ph}}{R_{ph}^2 + X_d \cdot X_q} \quad (3.18)$$

The electromotive force is proportional to the frequency, the number of turns, the air-gap flux per pole and the demagnetization coefficient:

$$E_{ph} = \sqrt{2} \cdot \pi \cdot f_s \cdot N_t \cdot k_{ws} \cdot \Psi_{gap} \cdot k_{dpm} \quad (3.19)$$

Next, the electromechanical characteristics can be calculated, namely:

- the input power:

$$P_{in} = n_{ph} \cdot U_{ph} \cdot \left(I_q \cdot \cos(\delta) - I_d \cdot \sin(\delta)\right) \quad (3.20)$$

- the output power (function of the sum of losses) and axis torque:

$$P_{out} = P_{in} - \sum \text{Losses} \quad (3.21)$$

$$T_m = \frac{P_{out}}{\Omega} \quad (3.22)$$

- the energetic performances (power factor and efficiency, respectively):

$$\cos\varphi = \frac{P_{in}}{n_{ph} \cdot U_{ph} \cdot I_{ph}}$$
$$\eta = \frac{P_{in}}{P_{out}} \quad (3.23)$$

3.2.2 The losses of the PMSM

The sum of losses contains the copper, iron and mechanical losses. A detailed view on the category of losses, depending on the machine type, winding variant and skewing effect was presented in [65]. Here, some loss components are neglected (for example, for small power and reduced current the effect of leakage flux, on the copper loss component, can be neglected; the time and harmonic iron loss are not considered; the ventilation losses are neglected because, for servomotors, there is no fan on the rotor shaft).

For the copper losses the well-known mathematical expression is used:

$$P_{co} = n_{ph} \cdot R_{ph} \cdot I_{ph}^2 \tag{3.24}$$

The iron loss calculation is another parameter which has to be very carefully evaluated. Some empiric mathematical expressions have been presented already in [31], [62], [64], [65]. The iron calculation presented here is based on the same mathematical expressions used in the finite element analysis, employed with Flux2D software. For each part of the stator (yoke, teeth and isthmus) the power density is calculated with the equation:

$$P_{d\_x} = \underbrace{k_{hyst} \cdot B_x^2 \cdot f_s}_{hysteresis\ loss} + \underbrace{\pi \cdot \sigma_{iron} \cdot \frac{d_{lam}^2}{6} \cdot (B_x \cdot f_s)^2}_{eddy\ current\ loss} + \underbrace{k_{exc} \cdot (B_x \cdot f_s)^{3/2}}_{excess\ loss} \tag{3.25}$$

where the 'x' subscript replaces the yoke, tooth and isthmus, σ_{iron} is the iron conductivity, d_{lam} is the lamination sheet width, k_{hyst} and k_{exc} are the hysteresis and excess loss coefficients obtained from the material characteristic, based on a given flux density value and its corresponding specific iron loss. Next, by multiplying the power density (obtained from equation (3.25)) by the volume of the yoke, teeth and isthmus we will get the iron loss in the machine.

Usually the rotor iron loss is neglected because the armature field rotates synchronously with the rotor. Other researchers tried even to estimate the PMs loss, based on empirically defined expressions, like:

$$P_{pm} = k_{md} \cdot p_{pm} \cdot m_{pm} \tag{3.26}$$

where the k_{md} is the magnetic field distortion coefficient (empirically defined, p_{pm} is the PMs specific loss and m_{pm} the mass of the PMs.

The mechanical losses contain the ventilation, friction of the bearings and aerodynamic losses. Since no ventilation is mounted on the rotor's shaft only the bearing frictions and aerodynamic losses are calculated.

The friction torque calculated at rated speed and for a shaft mounted horizontally on two horizontal bearings is calculated by:

$$P_{bf} = 2 \cdot T_{bf} \cdot 2 \cdot \pi \cdot n_N \tag{3.27}$$

where T_{bf} is the bearings friction torque which depends on the mass of the rotor (M_R) including the passive elements, the average bearing radius (R_{ab}) and the bearing coefficient (k_b) which depends on the type of the bearing:

$$T_{bf} = M_R \cdot R_{ab} \cdot k_b \tag{3.28}$$

The aerodynamic loss for constant air-gap is calculated as [65]:

$$P_{ad} = \frac{1}{Re_n} \cdot D_{pm} \cdot L_m \cdot \gamma_{air} \cdot v^3 \tag{3.29}$$

where Re_n is the Reynold's number, γ_{air} is the air density, for a given temperature [65] and v is the peripheral speed of the rotor, including the PMs. Thus, the mechanical losses are:

$$P_{mec} = P_{bf} + P_{ad} \tag{3.30}$$

3.2.3 The mass and the cost of the active parts of PMSM

The mass of the active parts is obtained based on the following mathematical expressions:

- the mass of the PMs:

$$m_{PM} = 2 \cdot \pi \cdot \left(\frac{D_{pm}}{2} - h_{pm}\right) \cdot \alpha_{pm} \cdot h_{pm} \cdot L_m \cdot \gamma_{pm} \tag{3.31}$$

- the mass of the rotor's yoke:

$$m_{ry} = \pi \cdot \left(\left(\frac{D_{or}}{2} \right)^2 - \left(\frac{D_{sh}}{2} \right)^2 \right) \cdot L_m \cdot \gamma_{iron} \quad (3.32)$$

- the mass of the stator's yoke:

$$m_{sy} = \pi \cdot \left(\left(\frac{D_{os}}{2} \right)^2 - \left(\frac{D_{os}}{2} - h_{sy} \right)^2 \right) \cdot L_m \cdot k_{fe} \cdot \gamma_{iron} \quad (3.33)$$

- the mass of the stator's teeth:

$$m_{st} = Z_s \cdot h_t \cdot w_t \cdot L_m \cdot k_{fe} \cdot \gamma_{iron} \quad (3.34)$$

- the mass of the stator's tooth isthmus:

$$m_{sistm} = Z_s \cdot h_{istm} \cdot 2 \cdot w_{istm} \cdot L_m \cdot k_{fe} \cdot \gamma_{iron} \quad (3.35)$$

- thus, the mass of the stator's iron is:

$$m_{siron} = m_{sy} + m_{st} + m_{istm} \quad (3.36)$$

- the mass of the copper:

$$m_{co} = n_{ph} \cdot k_{pc} \cdot S_c \cdot l_t \cdot \gamma_{co} \quad (3.37)$$

- finally, the mass of the total active part of the machine:

$$m_{a\_tot} = m_{pm} + m_{ry} + m_{siron} + m_{co} \quad (3.38)$$

For the calculation of the mass of the shaft, we should estimate the length of the machine, having in mind also the diameter of the shaft capable to sustain the demanded axis torque. On the shaft length, there will be two diameters: the diameter of the shaft under to active part of the machine, and the shaft which will be connected to the load, having the outsider diameter equal to the inner diameter of the bearings, D_b. The mass of the shaft can be estimated as:

$$m_{sh} = \pi \cdot D_{sh}^2 \cdot L_m \cdot \gamma_{sh} + \pi \cdot D_b^2 \cdot L_m \cdot \gamma_{sh} \quad (3.39)$$

The main results of the RF-PMSM designed machine are given in Table 3-2, because they will be compared with the results from the numerical approach, from subchapter 3.5.

TABLE 3-2. THE PARAMETERS OF THE DESIGNED RF-PMSM

PARAMETER	***VALUE***	***UNIT***
Output power	1200	W
Rated speed	3400	r/min
Rated torque	3.37	N·m
Battery voltage	24	V
Number of phases	3	-
Number of pole pairs	3	-
Number of slots	18	-
Stator outer diameter	87.4	mm
Machine's active part length	80	mm
Air-gap length	1	mm
Phase resistance	7.74	mΩ
d,q axis inductance	0.1306	mH
Induced emf on 1 phase	11.26	V
emf coefficient	0.67	V·s
Torque coefficient	0.094	N·m/A
Rated current	35.6	A
Total losses	90.74	W
Power factor	87.5	%
Efficiency	92.9	%
Raw material active part cost	18.93	€
Active part mass	2.96	kg
Power/active_mass	405.5	W/kg

In the above equations, the following parameters were introduced:

- for the rotor: γ_{pm}, γ_{iron} are materials densities for the PM's, rotor iron and shaft.
- for the stator: h_{sy}, Z_s, h_t, w_t, h_{istm} and w_{istm} are the height of the stator yoke, the number of stator slots (or teeth), the height of the tooth, the width of the tooth, the height of the tooth isthmus and the width of the tooth isthmus.
- for the copper: k_{pc} and γ_{co} are number of parallel conducters per one turn and the copper's material density.

3.3 The armature reaction calculation based on equivalent reluctance circuit

The armature reaction effect was evaluated for a six-phase PMSM. This approach is presented here.

A relatively precise method to computer the flux density in the machine's iron, by taking into account the leakage, can be made based on the so called *equivalent reluctance circuit*. The studied machine is, this time a six-phase PMSM, which has a common stator and surface mounted PMs (the PMs are glued in small pieces, to reduce the air-gap flux harmonic content). The winding configuration is given in FIGURE 3-5 and the rotor is in FIGURE 3-6.

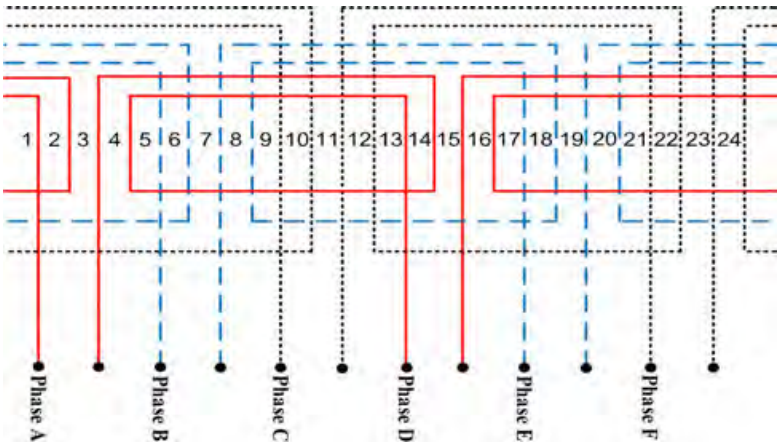

FIGURE 3-5. PMSM6 stator winding.[51]

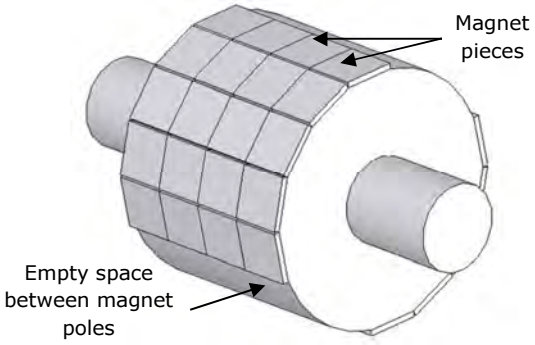

FIGURE 3-6. The rotor of the six-phase PMSM. [51]

The six phases are spaced-shifted by 60°. For the 24 stator slots, 12 coils are used to complete the winding. The phase *A* winding starts in slot 1 and continues in slots 17, 2 and 16.

For the phases *B*, *C*, *D*, *E* and *F*, they are placed in different slots by moving 4/3 of a pole (4 slots pitches). All coils per one phase are connected in series to form one current path.

After the calculation of the magnet's volume, necessary to assure the demanded torque, all the other geometry dimensions have been obtained (based on a similar approach like the one presented into 3.2.1 sub-chapter). The nonlinearity of the magnetic core has been taken into account. For that, the magnetic equivalent circuit of the PMSM6 was drawn, FIGURE 3-7. The advantage of the proposed lumped equivalent circuit is given by the fact that it takes into consideration the armature reaction effect.

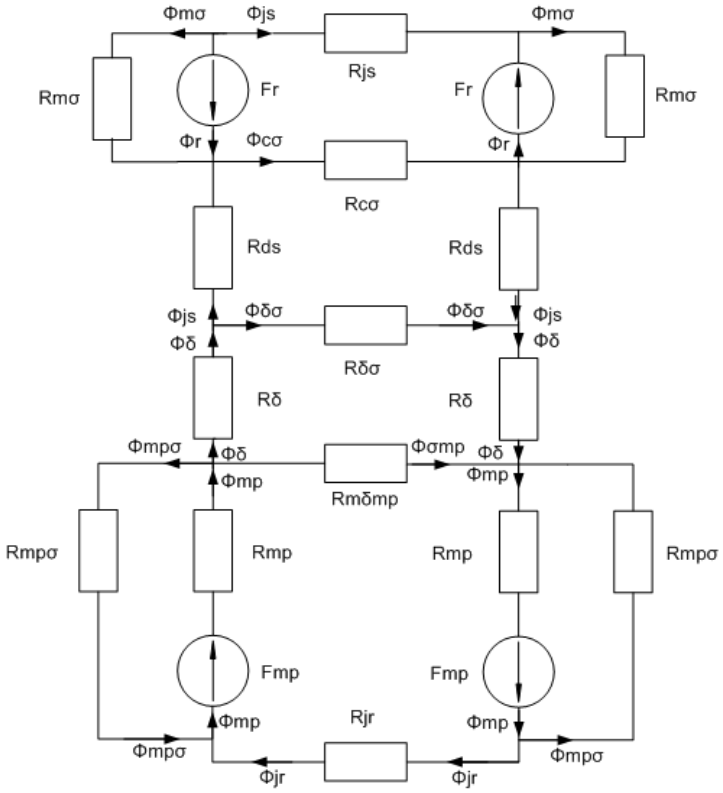

FIGURE 3-7. The PMSM6 magnetic equivalent circuit, with armature reaction. [51]

A magnetic equivalent circuit has one or more closed loop paths, and contains one or more magnetic fluxes. To determine the flux densities in the PMSM6, the coil's magnetomotive force is introduced. The equations (3.40) to (3.50) represent the analytical expression of the magnetic behavior of the studied six-phase PMSM.

$$2 \cdot \boldsymbol{Fmp} + 2 \cdot \boldsymbol{Rmp} \cdot \Phi\boldsymbol{mp} + \Phi\sigma\boldsymbol{mp} \cdot \boldsymbol{Rm\sigma mp} + \Phi\boldsymbol{jr} \cdot \boldsymbol{Rjr} = 0 \quad (3.40)$$

$$\Phi\boldsymbol{mp} \cdot \boldsymbol{Rmp} + \Phi\boldsymbol{mp}\sigma \cdot \boldsymbol{Rmp}\sigma + \boldsymbol{Fmp} = 0 \quad (3.41)$$

$$-\Phi\boldsymbol{c}\sigma \cdot \boldsymbol{R}\sigma\boldsymbol{c} + \Phi\boldsymbol{js} \cdot \boldsymbol{Rjs} - 2 \cdot \boldsymbol{Fr} = 0 \quad (3.42)$$

$$\Phi\boldsymbol{m}\sigma \cdot \boldsymbol{Rm}\sigma + \boldsymbol{Fr} = 0 \quad (3.43)$$

$$2 \cdot \Phi\delta \cdot \boldsymbol{R}\delta + \Phi\delta\sigma \cdot \boldsymbol{R}'\delta\sigma - \Phi\sigma\boldsymbol{mp} \cdot \boldsymbol{Rm\sigma mp} = 0 \quad (3.44)$$

$$2 \cdot \Phi\boldsymbol{ds} \cdot \boldsymbol{Rds} + \Phi\boldsymbol{c}\sigma \cdot \boldsymbol{Rc}\sigma - \Phi\delta\sigma \cdot \boldsymbol{R}'\delta\sigma = 0 \quad (3.45)$$

$$\Phi\boldsymbol{ds} - \Phi\boldsymbol{c}\sigma - \Phi\boldsymbol{r} + \Phi\boldsymbol{m}\sigma = 0 \quad (3.46)$$

$$\Phi\boldsymbol{r} - \Phi\boldsymbol{m}\sigma - \Phi\boldsymbol{ds} = 0 \quad (3.47)$$

$$\Phi\boldsymbol{jr} + \Phi\boldsymbol{mp}\sigma - \Phi\boldsymbol{mp} = 0 \quad (3.48)$$

$$\Phi\boldsymbol{mp} - \Phi\delta - \Phi\boldsymbol{mp}\sigma - \Phi\sigma\boldsymbol{mp} = 0 \quad (3.49)$$

$$\Phi\delta - \Phi\delta\sigma - \Phi\boldsymbol{ds} = 0 \quad (3.50)$$

The following notation was used: Rmpσ – the leakage reluctance of PM; Rmp- the magnetic reluctance of the PM; Rδ – the reluctance of the air-gap; Rδσ – the leakage reluctance of the air-gap; Rds – the magnetic reluctance in the stator tooth; Rjs – the magnetic reluctance in the stator yoke; Rjr – the magnetic reluctance in the rotor yoke; Rmσmp – leakage reluctance between consecutive PMs; Rcσ – the leakage reluctance of the stator slot; Rmσ – the frontal leakage reluctance of the winding; Rdσ – the leakage reluctance of the stator tooth to the air-gap; Fmp – magnetomotive-force of the PM; Fr – the magnetomotive-force of the armature reaction. The Φ parameter refers to the magnetic flux, while the associated indices (i.e., mp, σ, δ, ds etc.) refer to the circuit elements indicated by the specific magnetic reluctances.

The calculated flux density values are presented in Table 3-3.

TABLE 3-3. FLUX DENSITY VALUES OF THE SIX-PHASE PMSM [51]

PARAMETER	*UNITY*	*WITH ARMATURE REACTION*	*WITHOUT ARMATURE REACTION*
Byr	T	0.83	0.982
Bys	T	1.192	1.448
Bt	T	1.117	1.349
Bδ1	T	0.537	0.636

(In the above table, Byr is the rotor yoke flux density, Bys is the stator yoke flux density, Bt is the stator teeth flux density and Bδ1 is the air-gap flux density.)

3.4 The main designing parameters of a SRM

For the SRM, the air-gap flux density is computed function of the magnetic flux and the air-gap's surface. The magnetic flux is obtained by solving the magnetic equivalent circuit (MEC) corresponding to the machine's geometry.

$$B_g = \frac{\Psi_{ps2}}{b_{pS} \cdot l_a} \tag{3.51}$$

where Ψ_{ps2} is the magnetic flux in the air-gap and l_a is the machine's active stack length.

The SRM's mean diameter (the diameter till the half of the air-gap length) is computed as:

$$D_g = \sqrt[3]{\frac{P_{2N} \cdot Q_S \cdot k_\sigma}{Q_R \cdot \pi^2 \cdot \eta_N \cdot k_L \cdot \frac{n_N}{60} \cdot B_{gmax} \cdot \left(1 - \frac{1}{K_{CR}}\right) \cdot As}} \tag{3.52}$$

where, P_{2N} is the output power, Q_R and Q_S are the rotor and stator number of poles. The coefficients k_σ and k_L consider the leakage flux in aligned position of the poles, respectively the aspect factor as ratio of the machine's main dimensions. The machine's efficiency and its rated speed, respectively the electrical loading are all taken into account in the mean diameter's computation. The Carter factor (K_{CR}) is commonly used when designing reluctance machines.

Having the mean diameter computed, the stator and rotor pole pitch can be calculated.

$$\tau_R = \pi \cdot \frac{D_g}{Q_R} \tag{3.53}$$

The stator pole width is considered half of the stator pole pitch, this in order to avoid increased saturation producing overheating of the machine.

$$b_{pS} = \frac{\tau_S}{2} \tag{3.54}$$

The same concept of design is applied to the rotor poles. Both the rotor and stator yoke's height are considered equal, representing 80% of the stator pole's width.

Sizing the coils represent other important step. The number of turns per pole are computed function of the air-gap width (g), the leakage flux factor, the maximum air-gap flux density (Bgmax), the air's permeability (μo) and the rated current (I).

$$b_{pS} = \frac{\tau_S}{2} \tag{3.55}$$

Knowing the number of turns per pole and the imposed current density, the coils can be easily designed in order to finalize the sizing of the stator pole slot opening to fit the winding.

Having all the dimensions of the machine computed, the magnetic equivalent circuit (MEC) of the machine can be designed and computed. Using such circuits, in each region of the machine the magnetic flux, respectively the flux density can be computed.

To calculate the machine's developed torque, a formula that considers the MMF and the mean diameter of the machine is used.

$$T_{SRM} = \left(N_f \cdot I\right)^2 \cdot \frac{D_g - g_x}{2} \cdot \mu_0 \cdot \frac{l_a}{g} \tag{3.56}$$

The losses of the SRM consist of iron loss (hysteretic loss and eddy current loss), winding loss and mechanical loss. The hysteretic and eddy current losses are computed function of the flux density of each region of the machine, and only a numerical approach, based on finite element method) will give us an appropriate estimation for such losses. On the other hand, the copper and mechanical losses can be computed in a similar manner, like the one presented for the PM machines in subchapter 3.2.2.

The main data and performances of the designed SRM are shown in Table 3-4. (More results, from the numerical analysis, will be presented in the 3.5.3 subchapter).

TABLE 3-4. THE PARAMETERS OF THE DESIGNED SRM

PARAMETER	*VALUE*	*UNIT*
Supplying voltage (U_N)	24 V	V
Imposed current (I)	80 A	A
Output power (P_{2N})	1.2k W	W
Rated torque (T)	3.4Nm	Nm
Rated speed (n_N)	3200 r/min	r/min
Number of stator teeth (Q_s)	8	-
Number of rotor teeth (Q_R)	6	-
Height of the stator tooth (h_{pS})	17	mm
Height of rotor tooth (h_{pR})	8.2	mm
Height of stator yoke (h_{jS})	7	mm
Height of rotor yoke (h_{jR})	7	mm
Width of stator tooth b_{pS}	10	mm
Width of rotor tooth (b_{pR})	11.5	mm
Active stack length (l_S)	80	mm
Air-gap length (g)	0.1	mm
Outer machine diameter (D_m)	115	mm
Motor's efficiency (η)	84	%

3.5 The analytical approach validation based on Finite Element Analysis

The analytical approach is intrinsically limited because it is based on several simplified hypothesis. Moreover, the precise calculation of the magnetic flux distribution within the machine's active parts and the electro-magnetical and mechanical parameters are very difficult to be evaluated. Mathematical methods, based on vector potential expressions, are very difficult to be employed. In order to facilitate the analysis of the electrical machine, many numerical solutions based on finite element method (FEM) were developed.

Some results from the FEM analysis were presented previously, in 2.4 subchapter, showing that the complex magnetic state of the machine and its dynamic behavior can be evaluated only with suitable software. One of the software package dedicated for the analysis of such machines, giving good results even when the control through the power converter was considered, is the Flux2D software.

3.5.1 FEM analysis of the RF-PMSM by using Flux2D software

The FEM analysis is realized for the validation of the analytical approach. Even if it is time-consuming, the FEM analysis offers trustfully performances' evaluation. Details on using this analysis in the Flux2D software are presented in [52]. Here, the main steps of the analysis will be presented. Firstly the geometry of the machine should be drawn. The mesh is associated to the machine's geometry. Next, the active parts are identified and specific regions name are assigned. The materials of the active parts are associated to the created regions. The physical application is defined by considering: the type and the dynamics of the simulation, the length of the machine, the boundary conditions and the possible load. Furthermore, the electric circuit, the supplying source and the association with the electric components or switches is made. If the application is correctly introduced, the next step is to solve it and to evaluate the electro-magnetic and mechanical performances. The steps of the FEM analysis are depicted here:

- *Geometry* (drawing the structure of the RF-PMSM).
    - Defining the reference system, the units and the periodicity or the symmetry conditions.
    - Defining the geometric parameters (even electric parameters can be considered, in order to control the application).
    - Defining the points, lines and building faces for drawing the geometry of the machine.
- *Mesh* (establishing the discretization of the network on which the vector potential is computed).
    - Defining the mesh points/lines and their association to the geometry's elements.
    - Associating the mesh elements to the discretization network and mesh building.
- *Physics* (establishing the application's parameters).
    - Defining the type of the application (electrostatic, magnetic or thermal) and dynamics (static or dynamic simulation) of the problem.
    - Defining the study domain (the machine's length and the boundary conditions, based on periodicity or symmetry).
    - Defining the specific name of the regions to be created and their association to the parts of the machine.
    - Defining the materials to be used and their association to regions.
    - Defining the magnetic orientation of the materials – in case of using permanent magnets.
    - Defining the electric circuit or the current sources to be used in the application and their association to the defined regions.

- Defining the mechanical properties of the application.

- *Solving* (solving the problem).
  - Defining the simulation conditions and the possible parameterization of the geometry or current sources.
- *Results* (evaluating the performances of the problem).
  - Computing the performances of the studied machine and their evaluation.
  - Validating the obtained electromagnetic and mechanical results.

The RF-PMSM was analyzed on Flux2D software and the electromechanical behavior was verified. The first result taken into consideration is the magnetic field lines within the active and non-active parts of the machine FIGURE 3-8. The possible mistake on magnets definition or current supply can be identified here. Also, the leakage flux can be seen (for example, in FIGURE 3-8 we can see the PM, the slot and the isthmus leakage flux).

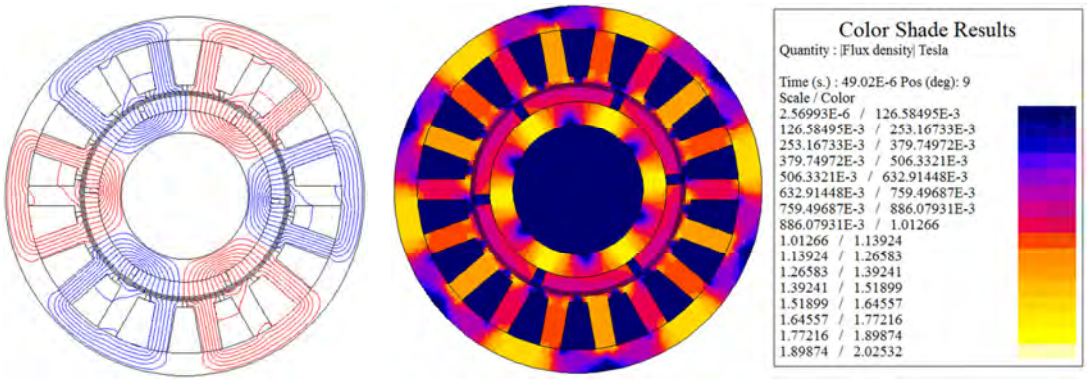

FIGURE 3-8. Field lines (left) and flux density (right) within the active parts of the studied RF-PMSM. [1]

Another very important parameter which is vital in establishing the machine's performances is the flux-density distribution within the active parts of the machine. The saturation level can be observed on FIGURE 3-8 too. For the studied machine (the one which was designed in 3.2) a maximum value of 2.025 T was found, which is acceptable for our application.

Another parameter which is evaluated is the air-gap flux density. From FIGURE 3-9 it can be said that the flux density varies between 0.58 T and 0.91 T. The effect of the slotted stator is obvious also.

Starting from the air-gap flux density, the other performances can be evaluated. Firstly, the axis torque is shown in FIGURE 3-10. The average torque of 3.42 Nm is obtained with purely sinusoidal current injected in the machine, see FIGURE 3-11. From FIGURE 3-10 it can be said that the torque ripples are quite high, 28.9%, thus affecting the machine's control dynamics. A solution to reduce the torque ripples is to skew the armature with a tooth pitch angle. This will slightly affect the torque level, but if the desired value is obtained we could consider it as an option.

The evaluation of the iron loss is made based on plotted curves given in FIGURE 3-12. The average stator iron loss is of 27.8 W at the stator yoke, and 25.7 W on the stator teeth. For synchronous machines the rotor iron loss is usually neglected (the rotor rotates synchronously with the armature field), but for the sake of comparison the rotor iron loss is given in FIGURE 3-12. An average of 1.84 W was found, which is very little in comparison with the stator iron loss.

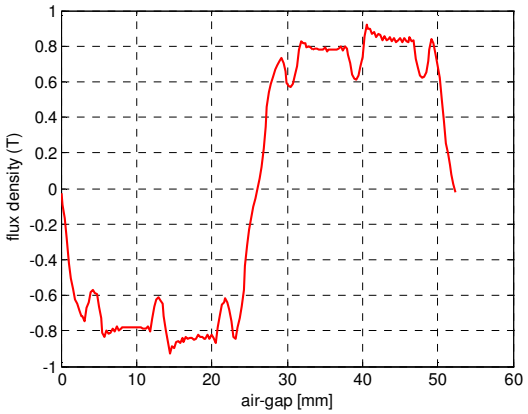

FIGURE 3-9. Air-gap flux density of the RF-PMSM. [1]

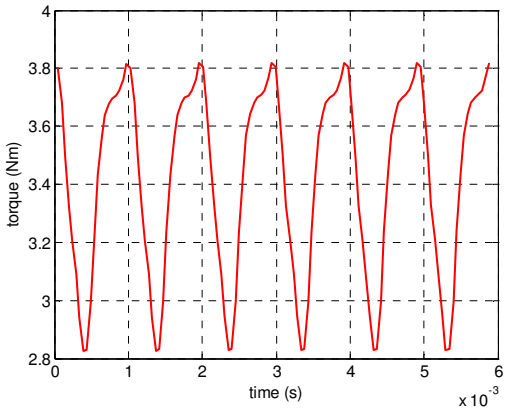

FIGURE 3-10. Torque of the studied RF-PMSM. [1]

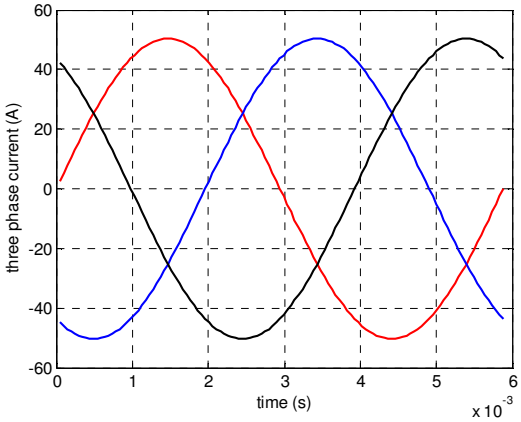

FIGURE 3-11. Three phase sinusoidal currents injected into the winding of the RF-PMSM. [1]

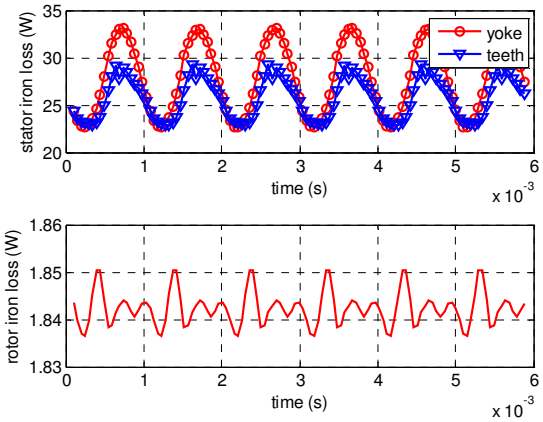

FIGURE 3-12. Iron losses within the active parts of the studied RF-PMSM. [1]

As stated before, the FEM analysis is made to validate the analytical approach. In Table 3-5 are given the main performances comparison. Here are given the variation limits of the flux density from the FEM analysis; the average value is below the analytical obtained one. This explains the fact that the iron loss from FEM is smaller, meaning an improved efficiency. We can observe that in the numerical analysis the results are sensitively improved. This can be explained by the fact that in the analytical approach the flux densities are estimated to be constant in the entire machine's active parts, while the FEM analysis expresses more realistic the flux density distribution, with some parts being saturated, and some other parts having very reduced value (see FIGURE 3-8).

TABLE 3-5. FEM - ANALYTICAL RESULTS COMPARISON FOR THE STUDIED RF-PMSM [1]

PARAMETER	*ANALYTICAL*	*FEM (MIN-MAX)*	*UNIT*
Rated torque	3.37	3.42	N·m
Flux density air-gap	0.74	0.58 – 0.9	T
Flux density on tooth	1.81	0.01 - 1.72	T
Flux density on stator yoke	1.65	0.0002 – 1.76	T
Flux density on rotor yoke	1.56	0.09 – 2.02	T
Iron loss in the stator yoke	34.89	27.8	W
Iron loss in the teeth	35.71	25.7	W

3.5.2 AF-PMSM results based on the Flux2D to Simulink coupling technology

Sometimes the dynamic behavior of an electrical machine cannot be simulated if we do not consider a proper control. Moreover, the switching effect, while the machine is supplied via a static converter, could influence drastically the machine's behavior. Such phenomena can be evaluated by coupling software: the *Flux2D*, where the machine is drawn, and *Simulink*, where the converter and control logic are employed.

In order to prove the implementation of the method, we will consider the study of the AF-PMSM. It is true that this type of machine is of 3D type, and the coupling technology is only possible with 2D geometries. But the 3D structure of the AF-PMSM can be seen, for simplicity, like a 2D machine [70]. After applying the design process, we have obtained the main geometry parameters based on which we have drawn the 3D geometry of the AF-PMSM, FIGURE 3-13. Also, the rated point operation parameters are given in Table 3-6.

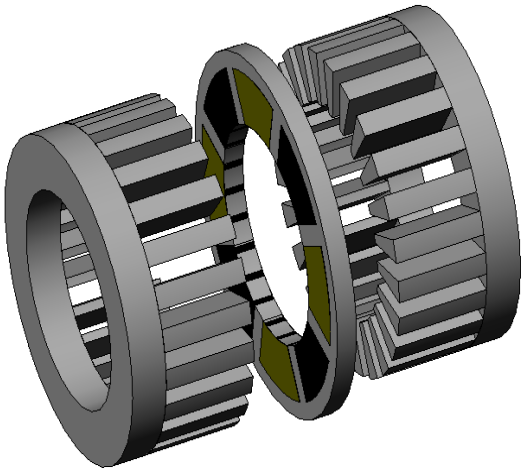

FIGURE 3-13. The 3D geometry of the AF-PMSM.

TABLE 3-6. THE PARAMETERS OF THE DESIGNED AF-PMSM

PARAMETER (UNIT)	*VALUE*
Output power (W)	1200
Rated speed (r/min)	3400
Rated torque (N˙m)	3.4
Battery voltage (V)	24
Number of phases (-)	3
Number of pole pairs (-)	4
Number of slots (-)	24
Outer diameter (mm)	85
Machine length (mm)	93.4
Airgap length (mm)	0.5
Airgap flux density (T)	0.63
Phase resistance (Ω)	0.03
Phase emf (V)	10.31
Rated current (A)	28
Losses (W)	182
Power factor (%)	0.81
Efficiency (%)	0.89
Active part costs (€)	47
Active part weight (kg)	3.5

In order to have a more comprehensive comparison between the analytical and numerical results and for a better accuracy, the other results were obtained in Flux2D. The studied AF-PMSM has been modeled as a RF-PMSM by means of 2D FEA at the geometric mean radius [70].

The magnetic flux density map in the cross-section of the machine is presented in FIGURE 3-14a. For no-load regime, the air-gap magnetic flux density distribution is depicted in FIGURE 3-14b, giving an average value of 0.68 T. The 2D FEA of an Axial Flux Machine is enough accurate for power, voltage and cogging torque calculation, but for determining the iron losses, 3D-FEA should be used [70]. The iron computation gave the following results, see FIGURE 3-14c.

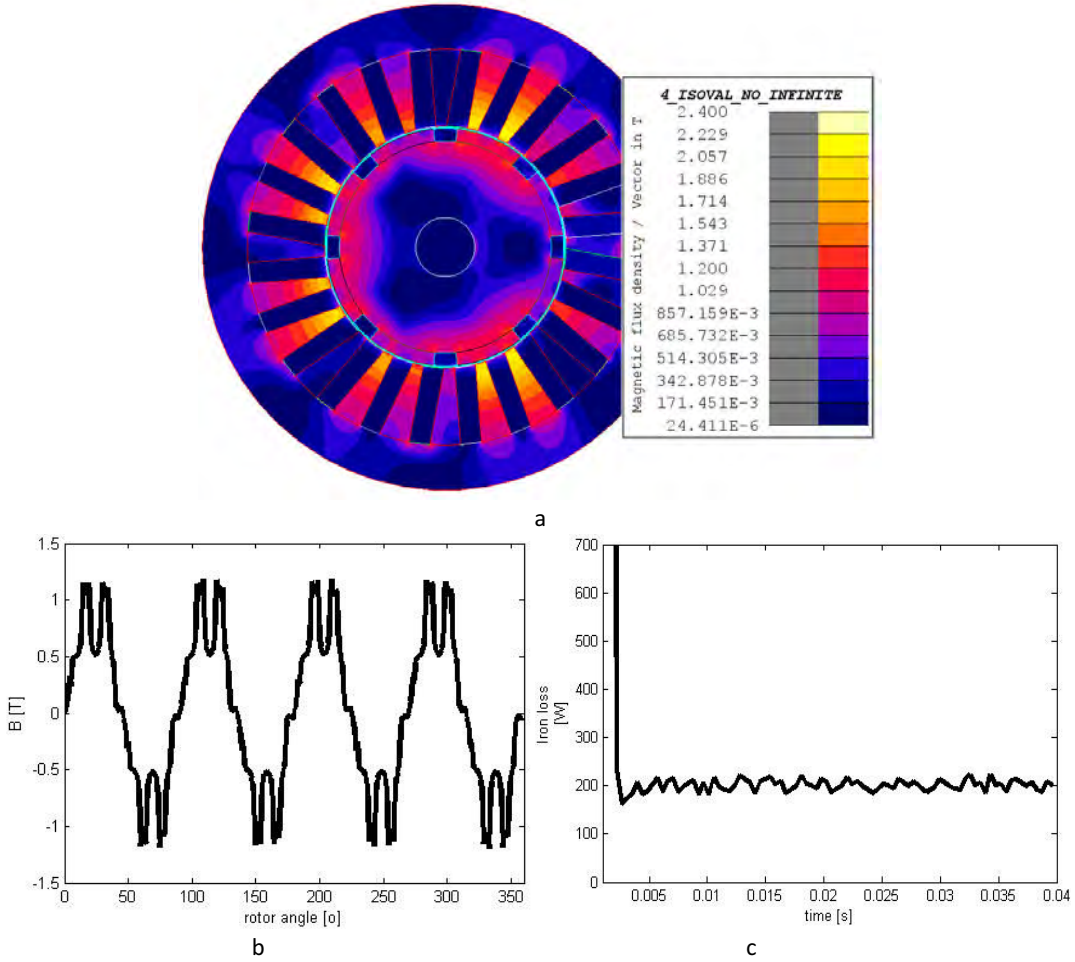

FIGURE 3-14. AF-PMSM result from FEM analysis:
a) flux density repartition; b) air-gap flux density; c) iron loss.

The transient regime simulation of the entire electrical drive system (the machine and its converter) was performed using the latest coupled simulation technique, the FLUX-to-Simulink link. This technology seems to be the most advanced tool for system designers, because it provides co-simulation capabilities for transient electromagnetic computations with a direct link to the finite element method (FEM) based model. It enables the users to account for drive and control parts within the device.

The FLUX to SIMULINK Technology combines the abilities of MATLAB Simulink for drive and control and the power of FLUX for transient electromagnetic computations. Using this link it was taken advantage of the high precision machine analysis capabilities enabled by the FLUX 2D FEM based numeric field computation program and easy-to-use, but also advanced Simulink/MATLAB environment, see FIGURE 3-15.

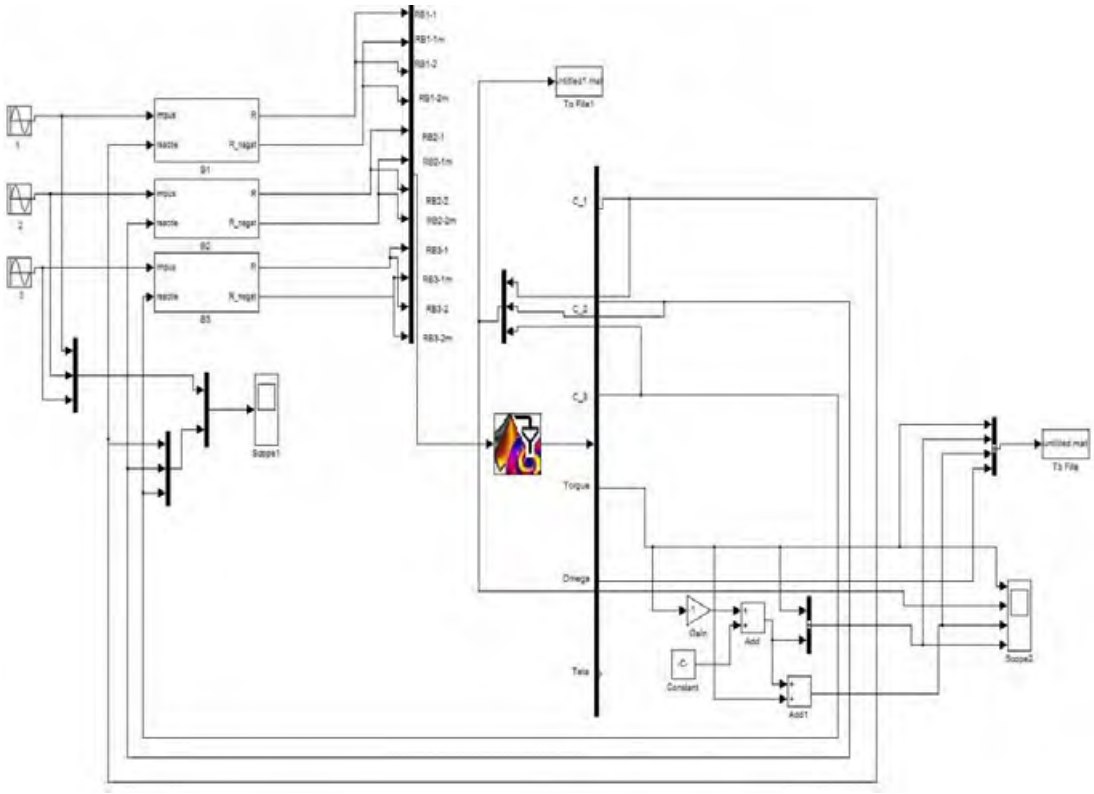

FIGURE 3-15. The Flux2D-Simulink coupling simulation implementation for the studied AF-PMSM.

The coupled simulation was performed at low time step in order to obtain accurate results. Hence the required simulation time should be very long. To reduce it, an optimized mesh of the machine's model in Flux 2D was imposed. This way a compromise between the simulation time and the required computer memory, respectively the precision of the results was obtained.

As the computer memory is limited to its physical value, the mesh quality had to be set for a lower value, but not to reduce significantly the accuracy of the computations. The model of the electric circuit of the power converter was build up in Flux2D is shown in FIGURE 3-16, and the main simulated results are shown in FIGURE 3-17.

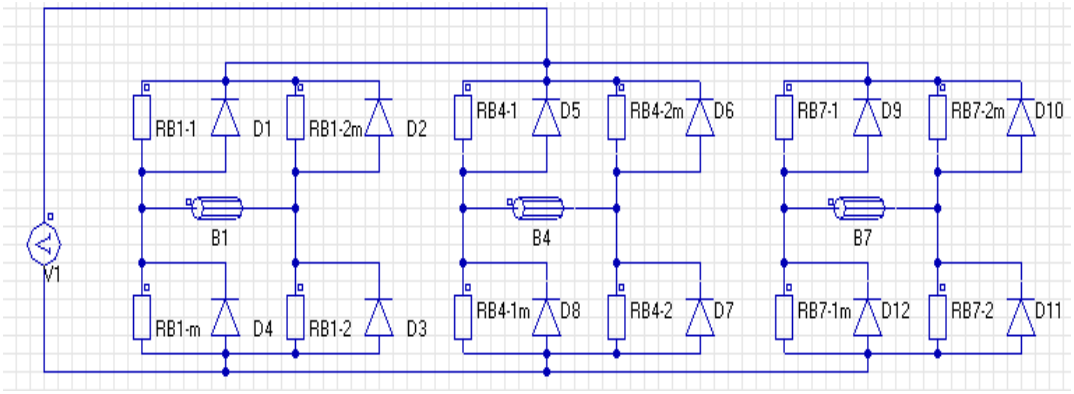

FIGURE 3-16. The Flux2D-Simulink coupling simulation implementation for the studied AF-PMSM.

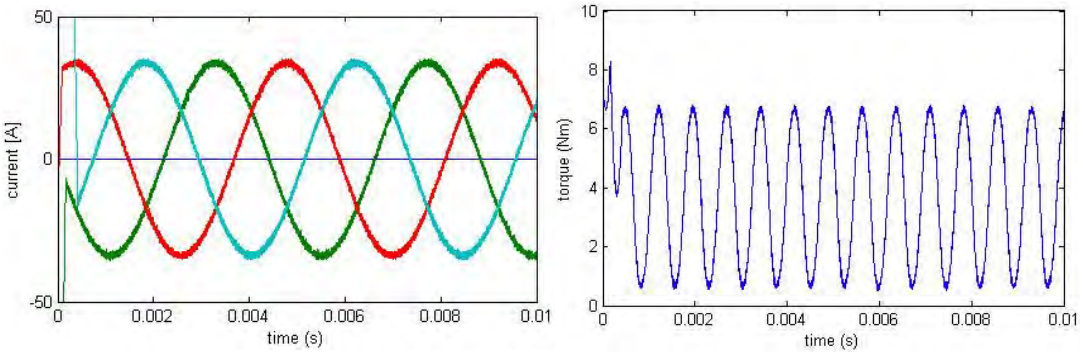

FIGURE 3-17. The commutated injected current (left) and the simulated torque (right) for the AF-PMSM.

The inverter, in the simulation model (the H bridge configuration was considered) needs to be made of resistors, to which we will consider the OFF state for a high value of the resistance (1e6), and the ON state for a reduced value of the resistance (1e-6) [52].

Because of the poor quality of the torque wave, we were trying to find a solution to reduce the torque ripples. Theoretically, skewing the stator or rotor core might produce very smooth torque wave. For that, we have analyzed the AF-PMSM with the Flux/Skewed computation module.

The geometry of the AF-PMSM-8/24 was drawn in 2D and after that we have considered an angle of incline of 1 slot (360/24=15°). The flux density repartition within the skewed AF-PMSM is shown in FIGURE 3-18-left. The effect on the inclined armature can be verified on the torque wave, in FIGURE 3-18-right. The torque varies now between 3.29 and 3.41, meaning that the torque ripples are of 3.58%! This is an important decrease of torque ripples. This gain can be decisive while preparing the control of the AF-PMSM.

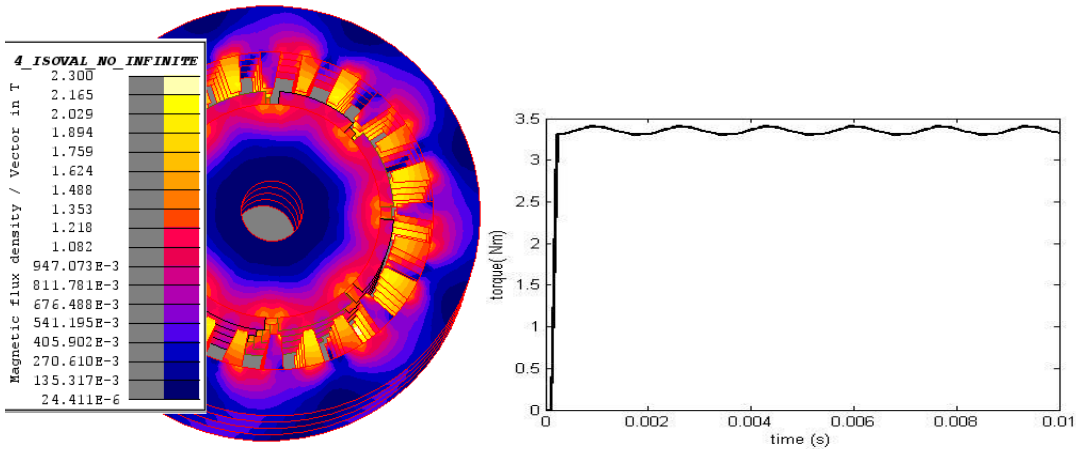

FIGURE 3-18. The skewed geometry of the 2D-AF-PMSM (left) and the simulated torque (right).

3.5.3 SRM simulated results based on the Flux2D-Simulink analysis

This analysis is realized for the SRM presented in 3.4. Considering that the machine is supplied at 80A, it is important to analyze if the currents is able to reach this value at rated speed, considering the inductance of the machine's phase. In this case, the tune ON angle has to be quite low, in order to start conducting and leave "space" for the current to increase close to 80A while the inductance of the phase is still very small.

The FEA model of the machine was implemented in Flux2D, considering a full geometry design. In order to do a hysteresis control of the currents in the phases of the machine, function

of the rotor position, the Flux2D model was coupled with Matlab/Simulink, accomplishing this way a time step based simulation.

The simulation results prove that the machine was well designed and the first observation is that no over-saturation of the core occurs in the SRM.

As it can be seen in FIGURE 3-19-left, the flux lines are closing diametrically through the rotor. In the same rotor position, the flux density distribution in the machine's core is displayed FIGURE 3-19-right. As stated previously, the stator yoke has to be saturated enough to ensure fast current fall at the end of each switching period. It can be seen that the saturation of the magnetic core is in acceptable intervals. The most severely saturated regions of the machine are the stator and rotor poles towards the air-gap - a normal phenomenon for the SRMs, in general.

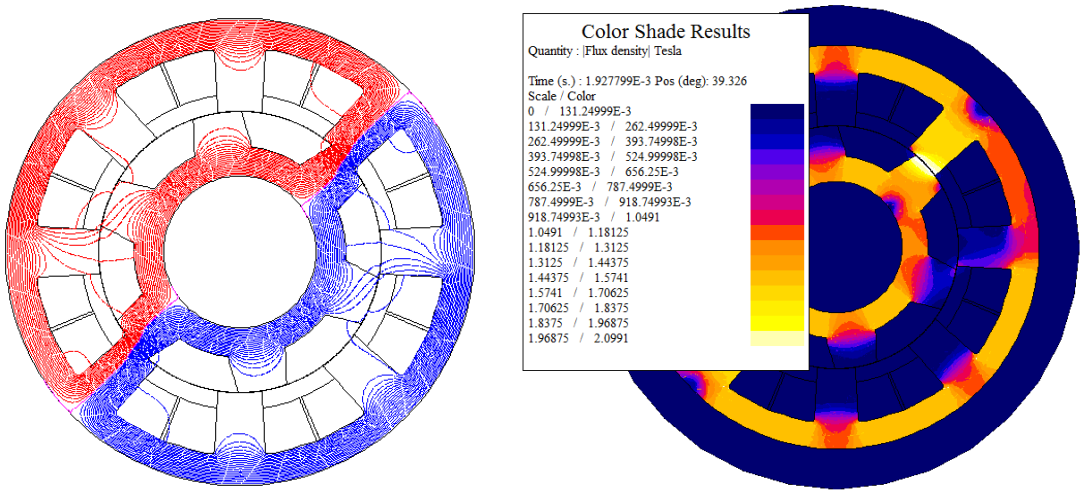

FIGURE 3-19. Field lines (left) and flux density (right) within and the active parts of the studied SRM.

Analyzing the overall flux density distribution, the machine is well balanced and the values do not exceed any maxima that a SRM cannot handle.

In FIGURE 3-20-left all the currents of the 4 phases of the machine are plotted. The current rated value is at 80A. The tail of the current, during OFF state of the power switches is quite long due to increased inductance of the phase in aligned position. This is a drawback of operating a machine at such high currents. In FIGURE 3-20-right, the electromagnetic torque developed by the machine is depicted. The developed torque reaches de desired mean value of 3.4 Nm.

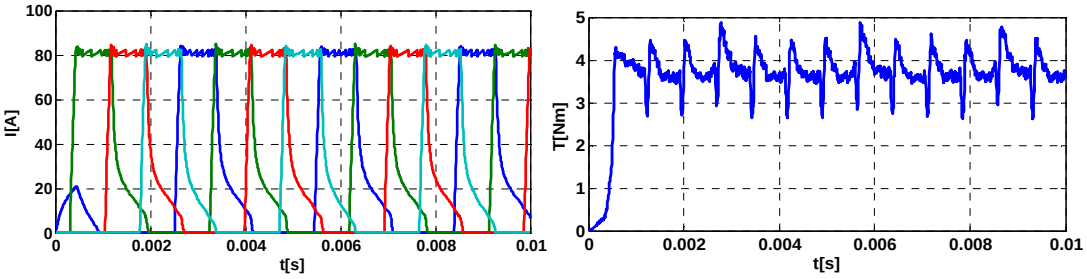

FIGURE 3-20. The four phase currents (left) and the torque wave (right) of the studied SRM.

4 THE OPTIMIZATION OF THE EV'S MOTORIZATION

4.1 Framework and summary of main results

This chapter presents the author's activity research with respect to the algorithms used or developed for the optimization of the EV's motorization. This topic has been employed in several collaborations with colleagues from UTBM or, lately, with Associated Professor Lhassane IDOUMGHAR from *Université de Haute-Alsace* (UHA), Mulhouse-France. At UHA the author has made two visits and he has been once *invited professor*:

- Research mobility at UHA, *Laboratoire de Mathématiques, Informatique et Applications* (LMIA) within the 4D-POSTDOC postdoctoral research program, subject MOEVEHU: from 20 January to 10 February 2011.
- Research mobility at LMIA within the 4D-POSTDOC postdoctoral research program, subject MOEVEHU: August 2012.
- Invited professor at UHA-LMIA, May 2013.

The collaboration with the French colleague, Lhassane Idoumghar, dates from 2009, while the author was Associated Professor at UTBM. From that moment to now (and even before that date), several articles, related to the optimization topic, were published:

- D.Fodorean, L.Idoumghar, and L.Szabo, "Motorization for electric scooter by using permanent magnet machines optimized based on hybrid metaheuristic algorithm", IEEE Transaction on Vehicular Technology, vol.62, n.1, pp.39-49, January 2013.
- D.Fodorean, L.Idoumghar, A.N'diaye, D.Bouquain and A.Miraoui: "Simulated Annealing Algorithm for the Optimisation of an Electrical Machine", IET Electric Power Applications, vol.6, n.9, pp.735-742, November, 2012.
- L.Idoumghar, D.Fodorean and A.Miraoui: "Using Hybrid Constricted Particles Swarm and Simulated Annealing Algorithm for Electric Motor Design", Proceedings of the 14th Biennial IEEE Conference on Electromagnetic Field Computation, Chicago, Illinois, USA, May 2010.
- L.Idoumghar, D.Fodorean and A.Miraoui: "Simulated Annealing Algorithm for Multi-Objective Optimization: Application to Electric Motor Design", Proceedings of the 29th IASTED International Conference: Modeling, Identification and Control'10, Innsbruck, Austria, February 2010, pp.190-196.
- S.Giurgea, D.Fodorean, G.Cirrincione, A.Miraoui, M. Cirrincione: "Multimodel Optimization Based on the Response Surface of the Reduced FEM Simulation Model With Application to a PMSM", IEEE Transactions on Magnetics, vol.44, n.9, pp.2153-2157, Septembre 2008.

4.2 The optimization topic related to the electrical machines

When thinking to an **optimization problem** we have in mind mainly the **minimization of a parameter**, or of a function which depends on several parameters. This is called **objective function**. If only one parameter should be minimized (optimized), it means that we have a **mono-objective problem**. If several parameters need to be minimized, a series of priorities need to be defined for these parameters (which usually interact to each other) and we have to solve a **multi-objective problem**. To reach the objective function, the designer needs to impose the space of available solutions in which the objective function is searched. This solutions space is defined by the designer, when establishing the variation intervals of specific parameters. These

specific parameters are the ones that affect mainly the objective function. Moreover, several constraints can be considered, especially when dealing with a multi-objective problem.

Mathematically, the optimization of a multiobjective problem can be written as:

$$\begin{cases} minimize_x \ [f_1(x)]^T \\ s.t. \\ g_j(x) \le 0 \quad j = 1,\dots,p \\ h_l(x) = 0 \quad l = 1,\dots,q \end{cases} \tag{4.1}$$

where:

- x: vector of n decision variables;
- f_i: the i^{th} objective function;
- g_i: the i^{th} of p inequality constraints;
- h_i: the i^{th} of q equality constraints.

A function which needs to be optimized could have the variation presented in FIGURE 4-1. Here, we can distinguish a local minimum and a global minimum. When searching to optimize a parameter (a function), we are interested in finding its global minimum, not just a local one. Moreover, a function could have more local minima. Thus, obtaining the global minimum will be very difficult, or practically impossible. This limitation of the optimization algorithm comes mainly from itself. If it is a linear optimization algorithm, like the gradient type, being trapped in a local minimum is very possible. A good optimization algorithm should permit to avoid being trapped in a local minimum, and this is usually obtained with genetic or evolutionary type algorithms.

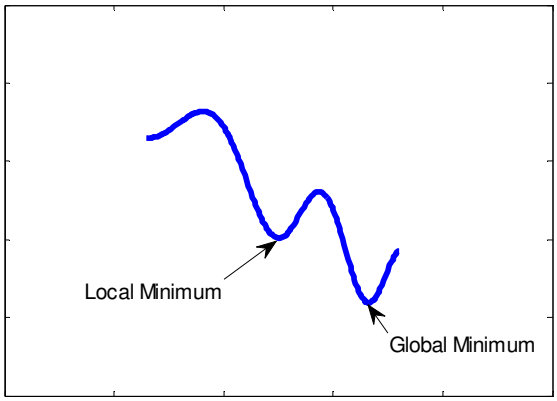

FIGURE 4-1. Sample of variation of a function that needs to be optimized.

Regarding the particular case of an electrical machine (EM), its optimization refers mainly to the minimization (decrease) of the weight of the machine, while keeping the output power at the desired level. In other words, when optimizing an electrical machine we need to increase its power density, meaning the ratio between the output power and the mass of the active part. It is important to keep the power at the desired level, because we need that the machine responds to the applications demands. In the previous phrase we have stated:

- the **objective function**=minimizing the mass of the EM;
- **a constraint**=keeping the power at the desired level.

Beside these two parameters we need to define **the solutions space**, imposed by the variation of the parameters which are mainly affecting the objective function.

Supplementary constraints could be added here, like, for example, the limitation of the current; no current increase is accepted because we do not want to increase the copper loss, which will decrease the efficiency. We could consider other constraints related to the energetic parameters (power factor and efficiency), which should be increased or kept at the same level. But most of all we are looking to obtain the best power density. This is true since:

- Keeping the current level or decreasing it (for the desired power), will maintain or increase the power factor;
- The efficiency is affected by the losses, which can be reduced if the machine's active part is reduced. (Remember that the iron loss is proportional with the frequency, flux density and the volume of the machine. Since the frequency is fixed, we can act only on the machine's volume, by reducing its mass, while avoiding the partial saturation of the machine. Again, since the mechanical loss is proportional with the volume of the machine, this means that by decreasing the machine's mass we will decrease the mechanical loss.)

In conclusion: **when thinking to the optimization of an EM, we want to reduce its mass, by keeping the desired torque**. And this is a mono-objective optimization problem.

The optimization of an electrical machine is a very important task in the designing process of the EV's motorization because:

- Permits the increase of the machine's power density, which has a direct influence on EV's autonomy, since a lighter machines will spear the life time of the battery;
- Depends directly on the designer, who has realized the designing process, and who has established the main parameters which are influencing the objective function and their variation limits - this means that a poor design will not produce better results;
- Choosing the right (or appropriate) optimization method will influence directly the optimization results.

When speaking about the last task, we should think to the complexity of the method, its limitation, the implementation time, the capacity to avoid local minimum[6] and the capacity to reach the global minimum[7].

The classification of the existing optimization methods is presented in the diagram below, FIGURE 4-2, [71].

The author, based on different research cooperation, has tested and evaluated several approaches found on the scientific literature. These ones are emphasized in FIGURE 4-2, meaning: gradient type, evolutionary and hybrid algorithms. Some of the results are presented in the next subchapters.

4.3 Optimization methods used for the studied electrical machines

4.3.1 SRM's optimization based on gradient type algorithm

The first optimization approach, used for the designed machines, was the Hook-Jeeves algorithm, [72]. The advantage for this algorithm is its simplicity, easily to be employed, it converges rapidly. On a contrary, it cannot avoid the local minimum, being limited to simple problems. In order to shown its capability, the algorithm was employed on a 350W SRM [73].

Here, only the main steps in the optimization algorithm are given:

[6] The local minimum it is not the best solution that can be reached; the algorithm can be trapped in such points – this is happening for the gradient type optimization algorithms, because this algorithm, when reaches a minimum value, search in the nearest space and it stop searching if the next value is not better than the previous one.

[7] The global minimum is "zero"; only rarely can be achieved, but there are some optimization algorithms which, when reaching the local minimum, they can avoid it and start to look in the solution space for the global minimum.

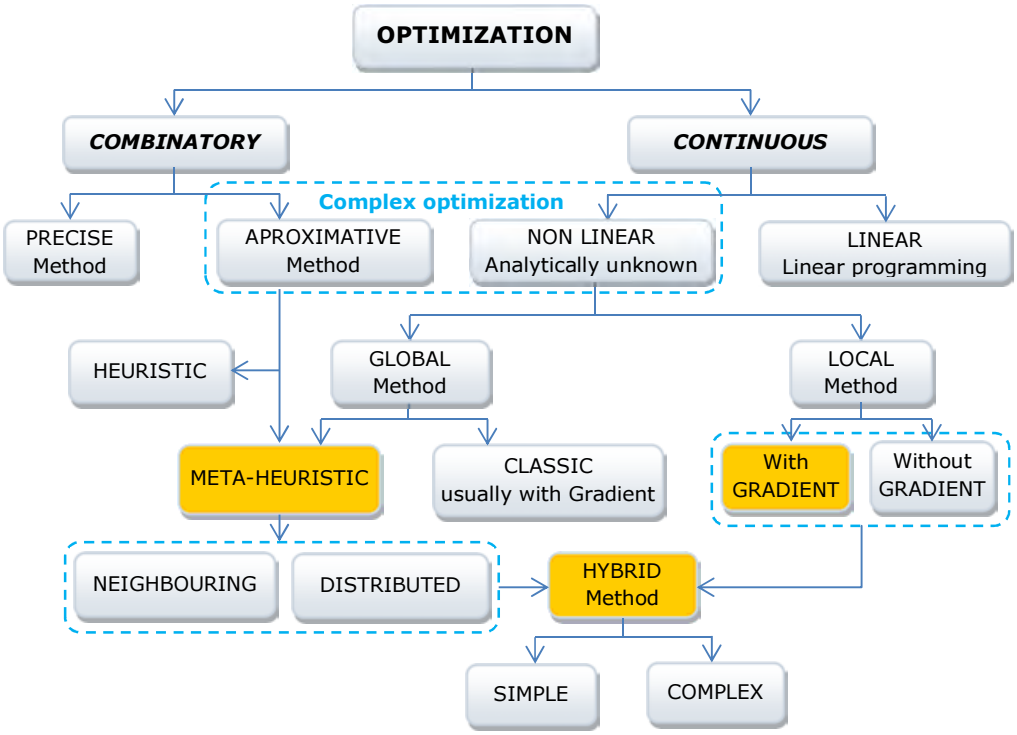

FIGURE 4-2. Optimization methods classification, of mono-objective type.

Step1. Choose the optimization variables (starting value and boundaries are imposed.)

Step2. Impose special limitations to other variables which can be altered during optimization process.

Step3. Define the objective function.

Step4. Set initial-final value of global increment. The objective values will be initially modified with larger increment, which will be further decreased, to refine the search space.

Step5. Compute geometrical dimensions, the electromagnetic parameters, the characteristics, and evaluate the objective function.

Step6. Make a movement in the solution space and recomputed the objective function and its gradient. Use partial derivative to find the worse and the track points.

Step7. Move to the better solution, while the objective function is decreasing.

Step8. Reduce the variation step and repeat the previous steps. The algorithm stops when the research movement cannot find better points, even with smallest variation step. The found value represents a local minimum; a different value can be found by changing the starting point.

The goal of the optimization process is to maximize the power/weight ratio; so, this is our objective function. The parameters which will be varied, while the optimization is employed, are: the length of the machine (la), the air-gap diameter (Dg), and the rotor and stator poles width (bpr and bps, respectively). The objective function evolution is presented in FIGURE 4-3. The evolution of geometric parameters (FIGURE 4-3a) involves the variation of energetic performances (FIGURE 4-3b), of the objective function (torque density, FIGURE 4-3c). The desired torque and power are reached with an optimum geometric configuration for which the aforementioned parameters play the most important role in affecting the objective function.

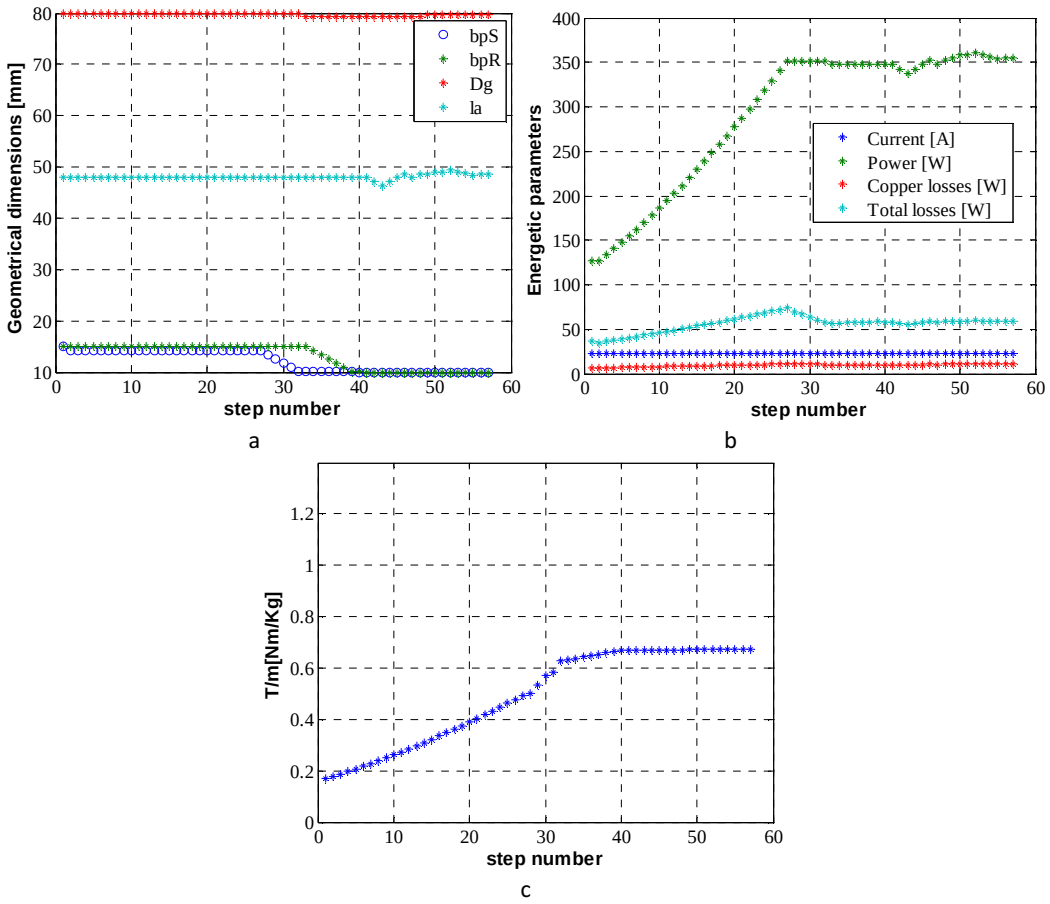

FIGURE 4-3. Parameters evolution in the optimization of a 350W-SRM. [73]

4.3.2 Radial-Flux PMSM optimization based on Response Surface method

The Response Surface (RS) optimization approach was applied to a PMSM, with ferrite magnets placed on the rotor to get the flux concentration [74].

Usually, in the design process some physical assumptions are made in order to have simple algebraic equations. With this regard, a higher accuracy can be obtained by using a model with the help of the numerical FEM, which takes into account the complexity as well as the multi-physical character of the EM. On the other hand, FEM based optimization has the drawback of requiring too much computing time for evaluating the objective function for each set of structural parameters. This seems to be incompatible with the large number of model parameters, which exponentially increases the number of objective function estimations. To overcome this drawback here it is proposed a unifying optimization methodology for improving the optimal design developed with the help of the analytical model, whereby a new simplified response surface is proposed to substitute the FEM model in the optimization algorithm. The existent models usually take into account only the significant parameters for the FEM model, but the proposed study is based on a reduced model obtained through the selection of the parameters with the greatest influence on the value of the error between the FEM and the analytical model. Also, it will be depicted that together with this selection method the obtained results are improved through the moving least squares (MLS) approximation.

4.3.2.1 The Algorithm

The proposed algorithm is presented in FIGURE 4-4, where are considered two functions of *n* parameters, which model the EM: an analytical model and a second model of FEM type [71]:

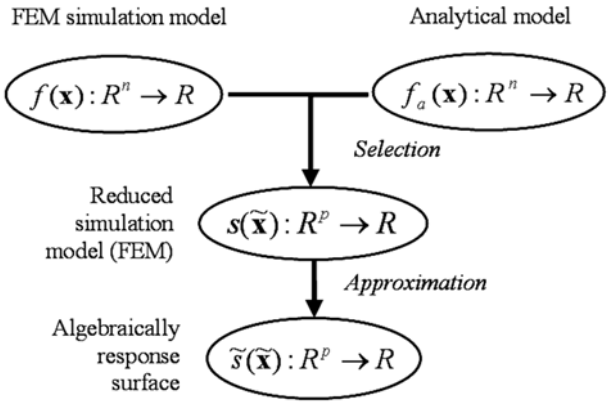

FIGURE 4-4. Creation of response surface. [71]

The analytical model provides an objective function $\boldsymbol{f_a(\mathbf{x}): R^n \to R}$, where $\mathbf{x}$ is the vector of parameters defined in the feasibility domain $\overline{\boldsymbol{D}}$ represented by simple algebraic equations. This simple model demands small computation time and it is therefore suitable for determinist and stochastic optimization algorithms, which solve for the following problem: $\mathbf{x}_a^* = \{\min \boldsymbol{f_a(\mathbf{x})} \mid \mathbf{x} \in \overline{\boldsymbol{D}}\}$.

The FEM model is more accurate and is for modeling the EM, providing an objective function $\boldsymbol{f(\mathbf{x}): R^n \to R}$. The high computation time demanded by this method limits the number of estimations of the objective function.

In the proposed algorithm the employed response surface, which will substitute the objective function, is based on the two following steps, summarized in FIGURE 4-4.

1st STEP: select the parameters $\tilde{\mathbf{x}}$ which present a significant interest for a subsequent optimization based on FEM simulation. The original FEM simulation model of *n* parameters $\boldsymbol{f(\mathbf{x}): R^n \to R}$ is transformed into a reduced simulation model with *p* parameters, $\boldsymbol{s(\tilde{\mathbf{x}}): R^p \to R}$ by choosing the significant parameters for an additional optimization. The selection method (a multi-model approach) uses both, the analytical and the FEM model.

2nd STEP: The reduced simulation model is replaced by a pure algebraically response surface model $\boldsymbol{\tilde{s}(\tilde{\mathbf{x}}): R^p \to R}$ (polynomial approximation). Different approximation techniques could be employed, such as:

- The Least Squares (LS) polynomial regression which generates a response surface on a minimal set of data simulations [75].

- The Moving Least Squares method (MLS) which is based also on the polynomial regression. This method provides both an accurate local approximation and a continuous gradient [76].

Once the response surface has been created, the optimization problem must be reformulated by using it.

Let $\boldsymbol{f(\mathbf{x}): R^n \to R}$ be the objective function of *n* dimensional optimization problem estimated through FEM. Then the general formulation of the OD problem can be formulated as the search of the solution given by:

$$\mathbf{x}^* = \{\min \boldsymbol{f(\mathbf{x})} \mid \mathbf{x} \in \overline{\boldsymbol{D}}\} \tag{4.2}$$

inside the feasibility domain, $\overline{\boldsymbol{D}}$. In the case of an electrical motor $\overline{\boldsymbol{D}}$ is generally a hyper-polyhedron delimited by the surfaces defined through the limits of each parameter, as shown beneath:

$$\overline{\boldsymbol{D}} = \left\{ \mathbf{x} \in \boldsymbol{R}^{n} \middle| \boldsymbol{x}_{i\min} \le \boldsymbol{x}_{i} \le \boldsymbol{x}_{i\max}, \forall \boldsymbol{i} \in 1 \ldots \boldsymbol{n} \right\} \tag{4.3}$$

The optimal design problem is completely defined by (4.2) and (4.3). This initial formulation of the optimization problem is then transformed by replacing the objective function with a response surface model over a feasibility domain $\overline{\boldsymbol{D}}_{\boldsymbol{R}}$ in a reduced dimension $p < n$ (p stands for the number of the most important parameters $\tilde{\mathbf{x}}$). Thus, the general formulation of an OD problem can be expressed as the search of the solution:

$$\tilde{\boldsymbol{x}}^{*} = \left\{ \min \tilde{\boldsymbol{s}}(\tilde{\mathbf{x}}) \,\middle|\, \tilde{\mathbf{x}} \in \overline{\boldsymbol{D}}_{\boldsymbol{R}} \right\} \tag{4.4}$$

The new feasibility domain is obtained by projecting the original feasibility domain onto the reduced space:

$$\overline{\boldsymbol{D}}_{\boldsymbol{R}} = \overline{\boldsymbol{D}} \cap \boldsymbol{R}^{\boldsymbol{p}} \tag{4.5}$$

This new model considers the unselected parameters as constant values $\boldsymbol{x}_{p+1} = \boldsymbol{x}^{*}_{a\,p+1} .. \boldsymbol{x}_{n} = \boldsymbol{x}^{*}_{a\,n}$, where $\mathbf{x}_{a}^{*} = \boldsymbol{x}^{*}_{a1} \ \ldots \ \boldsymbol{x}^{*}_{a\,n}$ represents the solution of the previous optimization problem:

$$\mathbf{x}_{a}^{*} = \left\{ \min \ \boldsymbol{f}_{a}(\mathbf{x}) \,\middle|\, \mathbf{x} \in \overline{\boldsymbol{D}} \right\} \tag{4.6}$$

obtained by using the equivalent simplified analytical model.

In order to find the reduced model improving the optimization result based on the analytical model, two selection methods are compared here:

- the selection of the most significant parameters from the FEM simulated objective function;
- the selection of the parameters by using the error gradient information.

One can see that the effect of any simple $\boldsymbol{x}_{i}$ in the global variability of the objective function depends on the feasibility domain range $\left| \boldsymbol{x}_{i\_\min} - \boldsymbol{x}_{i\_\max} \right|$. Therefore, the definition domain of each parameter has been normalized into the [-1, 1] interval.

A. Selection of the most significant parameter from the FEM simulated objective function

In order to select the parameters with the most impact on the proposed objective function, In the particular case of a non-stochastic model, as it is generally for EM models, it has been proved in [77] the efficiency of using the multiple correlation coefficients R^2 in order to obtain a hierarchy of the parametrical subsets $\mathbf{x}_{\mathbf{s}}$ based on their impact on the output result.

To obtain the set of simulation results needed for the application of the multiple correlation coefficient method, it is common to generate samples vectors $\mathbf{x}$. With a complete factorial design all distinct configurations of the parameters are presented.

In the case under study, the large number of the motor parameters generates a factorial design containing several thousands of samples. Moreover, the simulation time required to simulate an electrical motor, can even take several hours for a 3D analysis with a common PC.

To minimize the computation time an orthogonal array (OA) of experiments (named also *fractional experimental design*) has been used since it uses a subset of the factorial design containing distinct parameter configurations. This OA reduces the number of samples and at the same time offers sufficient information for calculating R^2. To evaluate the importance of n parameters and their interactions, the condition imposed for the OA is:

$$\boldsymbol{s} > \boldsymbol{n} \tag{4.7}$$

where s, represents the number of lines of the OA (the number of experiments).

B. Selection of the most important parameters by using the error gradient information – the multi model approach

In this case the selection of parameters which have the greatest influence on the value of the error between the FEM and analytical model is based on the sensitivity analysis of the error $\varepsilon(\mathbf{x}) = \left\| \boldsymbol{f}(\mathbf{x}) - \boldsymbol{f}_a(\mathbf{x}) \right\|_2^2$ with respect to each parameter by computing the partial derivatives $\partial\varepsilon/\partial\boldsymbol{x}_i \big|_{\mathbf{x}_a^*}$ $\boldsymbol{i}=1..\boldsymbol{n}$, where $\mathbf{x}_a^*$ represents the optimal point computed with the analytical model $\boldsymbol{f}_a(\mathbf{x})$ and $\boldsymbol{f}(\mathbf{x})$ the objective function computed with the FEM model . For a normalized domain, the value of $\partial\varepsilon/\partial\boldsymbol{x}_i$ quantifies locally the importance of parameter $\boldsymbol{x}_i$ in the variation of the error $\varepsilon(\mathbf{x})$ and then the capacity of the $\boldsymbol{x}_i$ parameter to improve the optimal value of the objective function computed by using the analytical model. As a result the unselected $(\boldsymbol{n}-\boldsymbol{p})$ parameters are fixed at the values given by the results obtained with the analytical model.

4.3.2.2 The Algorithm implementation for the optimization of a PMSM

This entire methodology has been employed with the help of developed software which implements an interface between the optimization algorithm and the analytical and FEM models. As previously specified, the EM which has been optimized is a PMSM with concentrated flux topology, presented in FIGURE 4-5.

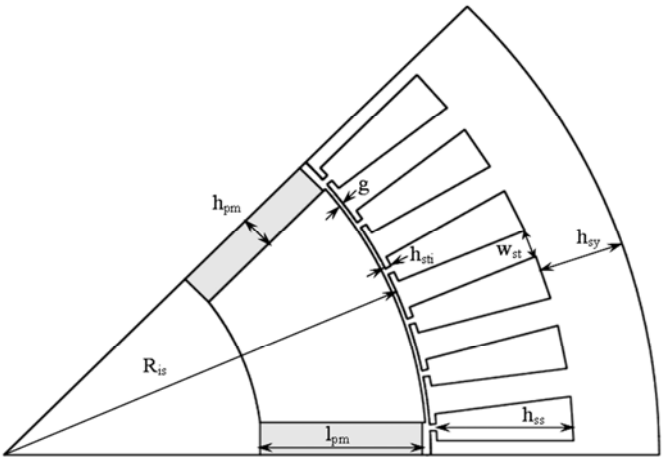

FIGURE 4-5. One pole cross section of the studied machine. [71]

There are eight poles, three phase winding of distributed type, rated power and speed of 2.2kW and 3000r/min respectively, and current $\boldsymbol{I}_s = \left(\sqrt{\boldsymbol{I}_d^2 + \boldsymbol{I}_q^2}\right) = 7\boldsymbol{A}$. Its main designing data and the feasibility domain are given in Table 4-1.

In order to obtain a maximum torque/weight ratio, we intend to minimize the weight (this is the objective function):

$$\boldsymbol{f}_{obj}(\mathbf{x}) = (\boldsymbol{T}(\mathbf{x}) - \boldsymbol{T}_n)^2\,(1-\gamma) - \frac{\boldsymbol{T}(\mathbf{x})}{\boldsymbol{w}_{tot}(\mathbf{x})}\gamma \tag{4.8}$$

where $\boldsymbol{T}(\mathbf{x})$ represents the developed torque for a set of geometrical parameters **x,** w_{tot} is the total weight of the motor. The first term of (4.8) expresses the minimization of the torque error, whereas the second term illustrates the torque per weight maximization. The trade-off between the two terms is adjusted by means of the weight coefficient γ, whose has been chosen to be 0.5. A preliminary optimization has been realized on the analytical model based on the reluctance network by minimizing the analytically computed objective function. The obtained analytical solution has the average torque *T=10.19 Nm,* the total weight w_{tot}*=9.03 Kg*, the objective function f_{obj} computed by (4.8) equal to -0.38.

TABLE 4-1. THE MAIN DATA DESIGN OF THE STUDIED PMSM FOR RESPONSE SURFACE OPTIMIZATION [71]

SYMBOL	*QUANTITY*	*FEASIBILITY DOMAIN*	*OPTIMAL VALUE* $\mathbf{x}_a^*$
L_m	motor length	[90÷108]mm	99.1 mm
R_{is}	inner stator radius	[47÷53]mm	50 mm
g	air-gap height	[0.4÷0.6]mm	0.5 mm
h_{pm}	permanent magnet height	[6÷9]mm	7.73 mm
l_{pm}	permanent magnet length	[23÷30]mm	27.8 mm
h_{sy}	stator yoke height	[9÷12]mm	9 mm
h_{ss}	stator slot height	[13÷19]mm	13 mm
h_{sti}	stator tooth isthmus height	[0.5÷1]mm	0.75 mm
w_{st}	stator slot width	[3.1÷3.7]mm	3.1 mm
T_n	rated torque		10 Nm
n_n	rated speed		3000 r/min
U_n	line supply voltage		200 V
p	number of poles pairs		4

1) Selection of the most important parameters of the objective function computed by using FEM.

As explained previously, an orthogonal array has been employed to reduce the number of parameters. To satisfy the condition in (4.7), an OA with 3 levels for each factor and 27 experiments has been selected. The used array is identified as OA.27.13.3.2, following the terminology introduced in [78]. Each parameter is associated with a column of the OA, so as to produce a table of levels for each parameter and for each FEM simulation. In this case, three representative levels have been chosen for each factor. To estimate the effects over the whole feasibility domain the minimal, the maximal and the central value have been considered as representative levels for each parameter. Replacing these levels in the OA, this last one generates the set of simulations, which are then used to compute the R^2 values. FIGURE 4-6 shows the results obtained for R^2 and the 3 most important parameters selected: R_{is}, l_{pm} and h_{pm}.

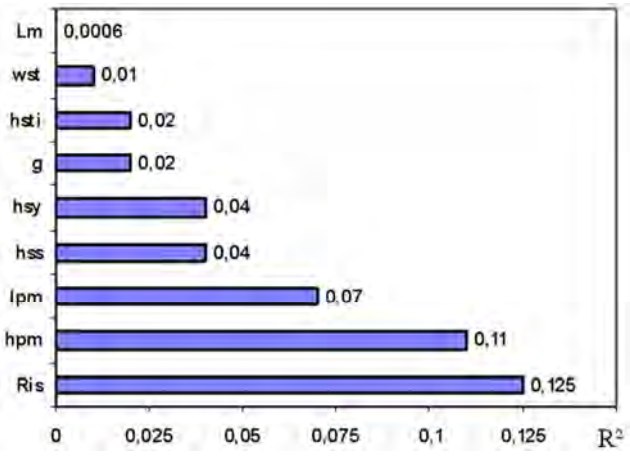

FIGURE 4-6. R2 analysis results. [71].

TABLE 4-2. THE ERROR SENSITIVITY *[71]*

x_i	$\frac{\partial \varepsilon(\mathbf{x}_a^*)}{\partial \mathbf{x}_i}$
L_m	***-1.5***
R_{is}	0.60
g	***-1.6***
h_{pm}	**-2.38**
l_{pm}	**-3.36**
h_{sy}	-0.05
h_{ss}	-0.13
h_{sti}	0.123
w_{st}	-0.24

1) Selection of the most important parameters by using the gradient of the error between the FEM and the analytical model (multi-model approach)

As explained previously, the partial derivatives $\left.\frac{\partial \varepsilon(\mathbf{x}_a^*)}{\partial \boldsymbol{x}_i}\right|_{i=1\ldots n}$ are computed at the point of the previous optimal parameters configuration for all of the 9 normalized parameters. A normalized variation of $\Delta \boldsymbol{x} = 0.2$ has been considered for each normalized parameter.

Table 4-2 shows that the error presents the greatest sensitivity for the next four parameters: l_{pm}, h_{pm}, g and L_m. It should be remarked that L_m and g have an equivalent sensitivity. On the other hand, the practical realization of an accurate value of g seems to be difficult, as actually it can only vary within a very small domain, between 0.4 and 0.6 mm. Thus it is more practical to consider only the parameters l_{pm}, h_{pm} and L_m for the second reduced simulation model.

Two different approximation techniques have been used to create a response surface model (RSM).

i. Polynomial regression

A quadratic approximation of the objective function has been employed to construct the Response Surface. A Composite Central Design (CCD) has been implemented to fit the coefficients of the response model. This CCD, proposed in [77], contains a complete factorial 2^k design, augmented with a group of $2\boldsymbol{k}$ axial points and one design center point. The distance from the center of the design space to an axial point is $\pm\alpha$ with $\alpha = 0.5$.

The polynomial model is obtained by using the least square method.

The first reduced simulation model (R_{is} l_{pm} h_{pm}) has been approximated by:

$$\tilde{\boldsymbol{f}} = -0.62 + 1.18\mathrm{R_{is}} + 1.27\mathrm{h_{pm}} + 0.049\mathrm{l_{pm}} + 0.68\mathrm{R_{is}}^2 + 1.38\mathrm{h_{pm}}^2 - \\ + 0.3\mathrm{l_{pm}}^2 - 2.08\mathrm{R_{is}}\,\mathrm{h_{pm}} + 0.58\mathrm{l_{pm}}\,\mathrm{h_{pm}} - 0.42\mathrm{l_{pm}}\,\mathrm{R_{is}} \tag{4.9}$$

which presents an optimal value $\tilde{\boldsymbol{f}} = -1.34$ for $\boldsymbol{R_{is}} = -1.0; \boldsymbol{l_{pm}} = -0.15; \boldsymbol{h_{pm}} = -0.62$.

For this configuration the results computed with the FEM are shown in Table 4-3, labeled as RSM_A model.

The second reduced simulation model (l_{pm}, h_{pm} and L_m) has been approximated through:

$$\tilde{\boldsymbol{f}} = -0.549 + 0.227\mathrm{L_m} - 0.48\mathrm{h_{pm}} + 0.051\mathrm{l_{pm}} + 0.177\mathrm{L_m}^2 + 1.2\mathrm{h_{pm}}^2 \\ + 0.162_{\mathrm{pm}}{}^2 - 0.189\mathrm{L_m}\cdot\mathrm{h_{pm}} + 0.64\mathrm{l_{pm}}\cdot\mathrm{h_{pm}} + 0.097\mathrm{l_{pm}}\cdot\mathrm{L_m} \tag{4.10}$$

which presents an optimal value $\tilde{\boldsymbol{f}} = -0.70$ for $\mathrm{L_m} = -0.15; \boldsymbol{l_{pm}} = -0.96; \boldsymbol{h_{pm}} = 0.44$.

For this configuration the results computed with the FEM are shown in Table 4-3, as RSM_B model.

ii. MLS approximation

The approximated value of the objective function and the gradient value were obtained by the MLS approximation on a pre-sampled uniform mesh grid with 5 values for each parameter. This method has been applied to the reduced simulation model. For the considered response surface with *p=3* parameters, 125 FEM simulations were necessary. In terms of computation, on a PC with PIV 1.8Mhz, 1Gb RAM configuration, the following computation time was needed for the implemented study: less than 30 minutes for FEM analysis, less than 1 second for the analytical calculation (equivalent magnetic reluctance) and less than 1 second for the response surface method based on MLS.

To solve the optimization problem, the response surface has been associated again to the BCGFS algorithm. The optimal point for the first reduced simulation model (R_{is} l_{pm} h_{pm}) was

obtained for R_{is}=-0.88 l_{pm}=-0.93 h_{pm} =-0.028 with an optimal value $\tilde{f} = -0.6279$. The results computed with the FEM are shown in Table 4-3 as RSM_C model.

With the second reduced simulation model (l_{pm}, h_{pm} and L_m) the optimal point obtained on the MLS approximation has been reached for $L_m = -0.98$; $l_{pm} = -0.97$; $h_{pm} = 0.24$ with an optimal value $\tilde{f} = -0.64$. The results computed with the FEM are shown in Table 4-3 as RSM_D model.

TABLE 4-3. COMPARISON BETWEEN THE ANALYTICAL AND RESPONSE SURFACE METHOD [71]

Model	Approximation	Selection	$\tilde{f}_{opt}$	f_{opt}	RMSE	R^2	Average Torque, [Nm]	Total weight, [Kg]
Analytical	-	-	-	-0.38	-	-	10.19	9.03
RSM_A	Polynomial regression	Most important parameters for the FEM	-1.34	-0.62	0.2281	0.99125	10.07	8.07
RSM_B	Polynomial regression	Multi-model approach	-0.70	-0.61	0.2249	0.9418	10.12	8.23
RSM_C	MLS	Most important parameters for the FEM	-0.63	-0.63	0.046	0.9992	10.09	7.98
RSM_D	**MLS**	**Multi-model approach**	**-0.64**	**-0.66**	**0.035**	**0.9984**	**10.05**	**7.59**

Table 4-3 shows the improvement for the analytical solution $\mathbf{x}_a^*$ obtained with the reduced response surface. The 4th column $\tilde{f}_{opt}$ represents the value of the approximated surface at the optimal point. The 5th column (f_{opt}) represents the value of the objective function, (7), obtained with the FEM simulation, at the same point. This column contains the proof for the validation test of the obtained results.

Firstly, the two approximation methods are compared based on RSM_A and RSM_C models. In the case of the polynomial regression (RSM_A) it can be observed a significant difference between $\tilde{f}_{opt}$ and f_{opt}. If in the one hand RSM_A appears better than RSM_C on the basis only of $\tilde{f}_{opt}$, on the other hand the column f_{opt} shows that the two solutions are practically equivalent. Moreover, in RSM_C the optimal value obtained on the approximation $\tilde{f}_{opt}$ is practically identical with the real value f_{opt}.

The same accuracy of the MLS approximation is apparent in the comparison between the solutions RSM_B and RSM_D where the selected parameters (l_{pm}, h_{pm} and L_m) are obtained with the multi-model approach.

In order to examine the fitted model which ensures the best approximation, the statistical analysis, ANOVA (analysis of variance), can be employed. Two typical statistic metrics have been used: R2, associated to the entire model, and the root mean square error (RMSE). This study has been realized by using the experiments associated to each approximation model. A better fitness is obtained for the largest R2 and for the smallest RMSE values, respectively (Table 4-3, columns 6 and 7). The results prove that the MLS response surface has a better accuracy than the polynomial regression.

The last two columns show that the motor weight was decreased of about 5% for RSM_D versus RSM_C, RSM_D versus RSM_B about 8%, and about 16% in comparison with the initial design based on the analytical model. In conclusion, the Multi-model approach selection, based on the error gradient, gives better results for the improvement of the analytical optimal solution. Furthermore, within this selection method, the response surface obtained by MLS approximation is more suitable than the polynomial regression.

4.3.3 Radial-flux PMSM optimization based on Methaursitic Algorithms

The Simulated Annealing SA is a probabilistic variant of the local search method, but it can, in contrast, escape local optima [79], [80]. SA is based on an analogy taken from thermodynamics: to grow a crystal, we start by heating a row of materials to a molten state. Then, we reduce the temperature of this crystal melt gradually, until the crystal structure is frozen in.

A standard SA procedure begins by generating an initial solution at random. At initial stages, a small random change is made in the current solution s_c. Then the objective function value of the new solution s_n is calculated and compared with that of the current solution. A move is made to the new solution if it has better value or if the probability function implemented in SA has a higher value than a randomly generated number.

Otherwise a new solution is generated and evaluated. The probability of accepting a new solution is given as follows:

$$\boldsymbol{p}=\begin{cases} 1 & \text{if} \quad \boldsymbol{f}(\boldsymbol{s_n})-\boldsymbol{f}(\boldsymbol{s_c})<0 \\ \exp\left(\dfrac{-\left|\boldsymbol{f}(\boldsymbol{s_n})-\boldsymbol{f}(\boldsymbol{s_c})\right|}{\boldsymbol{T}}\right) & \text{otherwise} \end{cases} \tag{4.11}$$

The calculation of this probability relies on a temperature parameter *T*, which is referred to as temperature, since it plays a similar role as the temperature in the physical annealing process. To avoid getting trapped at a local minimum point, the rate of reduction should be slow. In our problem the following method to reduce the temperature has been used:

$$\boldsymbol{T}_{i+1}=\gamma \boldsymbol{T}_i \tag{4.12}$$

where i = 0,1,... and γ = 0.99.

Thus, at the start of SA most worsening moves may be accepted, but at the end only improving ones are likely to be allowed. This can help the procedure jump out of a local minimum. The algorithm may be terminated after a certain volume fraction of the structure has been reached or after a pre-specified run time.

4.3.3.1 The SA Algorithm

The principle of our SA algorithm is described in FIGURE 4-7, where:

- Initial solution: Each solution X ∈ S is represented by its *n > 0* components, i.e., X = (x_1, x_2, ... , x_n), where *i = 1, 2, ..., n* and *n* represents the dimension of the optimization problem to solve. The SA algorithm starts with an initial solution which is initialized with uniform random value between the lower and upper boundaries of the interval defining the optimization problem.
- Variable *best_solution* keeps the best solution found,
- *Iter* counts the iterations of the main loop and *Notimprove* remembers the last iteration in which the algorithm improved the best solution.
- Evaluate function: Evaluate (or fitness) function in SA algorithm is typically the objective function that we want to minimize in the problem. It serves for each solution to be tested for suitability to the environment under consideration.
- The main loop proceeds until the number of iterations exceeds *Max_iteration* or optimal solution is attained or there was no improvement for the last *K* iterations.

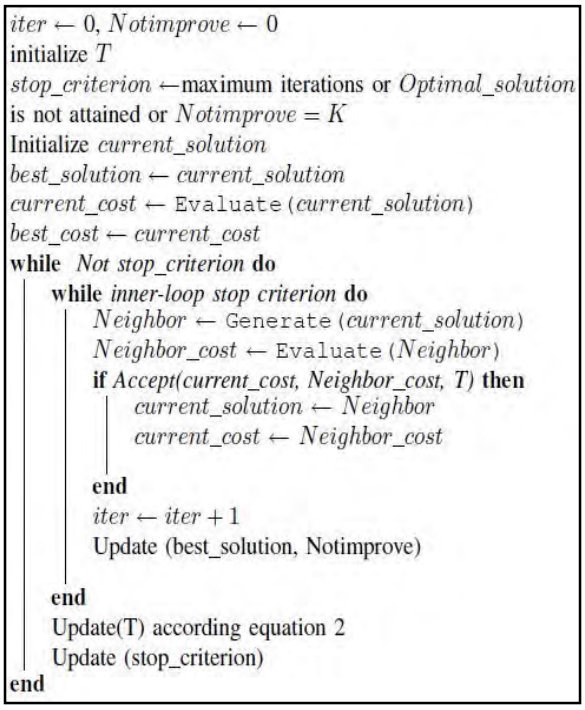

FIGURE 4-7. Simulated Annealing algorithm. [80]

- *Generate* function: Simulated annealing is a randomized algorithm for searching the space of feasible solutions using a notion of neighborhood relation. Let *S* be the set of all feasible solutions to the problem and $f : S \rightarrow R$ the objective function to be minimized. A neighborhood relation is a binary relation $N \rightarrow S \times S$ with some desired properties. The interpretation of *N(s, s')* is that solution *s* is a neighbor of solution *s'* in the search space of all solutions *S*. A neighbor heuristic proceeds in steps. It starts searching at some initial solution s_0 and in each step moves from the current solution to some neighbor according to some rules specific to the heuristic. At each iteration, our SA algorithm generates a random neighbor of the *current_solution* (line 11). In our case we define the neighborhood relation as follows. Any two solutions $s, s' \subseteq S$ are neighbors *N(s, s') iff* they differ by $m \in \{1,2,3\}$ items randomly chosen between *n*.
- *Accept* function: The key idea in the SA approach is the function *Accept* which specifies the probability of accepting the move from *current_solution* to a *Neighbor* solution, which also depends on so called temperature (*T*). The function *Accept* should satisfy the following conditions:
    1) *p = 1* if solution *Neighbor* is better then *current_solution* in terms of the cost function *f* (i.e. *f(Neighbor) < f(current_solution)* in a minimization problem).
    2) if *Neighbor* is worse than *current_solution* the value of *p* is positive (i.e. it allows for moving to a worse solution), but decreases with *|f(Neighbor) - f(current_solution)|*.
    3) for fixed *current_solution* and *Neighbor*, when *Neighbor* is worse than *current_solution* the value of *p* decreases with time and tends to *0*.

The function *Accept*(c_{cost}, n_{cost}, *T)* is decided by the probability of accepting configuration *Neighbor*. This probability is given by the following expressions:

$$\boldsymbol{p} = \begin{cases} 1 & \text{if} \quad \boldsymbol{n}_{cost} < \boldsymbol{c}_{cost} \\ \boldsymbol{rand} \times \exp\left(\dfrac{\boldsymbol{n}_{cost} - \boldsymbol{c}_{cost}}{\boldsymbol{T}}\right) < 2.0 & \text{otherwise} \end{cases} \tag{4.13}$$

where *T* is the temperature and *rand* is a random number independently generated within the range of [0,1].

- The best solution is updated in line 18.
- The temperature is updated according equation **2** in line 20 of the algorithm.

4.3.3.2 The SA capability based on five well-known benchmark functions

To testify the efficiency and effectiveness of SA algorithm will be tested on several known benchmark functions and compared with other optimization techniques found in the literature. Note that our SA algorithm is written in C++. The C++ compiler used is gcc version 2.95.2 (Dev-cpp). The laptop (Intel Core 2 Quad Q9000, 2 GHz CPU, 4 Gb memory) used to run our experimentation is running under Windows Vista x 64 Premium Home Edition.

The five benchmark functions [81] described in Table 1. These functions provide a good launch pad for testing the credibility of an optimization algorithm. For these functions, there are many local optima in their solution spaces. The amount of local optima increases with increasing complexity of the functions, i.e. with increasing dimension. In our experiments, we used *20* and *30*-dimensional functions.

TABLE 4-4. FIVE BENCHMARK PROBLEMS ADOPTED IN THIS WORK. [80]

Function Name	Problem	Range
Rastrigin	$\sum_{i=1}^{n}(x_i^2 - 10\cos(2\pi x_i) + 10)$	[-5.12;5.12]
Rosenbrock	$\sum_{i=1}^{n-1}(100(x_{i+1} - x_i^2)^2 + (x_i - 1)^2)$	[-30.0; 30.0]
Schwefel	$-\sum_{i=1}^{n}(x_i \sin(\sqrt{\lvert x_i \rvert}) = -418.9829\ n$	[-500.0; 500.0]
Noisy	$(\sum_{i=1}^{n}(i+1)x_i^4) + rand[0,1]$	[-1.28; 1.28]
Michalewicz	$-\sum_{i=1}^{n}\sin(x_i)\sin^{2m}(\frac{i - x_i^2}{\pi}), m = 10$	$[-\pi;\pi]$

This five benchmark functions are producing different variations and they are used to test the algorithm capability to converge to a solution in the most sever conditions. To have an idea about the problem complexity, several of the above benchmark functions are plotted in FIGURE 4-8. When tested in such functions, the algorithm proves its capacity in avoiding local minima, or its capability to get out if trapped in such points. Not only the capacity of the algorithm to avoid minima is tested with such functions, but also the knowledge and experience of the designer (programmer) to impose the constraints, limitations and to specify the limits of the test period and samplings until the objective function has reached the best possible value (not only the capacity to get out from local minima – the case of Rastrigin or Schwefel functions – represents a difficulty which needs to be surpass by the algorithm, but also when the variation from neighbor solution is too small - the case of Rosenbrock function, and even for Michalewicz – there is an important risk to be far away for the global minimum).

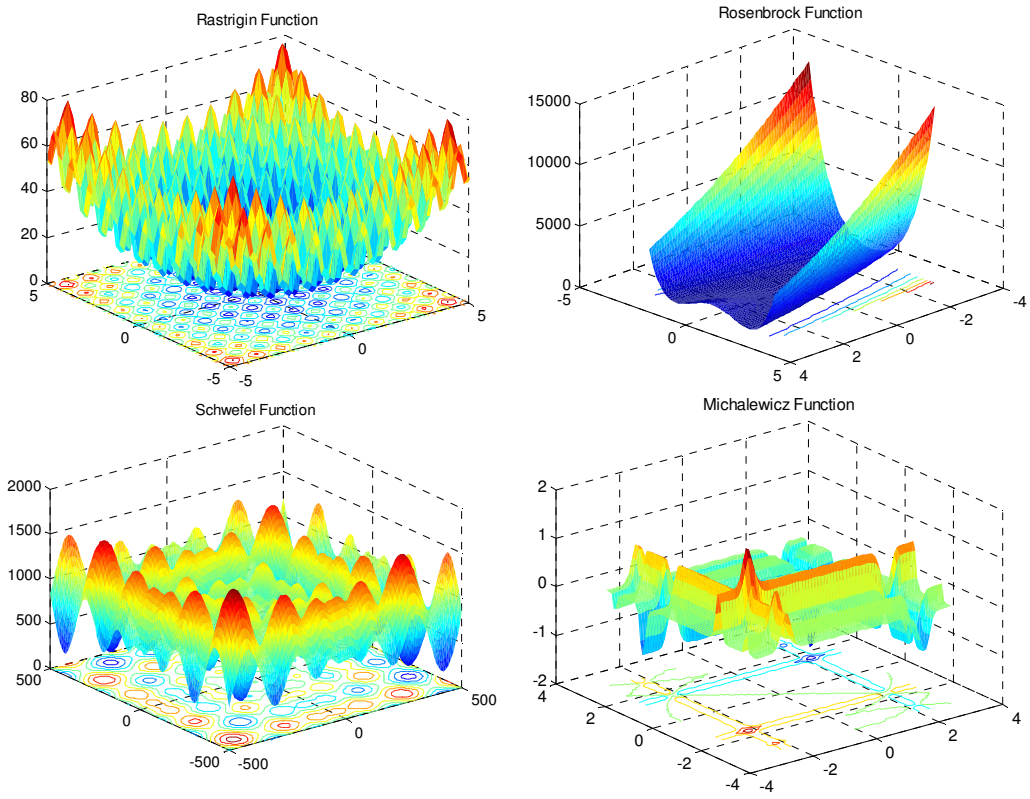

FIGURE 4-8. Benchmark functions variation.

4.3.3.3 The proposed SA Algorithm results against other approaches, like PSO and ACO

In this section we will compare our SA algorithm with three of the existing continuous-domain Ant Colony Optimization (ACO) algorithms [82].

As described in [82], we apply our algorithm to the three following benchmark problems: Rastrigin's, Rosenbrock's and Schwefel's function (dimension of searching *n = 30*) which are highly multimodal problems that represent a challenging task in continuous optimization.

For each benchmark problem considered in this section, we have, in Table 4-5, the mean and standard deviation produced by each algorithm after *30* independent runs.

TABLE 4-5. MEAN AND STANDARD DEVIATION VALUES OF THE BEST SOLUTION OBTAINED BY USING OUR SA ALGORITHM AND APPROACHES DESCRIBED IN [82] (N = 30 AND POPULATION OF *1000* ANTS WAS DEFINED FOR BOTH *CACS* AND *MACACO* ALGORITHMS). [80]

Function	ACO_R	*CACS*	*MACACO*	**SA**
Rastrigin	101.65	57.17	0.00058	**8.00 e-08**
	±21.01	±14.14	±0.00009	**± 2.59369 e-08**
Rosenbrock	29.93	1.23	7.48	**0.384**
	±35.14	±1.91	±11.68	**± 0.149790826**
Schwefel	−8703.26	−8934.57	−12569.49	**-12569.5**
	±721.53	±633.78	±0.01	**± 0**

Each algorithm should be allowed a maximum of 10^6 function evaluations for all the benchmark problems studied here, except for the Rosenbrock's function, which could be evaluated up to 6 10^6 times. Note that in [82] a population of *1000* ants was defined for both *CACS* and *MACACO* algorithms.

By analyzing Table 4-5 we can see:

- that *MACACO* algorithm outperforms the *CACS* and ACO_R in two of the three functions,

being worse than *CACS* on the Rosenbrock's function.

- that the results obtained by our SA algorithm are excellent in comparison with those obtained by ACO_R, *MACACO* and *CACS* algorithms. Our SA algorithm has a much smaller standard deviation for Rastrigin's and Rosenbrock's function and found the global optimum for Schwefel's function.

Performance of four Particle Swarm Optimization (PSO) algorithms, namely classical PSO, Attraction-Repulsion based PSO (ATREPSO), Quadratic Interpolation based PSO (QIPSO) and Gaussian Mutation based PSO (GMPSO) are evaluated in [83]. Whereas all the algorithms presented in this section are guided by the diversity of the population to search the global optimal solution of a given optimization problem, GMPSO uses the concept of mutation and QIPSO uses the reproduction operator to generate a new member of the swarm.

In order to make a fair comparison of classical PSO, ATREPSO, QIPSO, GMPSO and our SA approach we fixed, as indicated in [83], for each algorithm, the maximum number of iterations to *10000*. The number of particles, used by the four algorithm, in the swarm is *30* and use a linearly decreasing inertia weight *w* which starts at *0.9* and ends at *0.4*, with the user defined parameters $c_1 = c_2 = 2.0$.

A total of *30* runs for each experimental setting were conducted and the average fitness of the best solutions throughout the run was recorded. The mean solution and the standard deviation[8] found by the five algorithms are listed in Table 4-6.

TABLE 4-6. COMPARISON OF MEAN/STANDARD DEVIATION OF SOLUTIONS OBTAINED BY USING OUR SA ALGORITHM AND PSO APPROACHES DESCRIBED IN [3] (N = 20 AND SWARM SIZE = 30). [80]

Function	*PSO*	*QIPSO*	*ATREPSO*	*GMPSO*	**SA**
Rastrigin	22.339158	11.946888	19.425979	20.079185	**1.924398 e-06**
	15.932042	9.161526	14.349046	13.700202	**8.40864 e-07**
Rosenbrock	22.191725	8.939011	19.490820	14.159547	**0.840377**
	1.615544e+04	3.106359	3.964335e+04	4.335439e+04	**0.673092017**
Schwefel	−6178.559896	−6355.586640	−6183.677600	−6047.670898	**-8379.66**
	4.893329e+02	477.532584	469.611104	482.926738	**1.86624 e-12**
Noisy	8.681602	0.451109	8.046617	7.160675	**9.363985 e-04**
	9.001534	0.328623	8.862385	7.665802	**4.77749 e-04**
Michalewizc	−18.159400	−18.469600	−18.982900	−18.399800	**-19.634785**
	1.051050	0.092966	0.272579	0.403722	**0.002062516**

The numerical results given in Table 4-6 show that:

- all the algorithms outperform the classical Particle Swarm Optimization.
- SA algorithm gives much better performances in comparison to PSO, QIPSO, ATREPSO and GMPSO.
- the analysis of the results obtained by our approach for all five benchmark functions, studied in this work, shows the stability of our algorithm (i.e. SA algorithm has a much smaller standard deviation).

4.3.3.4 The proposed SA algorithm employed for the optimization of a PMSM with flux concentration

The Simulated Annealing algorithm was employed for the optimization of an electrical motor of synchronous type which is excited with permanent magnets (PMs). The PMs are rotor inset and the motor is of flux concentration type; practically it is the same machine that was presented earlier while being optimized with the Response Surface optimization method. This is why, no other details on the machine, application or variation of geometric parameters is given.

[8] Note that the standard deviation indicates the stability of the algorithms

In order to validate the SA optimization procedure, the authors have employed the analytical obtained parameters (the geometrical ones) on numerical simulation software based on finite element method (FEM). This approach is recognized in the field as a very useful tool for the design and the optimization of electrical machines.

It should be mentioned that the geometrical parameters were introduced manually for each valid experiment obtained through analytical optimization procedure and several simulations were launched; thus, the objective function was evaluated. The non-valid computed results were eliminated manually also (if the error between analytical and numerical computations has surpassed $\pm 20\%$).

The objective function for this study is the *torque/motor weight* ratio. Several simulations were employed. From several simulations it was possible to plot the objective function variation and thus the obtained results have proved the validity of the optimization algorithm. In FIGURE 4-9 one cans see the *torque/weight* ratio variation for several experiments and the error between the numerical and analytical results.

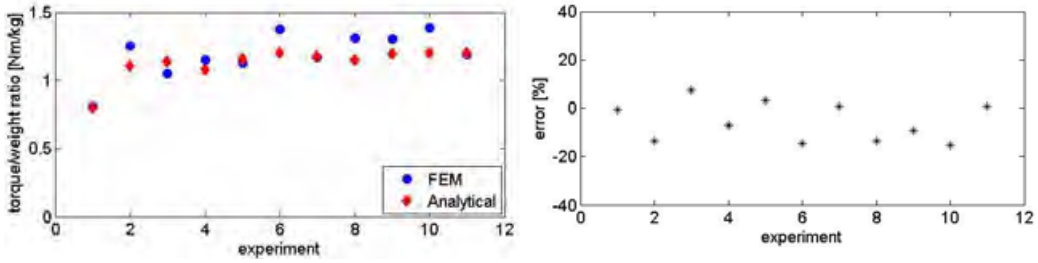

FIGURE 4-9. Objective function (left) and the error between the analytical (SA) and FEM (right). [80]

It can be said that all the plotted results are "good", and some of them are "the best": the experiments 4, 5, 7 and 11. The question is: how to choose among these results (several geometrical configurations are possible, finally)? In order to respond to this question, one should consider a multi-objective application, where other 'important' parameters interfere (like the electric consumption, the efficiency, the costs etc.).

If one compares the obtained performances with the ones presented with Response Surface Optimization (RSO), it can be observed a good agreement between the obtained results. The best result with the RSO is of *1.3241 torque/weight* ratio (*10 Nm* of rated torque), and here is of *1.2303* (for *7 Nm* of rated torque). It is well known that for large power motors this ratio is more important. So, for a *30%* torque decrease against the case given when optimization was employed with RSO method, the result obtained with the SA algorithm presented here is very optimistic.

4.3.4 Outer-rotor PMSM optimization based on Hybrid Methauristic Algorithm

4.3.4.1 Problem definition

Like in the previous optimization problems, the goal is to maximize the output power of the studied motor while minimizing its mass – in other words, it is intended to maximize the motor's power density [61]. Such design problem is the subject of multi-objective optimization that can generally be formulated as follows:

$$\begin{cases} minimize_x \ [f_1(x), f_2(x), \dots, f_m(x)]^T \\ s.t. \\ \quad g_j(x) \le 0 \quad j = 1, \dots, p \\ \quad h_l(x) = 0 \quad l = 1, \dots, q \end{cases} \tag{4.14}$$

To solve this problem, two main approaches (found in the scientific literature) can be considered:

- methods like [84], that try to find a set of equivalent solutions, called the Pareto's front, that are not dominated (equivalent) by any other solution for all objectives at the same time, and require an additional algorithm to choose the most appropriate solution that will be used.
- methods like [85], that aggregate all objective functions to create a composite single objective function to minimize, and then use a mono-objective optimization algorithms to obtain a single optimal solution. Aggregating several objective functions can be challenging, and tuning the weight to give to each objective may be problematic.

The second approach was used here, and our optimization problem consists in optimizing two given objective functions:

- The first objective function concerns the minimization of the mass of the active parts of the machine, here called m_{tot}. The total mass of the active parts of the machine needs to be minimized. m_{tot} is the sum of all active parts of the machine:

$$m_{tot} = m_{copper} + m_{stat} + m_{rot} + m_{PM} \tag{4.15}$$

where m_{copper} is the mass of copper used for windings, m_{stat} is the mass of the stator core (teeth and yoke), m_{rot} is the mass of the rotor core and m_{PM} is the mass of the PMs.

- The second objective function consists in the maximization of the output power P_{out} which is equal to the difference between the input power and the losses:

$$P_{out} = P_{in} - \sum Losses \tag{4.16}$$

The sum of losses contains mainly the iron and copper losses; the mechanical losses (usually estimated at *0.5%* of the output power) are neglected here.

The objective function is presented by the following equation:

$$\begin{cases} minimize_x \ F(x) = -\dfrac{P_{out}}{m_{tot}} + penality \\ where: \\ \text{penality} = 10^6 \times \sum_{i=1}^{5} |C_i - Limit| \\ Limit = \begin{cases} \text{LowerBound}(C_i) & \text{if } C_i < LowerBound(C_i) \\ \text{UpperBound}(C_i) & \text{if } C_i > UpperBound(C_i) \\ C_i & \text{otherwise} \end{cases} \end{cases} \tag{4.17}$$

In (4.16) the parameter C_i defines different constraints imposed for the objective function.

The decision vector *x* corresponds to the main geometrical parameters which have an important influence on motor's performances. The machine under study is the PMSM-17/39 presented into the subchapter 2.4. The geometry's parameters are extracted from the designing process and given in Table 4-7.

TABLE 4-7. THE MAIN PARAMETERS USED FOR MACHINE'S OPTIMIZATION [61]

PARAMETER	*SYMBOL (in MM)*	*VARIATION LIMITS*
Rotor inner diameter	*Dir*	[170 ÷ 210] mm
Rotor yoke height	*hjr*	[5 ÷ 9] mm
Tooth isthmus height	*his*	[1 ÷ 3] mm
Stator yoke height	*hjs*	[5 ÷ 10] mm
Tooth width	*ld*	[5 ÷ 9] mm
Air-gap length	*gap*	[0.5 ÷ 1.5] mm
PM height	*hmp*	[3 ÷ 7] mm
Machine's length	*Lm*	[30 ÷ 80] mm

The last column of this table contains the variation limits of the main geometrical parameters, which will establish the limits of the space of solutions for the objective function.

Table 4-8 presents the optimization constraints used in (4.16).

TABLE 4-8. CONSTRAINTS ("C_i") FOR THE OPTIMIZATION PROBLEM [61]

PARAMETER	SYMBOL	UNITY	VARIATION LIMITS
Output power	P_{out}	*W*	[1490 ÷ 1510]
Current consumption	I_s	*A*	[15 ÷ 25]
Axis torque	T_m	N˙m	[33.9 ÷ 34.3]
Efficiency	η	-	[0.9 ÷ 0.99]
Power factor	*PF*	-	[0.9 ÷ 0.99]

4.3.4.2 The Hybrid Particle Swarm Optimization algorithm

Particle Swarm Optimization algorithm (*PSO*) [86], [87] is a population based stochastic optimization technique inspired by social behavior of bird flocking or fish schooling. The idea of this algorithm is that particles (solutions) move through the search space with velocities which are dynamically adjusted according to their historical behavior. Therefore, the particles have the tendency to move towards the better and better search area over the course of search process.

The proposed algorithm starts with a group of random particles and then searches for optima by updating at each generation the following two best values:

- The best solution *pbest* it has achieved so far.
- The global best solution *gbest* obtained so far by any particle in the population.

At each iteration these two best values are combined, see FIGURE 4-10, to adjust the velocity (4.17), and that velocity is then used to compute a new move for the particle (4.18).

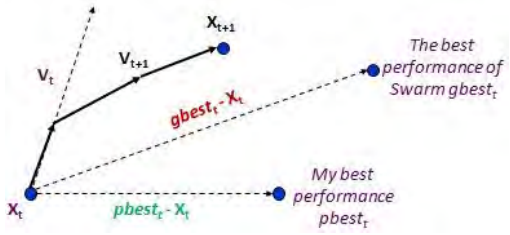

FIGURE 4-10. The movement of each particle in the PSO algorithm. [61]

$$v_{i,j}(t+1) = \chi.\left(v_{i,j}(t) + c_1.r_1.(pbest_{i,j} - x_{i,j}(t)) + c_2.r_2.(gbest_{i,j} - x_{i,j}(t))\right) \quad (4.18)$$

$$x_{i,j}(t+1) = x_{i,j}(t) + v_{i,j}(t+1) \quad (4.19)$$

Note that in the velocity equation (4.16), r_1, r_2 are random numbers generated within the range of [0, 1]. c_1, c_2 are two learning factors which control the influence of the social and cognitive components. χ is the "Constriction Factor" being defined by:

$$\chi = \frac{2}{\varphi - 2 + \sqrt{\varphi^2 - 4\varphi}}, \qquad \varphi = c_1 + c_2, \ \ \varphi > 4 \quad (4.20)$$

The major disadvantage of *PSO* approach is that, when a local optimal solution is reached, with all particles gather around it, escaping from this local optimum becomes difficult. To avoid premature convergence of *PSO*, in this paper it is proposed a new hybrid algorithm that combines the advantages of both Simulated Annealing algorithm (*SA*) (having very good local search ability) and *PSO* (having very good global-search ability).

To obtain a good combination of these two algorithms, *SA* is applied to *PSO* at every *L* iteration if no improvement of the *gbest* does not occur. Otherwise, if *SA* is performed at each iteration, the computational cost will increase sharply and at the same time the fast convergence ability of *PSO* may be weakened.

The *SA* algorithm is applied to the *gbest* in the swarm each *L* iteration that is predefined to be *60* (based on our experimentations). Therefore, the hybrid approach is able to escape from a local optimum with the aid of *SA*, and to keep fast convergence thanks to *PSO*.

In FIGURE 4-11 is summarized the principle of our hybrid algorithm, with the following stages:

```
Initialize swarm (30 solutions)
While maximum number iterations (10000) is not attained
  For each solution x_i do
    If Evaluate (x_i) < Evaluate (pbest_i)Then
        pbest_i ← x_i
    EndIf
    If Evaluate (pbest_i) < Evaluate (gbest) Then
        gebest← pbest_i
    EndIf
  EndFor
  For each solution x_i do
        Calculate solution velocity V_i according equation Eq. 5.
        Update solution position x_i according equation Eq. 6.
  EndFor
  If gbest solution is not improved during L=60 last iterations Then
    //Apply SA algorithm to the gbest solution
    Initialize T ← T_0
    StopCriterion ← maximum number of function evaluation = 2000
    current_solution ← gbest, best_solution ← current_solution
    f_c ← Evaluate(current_solution), fn ← fc
    While Not StopCriterion
      While inner-loop stop criterion
          x ← Generate(current_solution)
          f_n ← Evaluate(x)
          If f_n < f_c or random(0,1) < e^(-(f_n - f_c)/T) Then
              current_solution ← x, f_c← f_n
          EndIf
          Update (best_solution, StopCriterion)
      EndWhile
      Update T according equation: T ← 0.99 x T
    EndWhile
    gbest ← best_solution
  EndIf
EndWhile
```

FIGURE 4-11. The Implementation of the Proposed Algorithm. [61]

(a) Description of a solution (Particle). Each solution *x* is represented by its 8 components, that is, *x = (Dir, hjr, his, hjs, ld, gap, hmp, Lm)*.

(b) Initial Swarm. Initial Swarm corresponds to population

of particles that will evolve. Each particle x_i is initialized with uniform random value between the lower and upper boundaries of the interval defining the optimization problem.

(c) Evaluate Function. It corresponds to the objective function that we want to minimize in the problem, see (4.16).

(d) SA Algorithm. If no improvement of the *gbest* solution occurs during the last *L* iteration, then it means that the algorithm is trapped in a local optimum point. To escape out from local optimum, we apply *SA* algorithm to *gbest* solution. Note that the performance of *SA* depends on the definition of several control parameters:

(i) Initial Temperature. To determinate an initial temperature *T*0, Kirkpatrick [88] suggests that a suitable value of T_0 is one that results in an average probability λ_0 of a solution that

increases f being accepted of about 0.8. The value of T_0 will clearly depend on the scaling of f and, hence, be problem-particularity. It can be estimated by conducting an initial search (*100* iterations in next simulations) in which all increases in f are accepted and calculating the observed average objective increase, δf. T_0 is then given by:

$$T_0 = -\frac{\delta f}{\ln(\lambda_0)} \tag{4.21}$$

(ii) Generate Function. The neighborhood of each solution x is generated by using the following equation:

$$x_{i,j} = x_{i,j} + N(0,1).d.r_j \tag{4.22}$$

where *N(0,1)* is random number with Gaussian distribution, d is the direction of the new neighborhood and takes either 1 or −1, and r_j is a constant that corresponds to the radius of neighborhood generator.

(iii) SA Stop Criterion. The stopping criterion defines the reach of *2000 objective function evaluations.*

(iv) Inner-Loop. The length of each temperature level determines the number w = 100 of solutions generated at each temperature, T.

(v) Decrementing the Temperature. The most commonly used temperature reducing function is geometric.

4.3.4.3 The optimization results

As stated before, the proposed hybrid algorithm was employed for the PMSM-17/39.

In FIGURE 4-12 the variation of the main performances of the studied machine is presented.

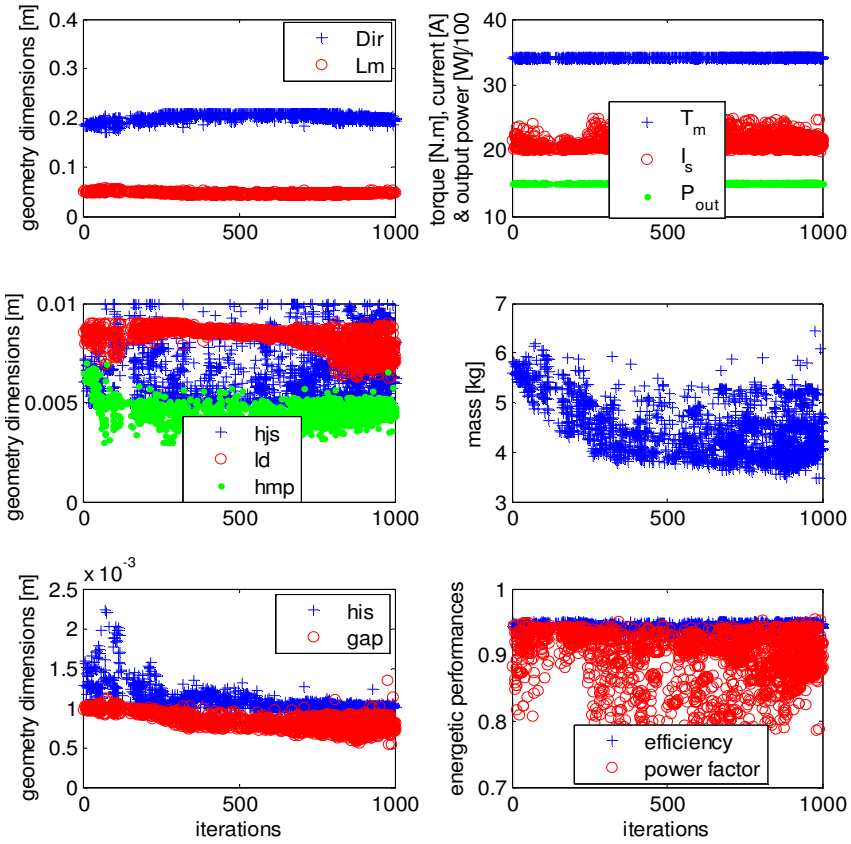

FIGURE 4-12. PMSM-17/39 optimization results. [61]

The algorithm starts from a random solution which will be continuously improved until the maximum number of iterations has been reached. Here, less than 3750 iterations were considered; beyond this limit, after several launch of the algorithm, no improvement has been found. For the sake of presentation, in FIGURE 4-12 only 1000 solutions were plotted (if all solutions should be shown, the plots become crowded and it will be very difficult to have an idea about the real results). It is noticed that the torque (T_m), output power (P_{out}) and current (I_s) constraints are respected. Also, the energetic performances are satisfactory. For a given geometrical configuration the best mass is 3.7697 kg. This mass gain is obtained with new geometrical parameters which variation is shown in FIGURE 4-12. The new values for the optimized geometrical parameters are given in Table 4-9.

TABLE 4-9. THE OPTIMIZATION RESULTS [61]

SYMBOL	***ORIGINAL MOTOR***	***OPTIMIZED MOTOR***	***GAIN (%)***
m_{tot}	5.91 kg	3.7697 kg	+ 36.21
P_{out}	1499.958 W	1500.0767 W	+ 0.0079
P_{out} / m_{tot}	253.8 W/kg	397.93 W/kg	+ 36.21
η	0.9124	0.9034	– 0.98
cosϕ	0.9203	0.9179	– 0.26
c_{tot}	73.99 €	59.39 €	+ 19.73
Dir	207 mm	210 mm	
hjr	8 mm	5 mm	
his	2 mm	1 mm	
hjs	6.5 mm	5 mm	
ld	7 mm	5 mm	
gap	1 mm	0.5 mm	
hmp	3 mm	5 mm	
Lm	50 mm	31.6 mm	

The optimized PMSM-17/39 was verified via FEM. The new geometrical and electrical parameters were considered and the machine's performances were computed. Since the machine's length was decreased significantly, a higher length of the PM was needed to obtain the torque. (The numerical results were presented into the subchapter 2.4) Analysis of optimization results given in Table 4-9 show that several important improvements should be noticed:

- the proposed algorithm presented here offers a mass decrease of 36.21%;
- since the active part mass has significantly decreased, the cost has decreased too; the percentage of cost's decrease (19.73%) is lower than for the mass (36.21%), because the PMs height has increased from 3 to 5 mm.

One should take a look on the '*Gain*' column from Table 4-9, to see the energetic performances of the optimized PMSM-17/39. The efficiency and power factor have practically kept their initial values.

5 THE THERMAL BEHAVIOR OF THE EV'S MOTORIZATION

5.1 Framework and summary of main results

The topic of the thermal analysis of the EV's motorization is still under study and at this moment we can present only few results. The following articles, which treat the thermal operation conditions of EV's motorization, are given here:

- D.Fodorean, A.Miraoui: "Permanent Magnets Thermal Operation Limits in a Hybrid Excited Synchronous Machine used on Wide Speed Applications", Proceedings of the 11th IEEE International Conference on Optimization of Electrical and Electronic Equipment – OPTIM'08, Brasov, Romania, 22-24 May 2008, pp.21-26.
- D.Fodorean, I.A.Viorel, A.Djerdir, A.Miraoui: "Mechanical and Thermal Designing Aspects for a PM Synchronous Machine with Wound Rotor", International Aegean Conference on Electric Machines, Power Electronics and Electromotion Joint Conference - ACEMP-Electromotion'07, Bodrun, Turkey, 10-12 Sept. 2007, pp.502-506.

The temperature influence on the EM behavior and the thermal analysis in different operation conditions is a very important subject in the analysis of the EV's motorization. Since the permanent magnets (PMs) have a temperature stability point, it is important not to surpass this limit. Also, the winding insulation can be permanently damaged if the temperature in the coils is beyond the acceptable limit. Regarding the iron, the steel can lose permanently its magnetic properties for temperatures beyond 700°C, and because our application is not intended to work in such conditions, we can say that the elements that have to be carefully designed are the PMs and the winding. Thus, when thinking to the thermal behavior evaluation of an EM, we think firstly to the material that is used.

5.2 The limits of the thermal analysis by FEM

Since the electromagnetic properties (resistivity and magnetic permeability) and the thermal ones (thermal conductivity and specific heat) are all temperature dependent, the magnetic field distribution and the transient thermal phenomena are dependent upon each other.

In EMs the phenomenon of eddy current generation produces induction heating. This is described by Maxwell's equations. The transient heating of the active parts of the machine, as a result of the Joule effect of induced currents, is described by a Fourier equation. The complexity of this type of computation can give satisfactory results only through numerical analysis, based on FEM. Such an analysis should take into account the interaction between electromagnetic and thermal phenomena.

Theoretically, the principle of the magneto-thermal coupling, which characterizes the induction heating processes in our machine, can be explained based on solving the magneto-harmonic and thermal transient equations at each time step. The derivation with respect to the variable time, in the Fourier equation, is approximated by finite differences and the study time domain (t_0 - *initial time,* t_f - *final time*) is replaced by a series of discrete time step values (t_0, t_1, t_2, … t_n …, t_f). At each time step t_n, $n = 0, 1, 2, …$, first the electromagnetic aspect is analyzed and then, the thermal one. The algorithm of this method contains:

- Computation of the Maxwell's equations and the surface power density generated by the Joule effect of eddy currents;
- Computation of the finite difference approximation of the Fourier equation;

- Computation of the new values of electromagnetic and thermal properties, which correspond to the final solution of the temperature field in step 2.
- Returning to step 1 for the computations of the next time step.

Concerning the numerical characterization of the thermal behavior of the studied machines, the author has encountered one major problem. Up to now we have not found a software package which takes into account the transient operation of the magneto-thermal coupling technique. On the other hand, since the thermal coupling modulus, of the used software, analyses the steady state magnetic with transient thermal regime, the carried out analysis did not gave satisfactory results. That is why the author is trying the extract from the EM's magnetic behavior (analyzed with FEM) the thermal limitations of the studied motorization variants. A second approach will be the use of the MotorCad software, which is based on thermal resistances equivalent circuit.

5.3 The thermal influence on the PMs stability operation for the DESM

Some phenomena occurring in the operation of an EM can be revealed only after the machine is tested and the performances evaluated, but some others can be predicted even in the design process. Such phenomenon is the heat of the machine. The thermal aspects should be taken into account for every built up electrical machine. The author is aware that he cannot take into account in his work all the thermal possible issues that could affect the behavior of the proposed machine, but some of them should not be ignored. A parameter which needs to be taken into account, absolutely, is the irreversible demagnetization of the PM.

When it comes to the PM motor one should give a special attention to their thermal behavior. The PMs operating point varies with the temperature. Usually, the Neodymium-Iron-Boron material is used, because it presents the best high density per volume. However, their weak point is the temperature operation limit: they lose their magnetization properties quite soon (in comparison with the Ferrites magnets – rather used for application with low dynamics because of their weak remanent flux density, [32], [33], [35], [36]). Because the DESM is more exposed to the irreversible demagnetization, due to auxiliary field winding supply, the problem of thermal stability of the magnets of the DESM will be treated here.

Two situations appear when thinking to the DESM: the field winding is fed to assure the necessary excitation flux (or to strengthen the PMs field), or to weaken the PMs field (if it is intended to explore higher speeds). In both cases feeding the auxiliary field winding involves supplementary joule losses, meaning heat that could irreversibly demagnetize the PMs. The analyzed DESM uses the PMs with the following demagnetization characteristic, given by the supplier, FIGURE 5-1.

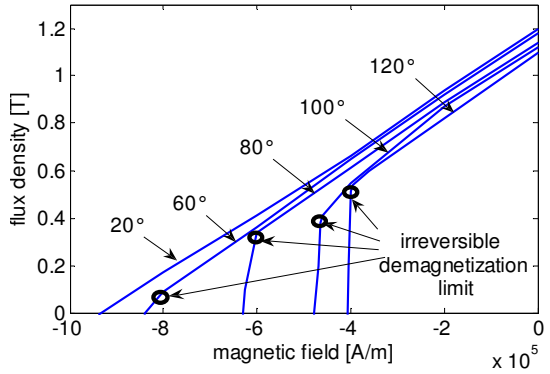

FIGURE 5-1. The magnetic characteristic of the PMs. [89]

In FIGURE 5-1, one can observe:

- The remanent flux density (B_r) at zero magnetic field;
- The coercitivity field (H_c) at zero flux density;
- The irreversible demagnetization limits function of the temperature. Below these limits it is sure that small portions or all the PM can be irreversibly demagnetized.

If the material is completely compromise, it is quite difficult to recover its properties.

On the other hand, the presence of the auxiliary winding can be used for magnetizing the PMs. This process is rough because the flux density cannot be correctly evaluated in all the PM's volume and can be made only with huge current pulses, which could damage the winding insulation. However, if the rotor is taken out, the PMs' flux density can be again restored.

The studied DESM (which design and numerical analysis was presented into subchapter 2.3) has the magnets mounted on the rotor pole's surface, and an auxiliary winding (of concentrated type) placed around the rotor poles, FIGURE 5-1-right.

The machine's magnetic analysis helps us to predict the PMs stability operation. While the machine operates at high speed values, as the air-gap field is weakened, we should prevent the irreversible demagnetization of the PMs. Several simulations, at no-load and load operation, have been employed. Feeding the rotor winding with a 'negative' auxiliary current (If), the air-gap flux density is decreased (see FIGURE 5-2), because the PM's operating point was modified. From the material characteristic given by the supplier (FIGURE 5-1) one can establish the lower limit of the PM operating point, function of the temperature, Table 5-1.

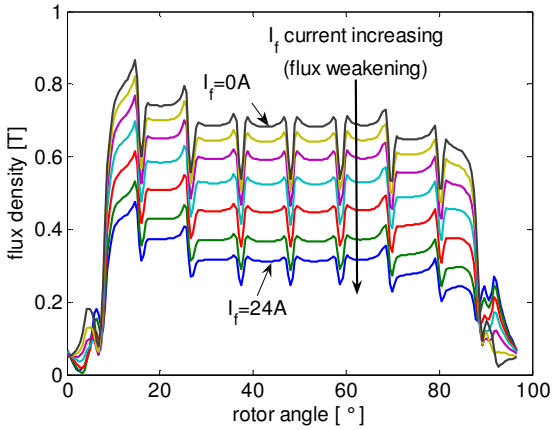

FIGURE 5-2. The airgap flux density curves function of auxiliary current values (I_f=0/4.2/8.5/12.7/17/21.2/24A) on *load* operation, 20°C. [89]

TABLE 5-1. THE PM FLUX DENSITY OPERATING POINT LIMITS [89]

TEMPERATURE	***FLUX DENSITY***
20°C	below 0T
60°C	0.05T
80°C	0.21T
100°C	0.4T
120°C	0.52T

One can clearly see that for 20°C operation temperature, the maximum injected current will not damage irreversibly the magnet material; a minimum of 0.197T is found. Thus, one can magnetically check the PM's thermal stability. As a sample of safe operation, the flux density repartition is given in FIGURE 5-3.

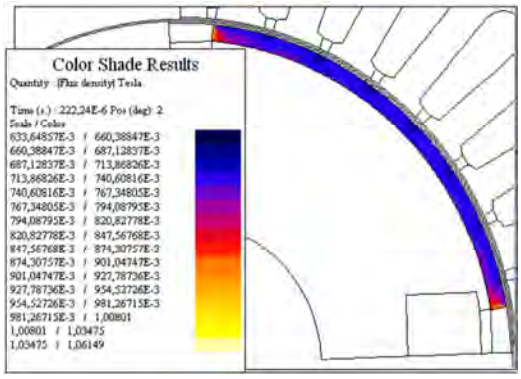

FIGURE 5-3. PM's flux density repartition: 20°C, I_f=0A. [89]

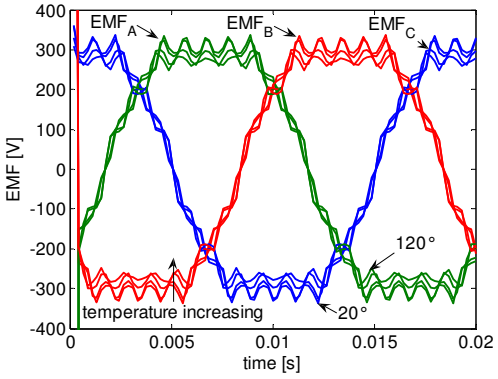

FIGURE 5-4. Back EMF function of temperature operating (20, 60, 80, 100, 120°C). [89]

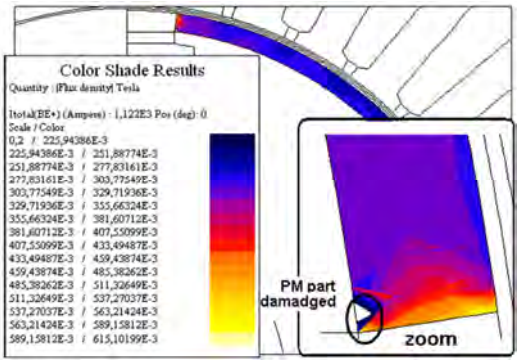

FIGURE 5-5. PM's flux density repartition: 80°C, I_f=18A. [89]

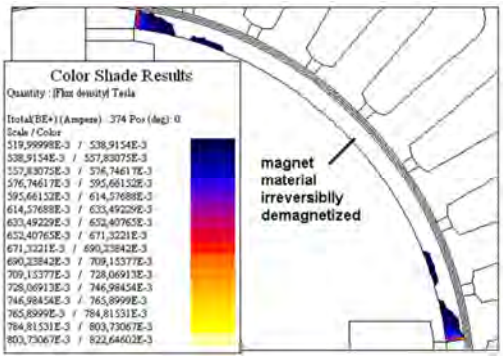

FIGURE 5-6. PM's flux density repartition: 120°C, I_f=6A. [89]

The authors have furthermore verified (by FEM) the thermal influence on the DESM operation. The PM material depending on temperature was introduced in the simulation software and several computations were carried out. Thus, the influence on the induced electromotive force (emf) was computed. One can see in FIGURE 5-4 how the emf is reduced, due to temperature effect. Thus, for the upper and lower temperature limits, one can measure a decrease of this voltage up to 12% – generally, an experimental measure of the EMF could be useful in order to estimate if the PMs were temporarily or permanently demagnetized.

For reduced temperature values, there is no problem regarding the irreversible demagnetization. On the other hand, as the temperature is increased, the demagnetization limit is reached. It can be seen that at 80°C, for 18A auxiliary current value, the PM is partially irreversibly damaged, FIGURE 5-5 – as the auxiliary current was increased, magnet material corners seem to have lower flux density values than those established by the supplier. Moreover, for 120°C the magnet material was entirely compromised, even at low values of auxiliary current, FIGURE 5-6 (no flux density colors shade).

In FIGURE 5-7 one can see the PM's thermal operation limits and the safe operation conditions of the studied DESM.

It should be noticed that in harsh temperature environments the proposed DESM cannot work properly if an increased speed is demanded (for example, one can imagine a hot day in summer, when the operation temperature of the electric vehicle surpasses 40°C; for wide speed operation, since the auxiliary winding involves temperature rising, the PMs can be destroyed). Several solutions can be employed, in order to avoid the magnet material damage:

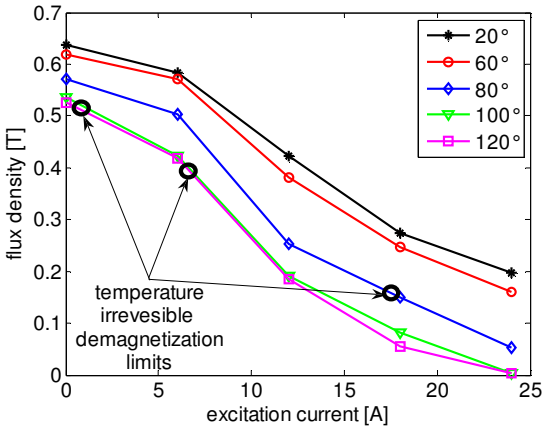

FIGURE 5-7. The flux density RMS and minimum values, in the PM, for different values of the operation temperature. [89]

- The use of another type of magnet material who presents better temperature characteristics (in our days, the manufacturers propose Nd-I-B magnet type at 1.4T and 210°C), but this can double the PMs cost. Also, the Samarium-Cobalt material is much more stable than the Nd-Fe-B.
- Increase the PMs height (and consequently the air-gap's thickness, since the emf must have a desired value), but this will reduce the machine's flux weakening capability.
- Supplementary conditions can be taken into account if high values of the temperature can affect permanently the machine's operation (artificial cooling for example).

5.4 Thermal aspects for the studied RF-PMSM

The thermal behavior can drastically influence the machine's performances. Thus a special attention should be paid on the heat transfer within the active and passive parts of the machine.

The heat sources on the machine are: the copper loss (while feeding the windings), the iron loss (for a more precise calculation, even the iron loss within the magnets can be considered) and the mechanical loss (in the bearings). If we do not consider an auxiliary cooling system (like a water pump), we should pay a special attention to the operating conditions. For example, we should check if the machine is running at permanent regime for a long period of time, or if the operating regime is intermittent.

When studying the motorization of an EV, the road conditions can be imposed. Here, the new european driving cycle (NEDC) is considered. If the vehicle is not running on highway, the EV can be tested on the european driving cycle (EDC). In the case of the EV for people with reduced mobility we have considered a slightly modified EDC, because the acceleration ramps are not a necessity (like for common electric scooter). Such a study was employed here, based on the Motorcad software.

5.4.1 Thermal analysis of the RF-PMSM by using MotorCad software

Here only the main steps of the thermal analysis employed in MotorCad will be resumed. Firstly the geometry should be introduced. Next, the winding should be defined. The cooling conditions (with air or water) are defined, as well as the heat sources (the losses), the rated torque and current/phase, the materials, the load conditions (speed and torque profile depending on time, due to various rolling conditions) etc. Finally, the performances of the studied machine are evaluated.

In resume, the MotorCad thermal model consists in following the next steps:

- *Geometry* (defining the geometry's parameters).
  - Introducing the correspondent type of machine (with surface mounted PMs, with inner or outer rotor etc.).
  - Defining the radial and axial geometry parameters.
  - Defining the non-active parts dimensions and stator-rotor configuration (number of poles and slots, straight or trapezoidal tooth, dimensions of the housing and cooling system etc.).
- *Winding* (defining the winding topology).
  - Defining the winding type.
  - Defining the conductor profile and diameter.
  - Defining the number of conductors per slot or the filling factor.
- *Inputs* (defining the inputs of the thermal modeling).
  - Defining the cooling conditions (water or air-cooling system).
  - Defining the heat sources: the losses, the load phase current and torque.
  - Defining the materials and evaluating the machine's weight.
  - Defining the load duty cycle.
- *Temperature* (evaluating the temperatures in the machine).
  - Automatic generation of the lumped thermal circuit.
  - Evaluation of the active and non-active parts temperatures in radial and axial cross section.
- *Outputs* (evaluating the temperatures in the machine).
  - Evaluation of the temperatures within the machine.
  - Evaluation of machine's performances.
- *Transients* (variation of the temperatures and losses in the machine).
  - Evaluation of the temperatures variation on the given EDC.
  - Evaluation of the losses variation on the given EDC.

5.4.2 Simulated results of the studied RF-PMSM

After the definition of the machine's geometry, cooling condition, heat source and materials, the loading conditions are defined. A slightly modified EDC was considered (see the Appendix section). This EDC is employed on 200 seconds. In order to reach the temperature stability, 54 duty cycles were considered, meaning that the simulation equivalent time is 10800 seconds (which is 3 hours).

The resume of results is presented in Table 5-2. A summary of the variation of the temperatures within the active and non-active parts of the machine is presented in FIGURE 5-8.

TABLE 5-2. RESUME OF RESULTS FROM THERMAL ANALYSIS WITH MOTORCAD [1]

PARAMETER	*VALUE*	*UNIT*
Temperature on the stator yoke	95.5	°C
Temperature on the stator teeth	96.9	°C
Temperature on the winding (average)	97.7	°C
Temperature on the PMs	92.5	°C
Temperature on the rotor yoke	92.4	°C
Temperature on the shaft	92	°C
Temperature on the front bearing	84.2	°C
Temperature on the rear bearing	88.5	°C
Temperature on the housing	91.1	°C

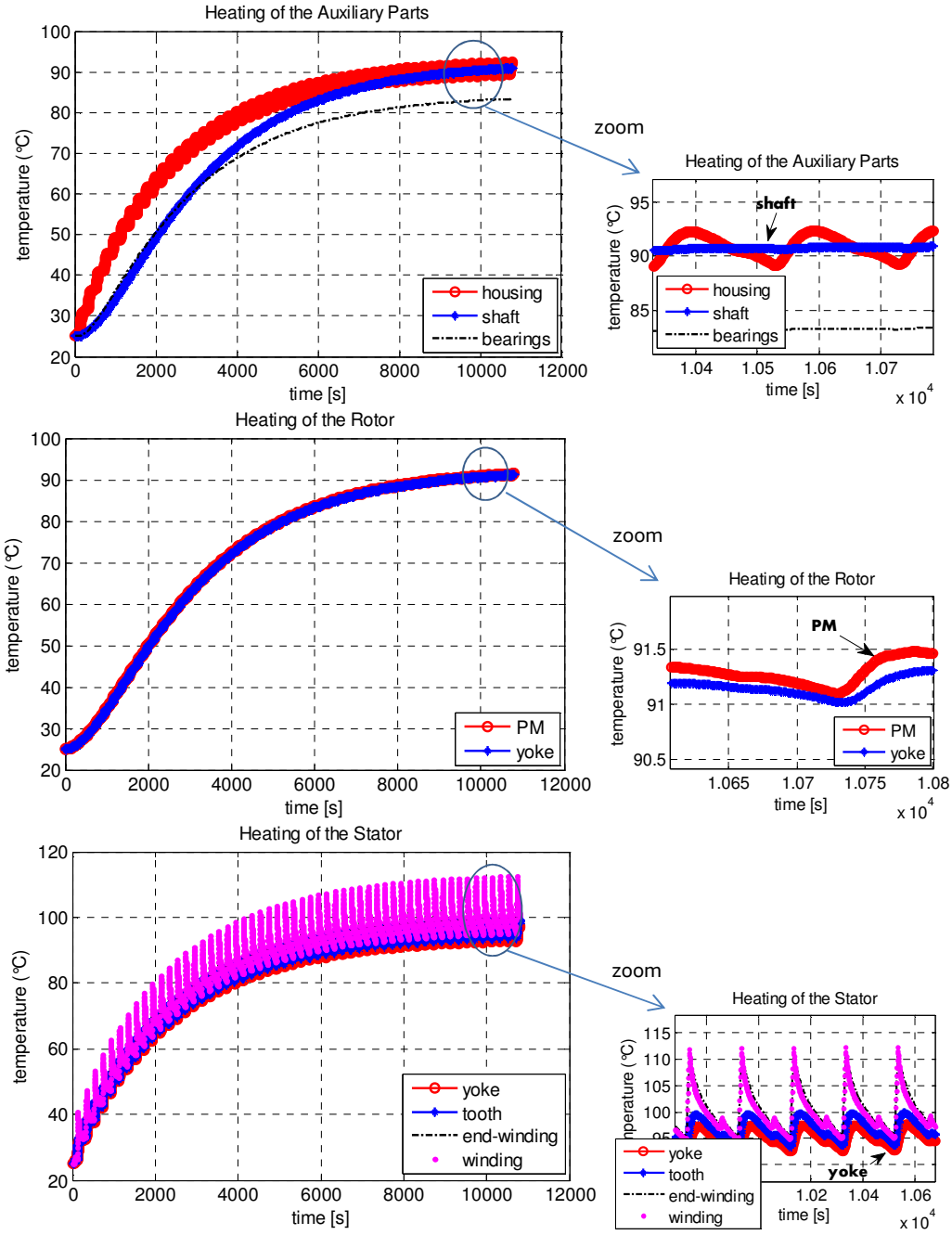

FIGURE 5-8. Temperatures on the active and non-active parts of the RF-PMSM. [1]

By consulting the temperature results, it can be said that the temperature limits are not surpassed for the winding, the PMs, the steel and housing materials. Concerning the bearings, the acceptable operating temperature is of 70°C, meaning that there is an important risk of burning the lubrication oil. So, for 3 hours operation we should consider an auxiliary cooling of the bearings. Anyway, the ES-PRM, for which the RF-PMS was designed (see 3.2 and 3.5.1 sections), perhaps will not run continuously for 3 hours; thus, no thermal risk exists.

6 FAULT TOLERANCE, CONTROL AND WIDE SPEED OPERATION

6.1 Framework and summary of main results

This chapter summarizes the author's research activities and results, with regard to the control of *ac* machines and drives, used in EVs. The topics stated into the chapter's title were not particularly treated into a research contract, but they resulted from several cooperation studies, with Romanian colleagues or researchers from abroad. The main results were published into the following scientific papers:

- M. Ruba, D. Fodorean, "Analysis of Fault-Tolerant Multiphase Power Converter for a Nine-Phase Permanent Magnet", IEEE Transaction on Industry Applications, vol.48, nr.6, pp.2092-2101, November/December 2012.
- D. Fodorean, D.C. Popa, M. Ruba, "On the Fault-Tolerance of Permanent Magnet Synchronous Machines and Drives used in Hybrid Vehicle Application", International Review of Electrical Engineering, vol.7, n.2, pp.3795-3803, March-April 2012.
- A.R. Matyas, K.A. Biro, D. Fodorean, "Multi-Phase Synchronous Motor Solution for Steering Applications", Progress In Electromagnetics Research, vol.131, pp.63-80, 2012.
- D.Fodorean, M.Ruba, L.Szabo, A.Miraoui: "Comparison of the Main Types of Fault-Tolerant Electrical Drives used in Automobile Applications", Proceedings of the IEEE International Symposium on Power Electronics, Electrical Drives, Automation and Motion – SPEEDAM'08, Ischia, Italy, 11-13 June 2008, pp.895-900.
- D.Fodorean, S.Giurgea, A.Djerdir, A.Miraoui: "Numerical Approach for Optimum Electromagnetic Parameters of Electrical Machines used in Vehicle Traction Applications", Energy Conversion and Management, vol.50, pp.1288-1294, Mai 2009.
- D.Fodorean, I.A.Viorel, A.Djerdir, A.Miraoui: "Performances for a Synchronous Machine with Optimized Efficiency while Wide Speed Domain is Attempted", IET Electric Power Applications, vol.2, n°1, pp.64-70, January 2008.
- D.Fodorean, A.Djerdir, A.Miraoui, I.A.Viorel: "FOC and DTC Techniques for Controlling a Double Excited Synchronous Machine", Proceedings of the IEEE International Electric Machines and Drives Conference, Antalya, Turkye, 3-5 May 2007, pp.1258-1263.

6.2 Fault tolerant electrical machines and drives

6.2.1 Three/six-phase induction machine for fault tolerant applications

By definition, a fault-tolerant drive is the machine-converter system which has the ability to operate in a satisfactory status even after faults have occurred. The potential faults can be divided in two categories: related to the electrical machine (winding open circuit and short circuit), and within the power converter (power device open circuit, power device short-circuit and dc link capacitor failure) [90]-[93]. When thinking to design a fault-tolerant machine-drive circuit, the aim is to develop a drive which can continue to operate with any one of these faults.

The induction machine is the industry's preferred variant, because of its construction and supplying simplicity. For the squirrel cage induction motor (SC-IM) different type of windings and coils faults will be analyzed. All analyses were carried out in terms of fault-tolerant capability, having in mind to get a smooth torque, as well as ameliorated energetic performances.

The FEM analysis offered up to now satisfactory results, so one can have confidence in it. Even if it is time consuming, many aspects of the drive operation can be simulated, verified, and different solutions could be employed, optimized or validated.

Four topologies of SC-IM were studied, having: 2 poles, 24 stator slots, 20 rotor bars, a double layer 3 phases and 6 phase winding with polar or shortened pitch (FIGURE 6-1). A specific electric circuit is associated to it, see FIGURE 6-2 (here, the end-winding effect is simulated with an inductance; also, on top of each phase, a resistor of 10^7 Ω, is placed to simulates a voltmeter).

Eight FEM cases were studied on the SC-IM: (**a**): health operation; (**b**): one short-circuited coil; (**c**): two short-circuited coils (only for 3-phase topologies); (**d**): one short-circuited phase; (**e**): one open phase; (**f**): one short-circuited coil from two different phases; (**g**): two short-circuited coils from two different phases; (**h**): two open phases (only for 6-phase variant). From simulations, one can see the voltage, current, torque, stator and rotor iron losses results.

The simulations were made in the following conditions:

- the phase resistance is 1.5 Ω, except the IVth case, where is 0.75 Ω.
- the voltage RMS value for the first three cases is 540 Vca (50 Hz), while for the IVth case it was chosen at 220 Vca in order to obtain, approximately, the same mean torque value as for the three phase topology.
- the computations were made to a constant speed, at 60% of the rated value, in order to simulate a supplementary effort (torque) of the SC-IM.

The simulation results of the healthy case of the three phase winding SC-IM, with polar pitch, are given in FIGURE 6-3. Similar results were obtained for all the other studied cases, in order to realize a comparison in terms of mean torque and iron losses, the simulation results being presented in stator and rotor iron losses, FIGURE 6-4.

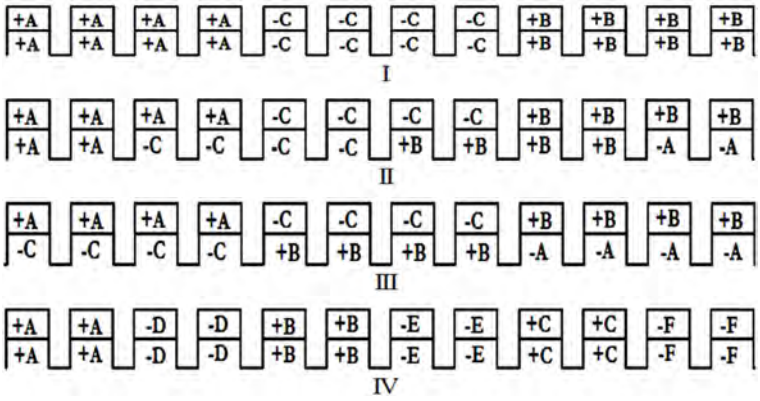

FIGURE 6-1. Phase arrangements in the studied SC-IM: (I) 3-phase winding with polar pitch; (II), (III) 3-phase winding, with shortened pitch; (IV) 6-phase winding with polar pitch. [94]

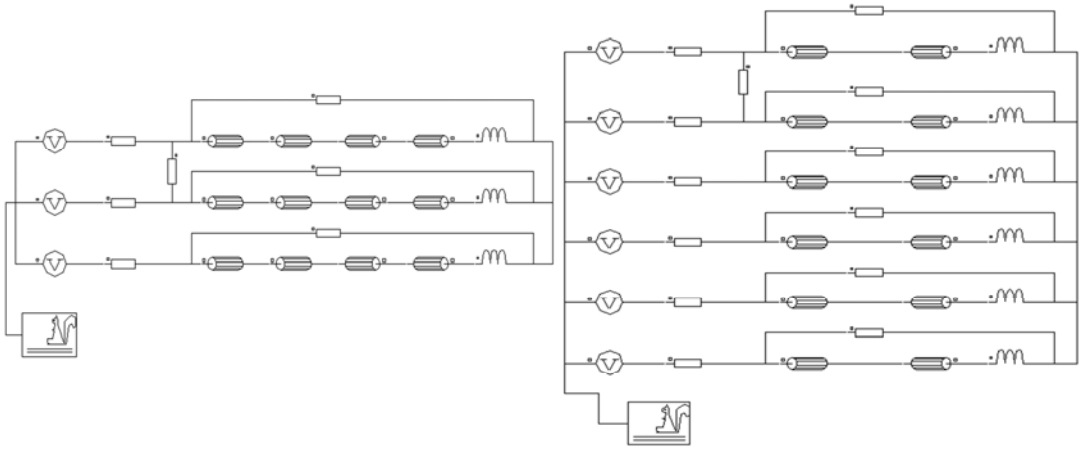

FIGURE 6-2. Electric circuits for the SC-IM supplying: the 3-phase (left) and 6-phase electric circuit. [94]

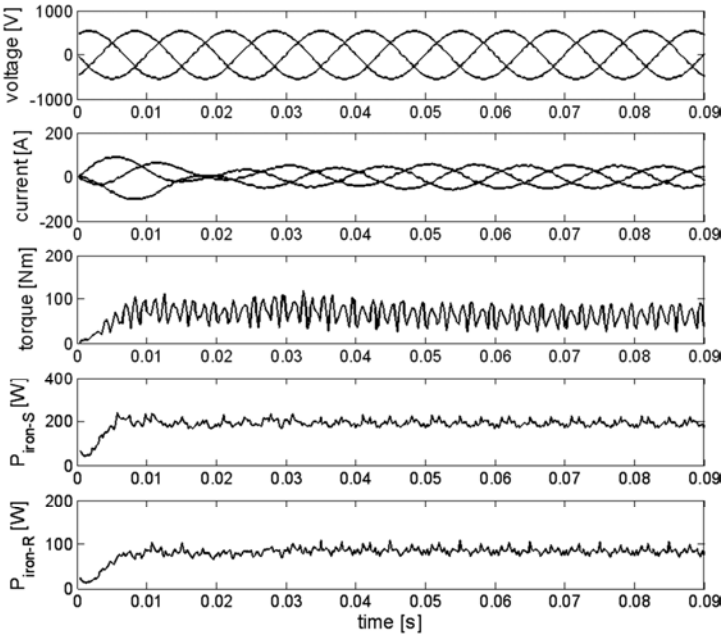

FIGURE 6-3. The three phase SC-IM (polar pitch winding) results in healthy case.[94]

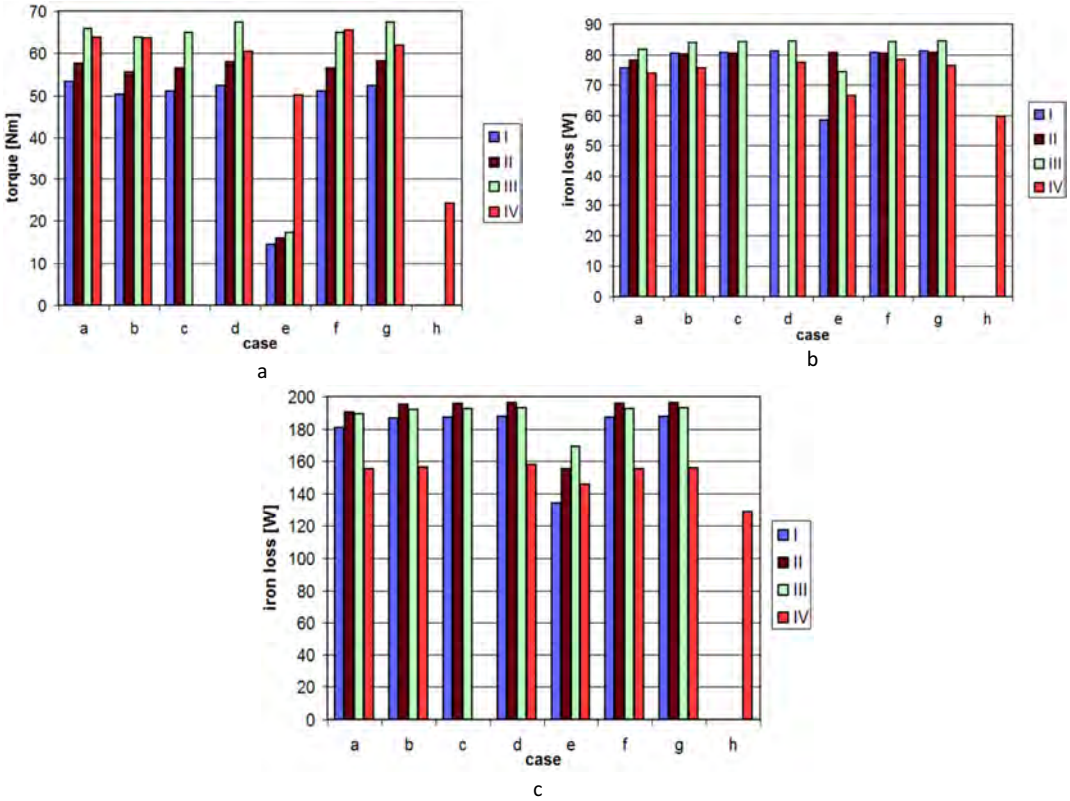

FIGURE 6-4. FEM results of the studied SC-IM: a) mean values of the torque for the studied SC-IM; b) mean values of the stator iron core loss; c) mean values of the rotor iron core loss. [94]

From the mean values of the torque and stator/rotor iron losses (FIGURE 6-4), one can see that the 3-phase shortened pitch (III) case gives better results than the polar winding (I) in term of maximum torque value, with relatively the same amount of iron losses, since the decrease of the harmonic content. The iron losses decrease it is much obvious for the 6-phase topology

(here the iron losses decrease also due to the low level of RMS voltage, meaning that one can reduce the absorbed power and the investment, while there are six electric sources and other network equipment which will increase the costs).

For several occurred faults (cases b, c, d, e, f, g, h), the mean values are approximately the same (the wave ripples are increasing as the faulted is more important, thus producing losses). The main differences appear for 1 phase or 2 phase open-circuit faults. The 6 phase topology offers a quite important torque capability even for 1 phase open circuit, while for 2 phases open circuit the torque reaches 40% of its mean value in health operation.

6.2.2 The SRM for fault tolerant systems

The switched reluctance motor (SRM) has the phase windings of concentrated type, thus being the researchers' favorite topology in terms of fault-tolerance operation. However, the fault aspect is a subject which cannot be forgotten, and therefore a more accurate characterization has to be made. The open-circuit and short-circuit of a phase will be verified, as well as the influence of the number of phases and poles.

By coupling SRM with an intelligent drive, will result in a fault-tolerant system. The machine studied here is a 12 stator poles against 14 rotor poles. Thus, it is possible to use the "two phase on" current feed technology. The present study was concentrated on the classical method of currents feeding, by using the pulse width modulation (PWM) method. The stator winding contains six channels, and each of them includes two phases which are fed for the same rotor position.

The electrical circuit of the drive is presented in FIGURE 6-5. One fault tolerance case is given by the phase separation from the drive. The switches are simulated by using resistances with floating levels between high and low values, corresponding to on/off states.

Four study cases have been employed: **(a)** normal (health) operation, **(b)** one phase fault, **(c)** two faulted phases, from different channels, **(d)** whole channel failure.

In FIGURE 6-6 one can see the torque and current waveforms for each study case. For one phase fault, the torque will decrease due to the missing current contribution. The loss of two currents, from two different channels, will determine two decrease regions in the torque characteristic, but its mean value still remains in the desired range.

In case of drive failure a sever fault can occur when there is no possibility to control one channel. Practically the machine will have now a dead zone. For passing through this zone, only the machine's inertia will be helpful. A serious problem interferes since the drive has to be able to use the rest of phases to take the rotor out from this situation. This corresponds to (d) case in FIGURE 6-6.

In Table 6-1 a comparison of the mean torque in healthy/faulty conditions is presented.

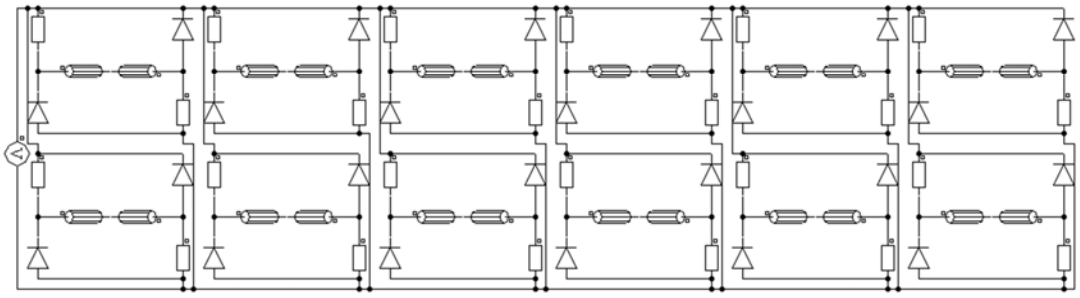

FIGURE 6-5. Electrical circuit for the SRM drive.[94]

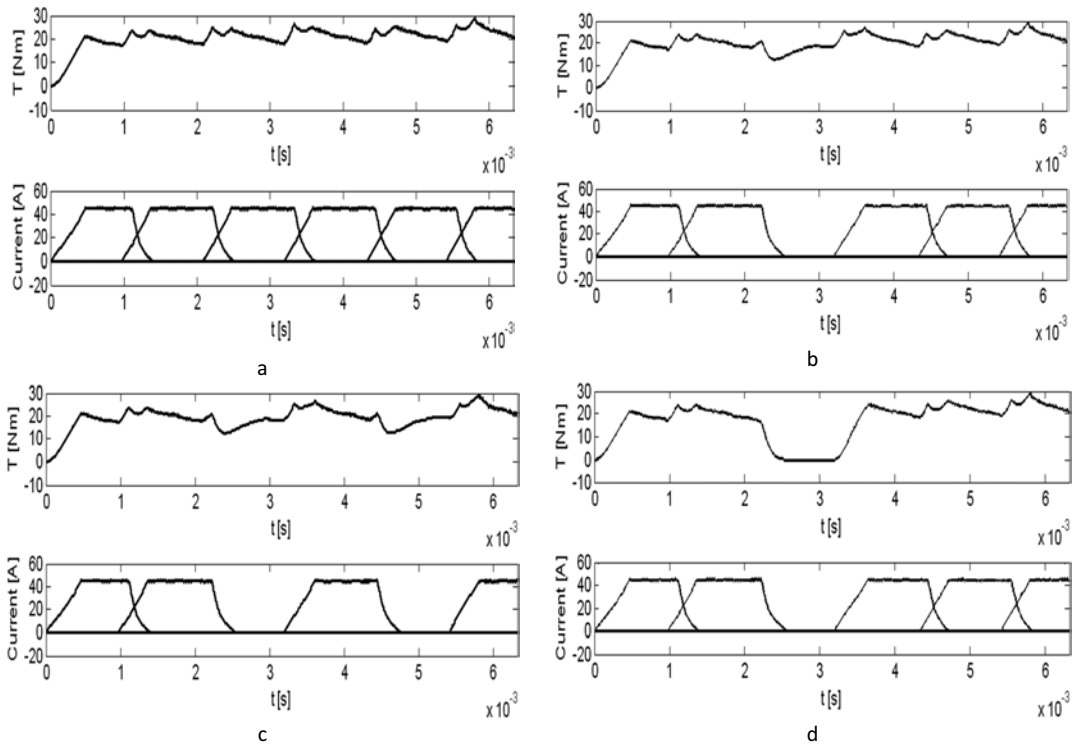

FIGURE 6-6. The SRM's torque & current wave forms in healthy (a) and faulty (b),(c),(d) operation. [94]

TABLE 6-1. MEAN TORQUE VALUES FOR THE SRM OPERATION [94]

PARAMETER \ *CASE*	*A*	*B*	*C*	*D*
Mean torque (Nm)	20.75	19.99	19.15	16.73

The loss of torque in case of one and two phase failure is very small. On the other hand, a high amount of torque is lost when a whole channel falls. Nevertheless, the operation could continue till the machine is stopped (or replaced).

6.2.3 The fault tolerance of a six-phase PMSM

The six-phase machine, analyzed here, from the fault tolerance capability point of view, was presented in subchapter 3.3. A multi-phase machine has intrinsically a fault-tolerance capability, meaning that in the case of one fault, the other phases should cover the lack of power due to faulted phase. Here, the motor's capability to operate in faulty conditions will be verified numerically. This numerical analysis is employed through FEM, based on JMAG-Studio software, on a 2D model.

The transient response analysis module was used to simulate the machine's magnetic behavior. Several results have been obtained, here being presented only the axis torque in healthy and faulty conditions, FIGURE 6-7. The torque ripples are influenced by the cogging torque, due to the strong PMs (1.4 T remanent flux density material has been used). The mean value of the electromagnetic torque is 0.341 Nm, which corresponds to the application's demands. On a contrary, the torque ripples are quite high for such a topology, FIGURE 6-7. A solution to reduce the torque ripples is to incline the stator.

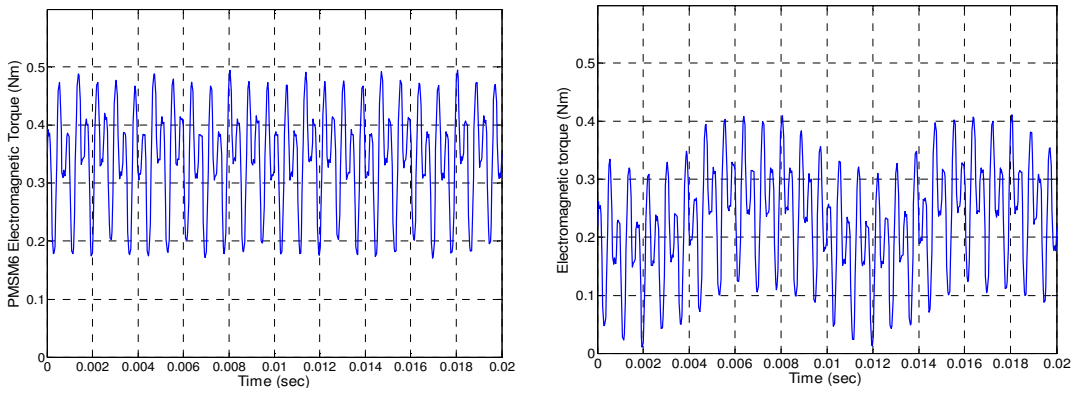

a b

FIGURE 6-7. PMSM 6 simulation axis torque in: a) healthy case; b) 2 open phases fault. [51]

The mean value of the electromagnetic torque for open phase operating of the 6-phase PMSM is 0.284Nm, which represents 83.28% from the mean value in no-fault operation. The electromagnetic torque for two-open-phase operating is 0.227Nm, 66.57% from the no-fault torque value. For this worst case, the torque is varying between the minimum value of 0.05 Nm and a maximum of 0.4 Nm. But we are still satisfied by the fact that even for a very severe operating case the machine can still operate. In order to improve the quality of the wave profile (to have a smother torque), we should provide a specific control technique, which could compensate the torque ripples (not discussed here).

To determine the characteristics of the proposed PMSM, a test bench was built, as shown in FIGURE 6-8. The test bench consists of: the proposed 6-phase PMSM, a DC motor used as a load, 2 three phase Semikron-SemiTeach inverters, PC+dSPACE for the control of the energy flow in the system, current transducers, incremental encoder of 2048 resolution for speed measuring and rotor detection. The control strategy was employed in dSPACE 1104. For simplicity a scalar control technique was built in Simulink. Since the PWM generator available on the dSPACE board is of three phase type, for the second-star of the 6-phase PMSM, an inverse signal has been used used. This is the advantage of this six-phase configuration, which permits the use of only 3 PWM generators to control 12 switches of the 2 inverters.

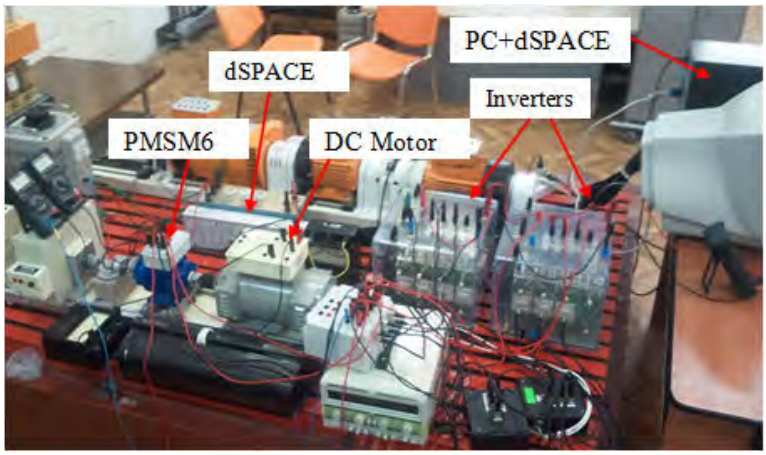

FIGURE 6-8. The test bench.[51]

Different measurements were made for different load operation. The six-phase currents and the comparison between the simulated and measured torque are plotted in FIGURE 6-9.

Another comment is needed with respect to the comparison between the calculated and experimental results, let's say, on the current characteristic. Here, for the same output power of

70 W, the difference between the current is equal to 0.233 A, meaning 19 %. This difference is common for very small electrical machine since the leakage inductance cannot be precisely calculated. Also, the winding of the machine is hand-made, thus the human error interfere here.

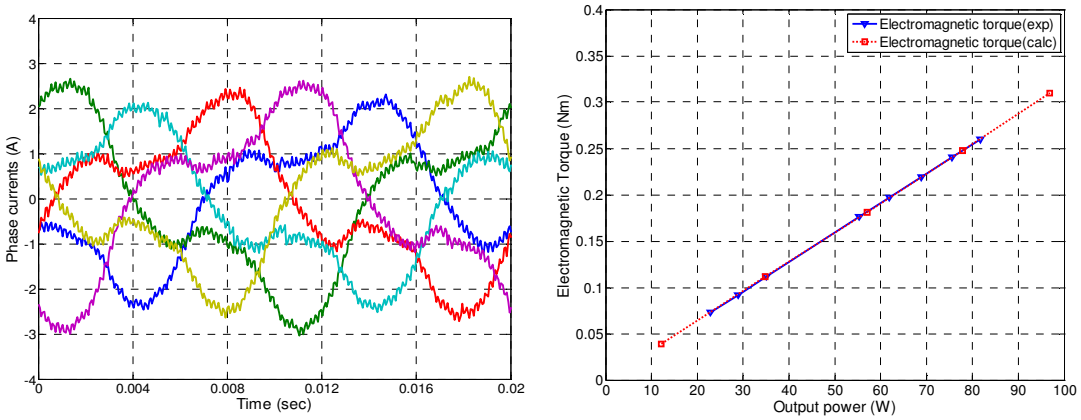

a b

FIGURE 6-9. PMSM 6 measured characteristics: a) the 6-phases currents; b) the torque. [94]

6.2.4 The nine-phase PMSM

Up to now, the researchers did not really exploit the solutions with higher number of phases. Studies like the one from [95] (where the vector control strategy was investigated for a 9-phase machine) are rather singular, and most of the time only theoretically approaches and results have been reported. One of the reasons is due to the controllability complexity when more than 6 phases need to be fed. The microcontrollers found on the market today cannot meet such specifications, meaning to assure the pulse width modulation (PWM) for more than 12 switches. Even with digital signal processors (DSP), the controllability of more than 12 switches is difficult. The field programmable gate array (FPGA) device has the computation power to control 9-phase drives, but the main issue is to employ the PWM for each switch, to elaborate the control technique and realize the analog to digital conversion (ADC) while acquiring the 9-phase measured currents. In the present study a control unit based on DSP is used, where the PWM and the ADC, as well as the control technique, are rather simpler to employ.

For a 9-phase machine, the inverter used, in the simplest configuration, needs 18 switches, FIGURE 6-10a. This variant do not assures the fault tolerance, if an inverter leg or machine's phase fault has been occurred (but the machine can still operate even with fewer phases). In order to have a complete fault tolerant inverter, an H-bridge-9-phase inverter is requested. Such variant is presented in FIGURE 6-10b, but this demands the control of 36 switches, which is practically prohibitive for the control units used today.

The goal and the main achievement of this research work was to propose, realize and employ a simplified 9-phase inverter dedicated for the supply of a 9-phase PMSM capable to assure the fault tolerance even when the most severe damage appears. The proposed converter configuration is presented in FIGURE 6-10c, having the same effect like the one from FIGURE 6-10b, but with a reduced number of switches: 24 switches are considered here, with 3 stars connections at the end of each group of three phases. This solution is not only much simpler, but offers also the possibility to have the operation even if 6 phases of the machine are not supplied. Moreover, even if 1 of the last 3 phases is not working, the system can still operate in compensation mode (only two phases being supplied)!

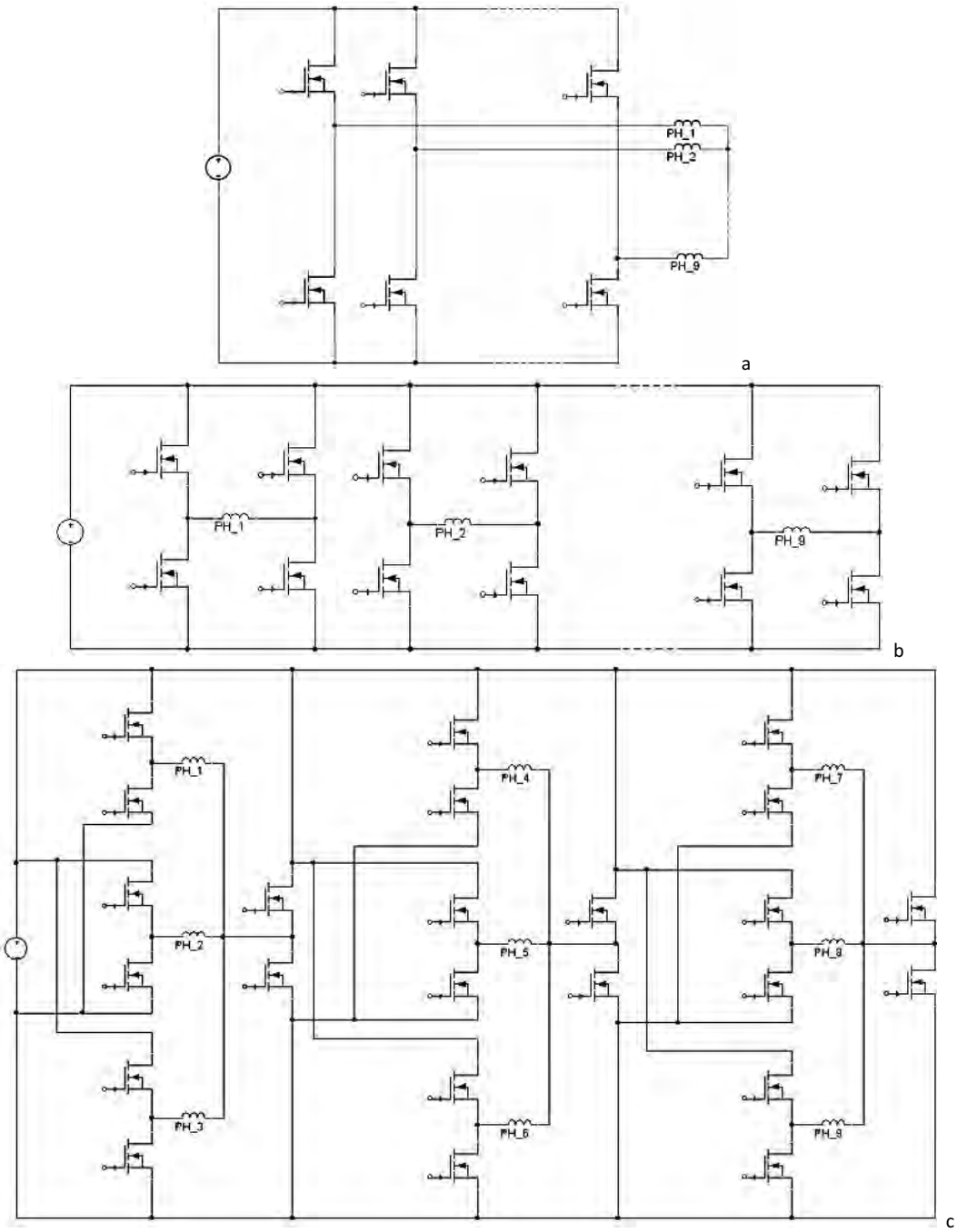

FIGURE 6-10. Topologies of 9-phase inverters: a) classical drive (common neutral point);
b) H-bridge 9-phase inverter with fault tolerant capability;
c) proposed simplified and fault tolerant 9-phase drive. [96][94]

The machine was firstly designed, analyzed numerically as well as its controllability and fault tolerance capability, by using the Flux2D-Simulink coupling technology [96]. Some of those results will be presented here. Finally, several cases of faults and the drive operation in faulty conditions will be verified experimentally, to prove the system's capability to operate in faulty conditions.

In FIGURE 6-11, the main assembly parts of the designed machine are presented.

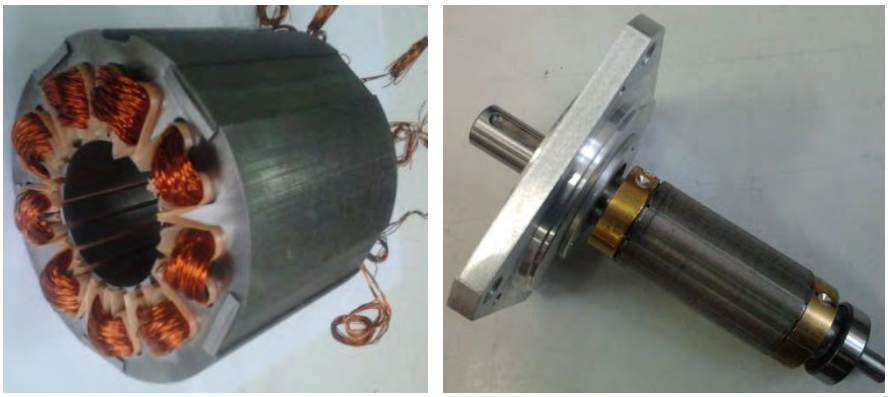

FIGURE 6-11. The stator with the coils around each tooth (left) and the rotor with the surface mounted magnets (right) of the constructed 9-phase-PMSM. [96]

In the literature there are many debates regarding the remedial strategies for such 9-phase converters. Some of them regard a safer yet more complex and expensive solution represented by the H-bridge based converter (see FIGURE 6-10b). The structure is designed using 36 switches, 4 for each phase of the machine.

Discussing about fault-tolerance, a fundamental danger of the full H-bridge topology should be mentioned here. A direct short-circuit can occur if the top and bottom switches of the same branch are turned “on” at the same time. In normal conditions, the top and bottom stages of a half of the H-bridge of a single branch are never “on” at the same time, unless a malfunctioning command is received from its controller. This can be avoided by monitoring the operation of the control system.

Moreover, a short circuited power switch is more difficult to manage. The solution is the total isolation of the entire branch by opening, and keeping permanently opened, all the corresponding power switches. This way the fault-tolerance is ensured by the physical separation of the damaged branch. Of course in this case the motor has to be fault-tolerant, to be able to continue its work (even at lower torque and at higher torque ripples).

In a more critical case, when both top and bottom switches of a branch failed shorted, the above mentioned branch exclusion method does not have effect. To solve this problem and to improve the performance/cost ratio of the power converter the classical H-bridge scheme given in FIGURE 6-10b is proposed to be changed by a simpler one, see FIGURE 6-10c.

In this special scheme the winding is divided in 9 phases, grouped 3 by 3. Star (Y) connections are created for each group of 3 windings. The 3 groups are connected to a common power supply. Obviously this special connection of the PMSM needs a particular converter.

The starting point was the standard three-phase voltage source inverter. To each of the three groups an extra inverter leg is added. This connection will be used since the PMSM under study has Y-connected winding groups.

If a winding fault occurs in the PMSM, the faulted phase is isolated by keeping open the corresponding two power switches. In this case, due to the appeared imbalance, the zero sequence component of the current is not null anymore and the I_0 current has to reach the source. Hence, the fourth inverter leg will allow this link.

The supplementary inverter leg will continue to drive the currents, assuring practically the normal current through the remained healthy phases. Since the additional inverter leg is connected to the neutral point of the PMSM, the neutral current caries the phase currents of the remaining phases:

$$\begin{aligned} \boldsymbol{I}_0 &= \boldsymbol{I}_a + \boldsymbol{I}_b + \boldsymbol{I}_c \\ \boldsymbol{I}_0 &= \boldsymbol{I}_a + \boldsymbol{I}_c; \quad \boldsymbol{I}_b = 0 \end{aligned} \tag{6.1}$$

It should be also mentioned that for a correct operation of the converter additional fault detection module has to be added, and as well a phase isolation logic, which will command the power switches during faulty operation.

There are two possible control strategies for the present machine: by using the scalar, or the vector control technique. This last one is more precise for transient control, but more complex, while increasing the computation time - thus, due to experimental limitations, the authors have decided to use the scalar technique.

In order to understand the compensation possibility when a fault occurred, some explanation will be given on a 3-phase-Y connected of the considered machine.

In normal condition, the 3 phase currents are given by:

$$\begin{aligned} \boldsymbol{I_a} &= \boldsymbol{I_d}\cdot\sin(\omega\boldsymbol{t}) + \boldsymbol{I_q}\cdot\cos(\omega\boldsymbol{t}) + \boldsymbol{I}_0 \\ \boldsymbol{I_b} &= \boldsymbol{I_d}\cdot\sin(\omega\boldsymbol{t} - 2\frac{\pi}{3}) + \boldsymbol{I_q}\cdot\cos(\omega\boldsymbol{t} - 2\frac{\pi}{3}) + \boldsymbol{I}_0 \\ \boldsymbol{I_c} &= \boldsymbol{I_d}\cdot\sin(\omega\boldsymbol{t} + 2\frac{\pi}{3}) + \boldsymbol{I_q}\cdot\cos(\omega\boldsymbol{t} + 2\frac{\pi}{3}) + \boldsymbol{I}_0 \end{aligned} \tag{6.2}$$

Equation (6.2) describes the well-known normal behavior of a machine in fixed rotating reference frame. Writing the same equations in fixed reference frame will give:

$$\begin{aligned} \boldsymbol{I_a} &= \frac{3}{2}\boldsymbol{I}_\alpha + \frac{\sqrt{3}}{2}\boldsymbol{I}_\beta \\ \boldsymbol{I_b} &= \sqrt{3}\boldsymbol{I}_\beta \\ \boldsymbol{I_c} &= 0 \end{aligned} \tag{6.3}$$

Generally, the electromagnetic torque is expressed like:

$$\boldsymbol{T_m} = \frac{3}{2}\cdot\boldsymbol{p}\cdot\left(\boldsymbol{I_q}\cdot\Psi_{\boldsymbol{m}} + \left(\boldsymbol{L_d} - \boldsymbol{L_q}\right)\cdot\boldsymbol{I_d}\cdot\boldsymbol{I_q}\right) \tag{6.4}$$

Hence, in case of faults, to have a constant torque, the *dq* components of the currents must remain the same.

The relation between rotating and fixed reference frame currents is given by:

$$\begin{aligned} \boldsymbol{I}_\alpha &= \boldsymbol{I_d}\cdot\cos(\omega\boldsymbol{t}) - \boldsymbol{I_q}\cdot\sin(\omega\boldsymbol{t}) \\ \boldsymbol{I}_\beta &= \boldsymbol{I_d}\cdot\sin(\omega\boldsymbol{t}) + \boldsymbol{I_q}\cdot\cos(\omega\boldsymbol{t}) \end{aligned} \tag{6.5}$$

In this case, to maintain the constant torque, one can replace equation (6.5) into (6.4) resulting the adapted control law to obtain fault remedy:

$$\begin{aligned} \boldsymbol{I_a} &= \sqrt{3}\boldsymbol{I_d}\cdot\sin\left(\omega\boldsymbol{t} + \frac{2\pi}{3}\right) + \sqrt{3}\boldsymbol{I_q}\cdot\cos\left(\omega\boldsymbol{t} + \frac{2\pi}{3}\right) \\ \boldsymbol{I_b} &= \sqrt{3}\boldsymbol{I_d}\cdot\sin(\omega\boldsymbol{t}) + \sqrt{3}\boldsymbol{I_q}\cdot\cos(\omega\boldsymbol{t}) \\ \boldsymbol{I_c} &= 0 \end{aligned} \tag{6.6}$$

It can be seen from (6.6) that increasing the phase currents with $\sqrt{3}$ will allow the machine to be able to develop the same amount of torque. In case the currents are not increased, the machine will develop only 2/3 of the rated torque. This way it is proved that controlling the magnitude of the *dq* components of the machine's currents, the torque can be developed at rated values even in the case of fault occurrence.

For this, the machine needs to be sized in the concept to accept higher currents without the risk of burnout. Hence, a compromise between the development of 2/3 of the rated torque and increasing with $\sqrt{3}$ the magnitude of the machine's currents must be taken into consideration. Of course, the method presented is applicable to 3 phase systems. But as a 9-phase machine, there are 3x3 phase windings; the procedure is applicable in the same way.

The scalar control will be implemented both in simulations and in real laboratory measurements. The reason for this is to prove operation of a 9-phase machine in faulty conditions, compensated by injecting currents in the neutral point of each star connection of the machine.

The already presented simulation program was used to analyze the behavior of the 9-phase-PMSM in several operation conditions, from normal to different winding faults. In the present study there is no compensation law applied to the drive, by means of current increasing. Hence the currents will not be increased in the machine with $\sqrt{3}$ but the torque will be diminished with 2/3 of its rated value. The simulation time was set to 0.05s, at the rated speed of the machine. The same acquisition time was used in the real laboratory measurements.

In FIGURE 6-12 the results of the simulations are plotted. For each study case the 9 currents and the developed torque is shown. In the first scenario, (FIGURE 6-12a), the normal behavior of the studied PMSM is presented. It can be seen that all the currents are present and the developed torque is about 1.8 N·m.

In FIGURE 6-12b, machine's operation in one phase fault is depicted. When time reaches 0.01 s, the fault is generated and the torque characteristic is modified by a ripple, normal for such operation condition. As the currents amplitude is not corrected, the developed torque is now 1.6 N·m.

For the second case under study, two faulted phases from two different Y connections are considered (see FIGURE 6-12c); the torque is rippled even more, having a mean value of 1.5 N·m. If the third fault occurs, on the third Y connection (see FIGURE 6-12d), the ripples tendency is to increase more. The maximum values now reach 2 N·m and the minimum values 0.2 N·m. Still, the machine is able to perform continuous operation, developing the rated speed and a mean torque of 1.35 N·m.

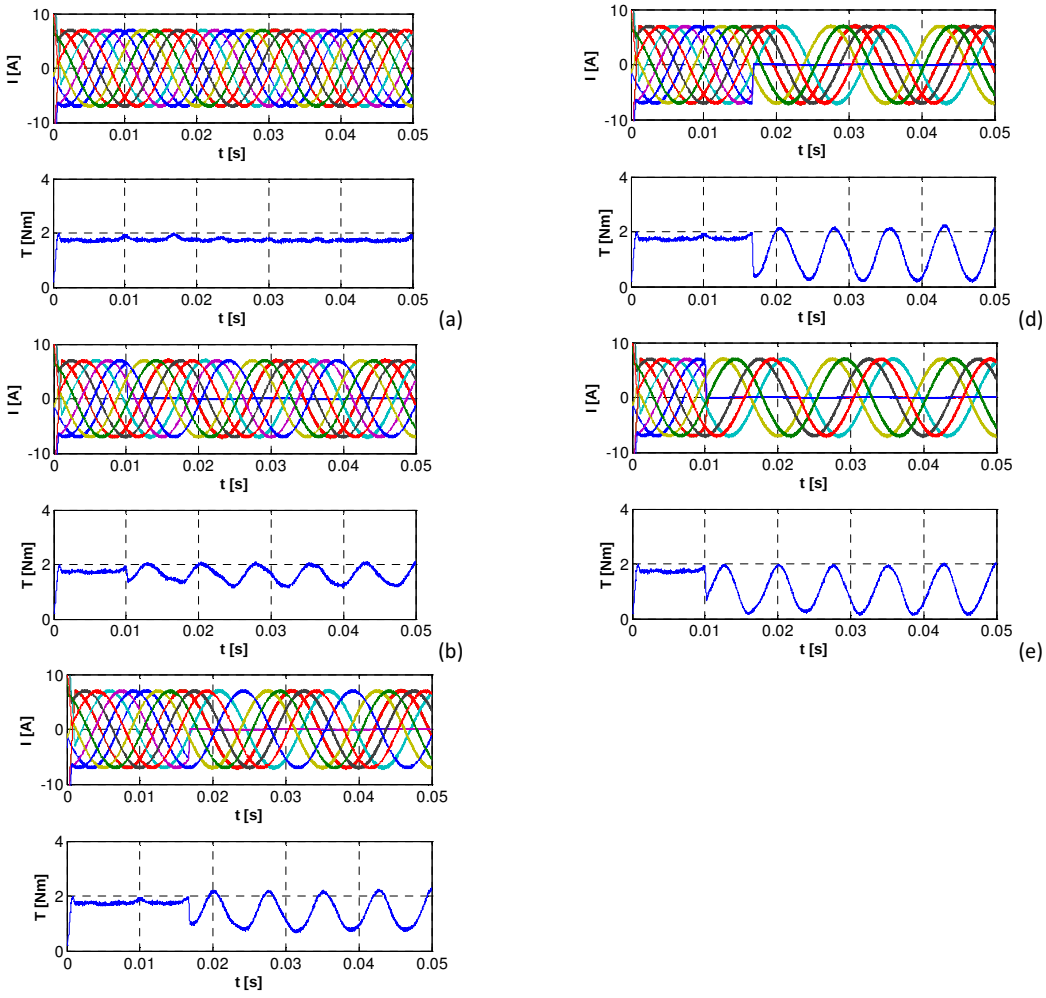

FIGURE 6-12. The simulation results for the studied 9-phase-PMSM. [96]

The last study taken into consideration is the case when only one phase from the first Y connection is operational and one phase from each of the remaining Y connections is faulted (FIGURE 6-12e). In this case practically 5 phases remain healthy in the machine. The ripples reach again consistent values and the developed mean torque is decreased to 1.19 N·m.

In all the above analyzed cases it is obvious that the torque is rippled and its mean value decreased but, overall, the PMSM can pursuit continuous operation despite all faults.

In order to validate, in real measurement, all the above discussed issues, the test bench setup was employed, as depicted in FIGURE 6-13. It contains the 9-phase-PMSM, a high precision torque meter and an induction machine (with its converter) as load. The 9-phase converter can be also seen in the figure, being built based on *IRFZ48N mosfet* switches. The control is designed in *Matlab/Simulink* and the program is uploaded on a dSPACE 1103 board. In order to perform the 9-phase PWM, software created PWM is used, setting the ON/OFF states of the switches via the digital I/O ports of the board. The main problem is that due to this, the switching frequency had to be reduced to 2.5 kHz (PC hardware limitation).

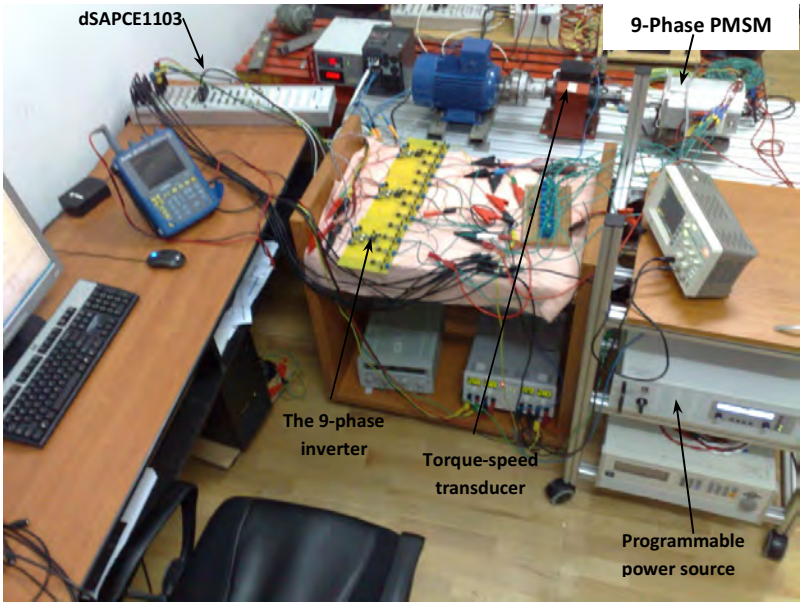

FIGURE 6-13. The test bench of the constructed 9-phase drive & PMSM. [96]

Firstly, the 9-phase currents of the machine-drive system are presented in FIGURE 6-14.

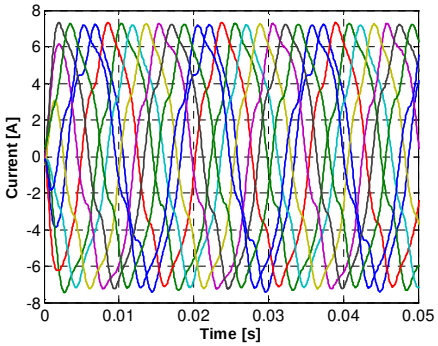

FIGURE 6-14. The currents on the constructed 9-phase drive & PMSM. [96]

To prove the fault tolerance capability of the drive, it is important to highlight the benefit of the 4th converter leg for each Y connection of the machine. The debate will be around one Y connection, the phenomenon being identical for the rest of the machine's phases. In normal condition, the currents on one star connection were acquired and depicted in FIGURE 6-15a.

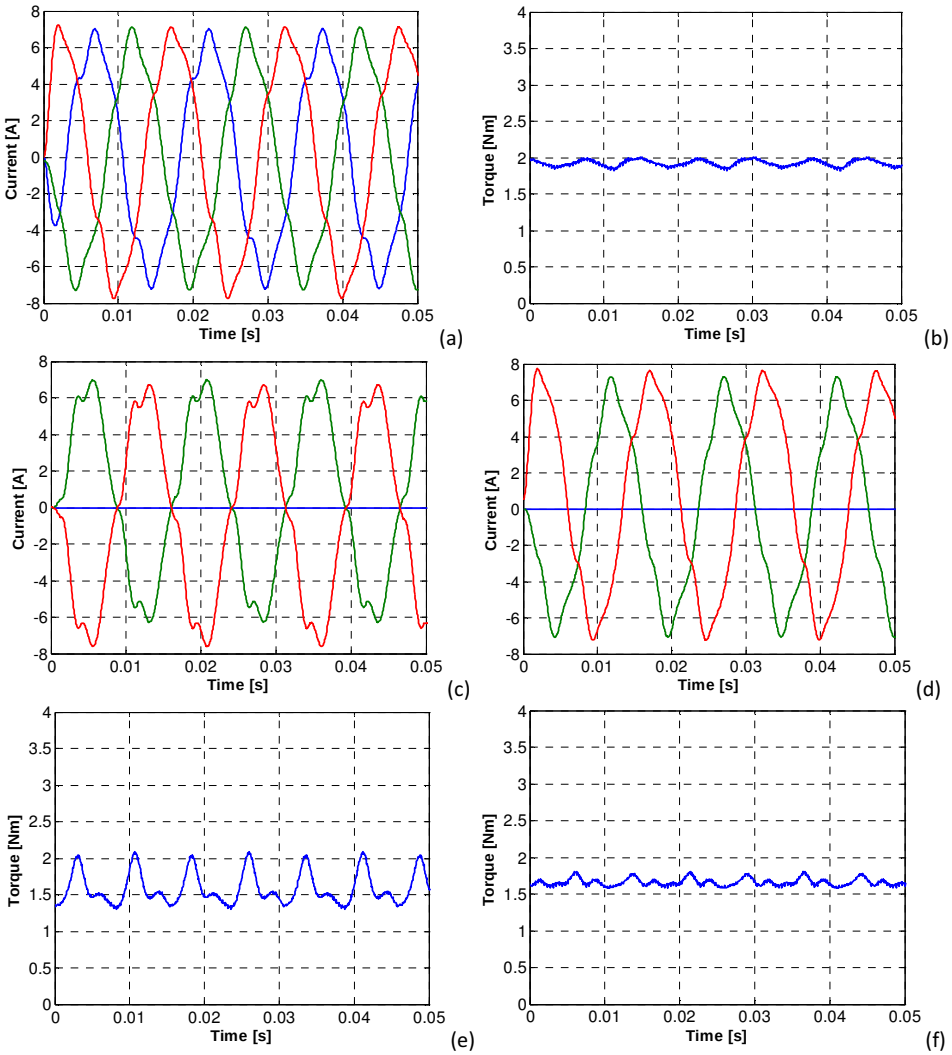

FIGURE 6-15. Measured results on one 3-phaseY-connection of the constructed 9-phase PMSM-drive: a) 3-phase currents on healthy operation; b) the measured torque in healthy operation; c) currents for 1-phase fault, no compensation; d) currents for 1-phase fault, with compensation; e) torque for 1-phase fault, no compensation; f) torque for 1-phase fault, with compensation. [96][94]

The torque characteristic (FIGURE 6-15b) is quite smooth having a mean value of 1.72 N·m, quite close to the one obtained via simulations.

The first step is to impose a fault on one winding Y. An open circuit of one phase is accomplished. Without connecting the 4th leg of the converter to compensate the loss, the remaining currents will become shifted with 180 degrees, like in FIGURE 6-15c.

It can be seen that the contribution of the auxiliary leg is mandatory. The operation of the auxiliary leg will complete practically the switching table for a 3 phase inverter. This way, the relative shifting of the currents will be set to the proper one, even in the case when one phase is missing from the star connection, see FIGURE 6-15d.

It is obvious that if the auxiliary leg is not in operation, the torque ripples are consistent and its mean value is decreased, (FIGURE 6-15e). In case it is connected (FIGURE 6-15f), the ripples are much smaller and a mean value of 1.62 N·m is developed. This value is very close to the one obtained in simulations. Overall, the usage of the auxiliary leg and its contribution in the torque development was proved via laboratory measurements.

6.3 *Flux weakening and the wide speed range motorization of the EV*

6.3.1 The speed-torque characteristic of the EV

One of the most important advantages of the electric motorization is the possibility to have, even at zero speed, the desired torque. The ICE vehicle will get the maximum torque after reaching around 2000r/min, for diesel engines, or even 4000r/min for the gas motors. From the speed-torque characteristic, we can distinguish three main operating regions, FIGURE 6-16:

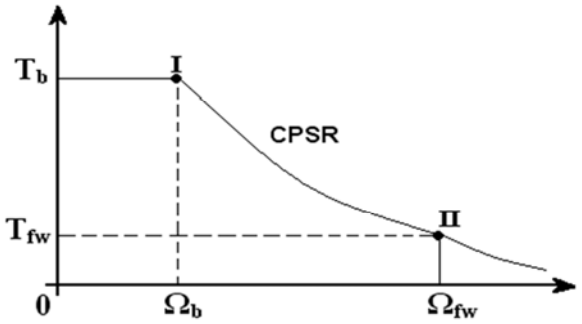

FIGURE 6-16. The torque-speed characteristic in electric traction systems. [97]

- Up to the rated speed, Ω_b (called also *base speed*), the motor is characterized by a constant torque, while speed and power increase;
- After the rated speed, in the constant power speed range (CPSR), as the speed increases the power should be kept constant and the torque has to be decreased;
- Beyond a certain value of the speed, Ω_{fw} (called the *field-weakening speed*), the power decreases as the torque goes to zero.

The operation in the CPSR zone is possible only it the flux wreaking technique is employed. This means that we need to reduce the air-gap flux in order to be able to go beyond the rated speed. This can be very simply shown on the *dc* motor case. For a *dc* motor, with parallel excitation, if we consider the stationary regime the time variation components of the armature are eliminated and the speed can be determined by: $\omega = \frac{U_a - R_a \cdot I_a}{k_E}$ equation, where the U, I and R denote the voltage, the current and the resistance, while the induced electromotive force coefficient is proportional with the excitation flux, the number of turns per phase, and other coefficients (like the number of parallel conductors per turn etc.). In the k_E coefficient only the flux parameter can be varied. And, it is obvious that if the flux decreases the speed, ω, increases, and if the flux increases the speed will decrease. Thus, increasing the speed beyond the rated value means to employ the *flux weakening technique*.

The problem for an electrical machine, which is excited through permanent magnets (PMs), is that the excitation flux is constant. For an electromagnet, the flux variation is simple, because we can control the excitation current, but the PMs is a constant flux source. Thanks to the flux-weakening concept we can employ the variation of the PMs flux.

The rotor topologies available today in PMSM are capable or not to assure the flux weakening capability. For example, the rotor variants presented in FIGURE 3-1 are more or less capable to produce speed variation, based on flux-weakening concept: the first variant, FIGURE 3-1a, has the lowest speed variation capability (up to 1.5 times the rated speed), while the FIGURE 3-1d variant permits the speed increase up to 4 times the base speed [98]-[101].

The study presented here will explore the speed capability variation of several machines: the IM, the PMSM and the variable synchronous reluctance machine (VRSM).

6.3.2 Optimizing the speed operation of electrical machines

The fast acceleration/deceleration and the speed variation capability of the thermal engine make it almost unbeatable in automobile industry. In order to compete with the thermal engine, the electrical motor should offer the same speed variation facility, and so improvements should be done. In this way, from the motorization point of view, the flux-weakening capability could be the right solution [98]-[101].

This theory, for PMSM, dates from 25 years ago, from Jahns [98], Morimoto [99] and Slemon [100]. In these papers, the electro-mechanical equations, which characterize the behavior of an electrical machine for speed variations, have been employed. After that, Bianchi has proposed a methodology called "parameters and volt-amper ratings" for PMSM [101], which has been presented as capable for giving the best parameters (*dq* axis inductances, linkage flux, rated current) for maximizing the speed of an electrical drive system.

The present work intends to validate some of the results obtained by the aforementioned authors. For that, an inverse-problem optimization approach has been used. This approach has been accompanied by FEM analysis, to prove more clearly the most proper choice of the electromagnetic parameters. Even the efficiency will be evaluated in the CPSR. This approach will be unified for (practically) all the types of machines.

In order to achieve the abovementioned goals, the next steps have been followed:

- Employing the optimization procedure, to find the optimum electromagnetic parameters which are maximizing the motor's operation at high speeds (the inverse problem method has been used).

- Employing a numerical study, by using the *Matlab* software for the analytical calculation of a non-linear system of equations.

The mathematical model of the PMSM, while operating in the speed range, contains several equations, written in in *per-unit* quantities: **the current** (6.7 - describing a circle), **the voltage**, (6.8 - defining an ellipse) and **the torque** (6.9 - describing a hyperbola) equation. In steady-state operation, if the iron saturation and the stator resistance are neglected, the PMSM is modeled by:

$$\begin{pmatrix} I_{d\_pu} = I_{pu} \sin\beta \\ I_{q\_pu} = I_{pu} \cos\beta \end{pmatrix} \tag{6.7}$$

$$V_{pu}^2 = \omega_{pu}^2 \cdot \left[\left(\lambda_{pu} + L_{d\_pu} \cdot I_{d\_pu} \right)^2 + \left(L_{q\_pu} \cdot I_{q\_pu} \right)^2 \right] \tag{6.8}$$

$$T_{pu} = \lambda_{pu} \cdot I_{q\_pu} + \left(L_{d\_pu} - L_{q\_pu} \right) \cdot I_{d\_pu} \cdot I_{q\_pu} \tag{6.9}$$

These equations, defining their trajectories, are given in FIGURE 6-17, where the optimum speed operation is given (from the current point of view) in solid-arrow representation. The currents starts from the current-circle center, continuing in CPSR (between points I to II) and finishing on the ellipse center. Here, theoretically, the speed is infinite. From the optimum speed trajectory point of view, two types of control strategies can be employed: the maximum torque and maximum power control strategies.

The curves plotted in FIGURE 6-17 were carried out for a PM motor, with saliency ratio (L_q/L_d) of "*2*" and a direct-axis inductance value of "*1.3*", in *p.u.*.

The approach for the speed wide range operation has to start with the definition of the desired maximum speed, Ω_{fw}. Thus, the employed computation follows an inverse approach, as shown in FIGURE 6-18. The following steps have to be performed:

- The designer has to determine the electro-magnetic parameters combination which gives the desired speed (from now on, this approach will be called *numerical analysis*)

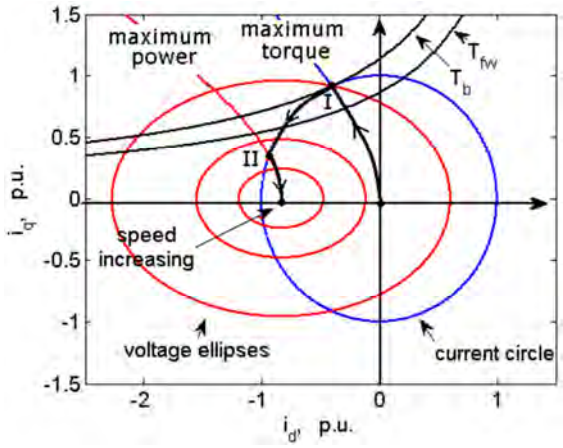

FIGURE 6-17. Current circle, torque hyperbola and voltage ellipsis of the PMSM on the *dq* frame. [97]

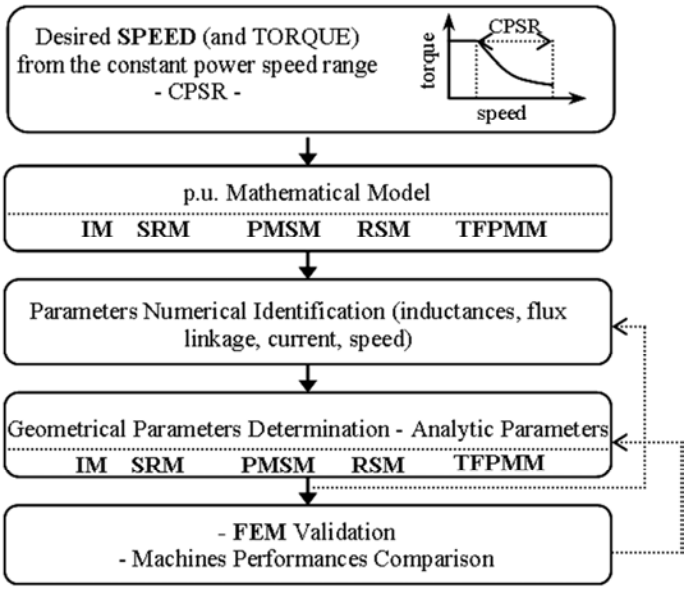

FIGURE 6-18. Diagram for the optimum speed operating range. [97]

- After that, the designer should find, analytically, the geometrical parameters of the rotor and of the stator cores which give the appropriate electro-magnetic parameters. Thus, the designer computes analytically the geometrical parameters based on a design procedure; if the analytical obtained electro-magnetic parameters do not correspond to the numerically obtained ones, modifications have to be made on his design until the *analytical* and *numerically computed parameters* have the same value.

- When passing to the FEM study, if the results obtained through this analysis do not match the ones predicted, the designer should iteratively operate modifications at the "Geometrical Parameters Determination" level (see the diagram from FIGURE 6-18), until the FEM results coincide with the requested ones.

All the machines have been studied by employing the above inverse optimization procedure, to validate and to compare the discussed motor topologies.

The studied IM is given in FIGURE 6-19a. This type of machine easily permits the speed variation below the rated value. On the other hand, the operation beyond the synchronous speed is obtained through the frequency variation (no flux-weakening discussion here). While the frequency is increased, the *V/f* ratio will not be maintained constant and the critical torque is reduced. FIGURE 6-20 shows the torque-speed characteristic of an IM for several frequencies.

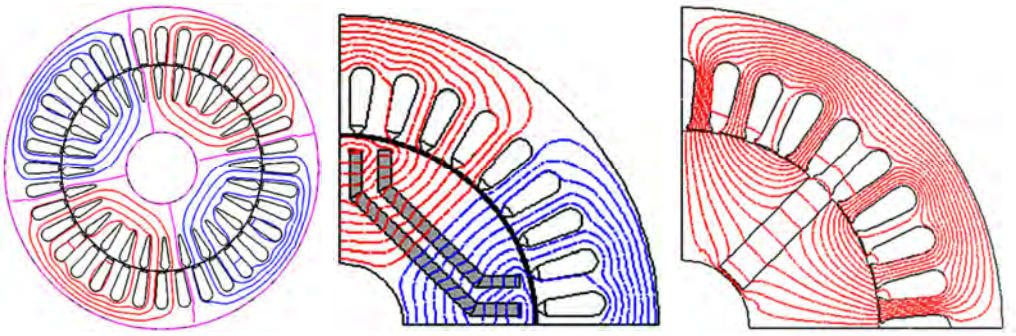

a b c

FIGURE 6-19. The analysed machine and the field-lines distribution from the FEM analysis. [97]

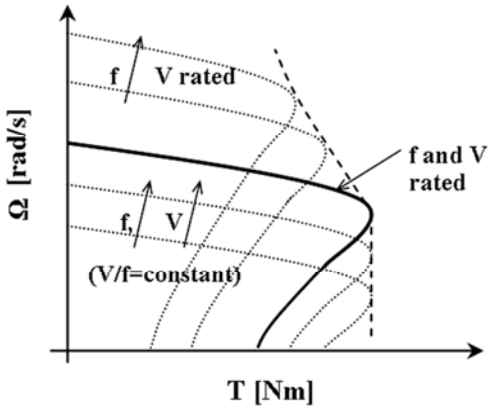

FIGURE 6-20. Torque-speed characteristic for the IM

For the flux weakening capability of the PMSM, with buried magnets on the rotor core, placed on two layers (see FIGURE 6-19b), in order to increase the flux linkage, as well as the saliency ratio. The system of equations which will model this machine is obtained by equating to "1" the normalized torque, speed and voltage, by solving the non-linear equation system, 6.7-6.9, and by adding the angle equation 6.10 - derived from 6.9:

$$\sin\beta = \frac{-\lambda_{pu} + \sqrt{\lambda_{pu}^2 + 8\cdot\left(L_{d\_pu}^2 - L_{q\_pu}^2\right)\cdot I_{pu}^2}}{4\cdot\left(L_{d\_pu} - L_{q\_pu}\right)\cdot I_{pu}} \tag{6.10}$$

The variation of the flux linkage and electromagnetic parameters is shown in FIGURE 6-21.

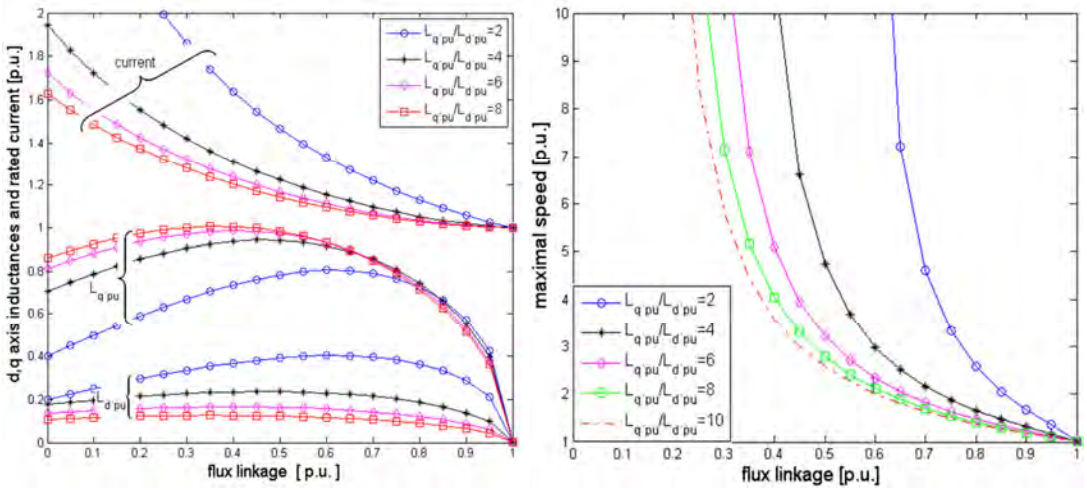

FIGURE 6-21. Parameters dependence for the PMSM operating in wide speed domain.

In FIGURE 6-21 the speed was computed by considering the maximum available speed, when the rated current equals the negative *d*-axis current, $I_{pu} = - I_{d\_pu}$, and the *q* axis current is $I_{pu} = 0$, meaning that the speed is $\omega_{pu} = V_{pu}/(\lambda_{pu}-L_d I_d)$). It can be seen that for a specific flux linkage and saliency ratio, a pair of *d-q* inductances gives a certain value of the speed. In fact, several combinations of the electromagnetic parameters give the desired speed.

The implementation of the algorithm from FIGURE 6-18 starts with the designer choice of the desired speed (for example $\omega_{pu}=2$). This speed gain (or flux weakening capability) is given by the electromagnetic parameter dependency, which is *numerically* obtained from FIGURE 6-21 (for example, for $\omega_{pu}=2$, one can have $I_{pu}=1.2$, $L_{d\_pu}=0.38$ and $L_{q\_pu}=0.76$, or, another possible combination could be $I_{pu}=2$, $L_{d\_pu}=0.3$ and $L_{q\_pu}=0.6$). After that, the designer can employ an *analytical approach* in order to obtain the requested electromagnetic parameter dependency, which gives him the desired speed. Of course, this electromagnetic parameters (obtained from the *numerical analysis*) are influenced by the geometrical ones and other parameters like the number of turns, the frequency etc. (coming from an *analytical approach*); these parameters can be varied to compute the abovementioned electromagnetic parameters (from FIGURE 6-21).

For a maximum power control strategy ($I_{pu}=1$) the power and torque equations are:

$$P_{pu} = \frac{\omega \cdot \cos\beta \cdot \left[1 - L_{d\_pu} \cdot (1-\xi)\right] \cdot \sin\beta}{\sqrt{\left(\xi \cdot L_{d\_pu} \cdot \cos\beta\right)^2 + \left(1 - L_{d\_pu} \cdot \sin\beta\right)^2}} \tag{6.11}$$

$$T_{pu} = P_{pu} / \Omega_{pu} \tag{6.12}$$

By using 6.11 and 6.12, the torque and power versus speed characteristics can be obtained, for certain inductance-saliency ratio dependence. For example, in the case of the direct axis inductance (L_d) variation, when the saliency ratio has been kept to $\xi=2$, the FIGURE 6-22 can be plotted. In the same way, for the variation of saliency ratio (ξ), when the d-axes inductance was $L_d=0.6$, the torque-speed dependence can be obtained, as shown in FIGURE 6-23. From this study it is quite obvious that at low values of ξ and L_d the CPSR is reduced.

Several computations have been carried out. Among the results that have been retained, a 3.5 speed gain has been obtained with good efficiency level, FIGURE 6-24 - here, for $L_d=0.6$, $\xi=4$, a maximum 0.9 efficiency has been found, for as much as 2 times the base speed. As the speed increases, the efficiency decreases also. Thus, the user can choose between the operation on high speed range and efficiency. The plotted results have been obtained by using the power balance of the system. Thus, the efficiency equation is given by:

$$\eta_{pu} = \frac{T_{pu} \cdot \Omega_{pu}}{P_{J\_pu} + P_{ir\_pu} + T_{pu} \cdot \Omega_{pu}} \tag{6.13}$$

where P_{J_pu} and P_{ir_pu} are the joule and iron losses, respectively.

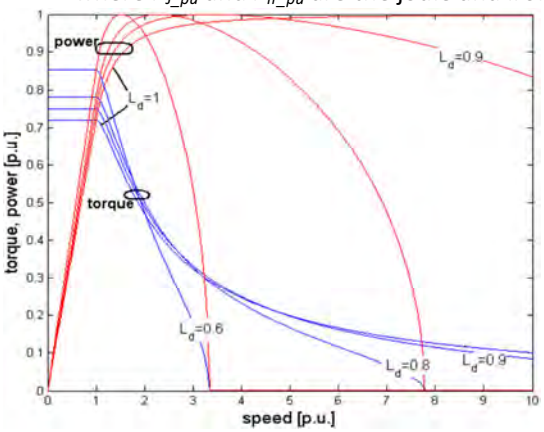

FIGURE 6-22. Torque and mechanical power vs. speed, function of ξ=2, for the studied PMSM

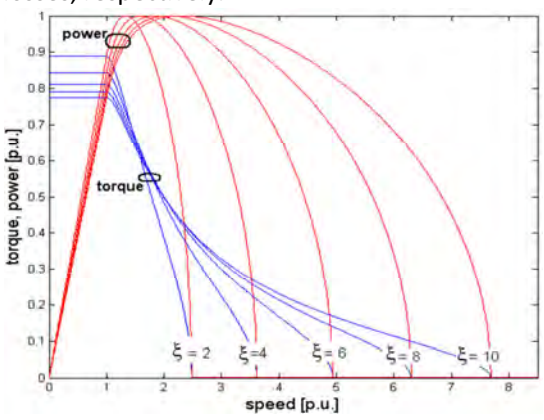

FIGURE 6-23. Torque and mechanical power vs speed, function of L_d=0.6, for the studied PMSM

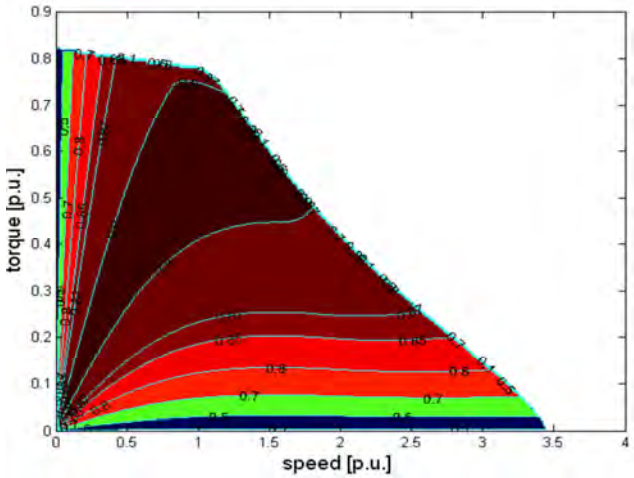

FIGURE 6-24. Efficiency on the torque-speed characteristic (L_d=0.6, ξ=4), fo the studied PMSM.

With the new electromagnetic parameters and volt-amper rates, the studied PMSM behavior has been simulated in the flux-weakening range. In order to test its performance (by means of simulation) a direct torque control (DTC) technique has been employed (the theory of this strategy is briefly discussed in the next subchapter).

After simulations, the obtained results are plotted in FIGURE 6-25.

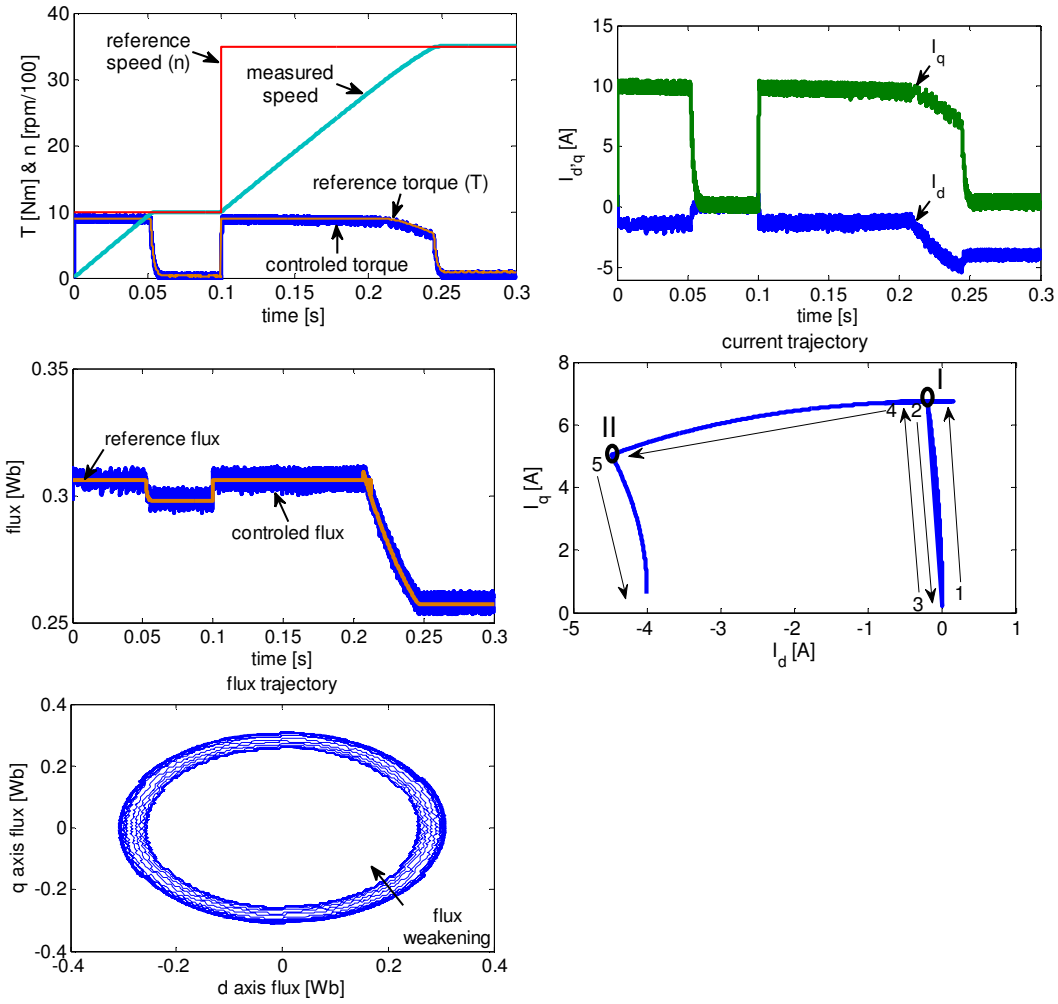

FIGURE 6-25. The simulated result from the DTC of the PMSM.

Here, a speed profile has been imposed, from the rated value (1000 r/min) up to 3.5 the base speed (3500 r/min). Concerning the torque, it can be seen that it has several distinctive areas: a constant torque (rated one) while the motor is accelerated, a region with zero torque (actually a small load torque is available due to friction and inertia), again the rated torque (due to the second acceleration) which cannot be maintained at constant value because the motors enters the flux-weakening region, and finally the "zero torque region" again (when the motor has reached the imposed speed, 3500r/min). Similar to torque variation, the linkage flux and I_q current variation can be seen, while I_q current has a negative value since the saliency ratio differs from unity value. The flux weakening is obvious on the flux locus variation (flux decreases while motor is accelerating) and the current locus variation.

The motor is running in 5 steps (with regard to the diagram presented in FIGURE 6-17):

- phase (1), the motor reaches the rated current value in the point (I) when the motors accelerates for the first time;
- since the reference speed was reached, there is only the friction and inertia which impose a small current value, phase (2);
- when a new reference speed is imposed, the current goes up to the rated value, phase (3), and stays there until the motor is entering the flux weakening region which determines …
- the flux to decrease, phase (4), up to point (II), when the second imposed value is reached, and thus…
- no current for acceleration is needed, phase (5), and the current value decreases down again (it can be noticed that here a relatively important value of the negative I_d current is reached).

A similar study is employed also for the VRSM. The use of this type of motor regards the applications where an important speed variation is demanded. The value of inductances ratio (L_q/L_d) can be seen as speed operation capability. Related to the rotor topology, several variants are possible (with flux barrier or axial sheets, this last one having the biggest saliency ratio: $\zeta>10$), but the axially laminated topology involves construction difficulties. That is why a flux barrier variable reluctance motor (VRSM) has been studied, FIGURE 6-19c.

Since we are still dealing with a synchronous machine, the VRSM system equation can be derived from 6.7-6.9, where the flux linkage of the PM is equaled to zero. Thus, the VRSM inductances and current equations (in *per-unit*) become:

$$L_{d\_pu} = \frac{\zeta - 1}{\zeta^2 + 1}$$
$$L_{q\_pu} = \frac{\zeta^2 - \zeta}{\zeta^2 + 1} \quad (6.14)$$

$$I_{pu} = \sqrt{\frac{2 \cdot \left(\zeta^2 + 1\right)}{(\zeta - 1)}} \quad (6.15)$$

The VRSM electromagnetic parameter variation is given in FIGURE 6-26, and FEM analysis of the motor shows how the magnetic field lines are affected by the flux barrier, for a *q*-axis stator winding supplying, FIGURE 6-19c.

All the studied machines' capability to operate in speed operation is evaluated and the following comments are made:

- The only way to increase the induction motor's speed, over the rated value, is to increase the supplied frequency. Also, a reduced power/weight ratio and a poor efficiency (due to rotor reaction obtain through stator supply) are the major drawbacks of this type of machine. On a contrary, the simplicity structure and the lack of PMs are its major advantages.

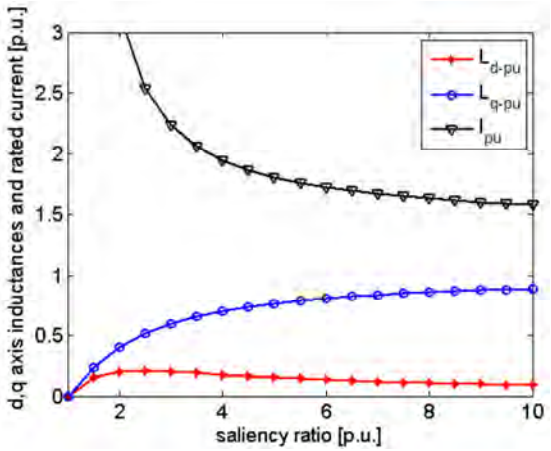

FIGURE 6-26. Parameters dependence for VRSM

- The PMSM will always have the risk of irreversible demagnetization of the PMs and difficulties to zero speed control. Otherwise, its very good power/weight ratio and wide speed range capability makes this motor the most common choice in electric vehicle traction.

- The variable reluctance synchronous motor has quite a low efficiency, and its speed capability cannot always be exploited since the electronic equipment cannot yet offer all the demanded frequency ranges. Nevertheless, the VRSM offers the best possibility on wide speed variation, even if this involves construction difficulties.

6.4 Control techniques for improved energetic performances

For *ac* drives, there are two main categories of control techniques [102]-[105]: the scalar control (SC) and the vector control (VC), see FIGURE 6-27. The SC, mainly employed for induction motors, supposes a constant magnetic state of the machine and thus the constant Voltage/Frequency ratio has to be assured (this technique is also known as the V/f control). This means that if sudden load change appears, the SC will not be capable to assure the machine's control. SC is mainly dedicated for constant load applications. If the application demands high dynamics, with fast accelerations and load variation, then the vector control technique should be used.

There are several types of VC techniques: the field oriented control (FOC), where the rotor or stator flux are considered as references, and the torque control, where the torque is considered as reference. For this last category, we have several variants: the direct torque control (DTC), the indirect torque control (ITC) and direct instantaneous torque control (DITC). Both vector control approaches can consider also the space-vector modulation (SVM).

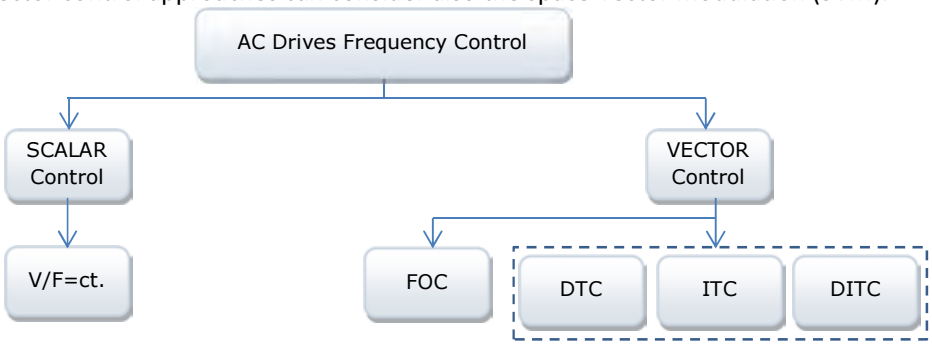

FIGURE 6-27. Variable frequency control techniques.

Vector-controlled drives were introduced about 35 years ago and they have achieved a high degree of maturity, being very popular in a wide range of applications in our days [102], [103]. It is an important feature of various types of vector controlled drives that they allow dynamic performance of *ac* drives to match or sometimes even to surpass that of the *dc* drive. At the present, the main trend is to use sensorless vector drives, where the speed and position information is obtained by monitoring input voltages or currents.

The VC technique consists in controlling the spatial orientation of the electromagnetic field and has led to the name of field orientation. The FOC usually refers to controllers which maintain a 90° electrical angle between the rotor *d*-axis and the stator field components. Thus, with a FOC strategy, the field and armature flux are held orthogonal. Moreover, the armature flux does not affect the main flux and the motor torque responds immediately to a change in the armature flux (or armature current). Hence, the *ac* motor behaves like a *dc* one.

A basic scheme of the FOC technique was used for the PMSM control. Having a speed and direct axis current as references, and using PI controllers, one can obtain the needed stator voltage components for the motor supply. The employed simplified FOC scheme for our simulations is given in FIGURE 6-28a.

DTC drives were introduced about 25 years ago [104], [105]. The principle of DTC is to directly select voltage vectors according to the difference between the reference and the actual value of the torque and the flux linkage. Thus, the torque and flux errors are compared in hysteresis comparators. Depending on the comparators, a voltage vector is selected from the well-known switching table of the DTC technique.

In general, compared to the conventional FOC scheme, the DTC is inherently a sensorless control method. It has a simple and robust control structure (however, the performances of DTC strongly depend on the quality of the estimation of the actual stator flux and torque).

The implemented simplified DTC scheme is given in FIGURE 6-28b. Here, from the current and speed controllers, the flux and torque references are obtained. Their values are compared with the measured ones, and from their errors one can get the voltage-vector selection in order to assure the PMSM supply (after an abc=>dq transformation).

In contrast to induction motors (IM) the initial value of the stator flux in PMSM is not zero and depends on the rotor position. In sensorless PMSM drives the initial position of the rotor is unknown and this often causes initial backward rotation and problems of synchronization. Otherwise, the DTC system possesses good dynamic performances, but in steady state regime the torque and the current waveforms present high ripples.

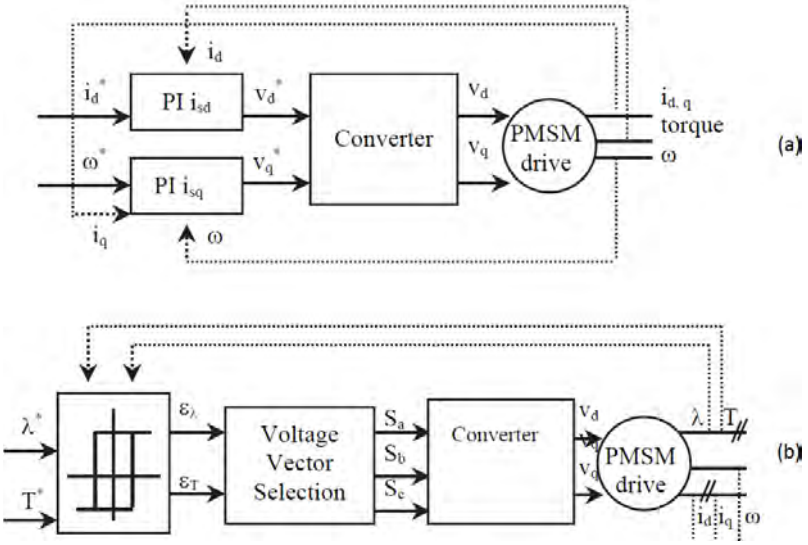

FIGURE 6-28. Simplified FOC and DTC techniques employed for PMSM drives [106].

In Table 6-2 are summarized the performances of both VC type techniques.

TABLE 6-2. SUMMARY ON THE VC TYPE TECHNIQUES PERFORMANCES

PARAMETER/PROPERTY	*DTC*	*FOC*
Dynamic response to torque	Very fast	Fast
Coordinates reference frame	alpha, beta (stator)	d, q (rotor)
Low speed (< 5% of nominal) behavior	Requires speed sensor for continuous braking	Good with position or speed sensor
Controlled variables	torque & stator flux	rotor flux, torque current iq & rotor flux current id vector components
Steady-state torque/current/flux ripple & distortion	Low (requires high quality current sensors)	Low
Parameter sensitivity, sensorless	Stator resistance	d, q inductances, stator/rotor resistance
Parameter sensitivity, closed-loop	d, q inductances, flux (near zero speed only)	d, q inductances, stator/rotor resistance
Rotor position measurement	Not required	Required (either sensor or estimation)
Current control	Not required	Required
PWM modulator	Not required	Required
Switching frequency	Varies widely around average frequency	Constant
Switching losses	Lower (requires high quality current sensors)	Low
Audible noise	spread spectrum sizzling noise	constant frequency whistling noise
Control tuning loops	speed (PID control)	speed (PID control), rotor flux control (PI), id and iq current controls (PI)
Typical control cycle time	10-30 microseconds	100-500 microseconds

For a synchronous machine, excited through PMs, the electromagnetic equivalent circuit is presented in FIGURE 6-29. From this graphical representation, one can get the mathematical model of the machine, while the iron loss is considered too. The voltage equations are:

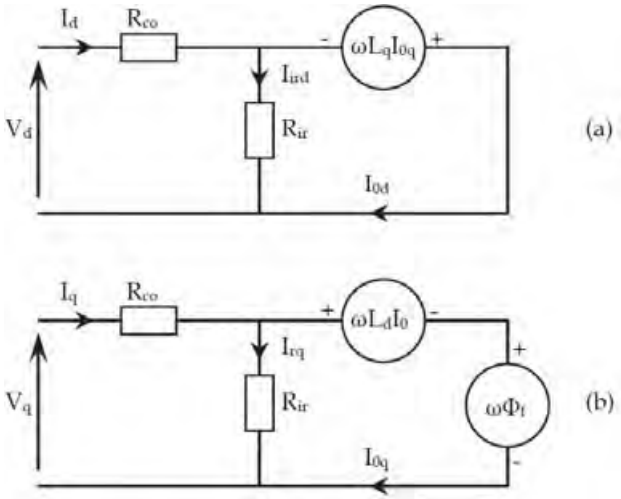

FIGURE 6-29. The equivalent circuit of the studied PMSM, in *d-q* reference frame [106].

$$\begin{bmatrix} \boldsymbol{V_d} \\ \boldsymbol{V_q} \end{bmatrix} = \boldsymbol{R_{ph}} \begin{bmatrix} \boldsymbol{I_d} \\ \boldsymbol{I_q} \end{bmatrix} + \begin{bmatrix} 0 & -\omega \cdot \boldsymbol{L_q} \\ \omega \cdot \boldsymbol{L_d} & 0 \end{bmatrix} \cdot \begin{bmatrix} \boldsymbol{I_{0d}} \\ \boldsymbol{I_{0q}} \end{bmatrix} + \begin{bmatrix} 0 \\ \omega \cdot \lambda_f \end{bmatrix} \tag{6.16}$$

The total voltage and electromagnetic torque equations are:

$$\boldsymbol{V}^2 = \left(\omega \cdot \lambda_f + \omega \cdot \boldsymbol{L_d} \cdot \boldsymbol{I_{0d}} + \boldsymbol{R_{ph}} \cdot \boldsymbol{I_q}\right)^2 + \left(-\omega \cdot \boldsymbol{L_q} \cdot \boldsymbol{I_{0q}} + \boldsymbol{R_{ph}} \cdot \boldsymbol{I_d}\right)^2 \tag{6.17}$$

$$\boldsymbol{T_e} = \boldsymbol{p} \cdot \left[\lambda_f \cdot \boldsymbol{I_{0q}} + \left(\boldsymbol{L_d} - \boldsymbol{L_q}\right) \cdot \boldsymbol{I_{0d}} \cdot \boldsymbol{I_{0q}}\right] \tag{6.18}$$

with $I_{0d}=I_d-I_{ird}$ and $I_{0q}=I_q-I_{irq}$.

The copper and iron losses are:

$$\boldsymbol{P_{Co}} = \boldsymbol{R_{ph}} \cdot \left(\boldsymbol{I_d^2} + \boldsymbol{I_q^2}\right) \tag{6.19}$$

$$\boldsymbol{P_{ir}} = \boldsymbol{R_{ir}} \cdot \left(\boldsymbol{I_{ird}^2} + \boldsymbol{I_{irq}^2}\right) = \frac{\left(\omega \boldsymbol{L_q} \boldsymbol{I_{0q}}\right)^2 + \left(\omega \lambda_f + \omega \boldsymbol{L_d} \boldsymbol{I_{0d}}\right)^2}{\boldsymbol{R_{ir}}} \tag{6.20}$$

The motor speed equation is:

$$\Omega = \frac{\boldsymbol{V}^2}{\boldsymbol{p} \cdot \sqrt{\left(\lambda_f - \boldsymbol{L_d} \cdot \boldsymbol{I_d}\right)^2 + \left(\boldsymbol{L_q} \cdot \boldsymbol{I_q}\right)^2}} \tag{6.21}$$

One of the major problems of *ac* machines is that their inductive character reduces the power factor. The surface-mounted PMs involve high inductances values, thus reducing the energetic performances of the machine.

There are two ways to increase the power factor. The first way is to use a capacitor battery connected to the stator winding. This solution involves equipment and maintenance costs. The second way is to use an appropriate control strategy. This demands computational power of the control unit, but is less expensive and no maintenance is needed. The second solution will be employed here.

The *unity-power factor control strategy* will be depicted further. From the phasor diagram of PMSM (FIGURE 3-4), it is possible to rewrite the *d,q*-axis currents by imposing β=(δ-ϕ). Thus, the currents are $i_d=-I_s \cdot \sin(\beta)$ and $i_q=I_s \cdot \cos(\beta)$.

The internal angle can be expressed function of *d,q* axis voltages, $\tan\delta = -V_d/V_q$. Then, introducing the current expression, in stationary regime (derivate terms are suppressed), one will get:

$$\tan\delta = \frac{\boldsymbol{R_{ph}} \cdot \boldsymbol{I} \cdot \sin\beta + \omega \cdot \boldsymbol{L_q} \cdot \boldsymbol{I} \cdot \cos\beta}{\boldsymbol{R_{ph}} \cdot \boldsymbol{I} \cdot \cos\beta - \omega \cdot \boldsymbol{L_d} \cdot \boldsymbol{I} \cdot \sin\beta + \omega \cdot \lambda_f} \tag{6.22}$$

Neglecting the phase resistance, the internal angle tangent becomes:

$$\tan\delta = \frac{\omega \cdot \boldsymbol{L_q} \cdot \boldsymbol{I} \cdot \cos\beta}{-\omega \cdot \boldsymbol{L_d} \cdot \boldsymbol{I} \cdot \sin\beta + \omega \cdot \lambda_f} \tag{6.23}$$

For unity power factor, β=δ, the following equality appears:

$$\frac{\sin\beta}{\cos\beta} = \frac{\omega \cdot \boldsymbol{L_q} \cdot \boldsymbol{I} \cdot \cos\beta}{-\omega \cdot \boldsymbol{L_d} \cdot \boldsymbol{I} \cdot \sin\beta + \omega \cdot \lambda_f} \tag{6.24}$$

After calculation, a second degree equation will be obtained, with the following solution:

$$\sin\beta = \frac{1 \pm \sqrt{1 - 4 \cdot \frac{\boldsymbol{L_d} \cdot \boldsymbol{L_q} \cdot \boldsymbol{I}^2}{\lambda_f} \cdot \left(1 - \frac{\boldsymbol{L_q}}{\boldsymbol{L_d}}\right)}}{2 \cdot \frac{\boldsymbol{L_d} \cdot \boldsymbol{I}}{\lambda_f} \cdot \left(1 - \frac{\boldsymbol{L_q}}{\boldsymbol{L_d}}\right)} \tag{6.25}$$

The mathematical model will be completed with the torque and motion equations:

$$\frac{\boldsymbol{d}\Omega}{\boldsymbol{dt}} = \frac{\left(\boldsymbol{T_e} - \boldsymbol{B} \cdot \Omega - \boldsymbol{T_l}\right)}{\boldsymbol{J}} \tag{6.26}$$

where *B* is the friction coefficient (measured in *N·m·s/rad*), Ω is the angular speed (measured in *rad/s*) and T_l is the load torque, *J* is the moment of inertia (measured in $kg \cdot m^2$).

The Simulink simulation interface of the FOC strategy and the simulated results for unity-power factor strategy are presented in FIGURE 6-30 and FIGURE 6-31, respectively.

Similar results have been obtained for the DTC technique, when the flux weakening has been employed: see FIGURE 6-32 for the Simulink block diagram which has produced the results form 6.3.2 subchapter – FIGURE 6-25).

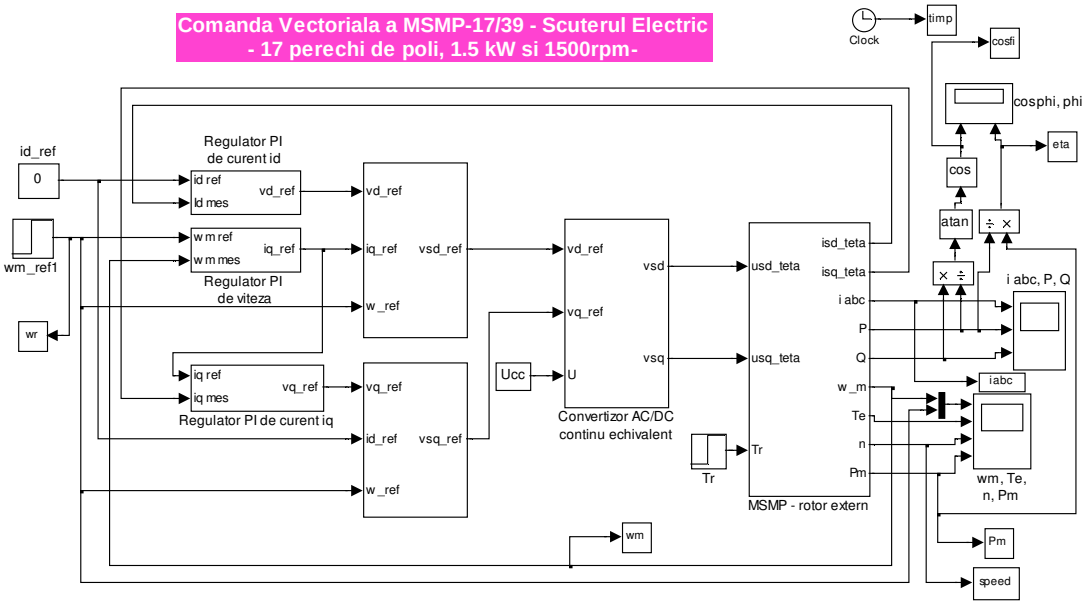

FIGURE 6-30. Simulink model for the FOC implementation for the PMSM-17/39 of the electric scooter from 2.4 sub-chapter.

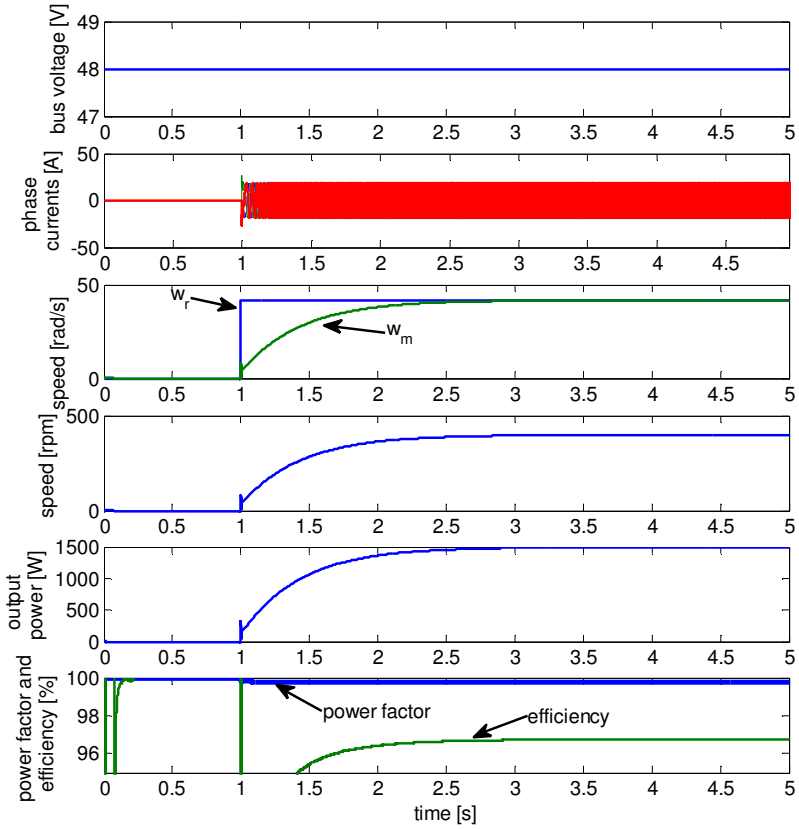

FIGURE 6-31. Simulated results of the FOC implementation for the PMSM-17/39 of the electric scooter from 2.4 sub-chapter: unity power factor control strategy.

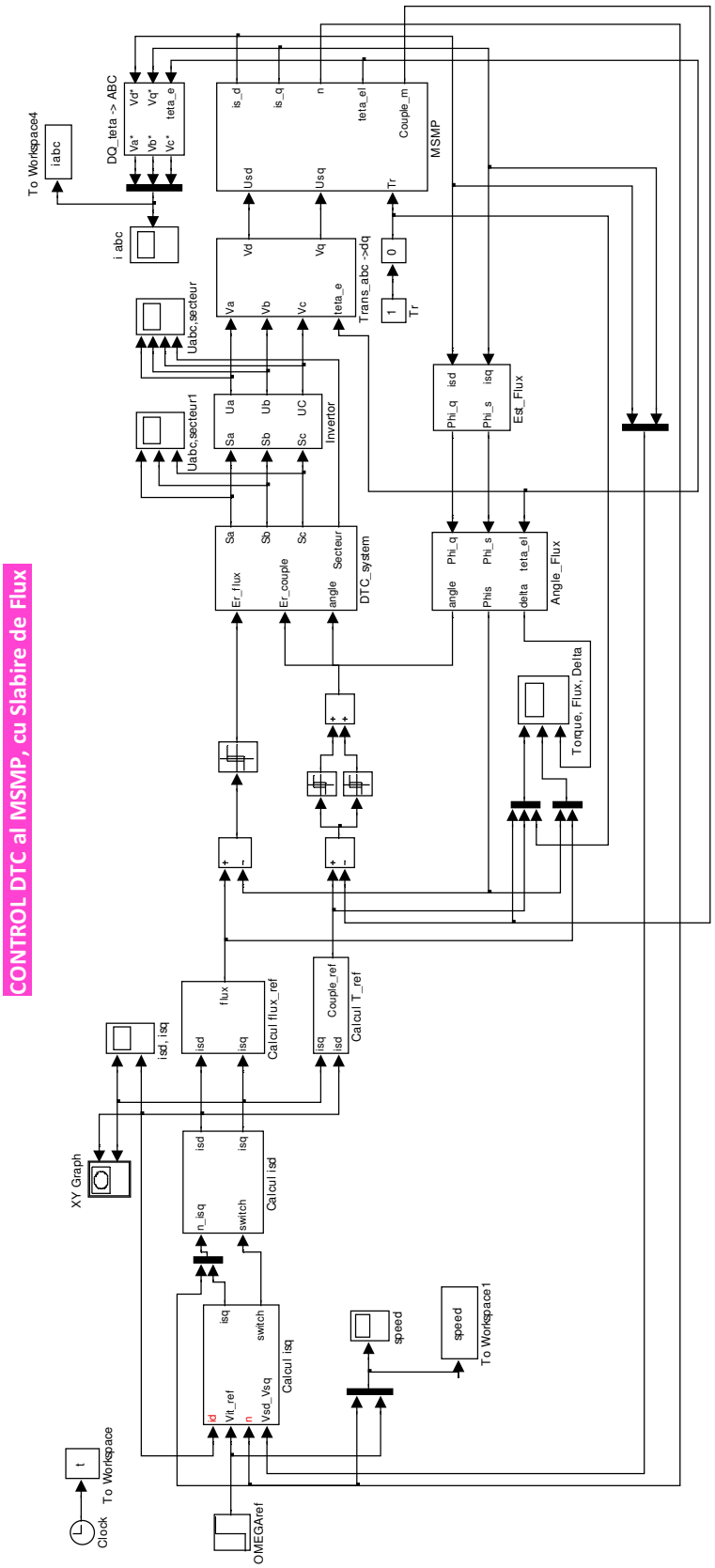

FIGURE 6-32. Simulink model for the DTC implementation for the PMSM presented into the 6.3.2 sub-chapter (giving the simulated results from FIGURE 6-25).

7 THE HYBRID SOURCE AND THE ENERGY MANAGEMENT

7.1 Framework and summary of main results

The research results obtained on the topic of hybrid sources and energy management on board of EVs have been obtained, mainly, in the frame of a research project financed by ALSTOM-Transport (Belfort, France), the author being a research team member. The project concerned the study of a hybrid vehicle of 5 kW, having a gas ICE and a PMSM motorization, and where different type of energy sources could be considered: Ni-M-H battery, UC and FC (for which a high speed compressor has been designed, based on a SRM). Some of the research results have been published in the following articles:

- T.Raminosoa, B.Blunier, D.Fodorean and A.Miraoui, "Design and optimisation of a Switched Reluctance Motor driving a Compressor for a PEM Fuel Cell System for Automotive Applications", IEEE Transactions on Industrial Electronics, vol.57, n°9, pp.2988-2997, September 2010.
- D.Fodorean, D. Bouquain, M.B. Camara and A.Miraoui, "Energy Management on board of a Reduced Scale Hybrid Automobile", Proceedings of the International Electrical Machines and Drives Conference, May 2009, pp.197-201.
- M.B.Camara, D.Fodorean, H.Gualous, D; Bouquain, A.Miraoui: "Hybrid Sources Control for Electric Drives Traction Applications", Proceedings of the IEEE International Symposium on Power Electronics, Electrical Drives, Automation and Motion – SPEEDAM'08, Ischia, Italy, 11-13 June 2008, pp.744-749.

Also, the energy management was a main topic in the MOEVEHU project, which was successfully ended in 30 April 2013, and for which not all results were already published; some of them are presented here.

7.2 Hybrid source EVs

The main supplying source on board of EV is the battery, which could assure an important amount of energy for a long period of time. Based on their materials, the batteries can have important energy density (for the lithium based batteries) or could be very stable in temperature and no balancing circuit electronics needed (for lead-acid batteries). If important accelerations are demanded by the application, the use of ultracapacitors (UC) will be a smart choice. The UC is able to deliver huge energy in a short period of time. And even if it is rapidly discharged, the UC can be rapidly re-charged in braking regime. So, with a hybrid source formed by a battery and UC, an increased autonomy of the electric car can be obtained. The fuel cells (FC) could replace the batteries, rather for static applications, since their auxiliaries have an important volume.

When considering a hybrid source to fed an EV, the designer should establish in the first place the driving conditions and the amount of energy needed by the propulsion and other auxiliary equipment. Next, based on a research regarding the available energy sources, he decides which equipment is best suited for the application. For example, energy density, the capacitance and the number of life cycles are very important parameters which have to be taken into account. Usually, for batteries and UC the manufacturer proposes small cells of 3.6Vdc for the battery, or 2.7Vdc for the UC. Based on the application, it is possible to configure the desired (hybrid) source. When the designer needs to build a battery or UC pack for a specific voltage and capacitance, he should be aware of the particularities of the devices. For example, for the lithium-ion (or polymer) batteries it is needed an electronic circuit for balancing the voltage

between the cells, since the internal resistance of each cell is very small and the charging can be unbalanced. For such batteries the manufacturer proposes a balancing management system (BMS) if more than 6 cells are linked in series connection. For the ultracapacitors a similar BMS is needed, if high capacity is necessary (for example, for cell units of 58F, the BMS is no longer needed).

These are a few tips in choosing the source device. After the acquisition of the desired source, it is needed to characterize it. This test will establish the behavior of the equipment when integrated into the application. Charging and discharging tests have to be done, to obtain the real operation capabilities of the energy source. For example, for the battery cell, the manufacturer presented a discharging characteristic of a 3.6Vdc lithium-polymer battery cell, of 60Ah, saying that such a battery will be discharged in 3 hours if the rated current is 20A, see FIGURE 7-1. After the tests, we have observed that only after two hours the cells are reaching their acceptable minimum discharge voltage level (which shouldn't be surpassed, otherwise part of the battery will be permanently damaged).

The UC cell pack consists in 6 cells and its characteristic are presented in FIGURE 7-2.

MODEL SE60AHA		
Nominal Capacity	60Ah	
Energy Density	98wh/kg@0.1C	
Float Voltage	3.4V	
Operating Voltage	Charge Voltage	3.6V
	Discharge Cut-off Voltage	2.0V
Max Charge Current	≤3CA	
Max Discharge Current	Constant Current	≤4CA(30s)
	Impulse Current	≤12CA(5ms)
Standard Charge/ Discharge Current	0.3CA	
Cycle Life	80%DOD	≥2000times
	70%DOD	≥3000times
Max Transient Temperature Resistance of Shell	170	
Long Term Shell Temperature Resistance	≤130	
Recommended Temperature	≤75	
Operating Temperature	Charge	0 55
	Discharge	-25 55
Low Temperature Discharge Efficiency	≥85%	
Self-discharge Rate/Month	≤3%(Monthly)	
Weight	2.2kg±0.1kg	

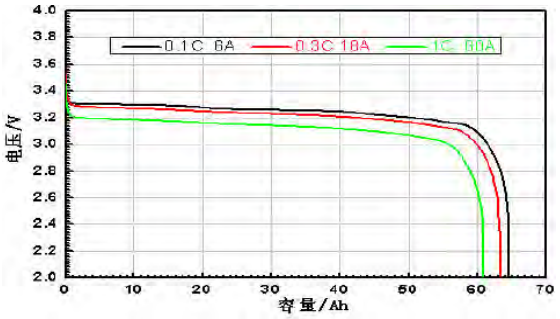

FIGURE 7-1. The lithium-polymer battery cell characteristics.

PRODUCT SPECIFICATIONS

ELECTRICAL	BMOD0058 E016 B02
Rated Capacitance[1]	58 F
Minimum Capacitance, initial[1]	58 F
Maximum ESR_{DC} initial[1]	22 mΩ
Rated Voltage	16 V
Absolute Maximum Voltage[1,4]	17 V
Maximum Continuous Current (ΔT = 15°C)[2]	12.0 A_{RMS}
Maximum Continuous Current (ΔT = 40°C)[2]	19 A_{RMS}
Maximum Peak Current, 1 second (non repetitive)[3]	200 A
Leakage Current, maximum (B02 Suffix - Passive Balancing)[4]	25 mA
Maximum Series Voltage	750 V
TEMPERATURE	
Operating Temperature (Ambient temperature)	
Minimum	-40°C
Maximum	65°C
Storage Temperature (Stored uncharged)	
Minimum	-40°C
Maximum	70°C

FIGURE 7-2. The UC cell characteristics.

For the electric scooter, studied in the MOEVEHU project, a test bench has been used for the discharge and charge of the battery and UC. The battery and UC packs are presented in FIGURE 7-3 and the measured characteristics in FIGURE 7-4 FIGURE 7-5.

FIGURE 7-3. The battery (left) and UC (right) pack needed for the supply of the electric scooter.

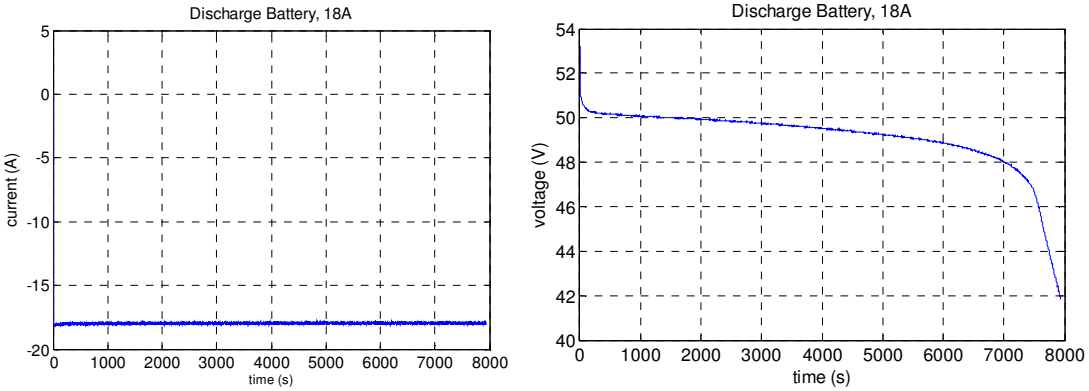

FIGURE 7-4. The discharge characteristic of the battery pack.

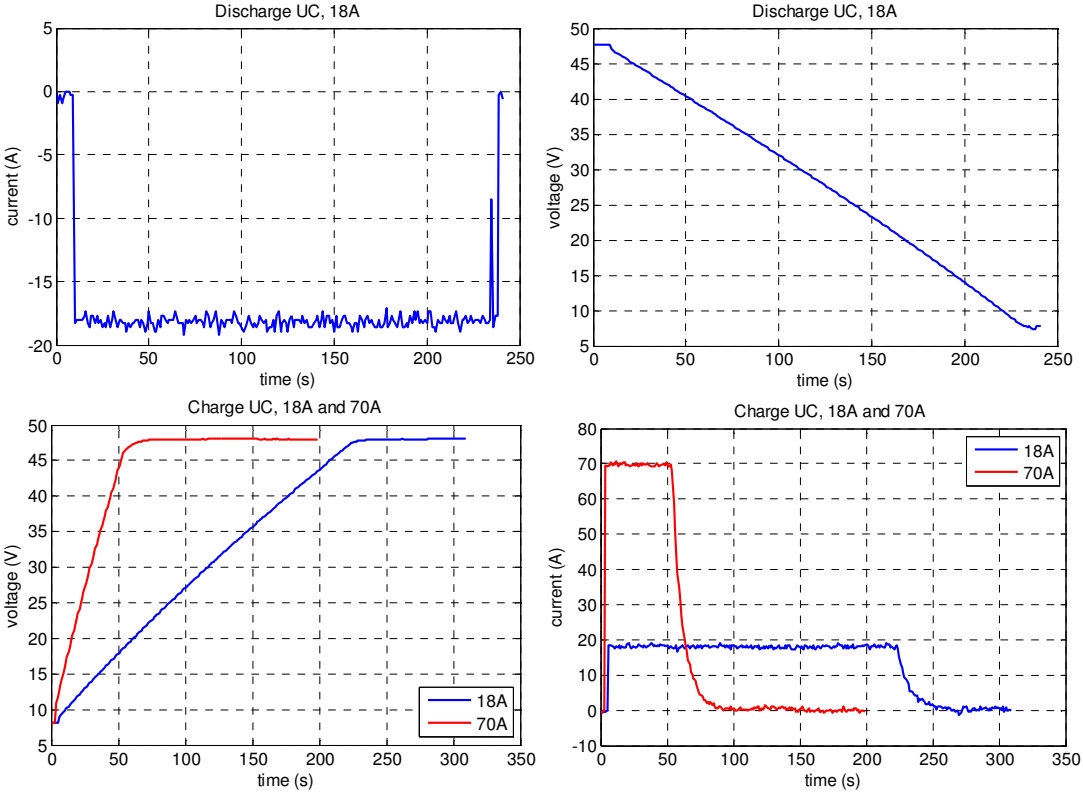

FIGURE 7-5. The discharge-charge characteristic of the UC pack.

The test bench of the electric scooter which is fed from the battery-UC source is presented in FIGURE 7-6. For comparison are presented some measured performances. The speed reference is inspired from a slightly modified European Driving Cycle (EDC) (the high-way period was neglected, and the acceleration ramp-time was increased), see FIGURE 7-7.

A comparison of the measured performances is presented in Table 7-1 (emphasizing that the cost is for a prototype machine).

FIGURE 7-6. The discharge-charge characteristic of the UC pack.

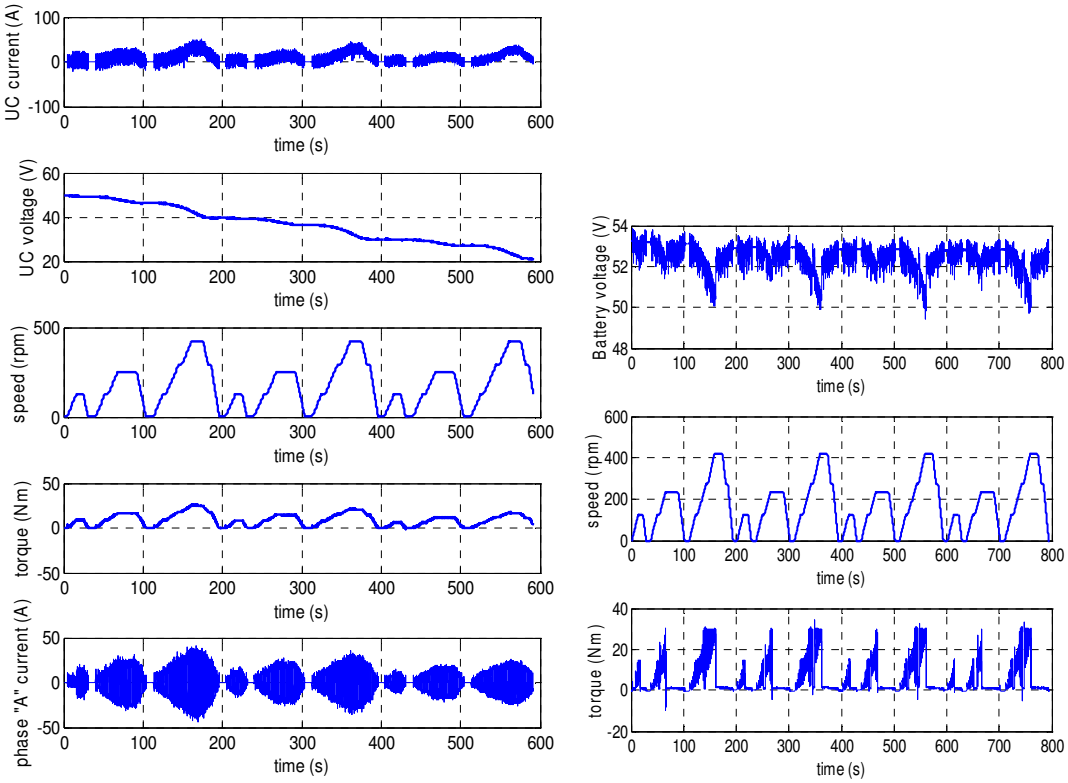

FIGURE 7-7. The electric scooter characteristics while being supplied from UC (left) or battery (right).

TABLE 7-1. SUMMARY OF PERFORMANCES FOR THE ELECTRIC SCOOTER SUPPLIED FROM BATTERY OR UC

PARAMETER \ *DEVICE*	*ELECTRIC MOTOR (PROTOTYPE)*	*BATTERY*	*UC*
Weight (kg)	14.5	35.2	17.6
Cost (€)	3100	864	3640
Autonomy at full load (km)		100	4
Autonomy on EDC (km, on straight line) – average speed: 20km/h		80km tested	3
Possible improvement: - use of 40Ah (or even 20Ah) batteries=> reduce the weight (by at least 11kg) and the costs of the power supply (!we should pay attention to the autonomy!)			

7.3 The energy management

Several control strategies could be employed [107]-[109]. Here, the used strategy is based on polynomial type (assures the energy transfer between batteries and UC) [110]. The control strategy must be of current type because the DC-bus voltage level is imposed by the batteries. The studied system is presented in FIGURE 7-8.

The analytical model is given by (7.1), where "k" and "α" define the sign of the UC current and the equivalent value of the duty cycle respectively (defining the buck/boost modes, (7.2)):

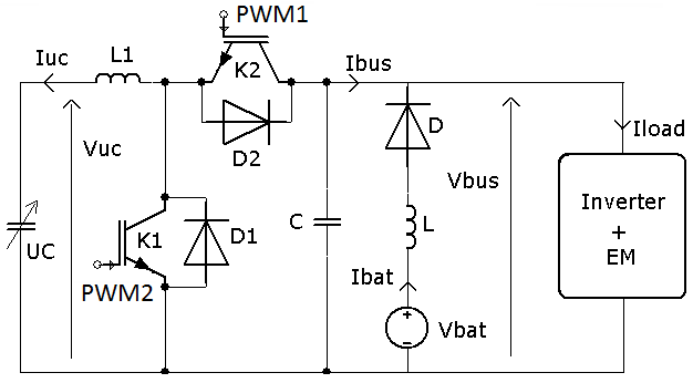

FIGURE 7-8. Layout of the studied hybrid system. [111].

$$\begin{cases} V_{L1} = L_1 \cdot \frac{d}{dt}(I_{uc}) = \frac{1}{k} \cdot (V_{uc} - \alpha \cdot V_{bus}) \\ I_{load} = I_{bat} + k \cdot I_{bus} \\ V_L = L \cdot \frac{d}{dt}(I_{bat}) = V_{bat} - V_{bus} \end{cases} \quad (7.1)$$

with

$$\underbrace{\begin{cases} k = -1 \\ \alpha = \alpha_2 = \frac{V_{uc} + V_{L1}}{V_{bus}} \end{cases}}_{buck}$$

$$\underbrace{\begin{cases} k = 1 \\ \alpha = 1 - \alpha_1 = \frac{V_{uc} - V_{L1}}{V_{bat} - V_L} \end{cases}}_{boost} \quad (7.2)$$

(Note: the meaning of the above notations, and the ones which follow, are linked to FIGURE 7-8.)

The buck-boost converter control strategy presents two distinct phases. The first phase is characterized by the charge of the UC with constant current; during this phase, the batteries current loop is not activated, so it can be said that only the PWM2 signal is activated. The second phase is characterized by the discharge of the UC with a variable current (7.3) (where $0 < \eta \le 95\%$ is the boost converter theoretical efficiency):

$$I_{ucref} = \frac{V_{bus}}{\eta \cdot V_{uc}} \cdot (I_{load} - I_{batref}) = \frac{V_{bus}}{\eta \cdot V_{sc}} \cdot I_{busref} \tag{7.3}$$

The UC reference current (I_{ucref}) is obtained starting from the electric energy exchange between batteries and UC. During this phase the UC and battery current loops with PWM1 control signal are activated (PWM1 and PWM2 signals cannot be activated simultaneously). To obtain a minimal static error with disturbance rejection, the "$R_{uc}(z^{-1})$", and "$S_{uc}(z^{-1})$" polynomials of the equation (7.4) are selected, where the polynomial coefficients are given by (7.5). The other parameters are "*L*", as the UC current smoothing inductance, "T_e" as the sampling period and the "ω_n" as control strategy band-width).

$$\begin{cases} S_{uc}(z^{-1}) = 1 - z^{-1} \\ T_{uc}(z^{-1}) = R_{uc}(z^{-1}) = r_{0uc} + r_{1uc} \cdot z^{-1} \end{cases} \tag{7.4}$$

$$\begin{cases} \omega_n \le \dfrac{2 \cdot \pi \cdot f_d}{10} \\ r_{0uc} = 2 \cdot (1 - \exp(-\omega_n \cdot T_e)) \cdot \dfrac{L_1}{T_e} \\ r_{1uc} = (\exp(-2 \cdot \omega_n \cdot T_e) - 1) \cdot \dfrac{L_1}{T_e} \end{cases} \tag{7.5}$$

By using the same principle, the polynomial coefficients for battery current control are given in (7.6):

$$\begin{cases} r_{0bat} = 2 \cdot (1 - \exp(-\omega_n \cdot T_e)) \cdot \dfrac{L}{T_e} \\ r_{1bat} = (\exp(-2 \cdot \omega_n \cdot T_e) - 1) \cdot \dfrac{L}{T_e} \end{cases} \tag{7.6}$$

The polynomial control (see FIGURE 7-9) consists in storing all measurement errors (ε) samples of the UC current to estimate the voltage drop. To make these estimations it is necessary to provide to the system the desired UC current reference (I_{ucref}), the polynomial coefficients (r_{0uc} and r_{1uc}) and the initial condition of the voltage:

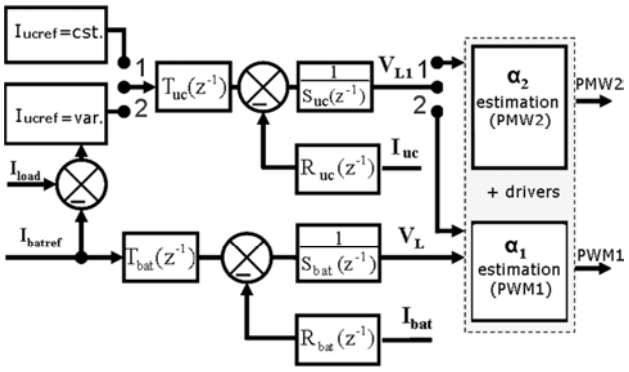

FIGURE 7-9. Layout of the polynamial controller. [111]

$$\begin{cases} \varepsilon_{I_{uc}}(n) = I_{ucref}(n) - I_{uc}(n) \\ \varepsilon_{I_{uc}}(n+1) = I_{ucref}(n+1) - I_{uc}(n+1) \\ V_{L1}(n+1) = V_{L1}(n) + r_{0uc} \cdot \varepsilon_{I_{uc}}(n+1) + r_{1uc} \cdot \varepsilon_{I_{uc}}(n) \end{cases} \quad (7.7)$$

The battery current control algorithm is employed in the same way as the UC current control. For $V_{bat}(n+1)$ estimation, it is necessary to provide to the system the battery current reference the polynomial coefficients (r_{0bat} and r_{1bat}) and the initial condition of the voltage:

$$\begin{cases} \varepsilon_{I_{bat}}(n) = I_{batref}(n) - I_{bat}(n) \\ \varepsilon_{I_{bat}}(n+1) = I_{batref}(n+1) - I_{bat}(n+1) \\ V_{L}(n+1) = V_{L}(n) + r_{0bat} \cdot \varepsilon_{I_{bat}}(n+1) + r_{1bat} \cdot \varepsilon_{I_{bat}}(n) \end{cases} \quad (7.8)$$

where *n* is the instant where a measurement is taken.

In order to prove the operability of the proposed control method, several simulation results can be presented. The hybrid system simulations parameters are shown in Table 7-2 and the simulations are carried out for boost converter state (PWM1=ON and PWM2=OFF).

TABLE 7-2. SYSTEM SIMULATION PARAMETERS

PARAMETER	*SYMBOL*	*VALUE (UNITY)*
IGBT control frequency	fd	10 kH z
DC-link maximal voltage	Vbus1	280 Vcc
Super capacitors maximal voltage	Vuc	81 Vcc
Boost converter average efficiency	η	86 %
Maximal DC-link current	L	25 µH
DC-link voltage smoothing capacitance	C	1500 µF
UC currents smoothing inductance	L1	50 µH

The main goal is to maintain the battery current at a constant value (10 A) while the system (meaning the UC, associate to its converter) will assure the excess of needed current. The simulated results are plotted in FIGURE 7-10.

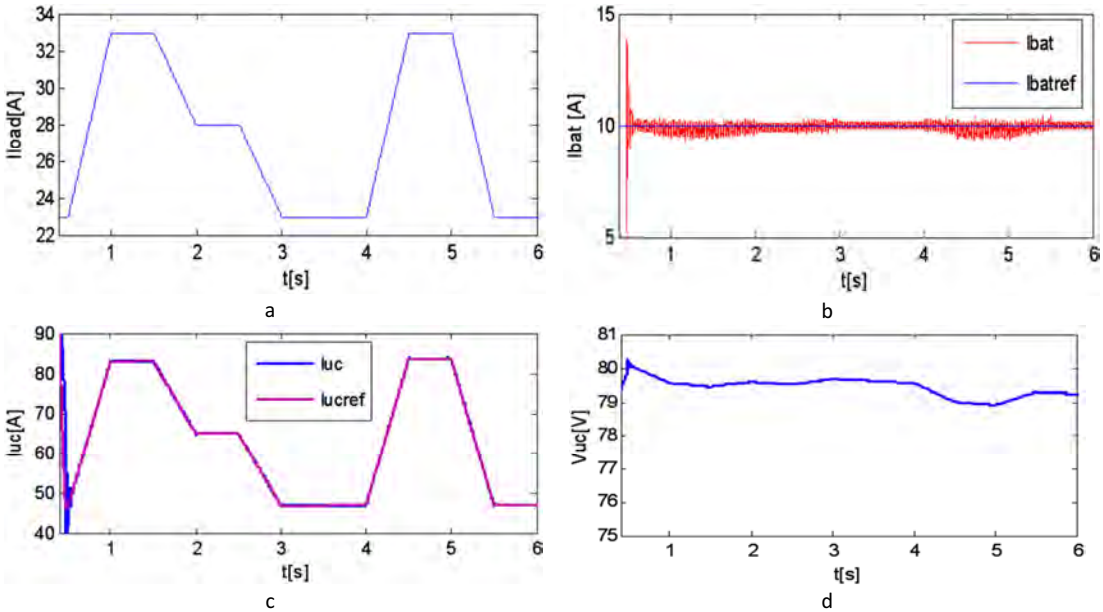

FIGURE 7-10. Hybrid source energy maangement: simulated results:
a) load current profile; b) battery current control; c) UC current control; d) UC voltage. [111].

In order to verify the boost converter control, the battery reference current (I_{batref}) is fixed at 10 A. The active load current (I_{load}) profile is shown in FIGURE 7-10a. The simulation results given in FIGURE 7-10b-d show that the boost converter control is satisfactory, except the instant around 0.5 second when the current loop does not have enough time to react. First of all, the battery current profile plotted in FIGURE 7-10b shows that the electric power transients are employed by the UC, and this is obvious in FIGURE 7-10c. Also, the UC module voltage (V_{uc}) is shown in FIGURE 7-10d and one can see how the UC voltage is rather decreasing while the UC current is increasing.

The simulation results give confidence for the implementation of the energy exchange on a reduced scale automobile system (test bench).

The setup of the studied reduced scale hybrid automobile contains a modular test bench which permits the evaluation of different new technologies of the electric and hybrid power train. The bench should be used for the validation and the correction of the design models and control laws. Thus, the expected modularity of all the components of the electric and hybrid power trains and the developed control strategies could be validate and ameliorated.

In order to have a representative bench for a real system, the authors have chosen to use as reference a car with 1:4 scale. The bench is shown on FIGURE 7-11.

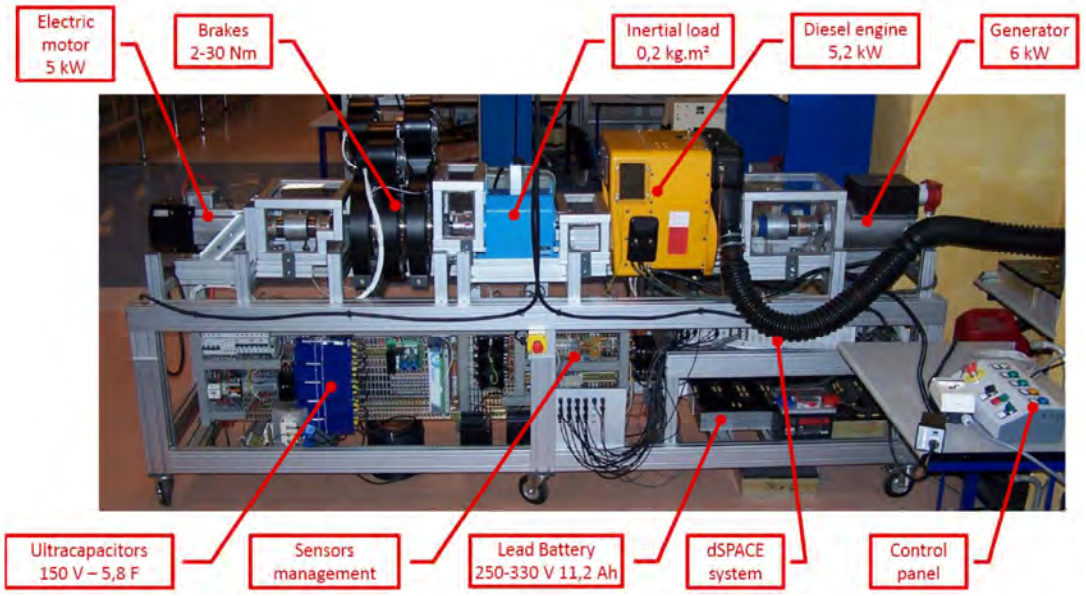

FIGURE 7-11. The test bench of the modular hybrid power train. [111]

The main components of the test bench are:

- diesel engine: direct injection, the output power is 5,2 kW and the maximal speed is 3600 r/min.
- generator: synchronous machine, power: 6 kW at 3000 r/min.
- electric motor: synchronous permanent magnets motor, with 5 kW of rated power and a rated speed of 3000 r/min (the maximal speed is 4300 r/min).
- mechanical load: electromagnetic brakes (2-30 Nm) and inertial load (0,2 kg.m²).
- lead battery: 250 – 330 V, 11,2 Ah.
- ultracapacitors: 150 V and 58 F, ultracapacitors in serial configuration with integrated balancing system.
- management system : dSPACE DS1103 real time control.
- sensors: voltage, current, speed, torque, temperature and fuel flow meter sensors.

The present work presents the results with regard to the energy management on board of this reduced scale hybrid automobile. To be more specific, the energy exchange between the UC, battery and the load was study, with a proper control technique.

In order to better situate the context of this study, several comments should be added, regarding the employed load cycle.

Each year, students of the Electrical Engineering department from UTBM participate in a contest which is called “Challenge SIA”. The SIA race is organized by the SIA (French Society of Automotive Engineers) and it concerns all education institutes. This competition takes place every year in the same time with the well-known competition: “the 24 hours course from *Le Mans*” (France). A nearby test circuit is used in the students’ competition.

It should been said that the European road cycle is very simple and, in authors’ opinion, does not reflect the real load profile for a common automobile. Thus, in order to exploit, in a more real manner, the system energy management, it has recorded, at the last edition of students’ race, the profile of the vehicle speed during this race. (The same type of motor, with the same data is placed on board of a small race car, with batteries of same type, and a 3-phase inverter to supply the motor). In FIGURE 7-12 is plotted the motor speed record for three laps.

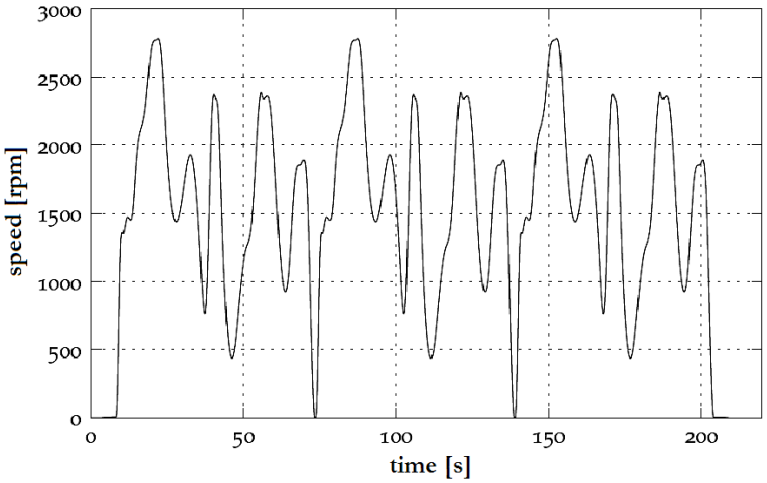

FIGURE 7-12. Motor speed profile recorded on a real road cycle nearby *Le Mans* circuit. [111]

So, the authors have chosen this experiment to reproduce the road cycle on the test bench in order to demonstrate the use of UC in this application where the dynamics of the vehicle is the most important thing. Finally, *it is a race*!

Some measured results are presented in FIGURE 7-13, in order to demonstrate the control capability on the tested reduced scale automobile.

As it was stated previously, the UC should assure the necessary pick current while load transients occurred. Thus, in FIGURE 7-13a is presented the battery current control with and without UC. It can be seen that the transient currents of the battery are smoothed by the action of UC, thus assuring the correct energy management. Also, the ultracapacitors current and the UC current on the dc bus are shown on FIGURE 7-13b.

So, here is the validation of the employed control technique for the reduced scale automobile system which operates in safe and real conditions.

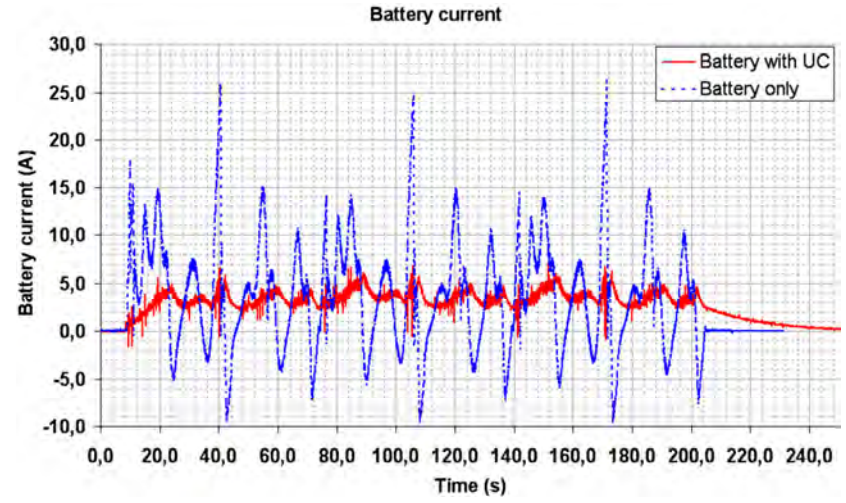

(a)

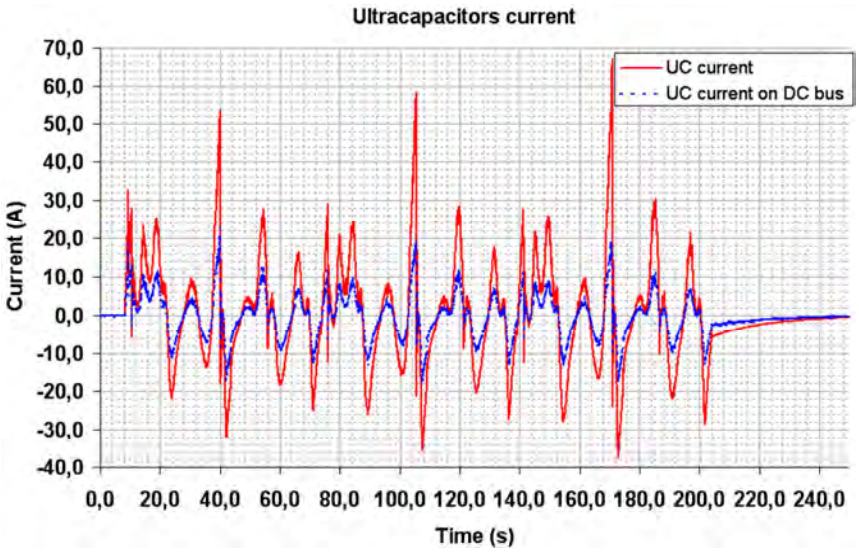

(b)

FIGURE 7-13. Obtained measured results. [111]

PART 2

FUTURE RESEARCH WORK

8 CONCLUSIONS AND PERSPECTIVES

8.1 Research perspectives

The main research field of the author, up to now, concerned the motorization of the light electric vehicles. Starting with the industrial projects (XANTOS, HYTEN and HiTECH-HEV), the author's interest is no longer limited to small power applications. The power range of the studies realized in XANTOS and HYTEN projects covered a power range of 120kW – for the KERS and TURBO applications for racing cars. Thus, new challenges have arisen. Some of these challenges are considered to be studied into the HiTECH-HEV project.

The HiTECH-HEV project concerns the realization of a modular platform for testing the components and performances of the energy management in a hybrid electric vehicle based on the Hardware-in-the-Loop concept. The goal is to propose high competitive HEV in terms of costs and autonomy. One objective of the research concerns the use of high-speed motorization. The idea is to use the high-speed motorization in order to reduce the volume and the weight of the power train.

Since the main element in the electric traction is the electric motor, by decreasing its volume we will reduce the overall weight of the EV. This will have a direct influence on the autonomy of the vehicle: by reducing the mass of the motorization we will spare important amount of the battery energy. Next, if the volume/weight have decreased, normally the investment on the motorization will decrease (this is not always true since the steel for example, has to meet some mechanical specification, in order to avoid the damage of the machine while running at high-speed). This is the main motivation of the high-speed motorization.

When working with high speed machines, three main questions need to receive an answer:

- Which motorization variant is best suited for such application?
- Which type of gear or distribution system will be used?
- How the control unit will manage the power flow?

These are the main challenges of the high speed motorization for (let's say) the future of electrical power train and for which the author proposes the following discussion.

8.1.1 The high speed motorization of EVs

High-power and high-speed electrical machines have been studied and realized mainly for ventilation systems and fuel cells compressors. In the literature a speed range of 40000…120000r/min, at high-power (beyond 15kW) has been reported [112]-[114]. Many studies are just theoretically, and the experimental results are only estimated. In such systems, because the demanded torque is rather constant, the control dynamics is reduced. The Parker company, for example, proposes a progressive increase of the speed of 60 seconds, each 1000 r/min (this mean that for their 15kW-40000r/min machine-drive system, the maximum speed will be reached in 40 minutes) [115]. On the other hand, in electrical traction systems the accelerations, decelerations and rapid change in machine's dynamic have to be promptly assured. For that, good materials should be used, a high performances power electronics unit need to drive the machine and a proper energy management should be employed. Water cooling of the machine is a must in such application. Thus, a supplementary water-pump system should be taken into consideration.

The research team from the HiTECH-HEV project has studied up to now three types of high-speed machines: permanent magnet synchronous machine (PMSM), variable reluctance

synchronous machine (VRSM) and induction motor (IM). The PMSM and IM are under construction process. We have decided to start from a first prototype of 26kW and 26000r/min, the supply being assured via a three phase inverter of 380Vdc, from a battery pack of lithium polymer.

For a long term research perspective, due to the current monopoly which exists on the permanent magnet market and even due to the European trend, the author's regard will be more and more oriented to the motorization variants which exclude the use of the PMs. One of the most interesting variants with this feature is the variable reluctance synchronous machine, which, for two poles configuration, could assure a very high power factor. (In the last call of European Cooperation Projects – FP7 project type – there was a topic specialy dedicated to the projects which are proposing the use of electrical machines without rear-earth magnet material. This is mainly because China, from several years, started to buy more and more companies which are producing PMs based on rear-earth materials, through that having a monopoly on the PMs market).

The high speed electrical machine has to be link to a gear, in order to send the expected torque and speed to the automobile's wheels. Thus, several possibilities have been considered: a mechanical distribution system, or a magnetically one. If the first one should be bought from the market, the second variant has to be firstly designed.

8.1.2 Magnetic gears

The advantage of a magnetic gear (MG) is obvious: there is no lubrication needed, there is no mechanical friction between the moving parts and the gear is intrinsically protected to breakage if a higher input torque is given [116]-[117]. The concept of magnetic gear was firstly present in the first quarter of the 20th century. In an American patent the idea of magnetic gear was proposed. At that time, the MG had the magnets on two armatures with different diameters (for low and high speed). But the first realized magnetic gear, which has copied the classical mechanical gear, was proposed in the beginning of the 1980s. This variant did not exploit, at maximum, the magnets presence. Thus, in 2001 has been proposed a magnetic gear with improved efficiency [116]. It contains a static, part made of steel, placed between the two rotors, and which serves to better transfer the flux between the rotating parts. Such variants are rather for reduced gear ratio. So, it can be said that the research in this field is unexploited yet.

A special design of such a gear needs to be done for high-speed application. Some solutions have been studied and the first results will be presented in a future international conference (COMPUMAG 2013, 30 June – 4 July 2013). The magnetic gear proposed in this paper is for a 40000 r/min electric motor, of 40kW (meaning a torque of 9.5Nm), and the output speed will be of 1500 r/min (meaning an output torque of 254 Nm).

In order to have an idea about the structure of the studied MG, few simulated results are presented in FIGURE 8-1. A special attention should be paid to the ratio between the poles of the high-speed (interior) and low-speed (exterior) rotors. In our case, the number of poles of the low speed rotor will be 26, while the number of iron pieces of the static part, is 27. The inner part (the high-speed rotor) has 2 poles. This has produced the lowest variation on the output torque. The capability of the MG to produce the desired torque, considering the abovementioned input and output speed is depicted in FIGURE 8-1, where the axis torque for different rotor positions is presented.

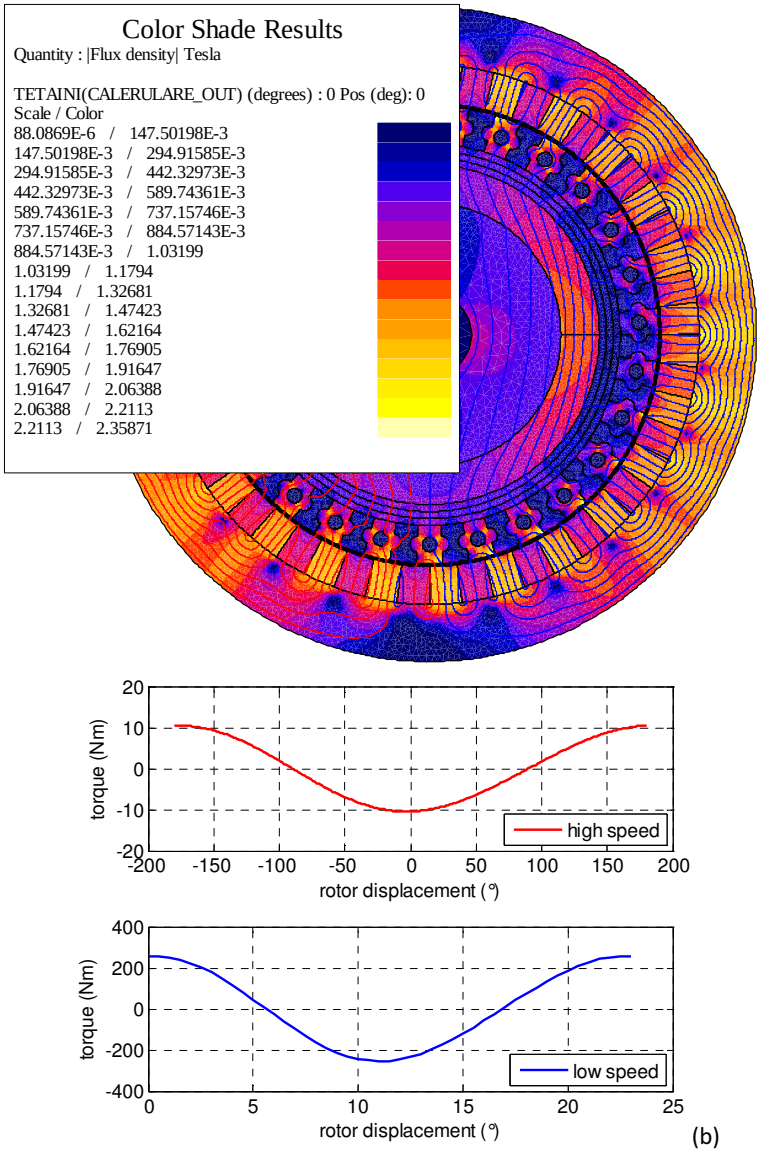

FIGURE 8-1. Proposed MG. a) cross section, field lines and flux density distribution; b) measured torque at the inner (high-speed) and outer (low-speed) rotor.

For a long term research perspective, the author is intending to take into consideration the use of a magnetic gear for wind power plants. The lifetime of a wind-power system will increase significantly if none mechanical multiplier is installed on the power plant and the solution should be much more compact. (Other similar applications could be taken into consideration, where a transmission system is used.)

8.1.3 High power-frequency converters and adequate control

The dynamics capability of the high speed motorization has to be realized with a high frequency inverter. If the industrial inverters found on the market today, for high power and frequency applications, are at 16 kHz, the dynamics of the high-speed motorization requests more.

Different variants can be considered here, based on MOSTFET or IGBT technology. The MOSFET can assure high frequency response. The research team from the HiTECH-HEV project

has studied experimentally such a technology up to 32 kHz, at 50Vdc-25A, and at 400Vdc-5A. More tests will be done. The IGBTs will be tested also to see which technology respond better to the applications' demands.

The control at such high speeds cannot be assured via classical microcontrollers. Dedicated digital signal processors or field programmable gate arrays have the computation power and the appropriate interface to control multiphase drives at high frequency (such devices should be considered for the study of the high speed control).

8.1.4 Scientific papers "in submission" or "in print" stage

In this moment there are several scientific papers in submission phase or waiting to be published.

- M. Ruba, D. Fodorean, *Design, analysis and torque control of low voltage high current SRM for small automotive applications*, IEEE EUROCON 2013 Conference, Zagreb, Croatia, July 1-4, 2013, in print.
- F. Jurca, D. Fodorean, *Analysis and Control of an Axial Flux Motor for Small Electric Traction System*, IEEE EUROCON 2013 Conference, Zagreb, Croatia, July 1-4, 2013, in print.
- D. Fodorean, *Study of a High Speed Motorization with Improved Performances dedicated for an Electric Vehicle*, the - COMPUMAG 2013, 19th Conference on the Computation of Electromagnetic Fields, Budapest, Hungary, June 30 – July 4, 2013, in print.
- D.C. Popa, D. Fodorean, *Analysis of a High Speed Induction Machine used for the Propulsion of an Electric Vehicle*, the - COMPUMAG 2013, 19th Conference on the Computation of Electromagnetic Fields, Budapest, Hungary, June 30 – July 4, 2013, in print.

8.2 Teaching perspectives

The technological transfer from university to industry is a very important aspect of the research activity, because ideas come to life in a real and competitive environment when an industrial partner is involved. In a similar manner, forming the students with quality skills, for the competitive environment in which they will be integrated, is another aspect of the mission of a teacher-researcher. In this way, the transfer of knowledge can be much more simply assimilated into the industrial environment since the people who form it have the ability to seize the novelty and to exploit it.

To make this thing possible, one important goal is to transfer concepts, methods, technologies, apparatus and work plans, used in the research projects, into the students' hands while they are involved in specific task of the research plan. Another possibility is, in the case that the project was successfully finished, to integrate a part of the equipment and materials into the teaching activities. Thus, the students will be able to work with new and high quality equipment that can be a solution for the industrial partners in their future production work.

Up to now the author's teaching activity was mainly concentrated on the use and performance measuring of electrical machines and drives, their modeling and control based on different control platforms, testing and monitoring of electrical equipment. Thus, a second goal of the author, from the teaching perspective, is to propose courses on rapid control prototyping (RCP) and Hardware-in-the-Loop (HiL). These concepts start to be more and more used in the industrial environment, especially for rapid integration of new control techniques or integration of new devices. A correct approach and a good methodology work can spare a lot of time, energy and budget for the series production stage. Such concepts and their use should be integrated into the teaching curricula of the electrical engineering domain.

Conclusions

This habilitation thesis report presents the main results, achievements and perspectives of the author's research-teaching activities.

First, the motivation of the research activity was introduced, to justify the author's activities in the present scientific context. The first chapter has started with a short state-of-the-art section, on electric vehicle (EV) application. From its birth, up to its present and taking a look toward the next 50 years, the EV's strong and weak points have been emphasized. Also, at the end of the first chapter, the main results and achievements of the teaching and research activities have been summarized.

The 2nd chapter has been dedicated to the motorization variants, especially for light EVs. A comparison of the main existent motorization topologies has been introduced, and the studied variants have been evaluated.

The 3rd chapter contains the main designing elements of the studied machines/topologies. Also, the numerical tool, based on finite element method, was introduced, because the design process relies on it. Some of the numerically obtained results have been compared with the analytical obtained ones, for validation.

Before its construction, the studied electrical machine needs to be optimized. Thus, in the 4th chapter several optimization techniques have been presented. Starting from the simplest (of gradient type) to the most complex ones (of evolutionary type, in hybrid implementation), the optimization algorithms and the obtained results have been presented for several machine topologies. Some of the optimized variants have been constructed. (The optimization problem was studied mainly in the context of international research cooperation.)

The 5th chapter presents the thermal behavior of the electrical machines, when specific driving cycles are considered in their operation. By means of specific software, complex thermal behavior of the studied machine has been evaluated.

In the 6th chapter, the control techniques used for the motorization of the EV, the motor-drive capability to operate in faulty conditions and the machines' possibility to work beyond the rated speed have been discussed.

The most common energy sources used in EVs, as well as their characterization or their use for improved energy management have been presented into the 7th chapter.

Some of the future activities of the author have been briefly introduced in the 8th chapter, the main scientific topics being: the high speed motorization, the magnetic gears, the high frequency power converters and high frequency control units.

We could conclude that the author's interdisciplinary scientific interest has involved knowledge, consistent effort and resources, which were well managed in the present national and international research context.

9 REFERENCES

[1] Fodorean D., Jurca F, Ruba M. and Popa D.C., *Motorization Variants for Light Electric Vehicles – design, magnetic, mechanical and thermal aspects*, AlmaMater, June 2013.

[2] Fuhs A.E., *Hybrid vehicle and the future of personal transportation*. CRC Press, 2009.

[3] Larminie J. and Lowry J., *Electric vehicle technology explained*. Wiley, 2003-1st/2012-2nd.

[4] Anderson D.C. and Anderson Judy., *Electric and hybrid cars – A history (2nd edition)*. McFarland & Company, 2010

[5] Pistoia G., *Electric and hybrid vehicles: Power Sources, Models, Sustainability, Infrastructure and the Market.* CRC Press, 2010.

[6] Soylu S., *Urban transport and hybrid vehicles.* Sciyo (Croatia), 2010.

[7] De Santiago J. et ali. *Electrical Motor Drivelines in Commercial All-Electric Vehicles: A Review*. IEEE Transactions on Vehicular Technology, vol.61, n°.2, pp.475-485, Feb.2012.

[8] Husain I., *Electric and hybrid vehicles: design fundamentals – 2nd edition.* CRC Press, 2011.

[9] Vogel C., *Build Your Own Electric Motorcycle.* McGraw-Hill Companies, 2009.

[10] Ehsani M., Gao Y., Gay S.E. and Emadi A., *Hybrid Electric, and Fuel Cell Vehicles: Fundamentals, Theory, and Design*. CRC Press, 2005.

[11] Ceraolo M., Caleo A., Campozella P. and Marcacci M.*A., parallel-hybrid drive-train for propulsion of a small scooter*. IEEE Transactions on Power Electronics, vol.21, n°.3, pp.768-778, March 2006.

[12] Chenh-Hu C. &and Ming-Yang C. *Implementation of a highly reliable hybrid electric scooter drive*. IEEE Transactions on Industrial Electronics, vol.54, n°.5, pp.2462-2473, March 2007.

[13] Wakihara M. and Yamamoto O., *Lithium ion batteries: fundamentals and performances*. Wiley VCH, 1999.

[14] Affanni A., Bellini A*.,* Franceschini G., Guglielmi P. and Tassoni Carla. *Battery Choice and Management for New-Generation Electric Vehicles*. IEEE Transactions on Industrial Electronics, vol. 52, n°.5, pp.1343-1349, October 2005.

[15] Mierlo JV, Maggetto G, Lataire Ph. *Which energy source for road transport in the future? A comparison of battery, hydride and fuel cell vehicles*. Energy Conversion and Management, vol.47, n°.17, pp.2748–2760, 2006.

[16] Lai J.-S., and Nelson D.J. *Energy Management Power Converters in Hybrid Electric and Fuel Cell Vehicles – invited paper*. Proceedings of the IEEE, vol.95, n°.4, pp.766-777, April 2007.

[17] Wessner C.W., *Building the U.S. battery industry for electric drive vehicles*. The National Academies Press (USA), 2012.

[18] ***- http://en.wikipedia.org/wiki/Electric_vehicle accesed on 10 March 2013.

[19] Hurd W. J., Morrow M.B., K.R. Kaufman and An K.N., *Wheelchair propulsion demands during outdoor community ambulation*. Journal of Electromyography and Kinesiology, vol.19, n°.5, pp. 942-947, October 2009.

[20] Boiadzjiev G. and Stefanov D., *Powered wheelchair control based on the dynamical criteria of stability*. Mechatronics, vol.12, n°.4, pp. 543-562, May 2002.

[21] Oonishi Y., Sehoon Oh. and Hori Y., *A New Control Method for Power-assisted Wheel Chair based on the Surface Myoelectric Signal*. IECON 2007, 33rd Annual Conference of the IEEE Industrial Electronics Society, pp.356-361, 5-8 Nov. 2007.

[22] Kim Y. K., Cho Y. H., Park N. C., Kim S. H. and Mok H. S., *In-Wheel motor drive system using 2-phase PMSM*. IEEE 6th International Power Electronics and Motion Control Conference, pp.1875-1879, 17-20 May 2009.

[23] Rahulanker R. and Ramanarayanan V.. *Battery assisted wheel chair*, India International Conference on Power Electronics, pp.167-171, 19-21 December 2006.
[24] Ohkita M. et ali, *Traveling control of the autonomous mobile wheel-chair DREAM-3 considering correction of the initial position*. 47th Midwest Symposium on A.; Circuits and Systems, vol.3, pp.215-218, 25-28 July 2004.
[25] Wang H., Salatin B., Grindle G.G., Ding D. and Cooper R.A., *Real-time model based electrical powered wheelchair control*. Medical Engineering & Physics, vol.31, n°.10, pp.1244-1254, December 2009.
[26] Cho S.Y., Winod A.P. and Cheng K.W.E., *Towards a Brain-Computer Interface based control for next generation electric wheelchairs*. 3rd International Conference on Power Electronics Systems and Applications, pp.1-5, 20-22 May 2009.
[27] Methil N.S. and Mukherjee R., *Pushing and Steering Wheelchairs using a Holonomic Mobile Robot with a Single Arm*. IEEE International Conference on Intelligent Robots and Systems, pp.5781-5785, 9-15 October 2006.
[28] Kamiuchi S. and Maeyama S., *A novel human interface of an omni-directional wheelchair*. ROMAN 2004 13th IEEE International Workshop on Robot and Human Interactive Communication, pp.101-106, 20-22 September 2004.
[29] Multon B., *Motorisation des véhicules electriques*. Techniques de l'Ingénieur, traité Électronique, document E 3996, pp.1-28, 2001.
[30] Kant M., *La voiture électrique Projet de motorisation*. Techniques de l'Ingénieur, traité Génie électrique document D 5561, pp.1-21, 1995.
[31] Fitzgerald A.E., et ali, *Electric Machinery – 6th edition*, McGraw-Hill, 2003.
[32] Miller T.J.E., *Brushless permanent magnet and reluctance motor drives*. Clarendon Press, Oxford 1989.
[33] Hanselman D.C., *Brushless permanent-magnet motor design*. McGraw-Hill, Inc., 1994.
[34] Gieras J.F., *Permanent Magnet Motor Technology: Design and Applications,* Springer 2010.
[35] Krishnan R., *Permanent Magnet Synchronous and Brushless DC Motor Drives*. CRC Press, 2009.
[36] Gieras J.F., Wang R.J., Kamper M.J., *Axial flux permannet magnet brushless machines.* Springer, 2008.
[37] Hughes A., *Electric Motors and Drives*. *Fundamentals, Types & Applications*. Newnes 2005.
[38] Krishnan R., *Switched Reluctance Motor Drives: Modeling, Simulation, Analysis, Design, and Applications*. CRC Press, (2001)
[39] Miller T.J. (2001). *Electronic Control of Switched Reluctance Machines*. Newnes.
[40] Inderka R.B., Menne M., De Doncker R.W.A. *Control of Switched Reluctance Drives for Electric Vehicle Applications*, IEEE Transactions on Industrial Electronics, vol.49, n°.2, pp.48-53, February 2002.
[41] Henneberger G. and Viorel I.A., *Variable Reluctance Electrical Machines*. Aachen: Shaker Verlag, 2001.
[42] Hadjidj D., Miraoui A. and Kauffmann J.M. *Modelling of a transverse vernier hybrid reluctance motor*. European Physics Journal – Applied Physics, vol.11, pp.183–188, 2000.
[43] Viorel I.A., Henneberger G., Blissenbach R. and Lövenstein L., *Transverse Flux Machines. Their behavior, design, control and applications*, Mediamira Puplisher (Romania), 2003.
[44] Henneberger G., Hadji-Minaglou J.R. and R. C. Ciorba, *Design and test of permanent magnet synchronous motor with auxiliary excitation winding for electric vehicle application*, Proc. of the European Power Electronics Symposium, Lausanne, Switzerland, Oct.1994, pp. 645–649.
[45] Radomski T.A., *Alternating current generator*, U.S. Patent 4 959 577, Sep. 25, 1990.

[46] Tapia J.A., Leonardi F. and Lipo T.A., *Consequent pole permanent magnet machine*, IEEE International Electrical Machines and Drives Conference, Boston, USA, 2001, pp.126–131.

[47] Rattei F., *Design of permanent magnet polyphase machine for hybrid a vehicle*, Proc. 4th Int. Symposium on Advanced Electromechanical and Motion Systems—Electromotion, Bologna, Italy, Jun. 2001, vol.1, pp. 99–101.

[48] Wroblewski J., *Magnetization of brushless synchronous generator with permanent magnets additionally excited—analysis conditions*, Proc. Of IEEE/KTH Power Tech Conference, Stockholm, Sweden, Jun.1995, pp.351–355.

[49] Amara Y., Lucidarme J., Gabsi M., Lecrivain M., Ahmed A.-H. B., and Akemakou A.-D., *A new topology of hybrid synchronous machine*, IEEE Transactions on Industry Applications, vol.37, no.5, pp.1273–1281, Sep./Oct.2001.

[50] Vido L., Amara Y., Gabsi M., L´ecrivain M. and Chabot F., *Compared performances of homopolar and bipolar hybrid excitation synchronous machines*, 40th Annual Meeting of Industrial Applications Conference, vol.3, Hong Kong, Oct. 2005, pp.1555–1560.

[51] Matyas A.R., Biro K.A., Fodorean D., *Multi-Phase Synchronous Motor Solution for Steering Applications*, Progress In Electromagnetics Research, vol.131, pp.63-80, Sept. 2012.

[52] Fodorean D. (2005). *Conception et Réalisation d'une Machine Synchrone à Double Excitation : Application à l'Entraînement Direct*. Université de Technologie de Belfrot-Montbéliard (Université de Franche-Comté), Belfort-France. PhD thesis report.

[53] Song B.-M. and Choi J.-Y., *A low-speed high-torque permanent magnet motor for electric scooters*, IEEE Vehicle Power and Propulsion Conference, Chicago, USA, pp. 1-6, Sept.2011.

[54] Ceraolo M., Caleo A., Campozella P. and Marcacci M.A., *A parallel-hybrid drive-train for propulsion of a small scooter*, IEEE Transactions on Power Electronics, vol. 21, no. 3, pp. 768-778, March 2006.

[55] K. Donghyun, H. Sungho, K. Hyunsoo, *Vehicle Stability Enhancement of Four-Wheel-Drive Hybrid Electric Vehicle Using Rear Motor Control*, IEEE Transactions on Vehicular Technology, vol.57, n.2, pp.727-735, March 2008.

[56] Amara Y., Vido L., Gabsi M, Hoang E., Ben Ahmed A.H. and Lecrivain M., *Hybrid Excitation Synchronous Machines: Energy-Efficient Solution for Vehicles Propulsion*, IEEE Transactions on Vehicular Technology, vol.58, n.5, pp.2137-2149, June 2009.

[57] Nguyen P.H., Hoang E. and Gabsi M., *Performance Synthesis of Permanent-Magnet Synchronous Machines During the Driving Cycle of a Hybrid Electric Vehicle*, IEEE Transactions on Vehicular Technology, vol.60, n.5, pp.1991-1998, June 2011.

[58] Magnussen F. and Sadarangani C., *Winding factors and Joule losses of permanent magnet machines with concentrated windings*, IEEE International Conference on Electrical Machines and Drives 2003, 1-4 June 2003, vol.1, pp.333-339.

[59] Jiabin W., Atallah K., Zhu Z.Q. and Howe D., *Modular Three-Phase Permanent-Magnet Brushless Machines for In-Wheel Applications*, IEEE Transactions on Vehicular Technology, vol.57, n.5, pp.2714-2720, June 2008.

[60] Fodorean D., Djerdir A., Viorel I.-A. and Miraoui A., *A Double Excited Synchronous Machine for Direct Drive Application - Design and Prototype Tests*, IEEE Transactions on Energy Conversion, vol. 22, n.3, pp. 656-665, September 2007.

[61] Fodorean D., Idoumghar L. and Szabo L., "Motorization for electric scooter by using permanent magnet machines optimized based on hybrid metaheuristic algorithm", IEEE Transaction on Vehicular Technology, vol.62, n.1, pp.39-49, January 2013.

[62] Pyrhonen, J., Jokinen, T. & Hrabovcova, V., *Design of Rotating Electrical Machines*, John Wiley & Sons, (2008).

[63] Huang, A.S., Luo, J., Leonardi, F. and Lipo, T.A. (1998). A general approach to sizing power density equation for comparison of electrical machines. *IEEE Trans. on Industry Applications*, Vol.34, No.1, (January 1998), pp.92-97, ISSN: 0093-9994.

[64] Fodorean D. and Miraoui A., *Dimensionnement rapide des Machines Synchrones à Aimants Permanents (MSAP).* Technique de l'Ingénieur, Paris, France. Doc.D3554, pp.1-24, 2009.
[65] Grellet G., *Les pertes dans les machines tournates.* Technique de l'Ingénieur, Paris, France. Document D3450, pp.1-31, 1989.
[66] Fodorean D., *Global Design and Optimization of a Permanent Magnet Synchronous Machine used for Light Electric Vehicle*, Intech, – book chapter in monograph: *Electric Vehicles – Modelling and Simulations*, edited by Serif Soylu, 2011.
[67] Chiasson J., *Modeling and high performance control of electrical machines*. IEEE Press series on power engineering. John Wiley & Sons Inc. Publication, 2005.
[68] Buja G.S. and Kazmierkowski P.,. *Direct torque control of PWM inverter fed AC motor – A survey*. IEEE Transactions on Industrial Electronics, vol.51, n°.4, pp.744-757, August 2004.
[69] Cimuca G.O., *Système inertiel de stockage d'énergie associé à des générateurs éoliens*. Ecole Nationale Supérieure d'arts et métiers (Centre de Paris), Thèse de Doctorat, 2005.
[70] Paunescu D., Paunescu Daniela, Popa D.C. and Iancu V.: *Design and Modeling of an Axial Flux Permanent Magnet Generator with Double Layer Tooth-Concentrated Fractional Windings,* in *Proc. of* ECMS 2011, Krakow June 2011.
[71] Idoumghar Lhassane, *Méthaeuristiques Hybrides et leurs Applications,* Mémoire d'Habilitation à Diriger des Recherches, Université de Haute-Alsace, 21 Novembre 2012.
[72] Tutelea L. and Boldea I., *Optimal design of residential brushless d.c. permanent magnet motors with FEM validation*, International AGEAN Conference on Electrical Machines and Power Electronics, pp.435-439, Sept. 2007.
[73] Fodorean D., Popa D.C., Jurca F., Ruba M., *Optimizing the Design of Radial/Axial PMSM and SRM used for Powered Wheel-Chairs*, Proceedings of the International Conference on Electrical, Computer, Electronics and Communication Engineering, Paris, France, 14-16 November 2011, pp.120-125.
[74] Giurgea S., Fodorean D., Cirrincione G., Miraoui A. and Cirrincione M., *Multimodel Optimization Based on the Response Surface of the Reduced FEM Simulation Model With Application to a PMSM*, IEEE Tran. on Magnetics, vol.44, n°9, pp.2153-2157, Sept. 2008.
[75] Kim S., Hong J., Kim Y., Nam H. and Cho H., *Optimal Design of Slotless-Type PMLSM considering multiple responses by Response Surface Methodology*, IEEE Trans. Mag, Vol. 42, No. 4, pp.1219-1222, April 2006.
[76] Youn B.D., Choi K.K., *A new response surface methodology for reliability-based design optimization*, Computers and Structures, vol.82, pp.241–256, 2004.
[77] McKay M.D., Morrison J.D. and Upton S.C., *Evaluating Prediction Uncertainty in Simulation Models*, Computer Physics Communications, pp.117:44-51, 1999.
[78] Sloane N.J.A., *A Library of Orthogonal Arrays*, http://www.research.att.com/~njas/oadir/.
[79] Michalewicz Z. and Fogel D. B. *How to Solve It: Modern Heuristics*. Springer-Verlag Berlin Heidelberg New, 2000.
[80] Idoumghar L., Fodorean D. and Miraoui A., *Simulated Annealing Algorithm for Multi-Objective Optimization: Application to Electric Motor Design*, 29th IASTED International Conference: Modeling, Identification and Control'10 Feb.2010, pp.190-196.
[81] P. N. Suganthan, N. Hansen, J. J. Liang, K. Deb, Y.-P. Chen, A. Auger, and S. Tiwari. *Problem definitions and evaluation criteria for the CEC 2005 special session on real-parameter optimization*. Technical Report 2005005, Nanyang Technological University, Singapore and IIT Kanpur, India, May 2005.
[82] Olivetti de Franca F., *Multivariate ant colony optimization in continuous search spaces*. In 10th Annual conference on Genetic and evolutionary computation, pp.9-16, 2008.
[83] Pant M., Thangaraj R. and Abraham A., *Particle Swarm Based Meta-Heuristics for Function Optimization and Engineering Applications*, 7th Computer Information Systems and Industrial Management Applications 2008, vol.7, pp.84 - 90, 26-28 June 2008.

[84] Deb K., *A fast elitist non-dominated sorting genetic algorithm for multiobjective optimization: NSGA II*, IEEE Transaction on Evolutionary Computation, vol.5, n.3, pp. 115-148, 2002.

[85] Idoumghar L., Idrissi-Aouad M., Melkemi M. and Schott R., *Metropolis particle swarm optimization algorithm with mutation operator for global optimization problems*, Proceedings of IEEE 22th International Conference on Tools with Artificial Intelligence, Arras, France, pp.35-42, October 27-29, 2010.

[86] Kennedy J. and Russell C.E., *Swarm intelligence*, Morgan Kaufmann, Academic Press, 2001.

[87] Xia W.-J. and Wu Z.-M., *A hybrid particle swarm optimization approach for the job-shop scheduling problem*, Journal of Advanced Manufacturing Technology, vol.29, n.3, pp. 360-366, March 2006.

[88] Kirkpatrick S., *Optimization by simulated annealing: quantitative studies*, Journal of Statistical Physics, vol.34, no.5, pp.975-986, 1984.

[89] Fodorean D. and Miraoui A., *Permanent Magnets Thermal Operation Limits in a Hybrid Excited Synchronous Machine used on Wide Speed Applications*, Proceedings of the 11th IEEE International Conference on Optimization of Electrical and Electronic Equipment – OPTIM'08, Brasov, Romania, 22-24 May 2008, pp.21-26.

[90] Welchko, B. A., Lipo, T.A., Jahns, T.M. and Schulz, S.E., "Fault Tolerant Three-Phase AC Motor Drive Topologies: A Comparison of Features, Cost, and Limitations", *IEEE Trans. on Pow. El.*, vol.19, no 4, pp.1108-116, July 2004.

[91] Jacobina, C.B., Ribeiro, R.L.A., Lima, A.M.N. and Silva, E.R.C., *Fault-tolerant reversible ac motor drive system*, *IEEE Trans. on Ind. Appl.*, vol.39, n.4, pp.1077-1084, July-August 2003.

[92] Ruba, M. and Anders, M., *Fault tolerant switched reluctance machine study*, *Int. Conf. in Power Electronics, Intelligent Motion and Power Quality,* Nuremberg, Germany, 2008.

[93] Wallmark, O., Harnefors, L. and Carlson, O., *Control algorithms for a fault-tolerant PMSM drive*, *IEEE Trans. on Ind. Elec.*, vol.54, no 4, pp.1973-1980, August 2007.

[94] Fodorean D., Ruba M., Szabo L., Miraoui A., *Comparison of the Main Types of Fault-Tolerant Electrical Drives used in Automobile Applications*, IEEE Int. Symp. on Power Electron, Electr.Drives, Automation and Motion, Ischia, Italy, 11-13 June 2008, pp.895-900.

[95] Grandi G., Serra G. and Tani A., *Space Vector Modulation of a Nine-Phase Voltage Source Inverter*, IEEE International Symposium on Industrial Electronics, 2007, pp.431-436.

[96] Ruba M., Fodorean D., *Analysis of Fault-Tolerant Multiphase Power Converter for a Nine-Phase Permanent Magnet*, IEEE Trans. on Ind. Appl., vol.48, nr.6, pp.2092-2101, Nov.2012.

[97] Fodorean D., Giurgea S., Djerdir A. and Miraoui A., *Numerical Approach for Optimum Electromagnetic Parameters of Electrical Machines used in Vehicle Traction Applications*, Energy Conversion and Management, vol.50, pp.1288-1294, Mai 2009.

[98] Jahns T.M.,, *Flux weakening regime operation of an interior permanent magnet synchronous motor drive*. IEEE Transactions on Industry Applications, vol.23, n.4, pp.681-689, 1987.

[99] Morimoto S., Takeda Y., Hirasa T. and Taniguchi K., *Expansion of operating limits for PM motors by vector control considering inverter capacity*, IEEE Transactions on Industry Applications, vol.26, n.5, pp.866-871, 1990.

[100] Slemon R., *Achieving a constant power speed range for PM drives*, IEEE Transactions on Industry Applications, vol.31, n.2, pp.368-372, 1995.

[101] Bianchi N. and Bolognani S., *Parameters and volt-ampere ratings of a synchronous motor drive for flux-weakening applications*. IEEE Transactions on Power Electronics, vol.12, n.5, pp.895-903, 1997.

[102] Takahashi, and T. Noguchi, "A new quick response and high efficiency control strategy of an induction motor", IEEE IAS Meeting, pp.496-502, 1985.

[103] Bae B-H., Sul S-K., Kwon J-H. and Shin J-S., *Implementation of sensorless vector control for super high speed PMSM of turbo-compressor*, IEEE Transactions on Industry Applications, vol.39, n°3, pp.811-818, May-June 2003.
[104] Buja G.S. and Kazmierkowski P., *Direct torque control of PWM inverter fed AC motor -A survey*, IEEE Transactions on Industrial Electronics, vol.5 1, n°4, August 2004.
[105] Fuengwarodsakul N.H., Inderka R.B. and Doncker R.W.D., *Instantaneous torque controller for switched reluctance vehicle propulsion drives*, 20th Electric Vehicle Symposium, 2003.
[106] Fodorean D., Djerdir A., Miraoui A., Viorel I.A., *FOC and DTC Techniques for Controlling a Double Excited Synchronous Machine*, IEEE International Electric Machines and Drives Conference, Antalya, Turkye, 3-5 May 2007, pp.1258-1263.
[107] Moreno J., Ortuzar M.E. and Dixon J.W., *Energy-Management System for a Hybrid Electric Vehicle, Using Ultracapacitors and Neural Networks*, IEEE Transactions on Industrial Electronics, vol.53, no 2, pp.614-623, April 2006.
[108] Schofield N., Yap H.T. and Bingham C.M., *Hybrid energy sources for electric and fuel cell vehicle propulsion*, IEEE Conference on Vehicle Power and Propulsion, pp.522-529, 7-9 September 2005.
[109] Gao L., Jiang Z. and Dougal R.A., *Evaluation of active hybrid fuel cell/battery power sources*, IEEE Trans. on Aerospace and Electronic Systems, vol.41, no 1, pp.346-355, January 2005.
[110] Camara M.B., Gualous H., Gustin F. and A. Berthon, *Design and New Control of DC/DC Converters to share energy between Super capacitors and Batteries in Hybrid Vehicle*, IEEE Transactions on Vehicular Technology, vol.57, n°5, pp.2721-2735, September 2008.
[111] Fodorean D., Bouquain D., Camara M.B. and Miraoui A., *Energy Management on board of a Reduced Scale Hybrid Automobile*, Proceedings of the International Electrical Machines and Drives Conference, May 2009, pp.197-201.
[112] Cho H-W., Jang S-M., and Choi S-K., *A design approach to reduce losses in high-speed permanent magnet machine for turbo-compressor*, IEEE Transactions on Magnetics, vol.42, n°.10, pp.3521-3523, October 2006.
[113] Seo J-H., Chung T-K., Lee C-G., Jung S-Y., and Jung H-K., *Harmonic iron loss analysis of electrical machines for high-speed operation considering driving condition*, IEEE Transactions on Magnetics, vol.45, n°.10, pp.4656-4659, October 2009.
[114] Binder A., Schneider T., and Klohr M., *Fixation of Buried and Surface-Mounted Magnets in High-Speed Permanent-Magnet Synchronous Machines*, IEEE Transactions on Industry Applications, vol. 42, n°.4, pp.1031-1037, July/August 2006.
[115] *** - Parker, High-Speed Motors for Test Rigs - MGV Series (flyer document available on web site: www.parker.com accessed on October 2012).
[116] Atallah K. and D. Howe, *A novel high-performance magnetic gear,* IEEE Transactions on Magnetics, vol.37, n°.4, pp.2844-2845, July 2001.
[117] Fukuoka M., Nakamura K. and Ichinokura O., *Dynamic analysis of planetary type magnetic gear based on reluctance network analysis*, IEEE Transactions on Magnetics, vol.47, n°.10, pp.2414-2417, October 2011.

PART 3

COPY OF THE MOST SIGNIFICANT RESEARCH PAPERS